GEOMETRY AND SIZE OF SUBSTRATE TOPOGRAPHY GUIDES THE NEURAL DIFFERENTIATION OF HUMAN EMBRYONIC STEM CELLS

SONEELA ANKAM

(B.Tech. Biotechnology, Anna University)

A THESIS SUBMITTED

FOR THE DEGREE OF DOCTOR OF PHILOSOPHY

DEPARTMENT OF BIOENGINEERING

NATIONAL UNIVERSITY OF SINGAPORE

2013

DECLARATION

I hereby declare that this thesis is my original work and it has been written by me in its entirety. I have duly acknowledged all the sources of information which have been used in the thesis.

This thesis has also not been submitted for any degree in any university previously.

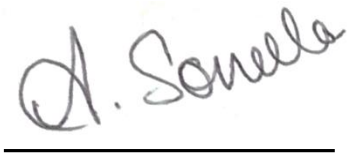

Soneela Ankam

ACKNOWLEDGEMENT

I wish to express sincere thanks to my supervisor, Dr. Evelyn Yim for her guidance and support provided during the last five years. This PhD would not have been possible without the research scholarship from NUS and funding from NRF-CRP. I thank Dr. G. V. Shivashankar for his discussions on the nucleus mechanism studies.

My colleagues from the Regenerative Nanomedicine Lab; Dr. Sandy Lim, Dr. Mie Yamamoto, Dr. Lesley Chan, Stephanie, Chua Jie Shi, Wong Sum Thai, Kung Yiu Shun, and Lim Choon Kiat, eased this journey with their consistent help. A special thanks to Sang Joon for teaching me the basics of cell culture techniques, Teo Kim Kiat for sharing tricks and tips on various techniques, Dr. Aung Aung Kywe Moe and Jason Tann for their friendly discussions, and generous help extended in maintaining the embryonic stem cells during my vacation.

I also thank Guillaume Thiery Marcy for his valuable suggestions and advice on neuronal differentiation of pluripotent stem cells. I sincerely thank Lee Shu Ying and the MBI microscopy core for their help with confocal imaging. My acknowledgement wouldn't be complete if I don't thank my undergrad mentor, Dr. Vaishnavo Pai who encouraged me to pursue research.

My greatest gratitude goes to my parents for allowing me to pursue research against the odds of my society. I thank my husband, Ramesh Ramji for his endurance and motivation that he has given me during the tough and challenging periods of my doctoral study. Finally, I would like to thank the almighty for his blessings.

TABLE OF CONTENTS

SUMMARY

Efficient derivation of neural cells from pluripotent stem cells remains an unmet need for the treatment and therapeutic development of neurological disorders. The limiting factors for current methods include being labour-intensive, time consuming and expensive. The *in vitro* stem cell niche should be carefully designed to support the growth of embryonic stem cells (ESCs) and their differentiation into a desired lineage. Several studies have shown that substrate topographies could guide the stem cell behaviours like adhesion, migration, proliferation and differentiation. In this study, it is hypothesised that the geometry, size and arrangement of the topographical cues could guide the neural differentiation of human embryonic stem cells (hESCs). The objective of the study is to efficiently differentiate hESCs to neurons using topographically patterned substrates and understand the mechanism of force induced neuronal differentiation.

A multi-architectural (MARC) chip containing fields of topographies varying in geometry and dimension was developed to facilitate high throughput analysis of topography-induced neural differentiation *in vitro.* The hESCs were subjected to "direct differentiation", in which small clumps of undifferentiated hESCs were cultured directly without going through the stage of embryoid body formation, on the MARC chip with N2 and B27 supplements for seven days.

This method was compared against "conventional method" of neuronal differentiation of pluripotent stem cells using embryoid body formation. The gene and protein expression analysis indicated that the anisotropic patterns like gratings promoted neuronal differentiation (20% Tuj1 positive) of hESCs while the isotropic patterns like pillars and wells promoted the glial differentiation (40% GFAP positive) of hESC. This

study also showed that optimal combination of topography and biochemical cues could shorten the differentiation period (7 days) and allowed derivation of neurons bearing longer neurites that were aligned (approximately 50%) along the grating axis. The MARC chip platform enabled high-throughput screening of customised topographical substrates that could maximize the efficiency of neuronal differentiation from pluripotent stem cells.

Using the MARC chip, we identified that the nano-grating substrate would be one of the optimal topographies for neuronal differentiation for hESCs. We then seek to understand the role of acto-myosin contractility in directing the neuronal differentiation on nano-gratings. It is hypothesized that the acto-myosin contractility is necessary for faster maturation of neurons derived from hESCs. In proposition, it is also speculated that hESCs grown on nano-gratings have higher contractility resulting in elongation and alignment of nuclei along the grating axis during neuronal differentiation. Inhibitors of acto-myosin contractility and ROCK activity like blebbistatin, ML-7 and Y-27632 were used to test the hypothesis.

From the temporal studies, acto-myosin contractility was indeed observed to be essential for expression of mature neuronal markers on nanopatterned substrates. Interestingly, nano-grating topography could promote the expression of immature neuronal markers like Tuj1 in spite of treatment with blebbistatin.

This thesis has contributed to the technological development of a novel high throughput screening biomaterials microarray and to the understanding of the roles of cytoskeletal contractility in the neuronal differentiation of human embryonic stem cells. A topographical chip, which is easily customisable and easily fabricated, was developed for studying the stem cell behaviour and differentiation on biomaterial substrates in a

high throughput manner. An efficient method called the “direct differentiation” utilising optimal topographical substrates and differentiation media was devised to drive the hESCs to commit to a neuronal or glial lineage in seven days, which is much shorter compared to other previously reported protocol. Using the high throughput array MARC chip, the arrangement, geometry and size of topographies were shown to be able to affect the differentiation of hESCs into neural lineage (20% neuronal cells). Using the optimal topography the 250nm gratings, a more in-depth study of the role of cytoskeletal mechanism along with changes observed in the nucleus gave us a better understanding of the role of topography in decreasing the time taken for efficient neuronal differentiation (7 days with direct differentiation method) as compared to the established methods (>21 days) thus far.

LIST OF TABLES

LIST OF FIGURES

LIST OF SYMBOLS/ABBREVIATIONS

AA – Ascorbic acid

AFM – Atomic force microscopy

AHPCs - Adult rat hippocampal progenitor cells

ANOVA – Analysis of variance

BCA – Bicinchoninic acid

BDNF – Brain derived neurotrophic factor

FGF2 - Fibroblast growth factor 2

BMP - Bone morphogenetic protein

BSA – Bovine serum albumin

ChAT – Choline acetyl transferase

CNS - Central nervous system

CNTF – Ciliary neurotrophic factor

DAT – Dopamine active transporter

DMEM/F12 - Dulbecco's modified eagle medium

DMF- Dimthylformamide

EB -Embryoid body

ECM - Extracellular matrix

EdU – 5 Ethynyl 2' deoxyuridine

EGF – Epidermal growth factor

FA - Focal adhesion

FBS – Foetal bovine serum

FGF8 - Fibroblast growth factor 8

GDF3 – Growth differentiation factor

GDNF – Glial derived neurotrophic factor

GFAP – Glial fibrillary acididic protein

hESCs - Human embryonic stem cells

HSPC -Hematopoietic stem and progenitor cells

iPSCs – Induced pluripotent stem cells

KOSR – Knockout serum replacement

KPa - Kilo pascals

LCST - Lower critical solution temperature

LIF – Leukemia inhibitory factor

MAP2 – Microtubule associated protein 2

MARC - Multi Architecture

MEF – Mouse embryonic fibroblasts

MgCl2 – Magnesium chloride

MLC – Myosin light chain

MSCs – Mesenchymal stem cells

NaCl – Sodium chloride

NCAM – Neural cell adhesion molecule

NEAA – Non essential amino acids

NIL – Nano imprint lithography

NMII – Non muscle myosin II

NPCs – Neural precursor/progenitor cells

NSCs - Neural stem cells

PA - Peptide amphiphile

PDMS - Polydiemthylsiloxane

pFAK – Phosphorylated focal adhesion kinase

pHEMA- Polyhemamethacrylate

PIPES - Piperazine-N,N'-bis (ethanesulfonic acid)

PLCL -Poly (L-lactic acid)-co-poly-(3- caprolactone)

PLGA- Poly (lactide-co-glycolide)

PLL -Poly-L-Lysine

PLLA – Poly-L-Lactic acid

PLO -Poly -L-ornithine

pMLC – Phosphorylated myosin light chain

PMMA - Polymethylmethacrylate

PSD 95 – Post synaptic density protein 95

RA- Retinoic acid

RGD – Arginine – Glycine - Aspartic acid

rhDLL4 – Recombinant human delta like ligand 4

ROCK - Rho associated protein kinase

RT-qPCR – Reverse transcription Quantitative polymerase chain reaction

SEM – Scanning electron microscopy

SHH - Sonic hedgehog

TCPS – Tissue culture polystyrene

TGFβ3 – Transforming growth factor β3

TH – Tyrosine hydroxylase

TiO – Titanium oxide

TUBB3- β tubulin 3

UV – Ultraviolet radiation

2x2µG – 2 micrometre grating width with 2 micrometre spacing

2x1µG - 2 micrometre grating width with 1 micrometre spacing

1x2µG - 1 micrometre grating width with 2 micrometre spacing

250x250nG – 250 nanometre grating width with 2µm spacing

1x6.5µP – 1micrometre diameter pillars with 6.5 micrometre pitch

2x12µW – 2 micrometre diameter wells with 12 micrometre pitch

2µG pr 250nG – 2 micrometre gratings with perpendicular 250 nanometre gratings

Chapter 1

1. Introduction

Neurodegenerative disorders are more prominent with aging and might be caused due to genetic and/or environmental influences. In most cases it leads to loss of function due to loss of neural cells in the affected region. Regeneration is limited in the adult brain and may be affected by factors like scaring by glial cells, accumulation of myelin associated inhibitors like chondroitin sulphate proteoglycans, free radical formation and the defect size [1-3]. Current treatment strategies for neurodegenerative disorders include the foetal neuron transplantation, surgery or drugs [4, 5]. These transplantation based therapies are limited due to ethical issues and also due to the limited number of neurons that can be obtained while the surgical procedures are technically challenging and propose higher risk. The continued use of psychotropic drugs could have other side effects and hence is not a solution but just offers therapy for the patient suffering from neurodegenerative disorders. Alternative sources for cell therapy include tissue engineering approaches to derive neurons from stem cells in vitro. The use of tissue engineered neurons could be a promising solution for neurodegenerative disorders.

In spite of several decades of research in the field of tissue engineering, the efficiency of deriving neurons for *in vitro* and *in vivo* studies is low, in the range of 0.5% – 40% depending on the technique and cell source used [6-9]. Recent advances in neuroscience, cell culture, genetic techniques, and biomaterials provide optimism for new treatments by bioengineering strategies [1]. These current challenges are the motivation for the work done in this thesis; to determine the optimal scaffold design for efficient derivation of neural cells from pluripotent stem cells. Neural tissue engineering

approach conventionally involves four components: scaffold designed to guide nerve regeneration over long distances, stem cell source to provide for sufficient differentiated and functional neuronal cells, trophic factors and cytokines that guide the growth and differentiation of stem cells.

The design of a suitable scaffold to guide the neural differentiation of human embryonic stem cells (hESCs) is dependent on providing a microenvironment similar to the stem cell niche *in vitro*. Stem cells can respond to changes in these microenvironments during development or injury resulting in their proliferation or differentiation. The stem cell niche is composed of a spatially arranged extracellular matrix (ECM) which presents a variety of biochemical and topographical cues that regulates stem cell fate for development and regeneration. In this study, the microenvironment is recreated *in vitro* by providing substrate topographies of various geometries and size. It has been shown by Weiss in 1945 that cells aligned and oriented along the substrate. Since then many interesting studies have shown the importance of other substrate features like geometry, size and curvature in the design of a tissue engineered scaffold. The study done by Yim *et al*. on transdifferentiation of human mesenchymal stem cells (hMSCs) into neurons when subjected to grating like topographies, leads us closer to exploring the full potential of stem cells [10]. These studies reiterate the importance of studying stem cell - substrate interaction to better recapitulate the stem cell niche and thus successfully be able to derive or maintain the tissue of interest *in vitro* for therapeutic purposes.

This thesis focuses on enhancing the neuronal differentiation from human embryonic stem cells (hESCs) for cell therapy. Embryonic stem cells (ESCs) are pluripotent cells derived from the inner cell mass of blastocysts with the potential to maintain an undifferentiated state. The ESCs remain as potential candidates for

regenerative medicine due to their ability to regenerate the three germ layers – ectoderm, mesoderm and endoderm. However one of the major challenges of using ESCs for therapeutic applications includes deriving a pure population of differentiated cells in an efficient manner [11]. Derivation of neurons from hESCs *in vitro* is of specific interest in this thesis. The molecular mechanisms that specify neuronal subtype when a stem cell becomes irreversibly committed to a particular neuronal subtype are not clearly understood at present [12]. This gap in knowledge and the rise in neurodegenerative disorders have aroused the interest of many researchers to bioengineer an optimal system for deriving specialised neural cells.

1.1. Hypotheses

It is hypothesised that the geometry and size of the topographical cues could guide the neural differentiation of human embryonic stem cells. The regulation of neural differentiation is hypothesized to be due to the involvement of the acto-myosin contractility. The acto-myosin contractility is necessary for faster maturation of neurons derived from hESCs.

1.2. Specific aims

The specific aims of this thesis are as follows:

1. **To characterise the hESC and optimise their culture on MARC chip**.

The objective of this study is to determine the optimal topographical pattern that could aid neuronal differentiation. In order to aid the screening process, a simple chip that contained the customised topography arrays was designed and fabricated. Seven different patterns of varying geometry and size were chosen for screening of the optimal topographical pattern. These seven patterns were chosen based on previous studies done

on either ESC derived neural precursors or neural stem cell elongation, differentiation and maturation [13-15]. The patterns comprised of gratings or wells or pillars of micro- and nanometre size and were assembled onto a single chip (MARC chip) to enable fast screening of topographies for understanding various stem cell functions.

2. **To devise a faster neural differentiation protocol using the MARC chip.**

It is important to understand the distinct role played by topography in the differentiation process in order to ascribe its importance to stem cell fate determination. Soft lithography was used to fabricate the different patterns from MARC chip onto polydimethylsiloxane (PDMS), a polymeric substance. The advantage of using PDMS is that it can be easily moulded to the required shape and specific stiffness. The topographical patterns were screened based on the expression of neuronal and glial markers observed during the neuronal differentiation of human ESCs on these patterned surfaces. The outcome of this study delivers the most suitable geometry and size that are important for neuronal differentiation of hESCs. After identifying an optimal topographical pattern, the effect of this particular topography on the neuronal differentiation is evaluated by measuring the neurite extension, alignment along the grating axis and branching.

3. **To understand the role of acto-myosin components in mediating the neuronal differentiation of hESCs.**

The objective of this study was to understand the role of acto-myosin components during neuronal differentiation of hESCs on unpatterned PDMS. Inhibitors of ROCK and myosin contractility were used to study their contributive role during neuronal differentiation. Temporal analysis of actin, myosin, focal adhesions and neuronal markers was done to enable a better understanding the dynamic role played by acto-myosin components.

4. **To understand the role of acto-myosin contractility during topography mediated neuronal differentiation.**

The previous studies focused on determining the optimal topographical cues and in understanding the response of hESCs to neuronal differentiation environment (neuronal differentiation media and unpatterned PDMS). This study is more interested in defining the role of topography in modulating the acto-myosin contractility. Temporal analysis of cytoskeletal components with or without inhibitors is done to reveal a schematic mechanism of topography induced neuronal differentiation of hESCs.

1.3. Conclusion

The derivation of neural cells from hESCs using suitable topographical cues forms the principal interest of this study. The hypotheses and aims are elaborated in this chapter while the relevant literature search to support the individual aims is given in chapter 2. The materials and methods used for the studies described in this thesis are detailed in chapter 3. Chapter 4-7 focuses on the individual aims of this thesis and chapter 8 provides the conclusion and future directions for these studies.

1.4. Significant contributions of this study

This thesis work has demonstrated in the technological development of a device in studying topography-directed stem cell differentiation and the scientific understanding of the roles of cytoskeletal contractility in the neuronal differentiation of embryonic stem cells. In terms of technological development, a simple and efficient protocol that could be used for deriving neurons or glial cells from human embryonic stem cells using topographically patterned substrates. The neuronal differentiation can be achieved by the direct differentiation method in only 7 days, and it was time-efficient as compared to the other established methods which need a minimum of 15 days for

neuronal differentiation. Moreover, a systematic study to determine the optimal geometry and substrate for both neuron and glial differentiation was conducted in this work. It is the first study to elucidate the role of acto-myosin components and focal adhesions during neuronal differentiation of embryonic stem cells on topographically patterned and unpatterned substrates.

Chapter 2

2. Literature review

2.1 Overview of the established biochemical methods for neuronal differentiation of pluripotent stem cells.

Stem cells are defined as cells with the ability to self-renew and differentiate into specialized cells in response to appropriate signals [16]. Because of its ability to differentiate into different types of functional cells, stem cells possess great value as therapeutics to regenerate and repair damaged tissue. Stem cells can be broadly classified into embryonic stem cells (ESCs) and adult stem cells.

ESCs are pluripotent cells derived from the inner cell mass of blastocysts with the potential to maintain an undifferentiated state [17]. The ESCs are hypothetically capable of regenerating all the cell types of the three germ layers - ectoderm, mesoderm and endoderm. Recent technologies also allow the re-programming of adult cells into pluripotent stem cells, which are referred as induced pluripotent stem cells (iPSCs) and they exhibit properties similar to ESCs [18]. Adult stem cells on the other hand, are derived from adult tissues. Adult stem cells can be multipotent; hence, they can generate progeny of multiple distinct cell types. Progenitor cells can also be isolated from adult tissues, and they have the capacity to differentiate into a specific type of cells; nevertheless, progenitor cells are committed to a specific lineage. With the properties of self-renewal and differentiation, stem cells have a huge potential for biotechnology and regenerative medicine.

Conventionally, pluripotent stem cells have been coerced to differentiate into neural cells by subjecting them to embryonic stages of development, with serial concoction of growth factors and neurotrophic factors. The various methods established

so far for neuronal differentiation of pluripotent stem cells like ESCs and iPSCs can be broadly classified into two methods namely, 1) embryoid body method, 2) adherent culture method, which will be discussed in detail.

2.1.1 Embryoid body formation

Several methods have been established for the generation of embryoid bodies from pluripotent stem cells (ESCs and iPSCs) to either demonstrate their pluripotency or to differentiate them to a particular tissue type or germ layer. The method of generating embryoid bodies (EBs) include suspension culture [19], stirred flask culture [20], hanging drop method [21], aggrewell^{TM} method [22] and using hydrogels [23, 24] (Figure 2.1).

In all these culture systems, either single cell or clumps are grown on low adhesion plates or systems (like aggrewell^{TM} and hydrogels) to enable the growth of these aggregates into the three distinct germ layers in the presence of serum and low growth factor concentrations. The liquid suspension culture method is the most commonly used method due to the cost-effectiveness and involves growing the pluripotent stem cells in ultra-low attachment plates in static culture. This method is not very suitable for generating homogeneous EBs. The hanging drop method is one of the earliest methods developed which involves adding small volume (20-25µl) of pluripotent stem cell aggregates on a lid covered with parafilm and carefully inverting the lid onto a buffer filled plated to avoid drying of the EBs. This method can be used to generate homogeneous EBs but is limited by being a time consuming and skill dependent process. The aggrewell^{TM} system is a more recent system developed by microfabrication techniques, containing thousands of microwells adhered to a standard multiwell plate. This system is reliable, reproducible, fast and more efficient to generate EBs from both

single cell and clumps, thereby allowing a precise control over the size and number of cells/EB formed.

The EBs can be tuned to a particular germ layer or tissue type by culturing them in the presence of suitable growth factors and media conditions. The pluripotent stem cells can be predisposed to a neural lineage by exposing the EBs to BMP inhibitors [25] or SMAD inhibitors [26] at an early stage of differentiation. Studies have shown that EB size also plays a role in the lineage preference during differentiation, viability and proliferation. The work done by Lee *et al*. on concave microwell arrays of 200, 500 and 1000μm sized wells show that cardiomyocyte differentiation and beating function can be significantly affected by the size of EBs [27]. Their work also demonstrated that there are significant differences in neurite formation and neurite length from EB's of different sizes during neuronal differentiation.

The EBs are generally grown in suspension for 3-15 days depending on the system used for generating them, followed by plating of EBs onto laminin coated coverslips in chemically defined medium (containing fibroblast growth factor2, FGF2, N2 and B27 supplements) to induce them to form neural progenitor cells. These neural progenitor cells are expanded in suspension neurosphere culture and replated onto suitable laminin coated or poly-L-ornithine coated substrates for neuronal or glial differentiation respectively. The neural progenitors are subjected to region specific cues like sonic hedgehog (SHH) and fibroblast growth factor 8 (FGF8) to induce differentiation of pluripotent stem cells into a dopaminergic subtype [28]. The other most commonly used patterning factor is retinoic acid (RA) during the neural rosette stage to induce anterio-posterior and dorsoventral patterning to drive hindbrain neuronal differentiation along with WNTs and FGF2 [29].

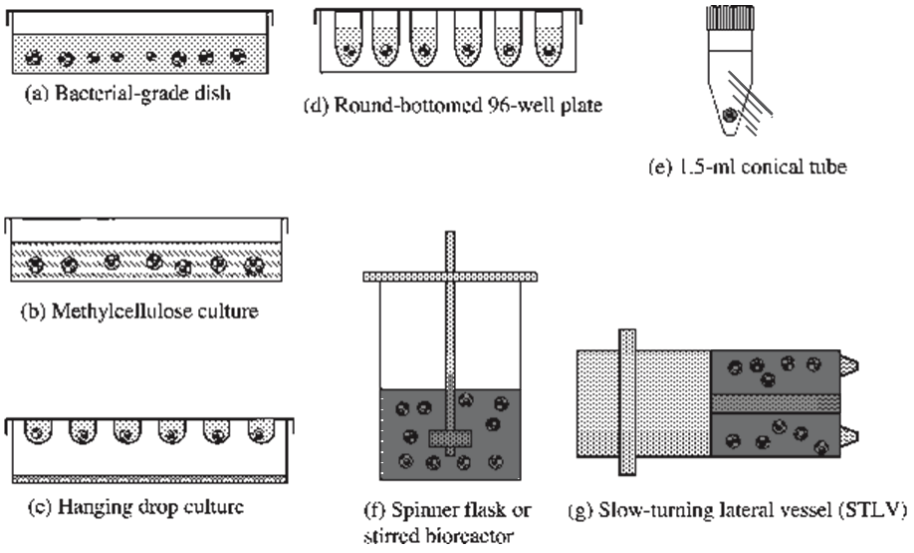

Figure 2.1 Schematic representation showing different methods employed for EB formation from pluripotent stem cells [21].

2.1.2 Adherent culture methods

The adherent culture system surpasses the aggregate formation steps and is done in chemically well-defined media, hence could be a good system to study the signaling pathways involved during neuronal induction and patterning from pluripotent stem cells. The hESCs were grown on matrigel or PLL/laminin (serial coating of poly-L-lysine followed by laminin) coated plates in the presence of N2B27 media (1:1 mix of DMEM/F12 supplemented with N2 and neurobasal medium supplemented with B27) and 100ng/ml Noggin (BMP inhibitor, to block extra embryonic endoderm differentiation) to derive neural progenitors after 30 days adherent culture. These embryonic stem cell derived progenitors could be maintained and expanded in culture by supplementing with FGF2 [30]. Studer *et al*., have shown that co-culturing hESCs on irradiated stromal cells for 28 days in serum replacement media (DMEM/F12 with 15% knockout serum replacement, 2mM L-glutamine and 10μM β-mercaptoethanol) to derive neural rosettes. These neural rosettes were manually picked from the feeder layers and grown on laminin coated plates in N2 containing media supplemented with

100ng/ml SHH, 20ng/ml FGF8 and 0.2mM ascorbic acid (AA) and 20ng/ml brain derived neurotrophic factor (BDNF) for 14 days with manual passaging once every 7 days. The neural progenitor cells committed to dopaminergic differentiation were finally cultured for another 10 days in N2 containing media supplemented with glial derived neurotrophic factor (GDNF), transforming growth factor β3 (TGFβ3) and ascorbic acid to derive up to 80% tyrosine hydroxylase (TH, dopaminergic neuronal marker) expressing neurons [31].

In a more recent study by Baharvand *et al*. where hESCs were co-cultured with chicken notochord (encapsulated in alginate bead), showed that they could differentiate into neuronal cells within 7 days of co-culture as opposed to control cells (not exposed to notochord co-culture) which could only form neural rosette like structures. This study showed that pluripotent stem cell derived neuronal cells attained anterior or hindbrain marker depending on whether they were co-cultured with notochord or somite, respectively [32].

In an interestingly simple system studied by Fei *et al*. showed that hESCs and iPSCs could be differentiated into neural lineage with dorsomorphin, a protein kinase inhibitor that inhibits both activin (co-operates with FGF signaling to maintain pluripotency of hESCs and iPSCs; activin/nodal signaling activates endoderm differentiation) and BMP signaling (involved in mesoderm and endoderm differentiation). Dorsomorphin (1μM) can suppress mesoderm, endoderm and trophoectoderm differentiation and induce rapid and high-efficiency neural conversion in both hESCs and hiPSCs (88.7% and 70.4%, respectively) [33]. Baharvand *et al*. established a four step (30 day) protocol that involves subjecting the undifferentiated hESCs grown on matrigel to noggin and FGF2 (stage 1), followed by induction with RA (stage 2), proliferation of neural rosettes with FGF2 (stage 3), isolation of neural tubes

and plating onto laminin coated plates to derive 96% microtubule associated protein 2 (MAP2) positive neuronal cells (stage 4) [34].

In summary, the established biochemical based methods of differentiating pluripotent stem cells involves subjecting them to embryonal stages of development by either embryoid body formation or by adherent culture in different media compositions. These methods are usually long but yield a purer population of desired neural cells because of the preconditioning steps involved during differentiation. Research has also shown that the various embryonal stages of development can be short-circuited to induce neural differentiation through use of inhibitors; however these methods are still limited by the long time needed for differentiation and low efficiency.

2.2 Biomaterial based structural cues for stem cell differentiation

The microenvironment is composed of extracellular matrix (ECM), which is a reservoir of biochemical as well as biophysical cues. Both of these cues can be presented on substrate surface with specific spatial arrangement, while biophysical cues can be presented in the form of substrate nanotopography and/or matrix stiffness. Both the controlled self-renewal and directed differentiation are keys to the application of stem cells in regenerative medicine, which aims to provide a therapeutic platform by creating or controlling the extracellular microenvironment in order to guide tissue growth for functional recovery and/or dictate stem cells differentiation into the appropriate cell type. In their *in vivo* environment, stem cell fate is controlled by intrinsic factors and microenvironment known as the stem cell niche [35, 36]. Meanwhile, as stem cells vary in sizes and shapes in the micron range, different types of stem cells require different biochemical and biophysical cues from their niche for differentiation or maintenance. It is not surprising to see that various type of stem cells do respond to topology at the micron- and nanoscale. In this section, we will discuss the role of topographical and

chemical patterns, in the maintenance and differentiation of ESCs and adult stem cells such as MSCs, hematopoietic stem cells, and neural stem cells/ neural progenitor cells (NSCs/NPCs).

2.2.1 Pluripotent stem cells (PSCs)

Embryonic stem cells (ESCs) are pluripotent cells that were extracted from the inner cell mass of a pre-implantation blastocyst [37]. The iPSCs are stem cells reprogrammed from adult cells. They were first demonstrated by Yamanaka using forced expression of four important pluripotent genes (Oct4, Sox2, c-Myc and Klf4) [38]. This research on iPSCs is gaining importance due to its applicability for providing personalized disease related solutions. Many new techniques have been established for reprogramming of adult cells since the first report in 2006, which includes both viral based systems (lentivirus, retrovirus) and integration–free system (plasmids, sendai virus, adenovirus or proteins) [39]. Although the extraction and culture methods of ESCs and iPSCs may differ, the PSCs share five characteristics: long-term self-renewal capacity, multi-lineage developmental potential, normal euploid karyotype maintenance over extended culture, cell-specific marker expression, and telomerase activity [40, 41]. These shared characteristics make PSCs unique and are the reason behind their enormous potential as an unlimited cell source for tissue engineering, regenerative medicine, drug discovery and testing, and studying human developmental biology [42]. However, before this potential can be realized, protocols for the efficient, reproducible, and xeno-free maintenance and differentiation of PSCs must be found.

Traditionally, PSCs were cultured on flat surfaces coated with a layer of extracellular matrix (ECM) or a layer of mitotically inactivated feeder cells. On these platforms, the PSCs were cultured in a serum-containing media that was supplemented with additional growth factors. This continues to be the culture condition of mouse

PSCs, which are conventionally grown on a layer of gelatin in serum-containing medium that is supplemented with leukemia inhibitory factor (LIF) [43]. Human PSC culture, however, continues to evolve towards a defined and xeno-free culture system in the hopes that human PSCs can be used for regenerative medicine. Human PSC culture has evolved from originally being propagated on inactivated mouse embryonic fibroblast (MEF) feeder layers [44], to being propagated on extracellular matrices like Matrigel^{TM}, laminin, and fibronectin with media conditioned by MEFs [45], and recently to being propagated on extracellular matrices with defined media [46]. Currently, xeno-free and fully defined culture media is being developed for human PSCs.

In addition to improving the PSC expansion culture conditions, there is also a push to direct the differentiation of PSCs into a specific terminally differentiated cell type. The current approaches to achieve this end goal are to use a 'differentiation medium' and/or embryoid body formation as discussed in the previous section [22, 47, 48]. The differentiation media often contains serum and chemicals, like retinoic acid, and does not include the requisite growth factors in the maintenance medium, like FGF2 or LIF. At present, PSC proliferation and differentiation are predominantly directed using biochemical cues from growth factors and the ECM; however, the ECM, like Matrigel^{TM}, also provide topographical cues. In the following section, the effect of topographical cues on PSC proliferation and differentiation will be discussed.

A. PSCs on Grating-like Structures

Grating-like topographies cause cells to become elongated. In the case of ESCs, this elongated morphology appears to be a cue for the PSC to differentiate. This has been shown by at least two studies which have demonstrated that differentiation is enhanced when a grating-like topography is used without differentiation medium, and an even greater enhancement is observed when differentiation media is used in

conjunction. Smith *et al.* also demonstrated that grating-like topographies promote mouse ESC differentiation [49]. Using a phase separation technique, this group created poly (L-lactic acid) (PLLA) matrices with nanofibrous architecture which had diameters ranging from 50 - 500nm. They then compared the effect of the PLLA matrix on mouse ESCs to the more conventional culture surfaces gelatin-coated tissue-culture polystyrene and PLLA film. When mouse ESCs were cultured on these three platforms with differentiation media or osteogenic media, which contained osteogenic supplements, the ESCs were observed to spread more on the nanofibrous matrix and to have an increase in early lineage and osteogenic markers. More specifically, they observed a greater increase in the expression of brachyury, β1 integrin, Runx 2, osteocalcin and sialoprotein, and decrease in nestin, as compared to flat films and the tissue-culture plastic control. In a more recent work done by Chan *et al*. it is understood that the efficiency of neural differentiation on gratings could be increased by preconditioning the hESCs into a neural fate (Figure 2.2). The work shows promising future directions in the use of gratings to not only direct the neuronal differentiation but also to increase the yield by temporal exposure to topographical cues [50].

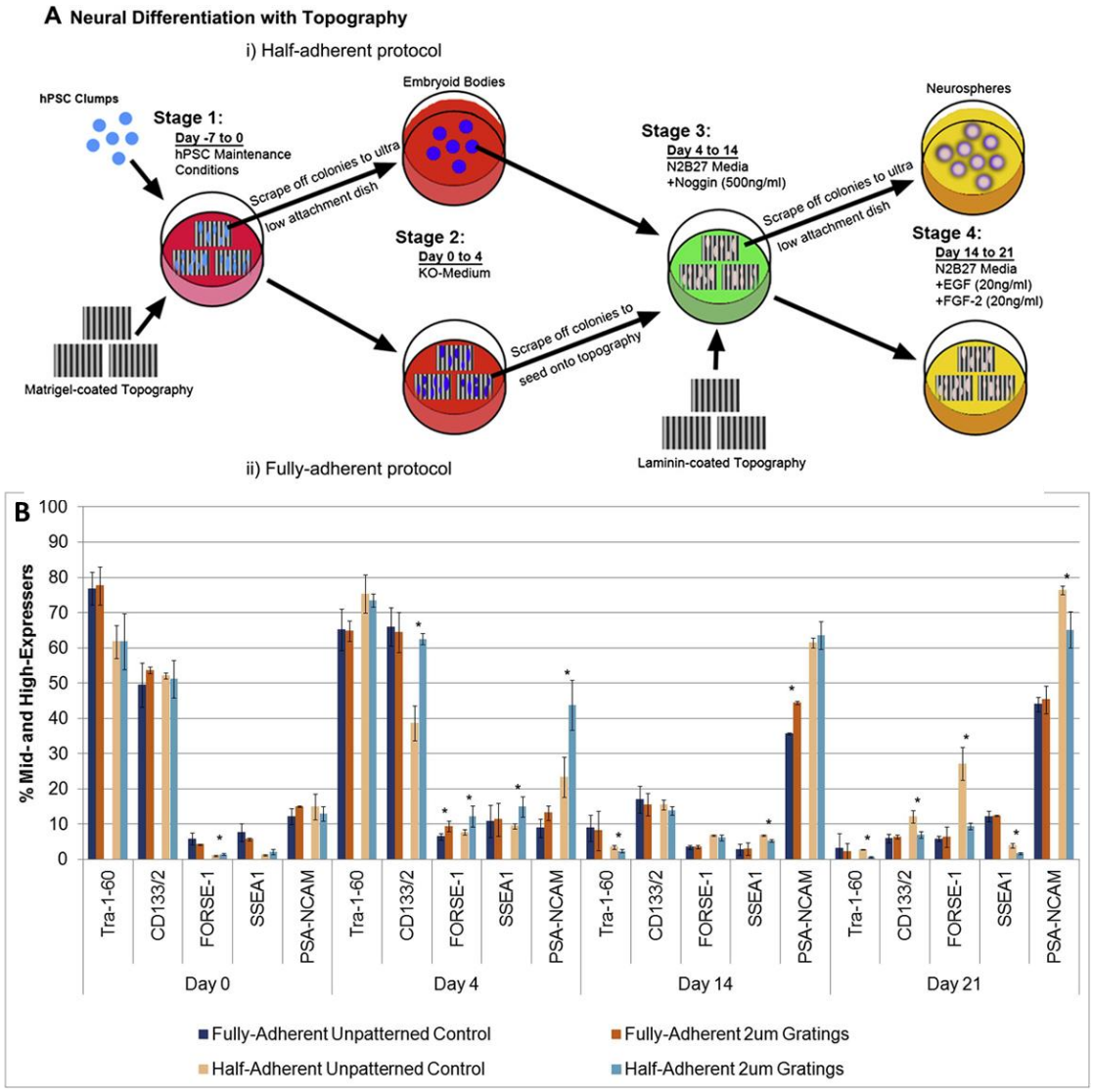

Figure 2.2 A) shows the schematic of neuronal differentiation using topographies in a fully adherent or half adherent protocol. **B)** The image shows the protein expression percentage for pluripotent (Tra-1-60, CD133/2) and neural stem cell markers (Forse1, SSEA1, PSA-NCAM) at different time points (0, 4, 14 and 21). The graph indicates that the half adherent protocol shows higher neuronal differentiation and lower pluripotent protein expression [50].

B. PSCs on Pillar-like Structures

Pillar-like topographies are supportive of mouse ESC proliferation as demonstrated by Markert *et al.* with the BioSurface Structure Arrays [51, 52]. With this structure array, Markert *et al.* surveyed the effects of pillar structures on mouse ESCs by utilizing pillars varying in shape (circle, square), placement (aligned, staggered), feature size (1, 2, 4, 6μm), spacing distance (1, 2, 4, 6μm), and feature height (0.6, 1.6, 2.4μm). This array of pillars was created in silicon and then coated with a thin layer of tantalum oxide. Using this array and expansion media, Markert *et al.* discovered that while pillar shape and placement have no effect on proliferation, the pillars with smaller feature sizes, bigger feature heights and increased spacing distance increase the proliferation of these mouse ESCs. The feature sizing combination which yielded the greatest proliferation rate are pillars with 1μm diameters and 2.4μm heights that were spaced 2μm apart. However, as these were the limits of the tested range, smaller feature sizes and taller feature heights may yield even greater proliferation rates. This was remarked upon by Markert *et al.* when they noticed that even without LIF in the culture media, the mouse ESC colonies exhibited rounded and more compact colonies as compared to the flat surface control. This is another indication that the cues supplied by pillar topographies are supportive of proliferation even without the support of the biochemical cues. In addition to physical pillar topographies supporting proliferation, it has been shown that circular ECM patterns can also be used to promote proliferation or induce differentiation.

Two studies conducted by Peerani *et al.* have shown that both mouse ESC and human ESC fate are influenced when constrained to a colony size due to the limitations of endogenous signalling [43, 53]. The colony size was constrained using micro-contact printing to pattern Matrigel^{TM} for human ESCs or a fibronectin-gelatin mixture for

mouse ESCs onto a tissue-culture treated microscope slide before cell seeding. In the study with human ESCs, the circular patterns had a diameter varying from 200-800μm and a pitch varying from 500-1000μm [53]. After 48 hours of culture in expansion medium, it was found that the cells in 200μm colonies differentiated, whereas the larger colonies of 400μm and 800μm remained undifferentiated, as determined by immunostaining and quantitative polymerase chain reaction.

The human ESC fate was determined by spatial colony size control with the secretion of the endogenous ligands BMP2, by human ESC-derived extraembryonic endoderm, and GDF3, by undifferentiated human ESC. In smaller colonies, the amount of GDF3 secreted is not enough to continue supporting human ESC self-renewal; as such the BMP2 ligand will activate the differentiation pathways. Similarly, mouse ESCs grown in colonies that were restricted to diameters of less than 100μm had a tendency to differentiate because endogenous Stat3 activation could not be maximized [43]. Since phosphorylated Stat3 is a transcriptional factor which directly regulates LIF receptor transcription and indirectly regulates pluripotency markers transcription, it is an important factor when determining mouse ESC fate. This study utilized a range of circular patterns with diameters varying from 50μm to 200μm and pitch varying from 200μm to 400μm. The cells were then cultured on these patterns for 24 hours in serum-free media without LIF. Using this range of patterns they found that generally mouse ESCs will proliferate as the pattern size and clustering increases, and as the pitch size decreases.

Restriction of the colony size by patterning can also be used to find an optimal aggregate size for differentiation, as shown by Sasaki *et al.* [54]. This group employed a mask-free photolithography system to develop adhesive circular micro domains with diameters ranging from 100μm to 400μm on glass substrates. After culturing the mouse

ESCs in differentiation media on these substrates for 12 days, they found that 200μm was the optimal diameter for the cardiac differentiation of uniform sized murine ESC aggregates. These simple micro-patterning techniques provide an efficient and high throughput method to probe the signalling within the ESC colonies and to determine the constraints that will drive differentiation towards a specific lineage most efficiently.

C. PSCs on Well-like Structures

Studies of the effect of well-like topographies on the proliferation of ESCs have been limited the micrometre range. Two groups have used soft lithography to show that well-like topographies made of polydimethylsiloxane (PDMS) will increase the proliferation human ESCs grown in aggregates. Mohr *et al.* used square microwells of PDMS coated with Matrigel™ with the following dimensional combinations (width, height): (50μm, 50μm), (100μm, 100μm), and (100μm, 120μm) [55]. All three of these topographical structures showed an improvement in the viability, proliferation rate, percentage of pluripotent ESCs (as measured by Oct4 expression level), and metabolic activity of the human ESCs when compared to the traditional culture surface, tissue-culture polystyrene. While in these microwells, the human ESCs grew as aggregates, which is unlike the traditional culture method of monolayers.

Similarly, Khademhosseini *et al.* also showed that human ESCs grown as aggregates in circular PDMS microwells coated with fibronectin and mitomycin C mouse embryonic fibroblasts also improved the homogeneity of the human ESC population and increased the proliferation rate [56]. However, unlike the Mohr group, Khademhosseini *et al.* used larger dimensions with a diameter of 200μm and a height of 120μm. Unfortunately, neither group explored smaller dimensions to determine the effect of human ESCs when grown at the nanometre scale.

2.2.2 Mesenchymal Stem Cells (MSCs)

The MSCs are stem cells of mesodermal origin that can be derived from the adult bone marrow. MSCs are multipotent in nature, capable of differentiating into osteoblasts, myoblasts, adipocytes, chondrocyte and skin [57-60]. It is now widely accepted that MSCs stimulate host recovery and regeneration through the secretion of numerous regenerative factors. *In vitro* studies have documented the secretion of multiple anti-inflammatory, angiogenic, neurotrophic, immunomodulatory, and antifibrotic factors from MSCs [61]. This therapeutic potential of MSCs could be tapped by enhancing the proliferation and directing their differentiation. The most common strategy used is a combination of growth factors / biochemical cues like bone morphogenetic protein 6 and transforming growth factor β3 for chondrogenic differentiation; ascorbic acid and dexamethasone for osteogenic differentiation; 5-azacytidine for myogenic induction; microRNA-21 (miR-21) and dexamethasone for adipogenic differentiation; retinoic acid for neuronal differentiation [62-65]. Nevertheless, various studies have shown nanotopography alone can enhance proliferation and/or induce differentiation of MSC [64, 66-68].

A. MSCs on Grating-like Structures

Generally grating-like topographies have been shown to induce differentiation in MSCs. In one such study by Yim *et al,* the proliferation, alignment, elongation and transdifferentiation of human MSC on the nano-grating axis were studied [64]. Gratings with line widths of 350nm, 1μm and 10μm on PDMS were used to study the transdifferentiation of human MSCs into neuronal lineage, with or without retinoic acid induction. They have successfully shown that the effect of nanotopography on the upregulation of neuronal marker is higher compared to the retinoic acid induction alone. In another interesting comparative study of different patterns by Martino *et al.*, uniform

grids and grooved nanopatterns on hydrogenated amorphous carbon film were compared for the differentiation of human bone marrow derived MSCs (huBM-MSCs) into osteogenic and adipogenic lineage [69]. These grooved nanopatterns exerted a higher effect on differentiation of huBM-MSC into osteogenic lineage due to the alignment and elongation cues presented by the grooves.

B. MSCs on Pillar-like Structures

Similar to ESCs, pillar-like patterns favour the proliferation of MSCs. However, the optimal size of the pillar-like feature for MSC proliferation appears to be dependent on the species. In the case of human MSCs, at least two studies have shown that the optimal feature size for adhesion and proliferation is 200nm. Khor *et al*. showed that human mesenchymal progenitor cells cultured on poly(styrene)-*block*-poly(4-vinylpyrindine) diblock copolymer with pillars of average height 6nm and width of 200nm resulted in an increased number of cell aggregates as compared to the smooth surface control on the first day post seeding [70]. Interestingly, by Day 7, the human MSCs cultured on these pillar structures had a flattened and cuboidal morphology with prominent and large adhesion sites and a diffused actin filament structure, which was quite different from the flattened and bat-like structure of the MSCs on the unpatterned mica surface.

Similarly, Dulgar-Tulloch *et al*. demonstrated that 200nm is the optimal feature size for human MSC adhesion and proliferation [71]. They cultured the human MSC on alumina and titania, whose surface was patterned with grain-like structures. This group also showed that the 200nm grain size was most favourable for human MSC proliferation independent of the surface chemistry, the surface roughness, and the crystal phase. When the grain size was increased to 1500nm, there was a decrease in the proliferation rate; however the 1500nm proliferation rate was still better than the

proliferation rate when the grain size decreased to 24nm or 50nm. The optimal topographical features seem to be different for proliferation of rat MSCs cultured on titanium oxide (TiO) nanotubes. Park *et al.* have demonstrated that rat MSCs have increased adhesion, spreading, motility and proliferation when cultured on these TiO nanotubes with a diameter of 15nm [72]. These 15nm TiO nanotubes also increased the osteogenic differentiation of the rat MSCs when cultured in induction media. However, when the tube diameters increased to 50nm and larger, the conditions became unfavourable to rat MSC culture and resulted in low cell attachment and apoptosis. The TiO nanotubes with 15nm diameter also showed optimal osteogenic differentiation of rat MSCs when cultured in osteogenic differentiation media. Engel *et al*. studied the human MSCs lineage commitment by varying the cell shape using topography. These human MSCs were cultured on microstructures in the range of 50µm to 100µm, imprinted on poly (methyl methacrylate) abbreviated as PMMA [73, 74].

When human MSCs are allowed to adhere, flatten and spread, they undergo osteogenesis, whereas compact, round cells become adipocytes [68]. The round pillars, 50µm width and 1µm height, aided adipogenic lineage differentiation while square pillars 2mm in width and 1µm in height, promoted osteogenic transition by changing the morphology of the cells to slightly elongated or star shape respectively. Cell shape is said to regulate the switch in lineage commitment of human MSCs, by modulating endogenous RhoA activity. The mechanism of topography induced differentiation will be discussed in greater detail in section 2.3. It was also demonstrated that the heights of topographical features could affect stem cell differentiation. In a study conducted by Terje *et al*., titanium nanopillar structures of near hexagonal order with varying heights of 15nm, 55nm or 100nm on titanium surfaces were synthesized by anodization through a porous alumina mask [75]. Osteogenic differentiation of human MSCs grown on these

titanium structures was observed. The 15nm high topographical features resulted in the most significant bone matrix nodule formation after 21 days of culture in comparison to the pillars of sizes 55nm and 100nm. In this study, the authors demonstrated that the stem cell behaviour is a function of pillar heights and not of the size and spacing. The parameter will serve as another important guiding parameter to consider when designing a scaffold for MSC differentiation.

C. MSCs on Complex Structures

There have emerged three different approaches toward the formation of nanofibrous materials: self-assembly, electrospinning and phase separation.

A substantial three dimensional (3D) network of nanofibers scaffold formed by the self-assembly of peptide-amphiphile (PA) molecules was fabricated by Hosseinkhani *et al* [76]. The chemical structure of PA contains RGD, a Glutamic acid (Glu) residue, four Alanine (Ala) and three Glycine (Gly) residues (A4G3), followed by an alkyl tail of 16 carbons. This PA is capable of self-assembly into sheets, spheres, rods, disks, or channels depending on the shape, charge, and environment. The fate of rat MSCs seeded on these nanofibers was then investigated. Improved cell attachment, significantly higher alkaline phosphatase activity and higher osteocalcin were observed for the rat MSCs seeded on PA with RGD compared to those grown on tissue culture plastic.

Commendable studies have also been carried out with differentiation of MSCs on electrospun fibers. Dang *et al.* fabricated a thermosensitive electrospun fibre scaffold that could be coupled with the drug encapsulation capacity of electrospinning to serve as a multi-functional platform to encapsulate growth factors as well as providing suitable topographical cues [77]. Thermosensitive polymers have a lower critical solution temperature (LCST) below which they are hydrophilic and water soluble. When the

temperature is increased above the LCST, they become hydrophobic and water insoluble. In this study, hydroxy-butyl chitosan, a thermosensitive material were electrospun into nanofibers, with an average diameter of 437nm, and myogenic induction of human MSCs was observed in response to topographical features without differentiating medium. This technique is beneficial in enabling us to differentiate MSCs as well as harvest the differentiated cells as a cell sheet without disrupting the cell-ECM interaction.

The work done by Murat *et al*. shows that even wrinkles on polyhemamethacrylate (pHEMA) surfaces can be controlled and could contribute significantly to the hMSC morphology and differentiation. Lamellar and hexagonal surface wrinkles were used in this study. Cells when grown on the lamellar wrinkles, spread and differentiated into an osteogenic lineage whereas cells grown on hexagonal wrinkles were rounded and differentiated into an adipogenic lineage. This work clearly shows that complex topographies like wrinkles can also be uniformly replicated in a simple replica molding process to study the stem cell fate [78].

The significance of a combinatorial approach of using both topographical cues and chemical cues in order to upregulate the neuronal markers has also been demonstrated by Prabhakaran *et al*. In their study, electrospun poly (L-lactic acid)-co-poly-(3-caprolactone)/Collagen (PLCL/Coll) nanofibrous scaffolds were used to study the transdifferentiation of bone marrow derived MSCs. The fibre diameter was in the range of 230 ±31nm and neural induction factors like BDNF, EGF (epidermal growth factor), and β-mercaptoethanol were used [79]. The mechanism behind transdifferentiation in response to nanotopographical cues has yet to be unraveled. Nonetheless, these studies contribute to materializing the enormous potential for the generation of functional neurons from patient derived MSCs.

Having learnt about the topographies and how geometry could affect proliferation and differentiation of MSCs, it is interesting to understand how symmetry of a topographical pattern can affect stem cell fate. Dalby and co-workers have shown that random topographies were better than ordered ones in inducing the MSCs to differentiate towards an osteogenic lineage [66]. In yet another study by the same group, a controlled disorder nanopit topography was fabricated by electron beam lithography [80]. It was termed NSQ50 with pits in a near square arrangement, 300nm centre–centre spacing and was used as a scaffold to direct osteoblast differentiation of human bone marrow osteoprogenitor cells. Their results showed that stem cells were sensitive to nanostructure regularity, and that the symmetry of structures had significant influence on stem cell differentiation. In addition to the mesenchymal lineage, MSCs have also been shown to acquire atypical neuronal-like phenotypes.

There has been one study by Khor *et al*. who showed that a complex topography pattern also described as 'worm-like' is able to support the proliferation of human MSCs. These patterns were fabricated by the assembly of poly (styrene)-*block*-poly (2-vinylpyrindine) diblock copolymer material on mica. This study showed that these 'worm-like' patterns of average height 3.2nm and average width 160nm yielded even higher numbers of cell aggregates as compared to a pillar-like topography on a similar material. The morphology of these human MSCs, however, was quite different from that on the pillar-like surface and smooth surface, exhibiting a more elongated morphology with parallel actin bundles and smaller adhesion sites. It was postulated that these worm-like patterns forced the cells into high tension, which allowed the microtubules to distribute homogenously throughout the cell, thus better supporting smaller adhesion sites for enhanced motility [70].

The work by Duy *et al*. presents an exciting new field of biomaterials and topography synthesis for studying stem cell response. They present a method to control MSC culture on dynamically temperature responsive polycaprolactone (PCL) surface. The shape-memory cycle begins by crosslinking liquid prepolymer into the desired primary shape followed by photocuring. The primary shape was then mechanically deformed into a secondary shape at 130˚C and subsequently cooled to -78˚C. To recover the primary shape, the compressive stress was removed and the polymer film was immersed in water at 40˚C for 10 min. Primary patterns like hexagon, boomerang and unpatterned surfaces could be converted to a square, round and channel like secondary pattern respectively using the shape memory cycle [81].

In this section, we have tried to recapitulate the importance of topography in MSC proliferation and fate regulation by various topographies and showed that topography were able to supersede the effect of biochemical cues but the overall outcome seems to be dependent on the species, cell type and topography. The next section will discuss about neural stem cells and neural progenitor cells giving a concise overview of some interesting studies to date in order to understand their interaction with topographies.

2.2.3 Neural stem cells (NSCs)/ neural progenitor cells (NPCs)

Neural stem cells are multipotent stem cells and are present in both developing and adult central nervous system. The NSCs are capable of self-renewal and differentiation into astrocytes, oligodendrocyte and neurons while the NPCs are lineage restricted and only capable of fewer divisions. The three major types of progenitors found in the adult human brain are ventricular zone neural progenitors, hippocampal neuronal progenitor cells and white matter glial progenitors. Isolation, expansion and *in vitro* differentiation of these stem cells and progenitors have been studied extensively in

the last two decades [82-89]. They can be grown either as neurospheres or adherent culture when grown in media containing basic fibroblast growth factor and epidermal growth factors [101]. NSCs and NPCs possess the potential for differentiation into transplantable neurons and so their identification and isolation gives the hope for treating debilitating neurodegenerative disorders.

Many studies have been done to direct differentiation of NSCs/ NPCs to neural cells using co-culture systems or biochemical cues like fetal bovine serum for NSC differentiation to astrocytes; Nerve growth factor, retinoic acid and laminin for neuronal differentiation and a combination of Sonic hedgehog, Fibroblast growth factor 8 and Brain derived neurotrophic factor for Dopaminergic neuron differentiation [90-92]. Our focus in this section will be on the role of topography in influencing the proliferation and directing differentiation of NSCs and NPCs.

A. Neuronal differentiation on Grating-like Structures

Topography often works synergistically with the appropriate biochemical cues as seen in the earlier section in a study conducted by Yim *et al*. Similarly, Recknor *et al.* have studied the effect of topography on neural differentiation of adult rat hippocampal progenitor cells (AHPCs) on micropatterned polystyrene substrates, chemically modified with laminin [14]. When these AHPCs were co-cultured along with the astrocytes on the micropatterns, the percentage of neuronal differentiation and the neurite outgrowth showed a clear increase, suggesting a synergistic effect of nanotopography and the biochemical factors secreted by the astrocytes. The orientation of the AHPCs on the micropatterned substrate seemed to depend on the alignment of the astrocytes with the micropatterns.

B. NSCs on Well-like Structures

Well-like topographies are able to support the proliferation of NSCs but when placed in differentiation culture media, the well-like topographies can promote differentiation. Leipzig *et al*. created a well-like topography from photopolymerizable methacrylamide chitosan hydrogels coated with laminin. The polymers of the hydrogel were tightly cross-linked to form a porous structure. They focused more on the Young's elastic modulus of the hydrogel rather than the size of the pores, but it was noted that as the stiffness increased, the pores became smaller. This group showed that proliferation of rat NSCs could occur when Young's elastic modulus was less than 10kPa, and was maximal at 3.59 ± 0.51kPa. They also showed that the stiffness of the hydrogel could change the type of differentiation being induced when coupled with suitable differentiating media. When the hydrogel stiffness was less than 1kPa, neuronal differentiation was enhanced while oligodendrocyte differentiation was enhanced when the hydrogel stiffness was greater than 7kPa, however, to promote maturation and myelination of the oligodendrocytes, the substrate stiffness needed to be decreased to less than 1kPa. Astrocyte differentiation appears to occur when the stiffness was less than 3.5kPa, however, even at this stiffness the astrocytes constitutes a very small percentage of the cell population. This study suggests that the spatial presentation of the extracellular matrix binding ligands to the integrin receptors of the cell is altered correspondingly with the compliance of the substrate, consequently changing the binding affinities between the ligand and receptors, which would affect the transcriptional regulation of the NSC fate to proliferate or to differentiate [93].

C. NSCs on Complex Structures

The effect of topography as contact guidance has been studied extensively with a focus on axonal guidance and neuronal regeneration. In addition to serving as contact guidance, topography can also affect the proliferation and differentiation of NSCs. One study done by Christopherson *et al*, found that electrospun polyethersulfone fibre mesh coated with poly-L-ornithine (PLO) and laminin will allow for the maintenance of rat hippocampus-derived adult NSC [94]. This study showed that as the diameter decreased from 1452nm to 283nm, the proliferation and spreading of the NSCs increased and aggregated less. However, the proliferation rates of the NSCs on the fibre mesh was still lower than that of the tissue-culture polystyrene flat surface control. The fibers instead were better at promoting differentiation when the NSCs were cultured under differentiation conditions, where they were cultured in the presence of fetal bovine serum and retinoic acid. They analysed the oligodendrocyte and neural differentiation of rat hippocampus derived neural stem cells seeded on nanofibers of various sizes. It was observed that in the presence of 1μM retinoic acid and 1% fetal bovine serum (FBS), rat NSCs showed a 40% increase in oligodendrocyte differentiation on 283nm fibers and 20% increase in neuronal differentiation on 749nm fibers, in comparison to tissue culture polystyrene surface. This study showed the significance of fibre topography and fibre dimension in regulating rat NSC differentiation as well as proliferation.

Table 2.1 Comparison of neuronal differentiation efficiency using either biochemical cues or topographical cues.

Stem cell	Topography or biochemical used	Efficiency of differentiation	Number of days to achieve differentiation	Reference
Human iPSCs	EB with FGF2, Noggin and TGFβ inhibitor.	70% PAX6 positive cells	21 days	[8]
Human ESCs	Dual inhibition of activin and BMP.	84% PAX6 positive cells	7 days	[33]
Human ESCs	EB with FGF2, BDNF and TGFα.	17% TH positive cells	21 days	[95]
Monkey ESCs	Co-culture with sertoli cells.	20% TH positive cells	21 days	[96]
Human ESCs	Co-culture with stromal cells	40% TH positive cells	50 days	[31]
Human ESCs	Micron-gratings	60% of PSA-NCAM positive cells	21 days	[50]
Rat hippocampal progenitor cells	Micron-gratings with astrocyte co-culture	35% Tuj1 positive cells	6 days	[14]
Rat neural stem cells	Nanofibers	60% Tuj1 positive cells	5 days	[94]
Mouse neural progenitor cells	Nanofibers	50% Tuj1 positive cells	7 days	[97]

2.2.4 Hematopoietic Stem/Progenitor Cells (HSPCs)

Hematopoietic stem and progenitor cells are multipotent stem cells predominantly found in the bone marrow of adults; however, other sources of HSPCs include the fetal liver, fetal spleen and the umbilical cord blood [98]. HSPCs are capable of self-renewal and differentiation into all blood cells of the myeloid lineage (e.g. macrophage, erythrocytes, dendritic cells, etc.) and of the lymphoid lineage (e.g. T-cells, B-cells, etc.) [98]. HSPCs are currently used for transplantations to treat haematological disorders and to support the treatment of malignant diseases [98]. Unfortunately, only a low number of HSPCs are able to be extracted and collected from their sources, as such *ex vivo* expansion of HSPCs is necessary to use HSPCs for widespread treatments.

The expansion of HSPCs is notoriously difficult to achieve *in vitro* as HSPCs will differentiate when removed from their niche. In the last several decades, however, scientists have persevered and developed two methods of culturing HSPCs *ex vivo* with some success. The first is to separate the HSPCs into Lin^+ and Lin^- cells, and then take the Lin^- cells and culture them in suspension within a cell culture bag with serum-free media and various growth factors [99]. As the culture progresses, the Lin^+ cells are removed from culture by magnetic separation, thus keeping the Lin^- cell population pure and preventing the Lin^+ cells from inducing the Lin^- cells to differentiate. The second method is to culture the HSPCs on tissue-culture plates, which produces a population with a far greater number of differentiated cells [99]. Both methods require the use of an orbital shaker.

A. HSPCs on Complex Structures

As stated above, the culture of HSPCs proves to be challenging. Chua *et al.* has explored the use of nanofibers to culture HSPCs while maintaining the HSPC phenotype ($CD34^+CD45^+$) [100]. They have shown that human umbilical cord HSPCs could be cultured on aminated electrospun polyethersulfone nanofiber scaffolds. Chua *et al.* have shown that aminated nanofiber mesh and films with average fibre diameters of 529 ±114nm can be used to expand the $CD34^+CD45^+$ cells by 195-fold and 178-fold, respectively, which is an improvement on the tissue-culture polystyrene culture system that only expanded the $CD34^+CD45^+$ cells 50-fold.

Chua *et al.* then continued their studies to show that they can improve the expansion of the $CD34^+CD45^+$ cell population by functionalizing these scaffolds with poly(acrylic acid) grafting and by performing the conjugation of the amino groups with different spacers – ethylene, butylenes and hexylene [101]. When the HSPCs are cultured on scaffolds with aminoethyl or aminobutyl conjugated nanofibers, they are able to obtain a total cell expansion of 773-fold and 805-fold, respectively, where the percentage of $CD34^+CD45^+$ cells were 25.9% and 29.2%, respectively. Culture on scaffolds of aminohexyl conjugated nanofibers only produced a total cell expansion of 86-fold, but the $CD34^+CD45^+$ cell population constituted 41.1% of the total population. All three of these substrates were an improvement over the unmodified nanofiber mesh scaffold, which had a total cell expansion of 85-fold and a cell population that was 13.3% $CD34^+CD45^+$; and the tissue-culture polystyrene control, which had a total cell expansion of 895-fold but only a cell population that was 5.9% $CD34^+CD45^+$. This group then concluded that substrates which "promoted cell adhesion also enhanced the preservation of the $CD34^+CD45^+$ phenotype and the primitive characteristics of cord blood $CD34^+$ HSPCs".

The Table 2.1 summarises the efficiency of neuronal differentiation and duration of differentiation for experiments carried out with either biochemical cues or structural cues. It is generally observed that higher percentages of neurons or specialised sub-type specific neurons could be derived using co-cultures and long term exposure to biochemical factors. However, faster neural differentiation could be achieved by using biomaterial substrates. Most of the studies for neural tissue engineering using structural cues are performed with mouse or rat progenitor cells and could only achieve very immature stages of neural cell derivation. It would be a great leap to increase the percentage of mature neuronal cells differentiation from human stem cells since it could be applicable for drug based studies.

2.3 High throughput screening of factors affecting stem cell interaction with the extracellular environment

The previous sections highlight the importance of substrate topography and material property is important in designing an optimal scaffold for stem cell based tissue engineering. Recently, with the development of technology and resources, the understanding of biomaterials, ECM and growth factors which are important for stem cell behaviour has been improved.

2.3.1 Biomaterial array

Biomaterials array was designed in an efficient nanoliter scale system by Anderson *et al*. in 2004 for studying the attachment, spreading and differentiation of hESCs (H9 cell line). This group used a modified fluid handling system to deposit 576 different combinations of 25 different acrylate, diacrylate, dimethacrylate and triacrylate monomers with a radical initiator onto a layer of poly(hydroxyethyl methacrylate) (pHEMA), on top of an epoxide-coated slide. Monomers were mixed at 70:30 ratios in

all possible combinations. Three blocks of 576 polymers were printed on each slide, with a centre to centre spacing of 740μm. Manual imaging was conducted to in this study to analyse the immunostained samples. This study identified monomers of biomaterials that inhibited hESC attachment. This screen could also compile the monomers which did not affect hESC attachment and proliferation either in the presence or absence of RA [102].

This group also conducted a similar study in 2005 based on poly (lactide-co-glycolide) (PLGA) biomaterial array interaction with hMSCs and neural stem cells (NSCs). In this study, 24 polymers of different composition and molecular weight were dissolved at 10% w/v in dimethylformamide (DMF), and mixed pairwise at ratios of 70:30 and 90:10, for a total of 1152 different combinations which were deposited in triplicate onto a layer of pHEMA, on top of an epoxide coated slide. To increase thickness, six layers of polymer were deposited on each spot resulting in circular but irregular polymer spots on the surface of the pHEMA. This study was able to show that only poly (ethylene glycol) (PEG) could inhibit hMSC attachment while just 30% of PLGA could reverse this condition [103]. These are one of the earliest studies showing on-chip polymerisation of biomaterial library and high throughput screening applications for stem cell studies. The imaging could be automated to decrease the time taken for analysis. Moreover, this is one of the pioneering studies showing the possibility of high throughput screening of biomaterials which could lead to more exciting areas of hybrid screens involving biomaterials, ECM and topographies.

As discussed in previous sections, hESCs and hiPSCs are grown in clumps but a defined system for clonal growth of hPSCs is not very well studied. In a recent work by Mei *et al*. the structure-function relationship of hPSCs and biomaterial substrate is studied using a high throughput biomaterial array. The effect of material properties like

wettability, surface chemistry and elastic modulus on clonal growth of hPSCs was investigated. Microarrays were prepared by co-polymerisation of 22 acrylate monomers of various hydrophobicity, hydrophilicity and crosslinking densities. In this study, 16 "major" monomers were mixed with each of the six "minor" monomers at six different ratios (100:0, 90:10, 85:15, 80:20, 75:25, 70:30 (v/v)). In this way, arrays with 496 different combinations were created, consisting of the major monomer (70-100%) and minor monomer (0-30%). These monomer mixtures were robotically deposited in triplicate on a non-cell adhesive layer of pHEMA covering conventional glass slides and then polymerized with a long-wave ultraviolet source. This study shows that the surface roughness does not have any effect on colony formation of PSCs unlike the elastic modulus of the substrate. The human vitronectin coating along with mTESR1 media had the highest efficiency for clonal growth of PSCs [104]. This study has paved a new direction for understanding biomaterial interaction with biological samples increasing the scope and possibilities.

2.3.2 Extracellular Matrix array (ECM array)

Flaim *et al*., 2005 showed that an ECM microarray platform could be created using a robotic spotter (150µm in diameter spot size) and much less protein (~10pg) than conventionally used. Effects of 32 different combinations of ECM (collagen I, collage III, Collagen IV, laminin and fibronectin) with 8 replicates on a glass slide coated with polyacrylamide were assayed for stem cell differentiation. This group optimised the printing buffer, microarray surface and deposition method. A contact style arrayer capable of depositing 150µm spots (can accommodate at least 20 cells) using 1-2nl of ECM was used. The spotting buffer had to be modified depending on the ECM assayed. The differentiation of mouse ESC to an early hepatic fate indicated by a β-galactosidase reporter fused to a fetal liver specific gene was studied on these ECM microarrays after

7 days of culture. Ten highest β-galactosidase expressions were seen from cells grown on matrices containing collagen I while the lowest eleven signals were obtained from cells grown on matrices lacking fibronectin. The ECM microarray enabled the identification of several counter-intuitive combinations of ECM providing the highest desired effect [105].

In an interesting study to understand the developmental fate of neural precursor cells and to investigate the ECM (laminin) component and signalling factors involved, Soen *et al* created a protein microenvironment using a non-contact arrayer (BCA arrayer, Perkin – Elmer) on a glass surface. Primary human neural precursor cells isolated from the whole cortex of a 22 week human foetus were used for the study. Each spot of the protein mixture was 400μm^2 in area capturing around 100 cells creating 8 replicates of each combination to derive statistically strong data (Figure 2.3). From immunostaining experiments, it was analysed that a combination of Notch ligand, jagged-1, rhDLL4 (recombinant human delta like ligand 4), TGFβ , CNTF (ciliary neurotrophic factor), BMP4 (Bone morphogenetic protein 4) encourage glial morphology while a combination of Wnt3a and laminin have a neurogenic effect [106].

Flaim *et al*. extended their ECM microarray to 240 unique combinations along with mixtures of soluble factors like wnt3a, activin A, bone morphogenetic protein 4 (BMP4), and fibroblast growth factor 4 (FGF4). Each of the 240 ECM mixtures was deposited with five replicates at a 450μm pitch. The cardiac differentiation of mouse ESCs (tagged to a green fluorescent protein, GFP reporter to myosin heavy chain) on these ECM microarrays has been studied. Wnt3A decreased the differentiation efficiency while BMP-4 and activin A promoted cardiac differentiation and these results correlate with previously established results. As compared to the ECM microarray developed by Soen *et al*. where soluble cues (growth factors, biochemical cues and

morphogenic factors) were presented in immobilized format, in this study soluble cues are available in a soluble non-immobilized format [107]. In this study, the ECM microarray was coupled with a laser scanning confocal microscope and a software used to analyse DNA microarrays to increase the resolution and throughput of previously established methods by 10 times.

The microarrayer based technology has been extended for study of long term proliferation and maintenance of pluripotency by hESCs (Hues1 and Hues 9). In a study by Brafman *et al*. human collagen I, collagen III, collagen IV, collagen V, fibronectin and laminin in 320 unique combinations with 5 replicates were used along with immobilized growth factors like basic FGF 2, BMP4, wnt3A and small molecules like retinoic acid (RA) on a polyacrylamide hydrogel substrate. The hESCs were grown for 5 days on the ECM microarray, fixed and stained for pluripotent markers, Oct4 and nanog. Their results suggest that single ECM component differentially supported hESC lines and were not optimal for both proliferation and maintenance of pluripotent stem cells. This study identified that laminin and fibronectin, used in combination with other ECMs were essential for proliferation of ESCs while collagen I, laminin and fibronectin individually could maintain the pluripotency of hESCs [108].

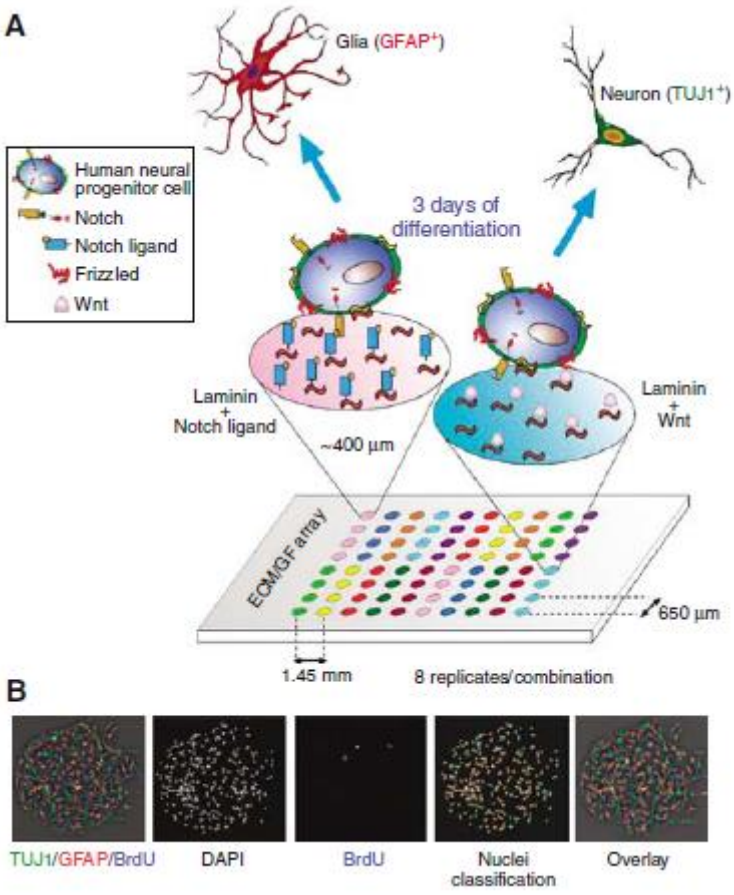

Figure 2.3 A) The image shows the schematic of ECM microarray. The spots were a combination of laminin and other recombinant proteins that were known to preferentially differentiate neural stem cells to glial or neuronal fate. **B)** The samples were fixed and stained for neuronal marker, Tuj1 (in green) or glial marker GFAP (in red). Automated analysis of the intensity of neuronal or glial marker expression based on the nuclei (DAPI) was performed on all spots. BrdU indicated the proliferating population [106].

These studies show the importance and need for high throughput screening of ECM interactions with stem cells to regulate their behaviour like adhesion, proliferation, differentiation. The ECM microarray printing technology has been well optimised and ready to be used for many different stem cell systems with multiple reporters.

2.3.3 Topography array

Lovmand *et al.* demonstrated this using an array of pillars-like topographies on silicon wafers from the BioSurface Structure Arrays [51]. These pillars varied in shape (circle, square), placement (aligned, staggered), feature size (1, 2, 4, 6μm), spacing distance (1, 2, 4, 6μm), and feature height (0.6, 1.6, 2.4μm). In general, they showed that proliferation decreased with increasing feature height and decreasing feature size. They also showed the converse, where differentiation increases with increasing height, decreasing feature size and decreasing spacing distance.

The efficacy of topographical cues to induce differentiation was recently shown by Markert *et al.* [52]. This group also used the BioSurface Structure Arrays [51] to screen the effect of 504 distinct topographical structures on murine ESCs. This array was etched onto a silicon wafer using standard lithography, before being sputter coated with tantalum oxide. This array contained a series of shark-skin structures which were formed by alternating lines of bars with lateral sizing ratios of 1:4 and 2:3. The lines and the bars were separated by 1μm, and the lateral size unit varied from 1μm to 8μm. Even though the culture took place in expansion media which contains LIF, the shark-skin structures promoted differentiation of the mouse ESCs as indicated by a decrease in alkaline phosphatase staining intensity, and an increase in cell elongation and colony spread.

A systematic study conducted by Unadkat *et al*. in 2011 lead to the development of TopoChip containing 2176 different topographies imprinted on a polylactic acid (PLA). This group studied the interaction of human mesenchymal stromal cells using highly automated imaging system followed by automated analysis of the results. This group also designed a Topochip carrier and a system for uniform cell seeding. This group

has not only studied the stromal cells but also ESCs and human endothelial cells. The whole system is easily available on a 6 well plate and can be customised to have nanopatterns. The authors show that by combining high-throughput screening with mathematical design of micrometre-range surface topographies, the "Braille code" of cell-topography interactions could be deciphered [109].

The above studies have clearly shown that high throughput screening of biomaterials, ECM and topography is possible and could lead to better understanding of stem cell behaviour. The major drawbacks of the current methods available are that the height of the individual topographies in a library cannot be varied. We would like to develop a chip that could be fabricated using simple techniques in every lab rather than using more difficult and expensive lithographic technique. The development of the high throughput topography chip will be discussed in Chapter 4.

2.4 Laminin and its role in neuronal development

Laminin belongs to a family of glycoproteins with diverse functions. The most commonly used and studied is laminin-1 purified from mouse EHS (Engelbroth-Holm-swarm) sarcoma basement membrane [110]. Laminin-1 is made up of $\alpha 1\beta 1\gamma 1$ chains and it has been shown to induce differentiation in neuroepithelial cells. The ultrastructure of laminin 1 was revealed using a rotatory shadowing electron microscopy to be a cross shaped structure with three short arms and one long arm [111]. Laminin consists of cysteine rich motifs that are structurally similar to the epidermal growth factor (EGF). Various studies have shown the importance of laminin-1 in promoting neurite outgrowth, axonal guidance, neuronal migration, neuronal differentiation and nerve regeneration [112-114].

Laminin-1 is the first ECM molecule present in between the cells of a developing mouse embryo and its presence has been confirmed at a very early 2 cell stage by

immunofluorescence using antibodies [115-117]. The expression of laminin is spatially and temporally regulated to express different chain during different stages of tissue development [118]. It has been shown that laminin in the adult brain are part of the basement membrane and created by astrocytes, while laminin in the developing brain can exist as soluble or polymerized forms [113, 119]. Astrocytes of the olfactory bulb in the adult mammalian CNS [120] and Schwann cells of mammalian PNS constitutively express laminin-1 [121]. These observations indicate that the expression of laminin-1 correlates with nerve regeneration. This has suggested many researchers to use laminin-1 grafts in the treatment of PNS injuries. Laminin has been applied in silicon or biodegradable tubes, in gels with the additional ECM components, or in collagen tubes containing fibronectin to promote neuronal regeneration and axonal guidance [122-126]. Furthermore, laminin-1 is also capable of neutralizing the inhibitory effect of myelin associate glycoprotein (MAG) [127].

Laminin can bind to either integrin based receptors or non-integrin based receptors to elicit functional outcomes in neuronal cells. Laminin-1 is known to bind to α1β1, α2β1, α6β1, α6β4, α7β1 and α9β1 integrins resulting in various cellular behaviours based on the integrins recruited [128-130]. Still, the reason why a particular integrin would be recruited preferentially over the others is unclear. The active peptide sequences in the alpha and beta chains of laminin elicit different signaling mechanisms. In particular, E8 fragment of laminin-1 was shown to promote neurite outgrowth and cell attachment [131, 132]. In 1991, Skubitz *et al.* synthesized biologically active synthetic peptides based on the α1 globular domain sequence of laminin-1 (KATPMLKMRTSFHGCIK, KEGYKVRLDLNITLEFRTTSK) that promoted neurite outgrowth [133]. Though some of the key peptide sequences in laminin 1 were identified to be important for neuronal differentiation, the exact molecular mechanism by which

laminin-1 preferentially binds to integrin based or non-integrin based receptors and promotes neuronal differentiation remains unclear. However, based on the numerous literature showing the importance of laminin in adult neurogenesis and migration, laminin was chosen to be the ECM used in this study.

2.5 Overview of the substrate topography mediated stem cell differentiation mechanisms.

2.5.1 Fate decisions through changes in cell shape

For anchorage dependent stem cells, the topographical approaches to control stem cell processes like proliferation and differentiation involves the precise control of cell spreading. In a pioneering study by Folkman and Moscona in 1978, cell shape was found to be linked intimately to DNA synthesis and growth in cells [134]. Changes in cell shape was also deemed to be a possible mechanism for myocardial development [135] and also the growth and differentiation of capillary endothelial cells [136]. With regards to stem cells, the previous sections have shown numerous studies that stem cell lineage can be dictated through the use of engineered topographical features (both geometric patterning or topographical cues) to regulate their cell shape. The manipulation of the physical stem cell shape using engineered extracellular topographical features can result from subsets of effects including altered adhesive interactions although the exact mechanism remains unknown. It will be important to recognise that the effects of cell shape on intracellular signalling pathways appears to be of higher complexity than adhesion signalling alone [137]. In the following sections of this chapter the components of the adhesion signalling pathway with a focus on the cytoskeleton and its postulated mechanism in translating these topography derived signals in the extracellular matrix into patterns of gene regulation in the nucleus for stem cell differentiation will be discussed.

Stem cell differentiation can result from biochemical cues, structural cues or likely a combination of both. The structural cues from topography changes the orientation of the cells, reorganizes its body, shape and functional state [138-140]. Studies employing simplistic 2D protein patterning to mimic native ECM demonstrated that mechanical cues do play an important role in regulating stem cell differentiation. Intriguingly, the cells must have an intrinsic fundamental mechanism to sense the underlying substrate topography, generating mechanical signals that are translated by intracellular signalling pathways before ultimately regulating the genomic expression and cell function [141]. This is also known as mechanotransduction. One important aspect of the existing theories [142-146] is the existence of a continuous physical connection from the ECM to the nucleus. The presence of such a physical continuity will allow cellular structural rearrangements to result in gene regulation, such as topography-induced stem cell differentiation.

2.5.2 Mechanotransduction

Mechanotransduction involves a complex interplay of different cellular organelles and components (e.g. focal adhesion and cytoskeleton) that by themselves are highly dynamic *in vivo*, making the process more convoluted [147]. However, advancement of experimental techniques has helped to provide increasing evidence to the mechanism and it appears that cellular components such as the integrins, focal adhesions and cytoskeleton organization collectively play important roles in topography-induced cellular behaviour [147-149].

The topographical extracellular signals have to be transduced from the ECM to the nucleus, where the genome can be regulated as a response to the extracellular signals. Under the effect of nanotopography, the physical substrates do exert differential

mechanical stress onto the cells, as indicated by the cytoskeletal reorganization. The important components of the mechanotransduction machinery include the integrins, focal adhesions with a particular focus on the cytoskeleton that translates these topographical cues into secondary pathways, ultimately affecting stem cell differentiation. The Figure 2.4 shows a schematic of the components involved in mechanotransduction of topographical cues from the underlying substrate.

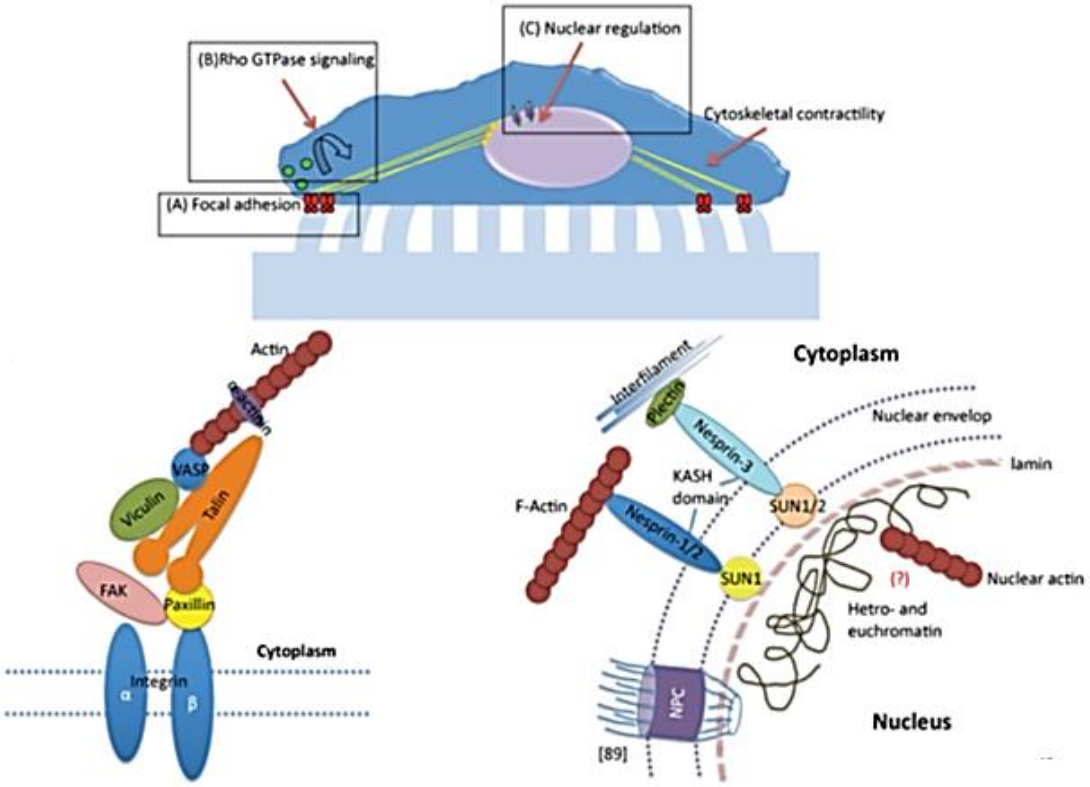

Figure 2.4 The image shows the schematic showing the key signalling components in the force mediated stem cell differentiation [150]. The focal adhesion complex is made up of many proteins which includes not only focal adhesion kinase, paxillin, vinculin and Talin. The actin microfilaments are connected to the nucleus through the SUN and KASH domains thereby effectively transmitting the underlying mechanical signal from the substrate to the stem cell.

2.5.3 Role of cytoskeleton in transduction of topographical cues to the cells

Force generation in the cytoskeleton is required for cell adhesion and migration on ECM. The cytoskeleton consists of actin (microfilaments), microtubules and intermediate filaments. They form a network of filamentous protein that extends throughout the cell cytoplasm in eukaryotic cells. The cytoskeleton has been well studied where it is involved in cellular metabolism and movement ranging from mitosis to migration [151, 152] and an increasing amount of evidence have demonstrated the importance of the cytoskeleton in stem cell differentiation [68, 153].

Different groups have tried to characterize the cellular forces that cells exert on the underlying substrate. An early method of cellular force measurement technique uses a silicon rubber membrane that deforms and wrinkles upon the exertion of force by adherent cells [154]. Another more recent study employs the use of an array of vertical elastomeric micro cantilevers that bends under the exertion of contractile force by cells [155]. The contractile forces present in the actin stress fibers of the cytoskeleton appear to be integral in modulating cellular functions like adhesion, migration and stem cell differentiation. The generation of contractile forces in non-muscle cells is mediated by a class of motor proteins, the non-muscle myosin II (NM II). Briefly, these NM II molecules assemble into filaments which then bind to actin through their head domains. A conformational change elicited from ATPase activity enables the contraction of the actin filaments. These thick cross-linked bundles of actin-myosin are also known as stress fibers. A recent concept suggested that cells use acto-myosin contractility for a two way interactions with the extracellular matrix. This cell contraction through the stress fibers will be resisted by the matrix at the sites of integrin sites with the subsequent recruitment of additional molecules for FA formation. Cells response to topography is thus not passive but rather they often are able to “tune” their mechanical properties

through the dynamic remodelling of the actin cytoskeleton. The balance of tension forces at these interfacial sites allows the cell to sense the ECM.

This tension mediated signalling is manifested in the reorganization of actin microfilaments or stress fibers with the observed alignment of these stress fibers to nano-gratings and differential organization to the other surface features [64, 148, 156]. This cellular force sensing in turn leads to altered levels of Rho GTPase and mitogen activated protein kinase (MAPK) activity as downstream biochemical signals for stem cell gene regulation. In a study by Engel *et al*., the use of matrices with different elasticity regulates the differentiation of MSCs into different lineages [153]. The use of specific NM II inhibitor blebbistatin blocked all elasticity-directed lineage specification without strongly affecting cell function and shape significantly, providing evidence of cytoskeletal force generation in ECM sensing. hESCs also appeared to be aligned and elongated when they were cultured on nanometre scale gratings [157]. It seems that the cytoskeletal-mediated nanotopographical sensing mechanism is also present in human ESCs where mouse ESCs were sensitive to local cyclic stress that were applied to focal adhesions. This applied stress led to the down regulation of Oct3/4 gene expression in mouse ESCs, and myosin II contractility is showed to be essential in mouse ESCs' stress sensitivity [158]. It is likely that the stem cells interpret such changes in force signals to regulate stem cell fate, although topography is probably only one of many contributing factors amongst others like mechanical and osmotic stress.

The ability of human MSCs to generate corresponding contractile forces in response to the underlying stiffness substrate suggests that the cell-generated forces is dissipated within the cell on a rigid matrix [159]. This has led to the postulation that these cellular forces changes protein conformation, exposing binding sites that enables plasma membrane proteins to become functional. It seems that optimal matrix elasticity

is crucial for a functional mechano-sensitive protein [160]. Similar force sensitive regulation of plasma proteins have been observed in mature cells although its role in stem cell regulation is largely speculative. However, a growing amount of evidence have demonstrated the importance of external force loading from the ECM [155] or actin-myosin contractility [149, 161] in the formation of FAs and ECM sensing. The cellular force contractility induces a downstream of events including the recruitment of adhesions molecules and kinases like the mechano-sensitive focal adhesion kinase (FAK), subsequently triggering the activation of Rho GTPases [162]. For example, increasing ECM stiffness activates Rho [163], which promotes acto-myosin stress fibre assembly [164], significantly changing the mechanical properties of the cell [165]. These stress fibers are constantly tuning its mechanical properties with feedback from these downstream molecules. It remains difficult to unravel the entire mechanism but an increasing amount of evidence directs the importance of cytoskeleton in mechanotransduction, with possibly a similar mechanism in topography-induced stem cell differentiation.

2.5.4 Topographical effects on the nucleus

The intricate physical network described previously sets the framework for the physical continuity spanning from the ECM to the nucleus. Mechanical signals such as topographical perturbations from the ECM can be transduced by structural alterations in the network to elicit differential gene expression in stem cells. This section briefly describes key components in nuclear mechanotransduction that might play key roles in topography sensing in stem cells.

While the actin microfilaments are anchored to the ECM through the integrins, they are also physically connected to the nuclear membrane on the other end. Nesprins

are a class of large outer nuclear membrane proteins onto which the actin microfilaments bind onto the KASH domains present in these proteins [166, 167]. The KASH domains are then physically connected to the SUN domain of the inner nuclear membrane forming a KASH/SUN complex to mechanically bridge the actin stress fibers to the nuclear membrane.

The other main structure of the nucleus that appears to be important in topography-mediated mechanotransduction is the nuclear lamina. Similar to the cytoskeleton, the nuclear lamina consists of a meshwork of intermediate filaments and lamin proteins that is associated with the KASH/SUN complex [168, 169] which in turn is connected to the chromatin (reviewed in [170, 171]). Recently, the LINC, a specialized structure that links both the nucleoskeleton and cytoskeleton has been identified, providing more evidence that mechanical forces that arise due to nanotopography can physically affect the structural organization of the nucleus [167, 172].

Forces that are transmitted to the nuclear scaffolds via LINC complex may regulate critical DNA enzymes or factors. Furthermore, in an earlier study, the disruption of intermediate filaments leads to the mechanical decoupling of the integrins and nuclei [173], demonstrating that a direct physical connection exists between the two. It has also been shown that local forces applied to apical integrins are indeed transmitted to the basal focal adhesions and nucleus, suggesting that a physical continuity does exist between the ECM and the cell nucleus [174, 175].

Similar changes in nuclei shape and altered gene expression in response to topography was observed both by other groups as well as our group [64, 176, 177]. While Dalby *et al*. observed spatial alteration of chromosomes in fibroblasts under

topographical influence, our work involving human MSCs on nano-gratings suggests that topography may exert an effect on the structural organization of the nucleus as indicated by the alignment and elongation of the MSC nuclei [64]. This study suggests the direct mechanical coupling of chromatin to the ECM through the intricate mechanotransduction network in stem cells. This physical coupling allows chromatin to be tightly regulated through cellular forces to unravel DNA regulatory motifs for transcription factors to interact, analogous to the exposure of cryptic binding sites in mechano-sensitive plasma proteins.

Although there are clearly evidences of nuclear mechanotransduction, the molecular and biophysical basis for such a mechanism is still left to be understood. In summary, this chapter has first reviewed the literature on established biochemical and biomaterial based stem cell differentiation, showing the different components like growth factors and scaffold design in regulating stem cell fate and the need of improvement in the differentiation efficiency. High throughput methods designed for screening ECM, biomaterials and topographies were discussed. These technologies help us to design a better throughput method that is customisable and easy to fabricate to investigate the differentiation efficiency (faster neuronal differentiation). Finally, the mechanisms and theories on understanding the mechanotransduction of mechanical signals from the substrate to the cells and their nucleus were discussed. These studies guided the experimental planning to better understand the role of nano-gratings during neuronal differentiation of hESCs in this thesis.

Chapter 3

3. Materials and Methods

3.1 Human embryonic stem cell maintenance

Human embryonic stem cell lines, H1 and H9 (WiCell Institute, Madison, http://www.wicell.org) were routinely cultured in a feeder free system using hESC-qualified matrigel (BD Biosciences) [178] and mTeSR1 medium (Stem Cell Technologies) with a daily medium change. Human ESCs were passaged enzymatically with dispase (1 mg/ml) after manual removal of differentiated colonies using an inverted microscope (Nikon TS100) and flame bent Pasteur pipette. The cells were passaged at a ratio of 1:4 – 1:6. Care was taken to remove the differentiated colonies before seeding onto the MARC to ensure uniform starting population of undifferentiated cells and to avoid biased outcomes. Fabrication of Multi-architecture (MARC) Chip

The schematic diagrams in Figure 3.1 shows the stages employed in the fabrication of the MARC chip: (A) patterning of topographies via nano-imprint lithography (NIL). (B) Assembly of topographies onto a single chip.

In the first stage, thermal NIL was primarily utilized to fabricate distinct topography separately onto individual free-standing thermoplastic polycarbonate (PC) sheet (0.25 mm thick, Innox, PC2151). The topographies (line-space gratings, pillars and complex three-dimensional hierarchical structures) are listed in Table 3.1 (Materials and Methods). The mold with the inverse structures of these topographies were made of silicon, quartz or nickel and supplied commercially. They were cleaned, treated in oxygen plasma (Reactive Ion Etcher, TRION) at 20 sccm O2, 80 W, 250mTorr for 3 minutes and further treated with an anti-stiction layer, (1H,1H,2H,2H)-Perfluorodecyltrichlorosilane (FDTS) (Sigma) to render the mold surface hydrophobic

to facilitate demolding. The thermal imprinting process of the PC sheet was performed on a nanoimprinter system (Obducat, AB), at a controlled imprint temperature above the glass transition temperature (Tg of PC=150°C) with an external imprint pressure from the system. Following this, the temperature of the nanoimprinter system was cooled down below the T_g. As different topographies were imprinted onto separate PC sheets, the imprinting conditions could be optimized with respect to the specific designs. For gratings, dimples and lens structures, a single imprinting condition is used: 180°C, 60 Bars, 600s. For delicate structures such as pillar structures, a preheating is performed at 180°C for 120s, before the imprinting at 180°C, 40 Bars, 300s to allow high yield imprinting of such structures. For hierarchical structures, a sequential imprinting process was employed: 180°C, 60 Bars, 600s for the primary imprint; followed by 140°C, 40 Bars, 300s for the secondary imprint. The pitch of the pillars or holes is defined as centre-to-centre side-to-side distance between two adjacent pillars or holes, which are in square arrangement. The dimensions of the gratings are described as ridge with the groove or spacing and depth, ridge being the plateau surface and the depth being the distance from the edge of the ridge to the floor of the groove or space.

In the second stage, assembly of these distinct topographies onto a single chip was carried out in a customized layout. Sections of each imprinted PC sheet were cut into a standard size of 2mm diameter "field" using an in-house-built puncher system. The remaining area of the silicon support surrounding the topographical "field" was covered by a pristine PC film without pattern. The bonding is carried out using PDMS (Sylgard^{TM}184, Elastomer Kit, Dow Corning) mixed in the ratio of 3:1 (base: curing agent). The assembled substrate was placed in a vacuum oven at 70°C for one hour to cure the PDMS, during which the "fields" were bonded firmly onto the solid substrate to form the multi-architecture microarray chip [179].

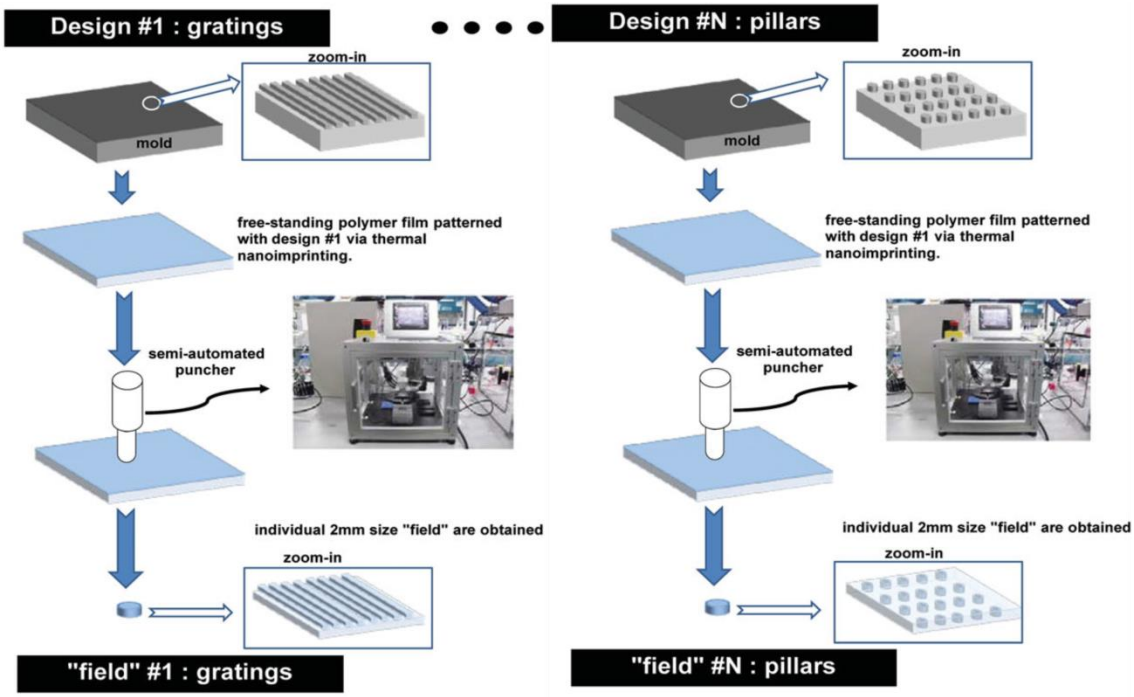

Figure 3.1 Schematic showing the fabrication of MARC. **A)** Shows the stage 1, fabrication of topographies by nano-imprint lithography (NIL) [179].

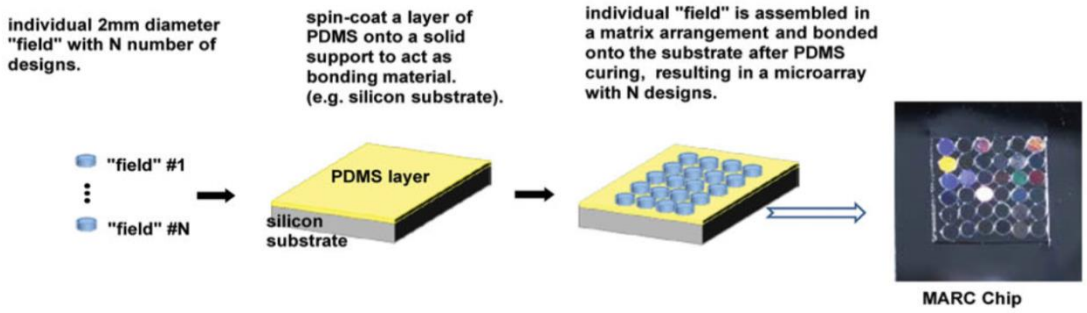

Figure 3.1 B) shows the Stage 2, assembly of individual topographical fields onto a single chip to form MARC [179].

3.2 Fabrication of micro- and nano-topographical features and replication by soft lithography

The topographies included gratings, pillars, wells and complex three-dimensional hierarchical structures, with different dimension, spacing and height (Table 3.1). Imprinted polymethylmethacrylate (PMMA) samples with 4cm^2 area [180], were used for gene expression analysis.

The MARC and imprinted PMMA were surface-treated with Trichloro (1H, 1H, 2H, 2H-perfluorooctyl)silane (Sigma Aldrich) and surfactant (0.01% TritonX 100, Sigma Aldrich) prior to using it for fabricating patterned polydimethylsiloxane (PDMS, Sylgard 184, Dow Corning) scaffolds by soft lithography, which were subsequently used for cellular study. PDMS was made by mixing the base and curing agent at 10:1 ratio, degassed for 1 hour and cured in the oven at 70˚C for at least 3 hours.

3.3 Replication fidelity inspected by scanning electron microscopy (SEM) and atomic force microscopy (AFM)

Replication fidelity of the patterns on MARC chip and nanoimprinted templates onto PDMS substrates were verified using JEOL SEM 6010 LV. In addition, 1µm pillars, 2µm gratings and 250nm gratings were examined by SEM to verify that the topographies are preserved after poly-L-ornithine (PLO) and laminin coating. Sample preparation of coated samples involved washing with phosphate buffered saline (PBS) followed by fixing with 2% glutaraldehyde in 0.1M sodium cacodylate and 3mM calcium chloride [181]. After fixing, the samples were dehydrated with an ethanol gradient and critical point dried. The coated and uncoated samples were sputter coated with platinum using Jeol JFC 1600 auto fine coater, for 20 seconds. The working distance was maintained at 10mm with an accelerating voltage of 10 -15 kV for imaging.

Coated and fixed 2µm well samples without dehydration were examined by AFM in tapping mode using DI NanoScope IV Multimode AFM and TESP-HAR tip (Veeco, 10nm tip radius).

Table 3.1. The geometry and dimensions of topographical patterns assembled on the MARC or imprinted polymethylmethacrylate (PMMA), used in this study, are listed.

Geometry/Representation (Abbreviated terms)	**Dimensions**		
	Width / Diameter	Spacing/Pitch	Height
Unpatterned PDMS control	NA	NA	NA
Grating 2x2µG	2µm	2µm	2µm
Grating 2x1µG	2µm	1µm	120nm
Grating 1x2µG	1µm	2µm	80nm
Grating 250x250nG	250nm	250nm	250nm
Pillars 1x6.5µP	1µm	6.5µm	1µm
Wells 2x12µW	2µm	12µm	2µm
Grating 2µG pr 250nGrating	2µm grating having perpendicular 250nm grating	2µm	2µm

3.4 Sample preparation for cell culture

PDMS samples were air plasma treated (Harrick expanded plasma cleaner) for 30 seconds at 10.5 W, sterilized by UV irradiation, and incubated overnight with 33µg/ml poly-L-ornithine (PLO, Sigma) at 37ºC followed by incubation with 20µg/ml laminin from Engelbreth-Holm-Swarm murine sarcoma (Invitrogen) for 8 hours at 37º C [182].

3.5 Optimization of neural differentiation medium

HES3 cells (a kind gift from Dr. Andre Choo, Bioprocessing technology institute, Singapore) were cultured on laminin coated PDMS MARC chip in unconditioned medium that comprises of 85% Knockout Dulbecco's Modified Eagle Medium, 15% Knockout Serum Replacement, 50U/ml penicillin, 50μg/ml streptomycin, 1mM L-glutamine, 0.1mM NEAA, and 0.1mM β-mercaptoethanol (adapted from Choo *et al.* [183]) for 10 days before staining for pluripotent markers.

3.6 Direct neuronal differentiation of hESC on MARC chip or patterned PDMS

Two methods of neural differentiation were tested. In the method termed "direct differentiation", hESCs were directly seeded on PLO and laminin-coated MARC or patterned and unpatterned PDMS in N2B27 medium (DMEM/F12 (Bio-rev Pte. Ltd): Neurobasal medium (Invitrogen) in the ratio 1:1 supplemented with 1X N2 and B27 supplements (Invitrogen)) for seven days, before staining for suitable neural markers. It was estimated that about 10 - 15 clumps ($2x10^4$ – $2.5x10^4$ cells) were needed to be seeded per cm^2 of PDMS substrate. Unpatterned PDMS was used as the control.

3.7 Neuronal differentiation of hESCs by "conventional method" using retinoic acid

As a comparison, the hESCs were also differentiated using a well-established protocol adapted from Zhang *et al*. [28], which is termed as the "conventional method" in this thesis. In brief, embryoid bodies (EBs) were formed by culturing the hESC in suspension culture on low adherent plates for 3 - 5 days in EB medium (DMEM/F12 supplemented with 20% KOSR (Invitrogen), 100mM L-glutamine (Sigma) with 2-mercaptoethanol (Sigma) and 1X non-essential amino acids solution (Sigma)). EBs were

dissociated with Accutase (Stem cell Technologies) and seeded onto laminin coated tissue culture polystyrene (TCPS) plates in neural induction medium (DMEM/F12 supplemented with 1X N2 and B27 supplements) supplemented with 1μM retinoic acid (RA, Sigma) for seven days [12]. After seven days, the medium was replaced with neuronal differentiation medium (DMEM/F12 supplemented with 0.5X N2 and 1X B27 supplements), and cultured for another 7-10 days on TCPS. Medium was replenished every other day. Neural rosettes were selected and propagated as neurospheres for 3-5 days in neuronal differentiation medium. The neurospheres were dissociated into single cells using accutase and seeded (5000cells/cm^2) on the laminin coated MARC PDMS in N2B27 medium. The samples were analyzed for neuronal markers after seven days of culture on the topographies.

3.8 Immunofluorescence analysis of neuronal markers

The differentiated samples were fixed in 4% paraformaldehyde (Sigma) and permeabilized in 0.2% Triton X. The samples were then blocked in 10% goat serum and 1% bovine serum albumin (BSA) for 1 hour before overnight incubation with primary antibodies at 4ºC. The antibodies and the dilutions used in this study can be referred from Table 3.2. The samples were stained for F-actin using phalloidin (Invitrogen) tagged to Alexa Fluor 546 or 633 and counterstained with DAPI (Invitrogen) at 2μg/ml. Human ESCs were stained for focal adhesion proteins like vinculin, pFAK (phosphorylated focal adhesion kinase) and paxillin by stabilizing them with cytoskeleton buffer [184] (10mM PIPES, 50mM NaCl, 150mM sucrose and 3mM MgCl2, pH 6.5-6.8) which includes freshly added protease inhibitor cocktail (1:100, Sigma Aldrich), followed by fixation, permeabilization and antibody incubation as elaborated above.

The samples were mounted using Prolong Gold anti-fade mounting reagent (Invitrogen) and imaged using Leica epi-fluoresence microscope or Leica TCS SP5 confocal microscope.

Table 3.2 The list of antibodies used in this study is listed.

Antibody	Dilution	Source/Company
mouse anti-SSEA4	1:200	Santa Cruz
mouse anti-Tra-1-60	1:200	Santa Cruz
rabbit anti-Oct4	1:500	Abcam
rabbit anti-nanog	1:200	Santa Cruz
mouse anti-Nestin	1:200	Santa Cruz
rabbit anti-Tuj1	1:750	Sigma
mouse anti-MAP2	1:500	Abcam
mouse anti-GFAP,	1:500	Chemicon
mouse anti-O4	1:50	Chemicon
mouse anti-vinculin	1:500	Sigma-Aldrich
rabbit anti-pFAK	1:200	Abcam
mouse anti-paxillin	1:200	BD Biosciences
rabbit anti-MLC	1:200	Cell signalling
rabbit anti-pMLC	1:200	Cell signalling
rabbit anti-H3K9me3	1:200	Abcam
mouse anti- H3K9ac	1:500	Abcam

3.9 Gene expression analysis by reverse transcription polymerase chain reaction (RT–PCR) and quantitative PCR (RT-qPCR)

RNA was isolated using Trizol (Invitrogen) after 1, 4 and 7 days of culture on patterned and/or unpatterned substrates. The A260/280 ratios were verified to be >1.8 using Nanodrop 2000. Reverse transcription PCR was done using Qiagen One-Step RT PCR Kit and Biorad MyCycler. The primers for RT-PCR were designed using Primer 3 software. The primer sequences, annealing temperatures and number of cycles are given in Table 3.3. cDNA for RT-qPCR was generated using Sensiscript RT kit (Qiagen). RT-qPCR was done on ABI 7500 fast with Taqman universal master mix II (ABI/ Invitrogen) and Taqman probes for Oct4, nanog, Nestin, Sox1, Sox2, Musahi1 (Msi1), Neurofilament (NEFL), MAP2 and GAPDH (housekeeping gene) in triplicates. A no template control was also included. The relative quantitation values expressed in the graphs were normalized to the unpatterned control and housekeeping gene, GAPDH.

3.10 Analysis of proliferating cell population using 5-ethynyl-2'-deoxyuridine (EdU)

The cell proliferation assay was conducted using the commercially available Click-iT EdU Alexa Fluor 647 imaging kit (Invitrogen) according to the manufacturer's instruction. In brief, the samples were incubated with 10μM EdU reagent for 4 hours before fixing with 4% PFA and permeabilization with 0.2% triton X. The EdU is a nucleoside analog for thymidine and incorporated into the DNA during DNA synthesis. The incorporated EdU is detected using a detection cocktail that includes copper sulfate and fluorescent dye azide. It is a copper catalyzed covalent reaction between the azide in the dye and alkyne in the EdU. The samples were then imaged under Leica TCS SP5 confocal microscope.

Table 3.3. The primer sequences used in this study for reverse transcription polymerase chain reaction (RT- PCR) are listed.

Gene	Forward Primer	Reverse Primer	Annealing temperature	Cycle number	Reference paper (or) Genbank Accession number
PAX6	ACCCATTATCCAGATGTGTTTGCCCGAG	ATGGTGAAGCTGGGCATAGGCGGCAG	63º	30	NG_008679.1
Vimentin (VIM)	CTTCGCCAACTACATCGACA	ATTCCACTTTGCGTTCAAGG	56º	35	NM_003380.3
NCAM	CAGTCCGTCACCCTGGTGTGCGATGC	CAGAGTCTGGGGTCACCTCCAGATAGC	68º	38	NM_001076682.3
TUBB3	GGCCTTTGGACATCTCTTCA	ATACTCCTCACGCACCTTGC	60º	35	NM_005612.4
Synapsin1 (SYN1)	TGCCTTCAACCTTCCAGAGCCAGC	GGAAACCAGGGGCGGAGGTCTT	63º	38	NG_008437.1
Synaptophysin (SYP1)	GATGCTGCTGCTGGCGGACA	GTAGGTGGCCAGAGCCCCCA	63º	38	NG_012532.1
PSD 95 (DLG4)	GAACCCACGGAGGGGAGGAACGAA	GGGCTTCCGGCGCATGACATA	63º	35	NM_001365.3
PAX2	ATGTTCGCCTGGGAGATTCG	GCAAGTGCTTCCGCAAACTG	56º	35	NG_008680.1

PTX3	TGCAAGCCACGGACGACGTC	GCAGCTCCTCTAGCACCGCG	63º	35	NM_002852.3
LMX1b	CTGATGCGAGTCAACGAGTC	TAGTCACCCTTGCACAGCAG	60º	35	NG_017039.1
DAT	ACAGAGGGGAGGTGCGCCAGTTCACG	ACGGGGTGGACCTCGCTGCACAGATC	70º	35	[38]
ChAT	GGAGGCGTGGAGCTCAGCGACACC	CGGGGAGCTCGCTGACGGAGTCTG	70º	35	[38]
OLIG1	CTCCCTTCGCTCAGCTTC	CAACTCCAGGGACAAGGAGA	60º	35	NM_138983.2
GFAP	GGCCCGCCACTTGCAGGAGTACCAGG	CTTCTGCTCGGGCCCCTCATGAGACG	68º	38	NM_002055.4
Beta actin (ACTB)	TCGTGCGTGACATTAAGGAG	AGCACTGTGTTGGCGTACAG	54º	32	NM_001101.3
GAPDH	GAGTCAACGGATTTGGTCGT	TTGATTTTGGAGGGATCTCG	54º	32	[185]

3.11 Image analysis

Representative images were taken at four random locations on each sample. Image analysis for cell count were done using ImageJ (NIH) cell counter module. Cell length ratio was calculated as the ratio of the long axis to the short axis. Cell length ratio refers to the extent that the cell is stretched. Alignment of the cells was calculated by measuring the angle between the long axis of the cell and the grating axis. Cells that had an alignment angle <15º were considered to be aligned. For intensity measurements, the region of interest was created around the cell and the nucleus followed by using the ImageJ module for intensity measurements. Imaris was used to determine the nucleus volume. For step by step description of using Imaris and Image J for image analysis is elaborated in appendix C. The AFM images were processed using WSxM 4.0 Beta 3.1 [186].

3.12 Determination of the role of acto-myosin components using inhibitors

The hESCs were treated with myosin II inhibitor, blebbistatin (Tocris biosciences); Myosin light chain kinase inhibitor, ML-7 (Tocris Biosciences); ROCK inhibitor, Y-27632 (Tocris Bioscience); actin polymerization inhibitor, Cytochalasin D (Tocris Bioscience) to determine the effect of actin, myosin and ROCK activity on hESCs during neuronal differentiation. They were added at different concentrations (detailed concentrations used are listed in Table 3.4) for 2 or 5 consecutive days in N2B27, neuronal differentiation media, The inhibitors were added one day after attachment of hESCs to the laminin coated substrates and analysed on day 4 or day 7 for cytoskeletal components and neuronal markers by immunofluorescence staining.

Table 3.4 The concentrations of inhibitors used to study the role of acto-myosin contractility in neuronal differentiation of hESCs.

Inhibitor	Concentrations used
Blebbistatin	2µM, 10µM, 20µM (for 4 day experiment) 5µM, 10µM, 20µM (for 7 day experiment)
ML-7	2µM, 10µM, 20µM
Y-27632	2µM, 10µM, 20µM
Cytochalasin D	0.1µM, 0.5µM, 2µM

3.13 Statistical analysis

The experiments were repeated atleast three times independently, with atleast two technical replicates per run. For cell and nucleus based measurements at least 100 cells were analyzed. One way ANOVA and Bonferroni Post Hoc tests were conducted to test the level of significance ($p<0.05$, $p<0.01$, $p<0.001$).

Chapter 4

4. Fabrication and characterization of hESCs culture on Multi Architectural Chip (MARC) with an array of topographies.

4.1. Introduction

Neurodegenerative diseases like Parkinson's disease are very prominent in the current increasing aging population; the lack of sufficient cell therapies for such disorders encourages us to develop novel and efficient methods of deriving neural cells from ESCs. Many interesting studies have shown the importance of substrate features like geometry, size and curvature in the design of a tissue engineered scaffold. Previous works have shown that nano-gratings and electrospun fibers can provide contact guidance for stem cells facilitating neuronal differentiation [64, 94, 187]. Micro-wells can be used for controlling the size of the embryoid bodies derived from hESCs thereby determining their fate [54]. These together highlight the importance of substrate topography and the need to provide an artificial niche for stem cells that closely mimics the *in vivo* microenvironment of the desired cell type. Optimal topography design is yet to be identified for many other cell types, indicating the need for high throughput systems to screen for factors influencing the artificial stem cell niche.

Recently, various high throughput assays have been designed to enable the screening of several parameters in a single experiment. In one such interesting study conducted by Soen *et al*. a combinatorial array of extracellular matrix (ECM) proteins was used to study the developmental fate of neural precursor cells [188]. In spite of the advances in high throughput chip generation [52, 188, 189], automated imaging systems and quantitative analysis software, there has been no comparative study on the effects

of various geometries with dimensions smaller than 3 μm and with different feature height on hESCs in one platform. One of the limitations was challenges in the micro- or nano-fabrication of different topographical patterns such as a combination of 2-dimension, 3-dimension and curved structures with different aspect ratio and micro/nano feature resolution on the same sample using lithography based techniques. Conventionally, different techniques have to be employed for patterning specific geometries, resolution and aspect ratio patterns: optical lithography for micron scale resolution, electron-beam lithography for nano scale resolution, optical and isotropic etching for curved features, and interference lithography for 3-dimensional structures. Furthermore, combination of these different techniques to fabricate multiple topographies on a single substrate adds further challenge using conventional means. The 'Topochip' fabrication, shown by Unadkat *et al.* has topographies of >10μm and only the lateral dimensions could be varied, but not the height [189].

In this study, we have developed a Multi Architectural (MARC) Chip, an innovative high-throughput system designed to overcome the limitation of screening topographies one at a time and fabricating complex topographies on a single chip. The MARC chip can combine topographies ranging from micro- to nano-dimensions with not only varying lateral dimensions but also allows the incorporation of different heights and complexity. Based on earlier studies, a combination of anisotropic patterns namely the gratings [64, 187] and isotropic patterns like the wells [54] and pillars [190] along with hierarchical structures were chosen to be assembled on the MARC (Size and geometry of the topographies used in this study are listed in Chapter 3, Table 3.1). Gratings of varying lateral dimensions and height were designed to investigate whether height and spacing also play a role in neural differentiation. The hESCs are characterized and the neuronal differentiation of hESCs on PDMS MARC chip is studied.

4.2. Results

4.2.1. Maintenance of hESC pluripotency and karyotypic stability

The pluripotency of hESCs were verified before seeding onto the MARC (Figure 4.1 A-H). We observed that > 90% of the colonies, in both H1 and H9, expressed the pluripotent surface markers, SSEA4 and TRA-1-60, and transcription factors, Oct4 and nanog, which are important for maintaining pluripotency. Karyotyping analysis was performed at Kandang Kerbau Women's and Children's Hospital, Singapore on 16G-banded metaphases to inspect if the hESCs had become genetically abnormal during *in vitro* passaging. In order to verify the genetic stability of H1 and H9 cell lines, they were cultured on matrigel coated flasks with mTeSR1 and karyotyped at passage 24 (3 months) and 54 (6 months) for H1, and passage 11 for H9 (1.5 months). Karyotyping confirmed that no abnormal clones were present even after long term culture (6 months) in feeder free conditions (Figure 4.1 I-K).

4.2.2. Replication of MARC chip and nano-imprinted template by soft lithography

Polydimethylsiloxane (PDMS) replicas were replicated from the MARC to be used for cell study. SEM analysis showed that all the seven patterns on the MARC were replicated with fidelity onto PDMS (Figure 4.2 A). PDMS was used as the substrate because of its ease of replicating complex topographical structures and imaging. The replication of nano-gratings from nano-imprinted templates required optimization to be done for curing temperature, curing time and surface treatments which are discussed in Appendix A (Figures A.1- A.5). Extracellular matrix (ECM) coating is required for hESC attachment, and hence PLO and laminin were chosen for neural differentiation in this study. One concern of ECM coating on the micro- and nano-topographies was the

potential masking of the features by the ECM proteins. SEM analysis on coated 1 µm pillars, 2 µm gratings and 250nm gratings (Figure 4.2 B) and AFM analysis on non-dehydrated coated 2 µm wells (Figure 4.2 C, D and E), verified that the topographies were not masked by the ECM coating. The height of the 2 µm wells was measured to be 450nm by AFM; however, discrepancy in this height reduction was believed to be an artifact created by the AFM tip inability to reach a 2 µm height in this scenario [191]. This conclusion is further supported by Wang *et al*. who showed that the laminin deposited on PDMS is only 50nm thick [192] lending support to the observation that the topographies were not masked by the ECM. In order to verify that the same amount of laminin was absorbed onto different patterns, fluorescent laminin was used to coat the surface of an unpatterned and 250nm gratings substrates. When coated without PLO, non-uniform coating was observed (Figure 4.2 F).

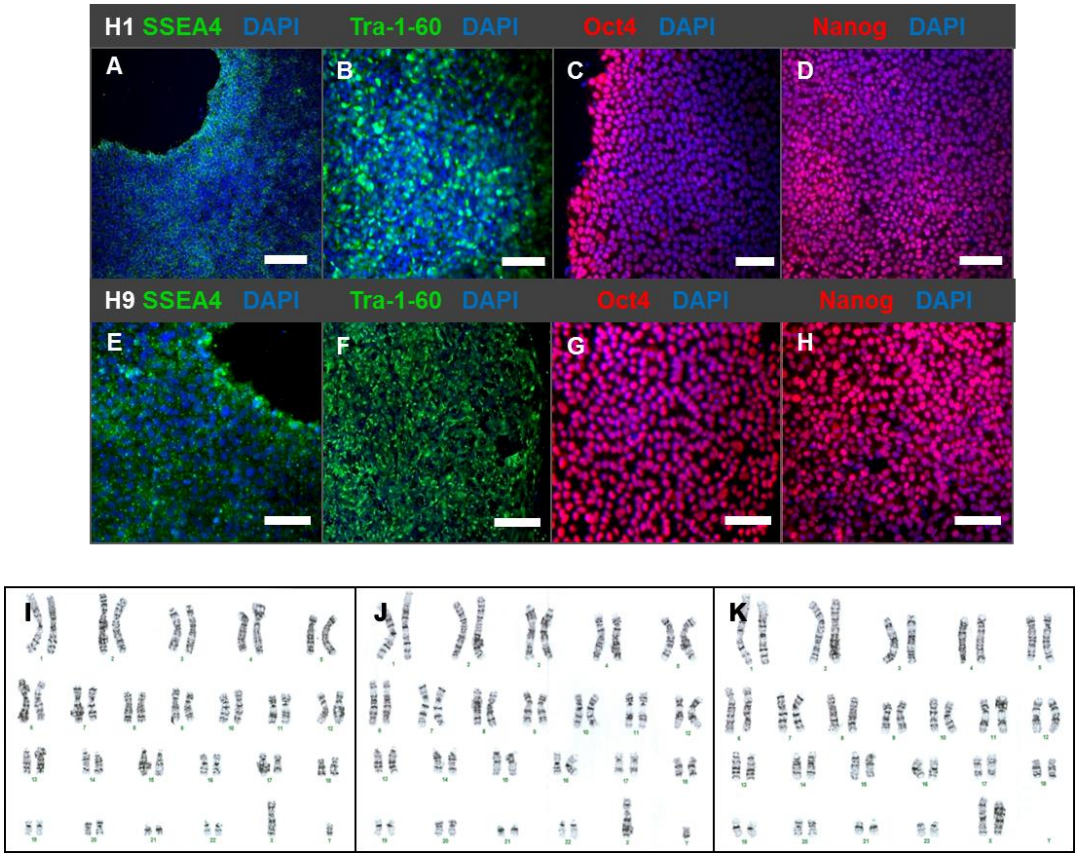

Figure 4.1 Human embryonic stem cells (hESCs) expressed pluripotent markers before differentiation was induced, as shown by immunofluorescence. Immunofluorescent images of cells expressing pluripotent surface markers, **A)** SSEA4 and **B)** Tra-1-60; transcription factors, **C)** Oct4 and **D)** nanog, in the H1 cell line. Immunofluorescent images of cells expressing **E)** SSEA4, **F)** Tra-1-60, **G)** Oct4 and H) nanog in the H9 cell line. SSEA4 (A, E) and Tra-1-60 (B, F) are stained green while Oct4 (C, G) and nanog (D, H) are stained red. The nucleus is counterstained with DAPI (blue). Scale bars: 200µm (A-H). Karyotyping analysis was performed on 16 G banded metaphases of H1 (I, J) and H9 (K) cells grown on Matrigel **I)** Karyotyping results for H1, passage 24. **J)** Karyotyping results for H1, passage 54. **K**) Karyotyping results for H9, passage 11 [193].

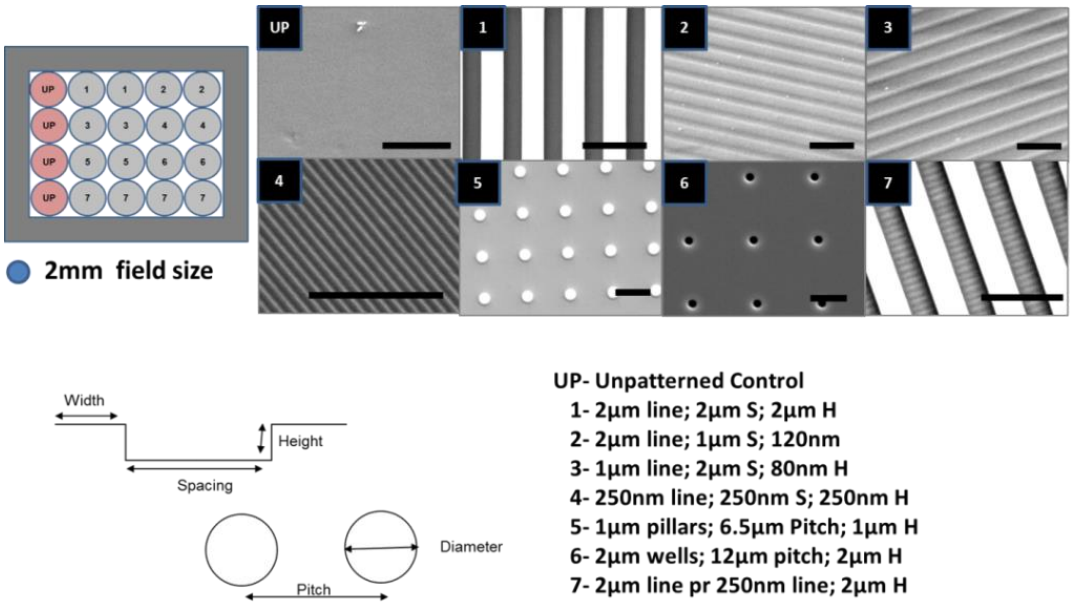

Figure 4.2 A) shows the schematic of MARC and the scanning electron microscopy images of the individual fields of topographies. The scale bar represents 5µm [193].

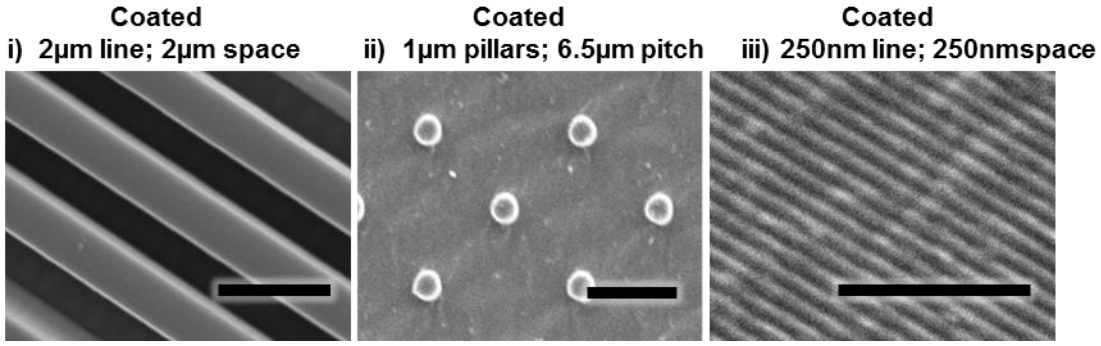

Figure 4.2 B) shows the scanning electron microscopy images of coated topographies i) Laminin-coated 2µm grating with 2µm spacing and 2µm height. ii) Laminin-coated 1µm pillars with 6.5µm pitch and 1µm height. iii) Laminin-coated 250nm gratings with 250nm space and height. The Scale bars represent 5µm [193].

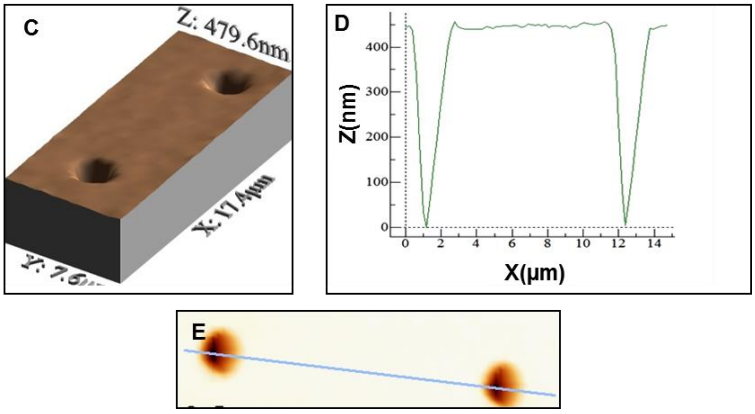

Figure 4.2 Atomic force microscopy analysis of coated 2µm wells. **C)** The three-dimensional view of the coated 2µmwells. **D)** Height analysis shows the height of the coated samples to be 450nm and the diameter of the well is 2µm. **E)** Cross section of the wells for height analysis [193].

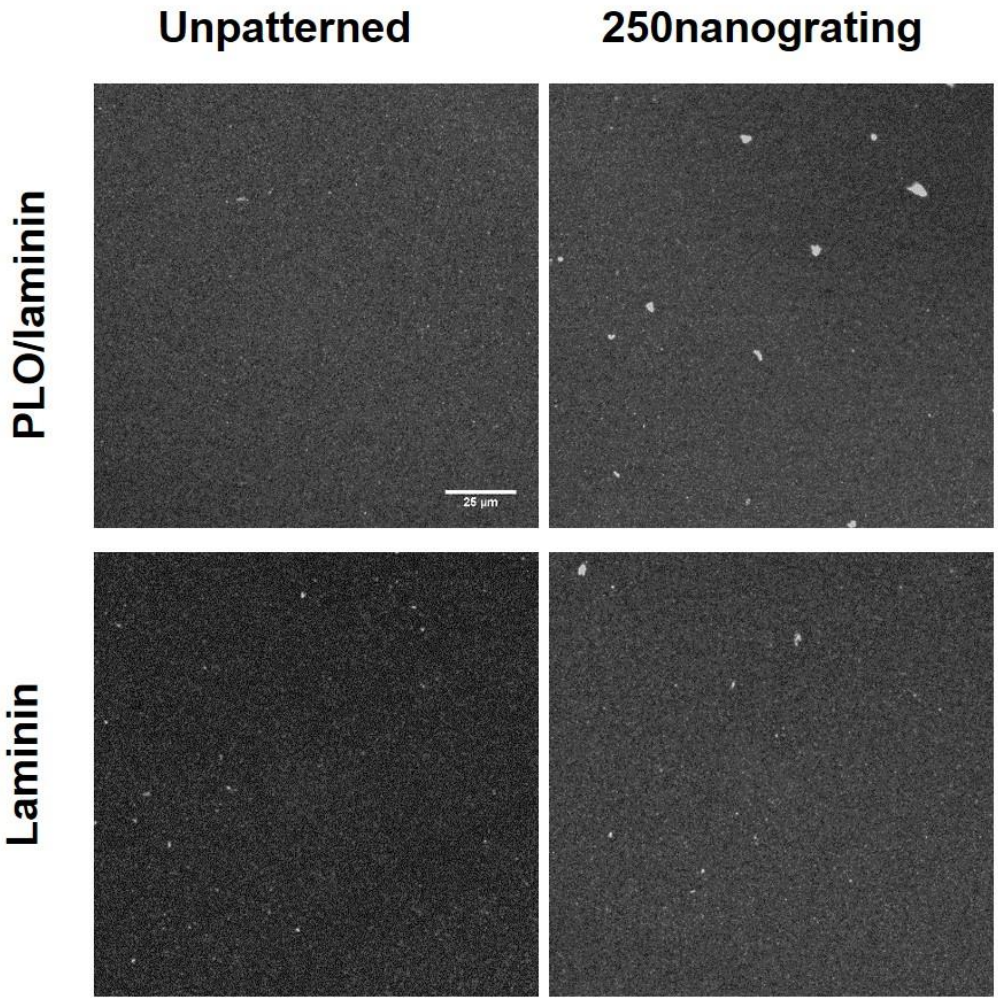

Figure 4.2 F) Fluorescently-labelled HiLyte laminin 488 was coated onto patterned (250nm gratings) and unpatterned substrates to verify that uniform amount was absorbed onto both surfaces. When coated without poly-L-ornithine (PLO), there were differences in laminin absorption. Hence the preferred method of coating was PLO followed by laminin. The scale represents 25µm.

4.2.3. Neuronal differentiation of hESCs by embryoid body formation and using MARC

A schematic of the conventional method of neuronal differentiation adopted in this study is shown in Figure 4.3.A. The hESCs were subjected to neuronal differentiation by established methods of embryoid body formation (Figure 4.3 B), followed by induction to neural rosette stage (Figure 4.3 C) and neurosphere derivation. The EBs was approximately 150µm in size (Figure 4.3 B). The EBs were dissociated into clusters and seeded onto laminin coated well plates with various concentrations of Retinoic acid (RA, 0.5, 1 and 2µM). 1µM RA was sufficient to induce neural rosette formation (Figure 4.3 C). The neural rosettes were then picked to expand the neural precursor cells by neurosphere culture in a low attachment plate for 4-7 days. These hESCs derived neural precursor cells were then seeded as single ells onto the MARC PDMS coated with PLO and laminin. The MARC PDMS samples were fixed and immunostained after 7 days culture in neuronal differentiation media (N2B27). The samples were stained for immature neuronal marker, Tuj1 and mature neuronal marker, MAP2 (Figure 4.3 D). Human ESCs when subjected to differentiation through EB formation, all the topographies supported neuronal differentiation but the total numbers of cells available for study were very low after the long differentiation protocol.

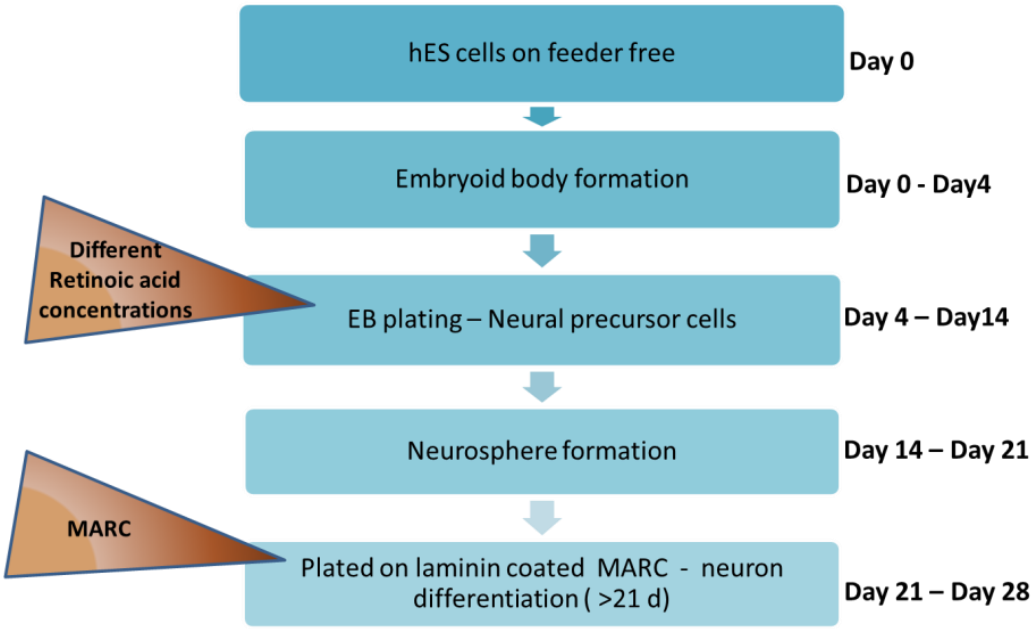

Figure 4.3 A) shows the schematic of conventional neuronal differentiation protocol used in this study. The hESCs are subjected to EB formation followed by induction to neural rosettes and neurospheres to derive neural precursor cells which are plated onto MARC to study the effect of topographies on later stages of neuronal differentiation.

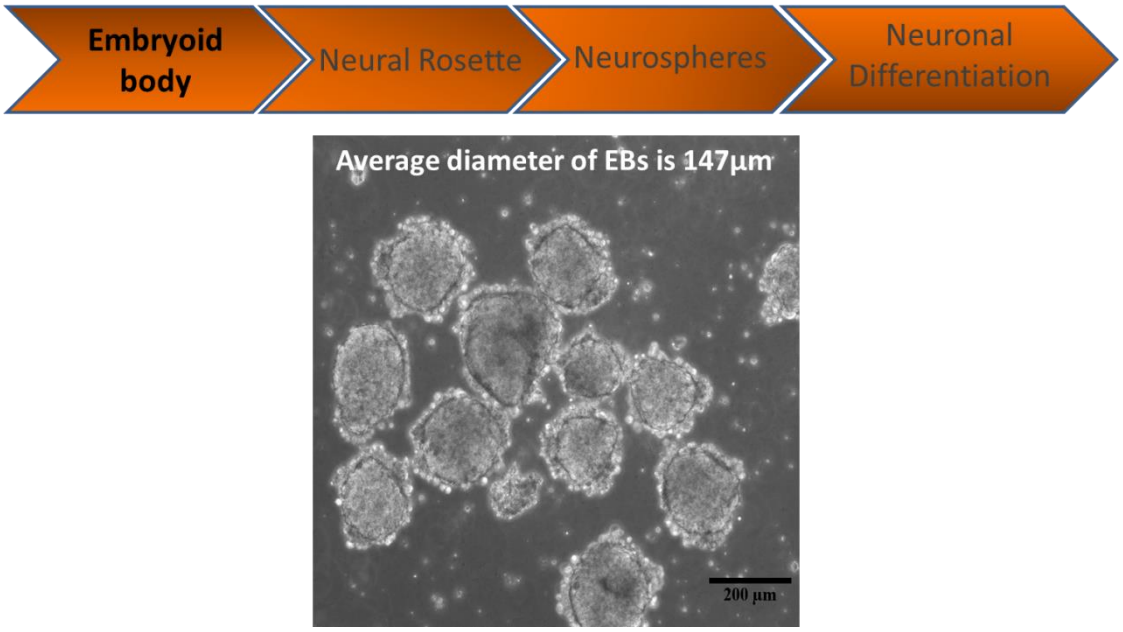

Figure 4.3 B) shows the Phase contrast image of fairly uniform embryoid bodies derived from H1, in suspension, with an average size of 150µm. The scale bar represents 200µm [193].

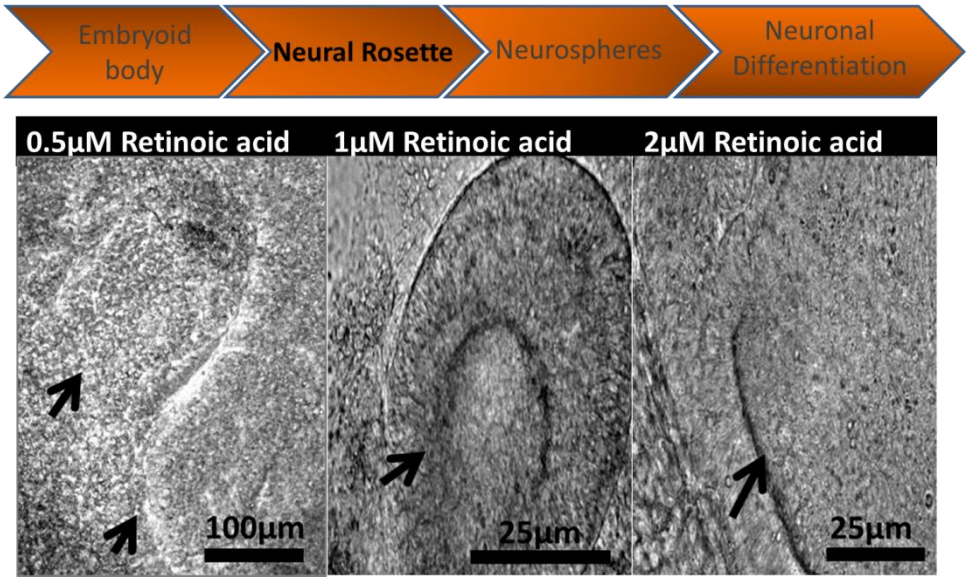

Figure 4.3 C) shows the phase contrast images of neural rosettes formed by retinoic acid induction (0.5, 1 and 2µM) after 12 days of culture in neural induction media [193].

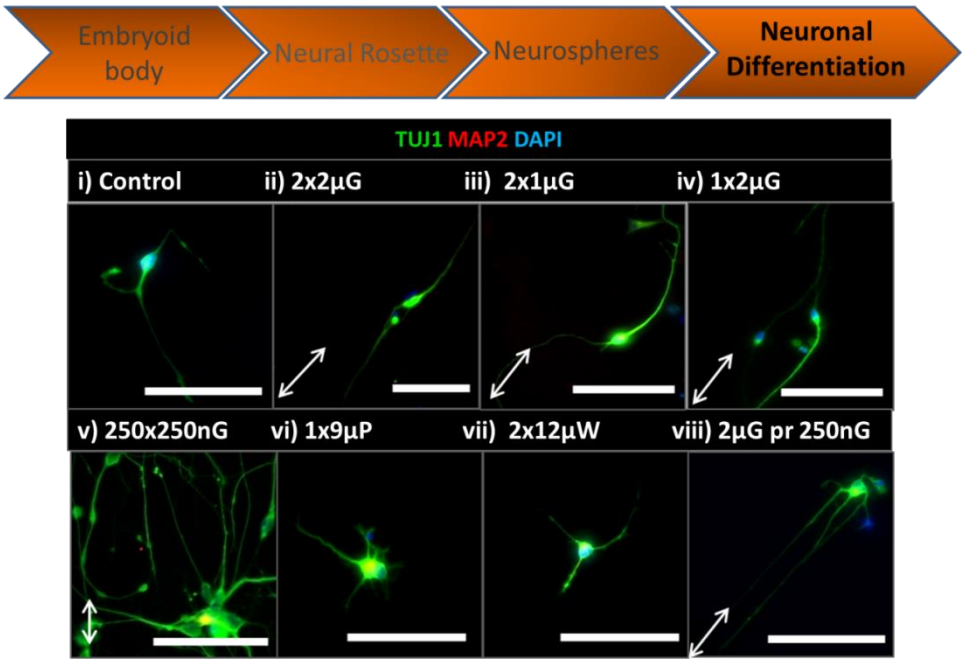

Figure 4.3 The neural rosettes were then selected and grown in suspension to expand the neural precursor cells (NPCs). The NPC's were seeded as single cells on the MARC chip and analysed after seven days. **D**) Shows the immunofluorescent images of hESC derived NPCs grown on MARC chip. They are stained with Tuj1 in green, Microtubule associated protein 2 (MAP2) in red and DAPI in blue. i) Control (unpatterned PDMS). ii) 2µm grating with 2µm spacing and 2µm height (2x2µG). iii) 2µm grating with 1µm spacing and 120nm height (2x1µG). iv) 1µm grating with 2µm spacing and 80nm height (1x2µG). v) 250nm grating with 250nm spacing and 250nm height (250x250nG). vi) 1µm pillar with 6.5µm pitch and 1µm height (1x6.5µP). vii) 2µm wells with 12µm pitch and 2µm height (2x12µW). viii) Hierarchical structures with 2µm gratings perpendicular to 250nm gratings (2µG pr 250nG). The scale bar represents 100µm. The white arrow marks show the direction of grating axis [193].

4.3. Discussion

The effect of topography-induced differentiation has previously been demonstrated on stem cells [64, 66, 194]; however, a systematic study on the effect of geometry and isotropy on neural differentiation of hESCs remains unknown. We hypothesized that by changing the geometry, isotropy and size of topography, hESC neural differentiation could be directed differently under the same conditions. In this study, a multi-architecture array was fabricated as a high-throughput screening method to identify the effect of different topographies on the neural differentiation of hESCs. The use of the MARC platform has made it possible to fabricate multiple topographies easily on a single substrate primarily through nanoimprint lithography (NIL). The use of the MARC chip for stem cell behaviour analysis also allows high-throughput investigation under similar culture conditions hence reducing the variability between samples, rendering a better comparison amongst the patterns and proving economical in the long-run. Exploiting the capacity of MARC to study different topographical influences on stem cells simultaneously, we utilized this screening system to study the influence of topography on hESC during spontaneous or conventional methods of neural differentiation in this chapter.

Karyotyping analysis is essential to avoid artificial results arising from abnormal or mutated clones. Human ESCs were tested for karyotypic changes because earlier studies have shown that continual enzymatic passaging could subject the ESCs to changes in their karyotype with no morphological changes. The hESCs are subjected to selective pressure during *in vitro* culture, which leads to death during passaging and accumulation of genetic abnormalities [195]. In order to avoid skewing of results due to use of karyotypically unstable hESC lines, the cell lines were tested at both early and late stage of passaging. The karyotype analysis was performed on cells cultured

continuously in vitro on Matrigel and mTESR1. Two different time points were chosen in this study to show that no karyotypic instabilities were present even after long periods of culture in vitro. The hESCs are passaged once every 6 days. The H1 hESC used for this study was between passage 10 and 15, and the H9 hESC was used between passages 5 – 10. The difference in passage numbers used was because of technical difficulties in expanding H1 as compared to H9. The choice of time point was based on the stage of cell cultures used for the experiments presented in this study, which is approximately 1.5 months for H9, 3 months for H1, which was around or beyond the oldest passage used in the experiments for the two hESC lines. For one of the cell line, H1, we further verified that even after long-term, 3 months, of continuous passaging in vitro, the H1 cells remained stable and did not show any karyotypic instability.

The ease of MARC fabrication allows us to combine micro and nano-sized patterns that mimic the ECM. Complex shapes like microlens, hexagonal holes and elliptical pillars could also be fabricated albeit of different heights. The MARC also included hierarchical structures which were a combination of micro and nanosized geometries superimposed, for example a micron line with nano scale lines imprinted perpendicular to it. These hierarchical structures were not replicated on the PDMS replica because the nanolines were on the grooves of the substrate rather than being on the ridges. However, a double replica of PDMS from PDMS master could resolve the problem of fabricating hierarchical structures. These hierarchical structures could serve as a platform for co-culturing glial cells with neuronal cells based on the geometry and shape of the topography suitable for the different cell types used in the study.

Before seeding the neurospheres on MARC, the PDMS substrates were coated with PLO and laminin. The pre-coating of PLO ensures uniform coating of laminin and reduces aggregate formation of laminin thereby resulting in uniform cell attachment

[182]. In order to verify that the ECM molecules do not change the topographical dimensions, SEM was conducted for 2µm gratings, 250nm gratings and 1µm pillars while a semi-dry AFM was conducted for 2µm wells. These patterns were chosen to represent the micro and nano-sized anisotropic patterns and the isotropic patterns. Since its more likely that the well like topographies could be covered up with ECM, AFM analysis was conducted to verify the height. However, the depth analysis indicated the depth of the coated samples to be 450nm instead of 2µm. We speculate that this could be due to an artifact created by the AFM tip's inability to reach the entire depth of the well [191].

The PDMS MARC chip is used to study neuronal differentiation of hESCs using established methods of embryoid body formation. Initial studies indicated that conventional method of differentiation were time consuming, pre-differentiated to a neuronal fate, hence yielded lower glial cells and required a very high starting population to end with sufficient cells for further downstream analysis like sorting, imaging or transplantation. The neuronal differentiation by conventional method predisposed the stem cells to a neuronal fate and hence when the neurospheres were seeded on the MARC, all patterns supported neuronal differentiation and it was difficult to distinguish the effects of individual topographies on the neural stem cells derived from hESCs. It was noted that all the topographies aided in neuronal differentiation of hESCs. It is speculated that the topographies were presented at a late stage of differentiation and hence it was difficult to choose a particular topography that specifically aided neuronal or glial differentiation. The cell number observed after the long period of differentiation was considerably low and hence did not allow the statistical analysis of determining the percentage of immature or mature neuronal population.

4.4. Conclusion

The MARC can be easily fabricated onto PDMS substrates using soft lithography without the loss of resolution of the topographical features. The main advantages of using MARC would be the ease of fabrication (NIL techniques), ability to include complex structures of varying heights onto the same platform, study of factors affecting stem cell behaviour in a high-throughput manner. The use of MARC for neuronal differentiation of hESCs by "conventional method" was discussed in this chapter. However, due to drawbacks like insufficient number of surviving cells at the end of the differentiation period, long time taken (> 21 days) and use of hESC derived NPCs that are predisposed to neurons, the role of topography is not yet clear. Hence the following chapter aims to investigate a suitable media formulation and devise a differentiation protocol to understand the effect of topographical features and efficiently differentiate the ESCs.

Chapter 5

5. Designing a fast and efficient method of deriving neural cells by determining the optimal geometry and size of topographical cues.

5.1 Introduction

Over the last decade, hESCs and iPSCs have been explored for their potential to be differentiated into cells of the three different embryonic germ layers and for their ability to self-renew [18, 196]. Neural cells, especially dopaminergic neurons for the treatment of Parkinson's disease and oligodendrocytes for stroke regeneration, are of particular importance in recent times due to the rapidly aging population [197]. There are two common approaches for neural differentiation of hESCs *in vitro*: i) embryoid body formation followed by neural precursor cell induction with stage specific cues such as fibroblast growth factor 2 (), retinoic acid (RA), FGF8 and/or sonic hedgehog (SHH), followed by neurosphere formation and adherent culture on laminin for neuronal derivation and maturation [198]; ii) adherent culture of hESCs with inhibitors of mesodermal and endodermal differentiation and/or by co-culturing hESCs with astrocytes [34, 199, 200]. The common disadvantages with these techniques are the extended periods of culture (> 20 days), labor intensity, the need for a larger starting population to get sufficient yield and/or the use of expensive growth factors at high concentrations and volumes. To address these problems, we hypothesize that an optimal combination of topographical and biochemical cues can enhance the neuronal differentiation efficiency. Stem cells have been demonstrated to be able to respond to biophysical and biochemical cues in their natural niche [201]. The influence of topography on cell behaviour and stem cell differentiation has been extensively

reviewed [201, 202]. The advent of tissue engineering approaches has enabled the design of substrates that mimics these cues *in vitro*.

To identify the optimal topographical structure, surface topographies of various geometries in nano-meter and micron sizes were used to examine the neural differentiation of hESCs on one chip under the same culture conditions. The effect of topography-induced differentiation has previously been demonstrated on stem cells [15, 54, 64, 66, 203-205]; however, a systematic study on the effect of geometry, size and on neural differentiation of hESCs remains unknown.

This chapter focuses on determining the optimal geometry and size for neural differentiation of human embryonic stem cell lines, H1 and H9 and to establish an easy and fast method for neuronal differentiation of hESCs using MARC. The MARC consists of both anisotropic patterns like gratings and isotropic patterns like pillars or wells assembled in a customized fashion. Gratings of varying lateral dimensions and height were designed to investigate whether height and spacing also play a role in neural differentiation. The use of MARC for stem cell behavior analysis will allow high-throughput investigation under similar culture conditions hence reducing the variability between samples, rendering a better comparison amongst the patterns and proving economical in the long-run. The efficiency of neuronal differentiation by the "direct differentiation method" is compared with "conventional method" of differentiation (chapter 4) in this chapter.

5.2 Results

5.2.1 Determination of suitable neuronal differentiation media

To explore the potency of topographical cues in inducing neural differentiation of hESCs, different sets of ECM coating and medium combinations were tested. First, the hESCs were cultured on a matrigel coated MARC for seven days in mTeSR1 to determine if any of the topographies induced differentiation in an environment strongly conducive to pluripotent maintenance. Despite the topographical cues, the hESCs maintained high levels of nanog, and they expressed low levels of the neural stem cell marker, Nestin (Figure 5.1 A). Low levels of early neuronal marker, Tuj1 was observed on 2µm gratings and 1µm pillars (Figure 5.2 B). This result was not surprising since mTeSR1 was designed to be extremely potent in maintaining the hESC pluripotent state [206]. In the next step, biochemical cues supporting pluripotent maintenance were greatly reduced by culturing cells on a laminin coated MARC in an unconditioned hESC medium without supplements for seven days. In these conditions, the percentage of cells expressing the pluripotent marker, Oct4, was slightly lower on 2µm gratings (1µm or 2µm space), suggesting that these patterns may have a higher potential to induce differentiation as compared to the others (Figure 5.1 C, D). Taken together, these results suggest that different topographical patterns play a role in both maintenance and differentiation of hESCs, but additional biochemical cues are necessary to fully achieve the desired effect.

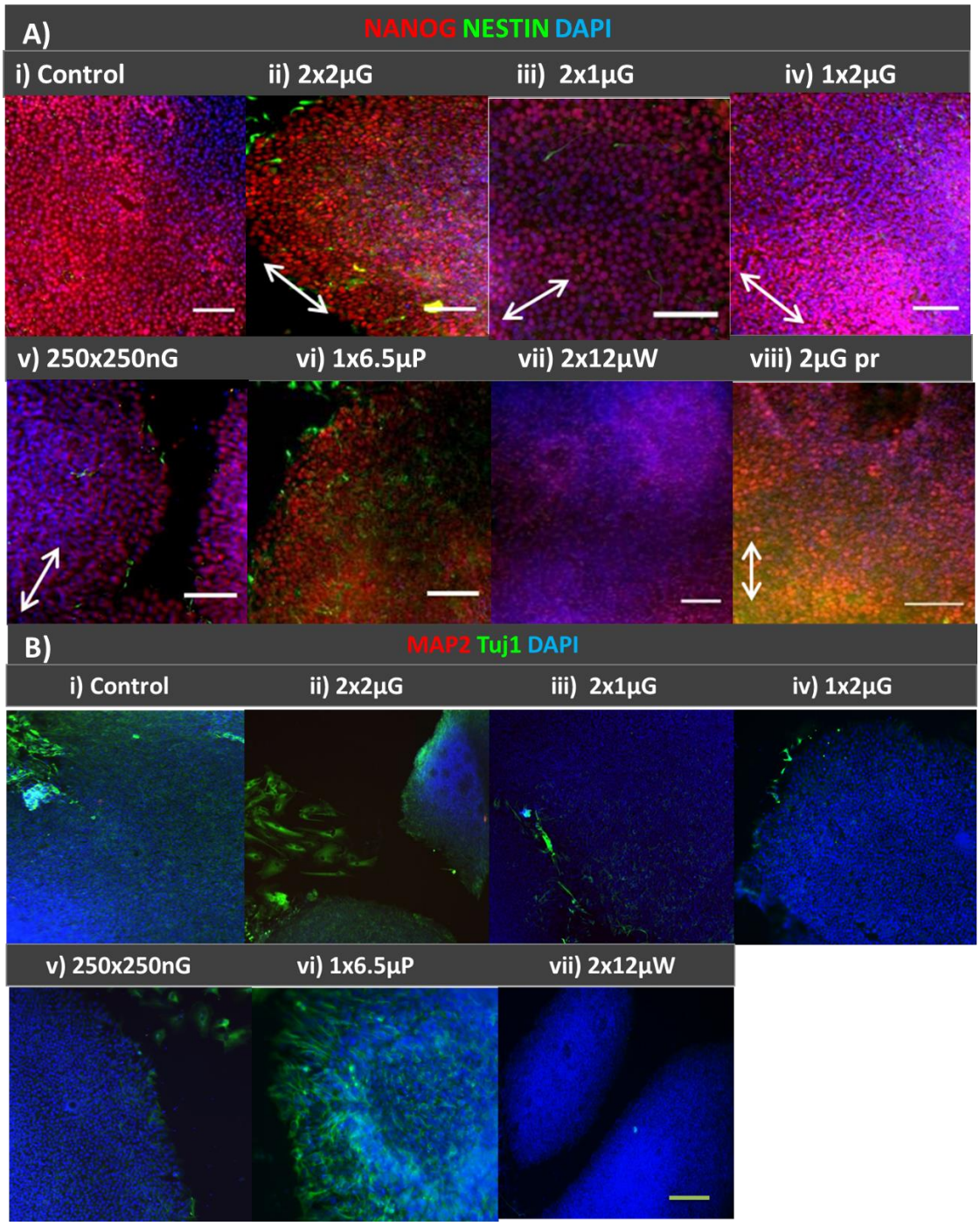

Figure 5.1 H9 cells seeded on MARC chip and grown under maintenance conditions with mTeSR1 and matrigel did not express neural stem cell marker, Nestin or neuronal markers, Tuj1 and MAP2. **Ai-viii)** Cells were stained for pluripotent marker, nanog (red), neural stem cell marker, Nestin (green) and nuclear stain, DAPI (blue). **Bi-viii)** Cells were stained for neuronal markers, MAP2 (red), Tuj1 (green) and nuclear stain, DAPI (blue). The scale bars represent 100µm. i) Control (unpatterned PDMS). ii) 2µm grating with 2µm spacing and 2µm height (2x2µG). iii) 2µm grating with 1µm spacing and 120nm height (2x1µG). iv) 1µm grating with 2µm spacing and 80nm height (1x2µG). v) 250nm grating with 250nm spacing and 250nm height (250x250nG). vi) 1µm pillar with 6.5µm pitch and 1µm height (1x6.5µP). vii) 2µm wells with 12µm pitch and 2µm height (2x12µW). viii) Hierarchical structures with 2µm gratings perpendicular to 250nm gratings (2µG pr 250nG) [193, 207].

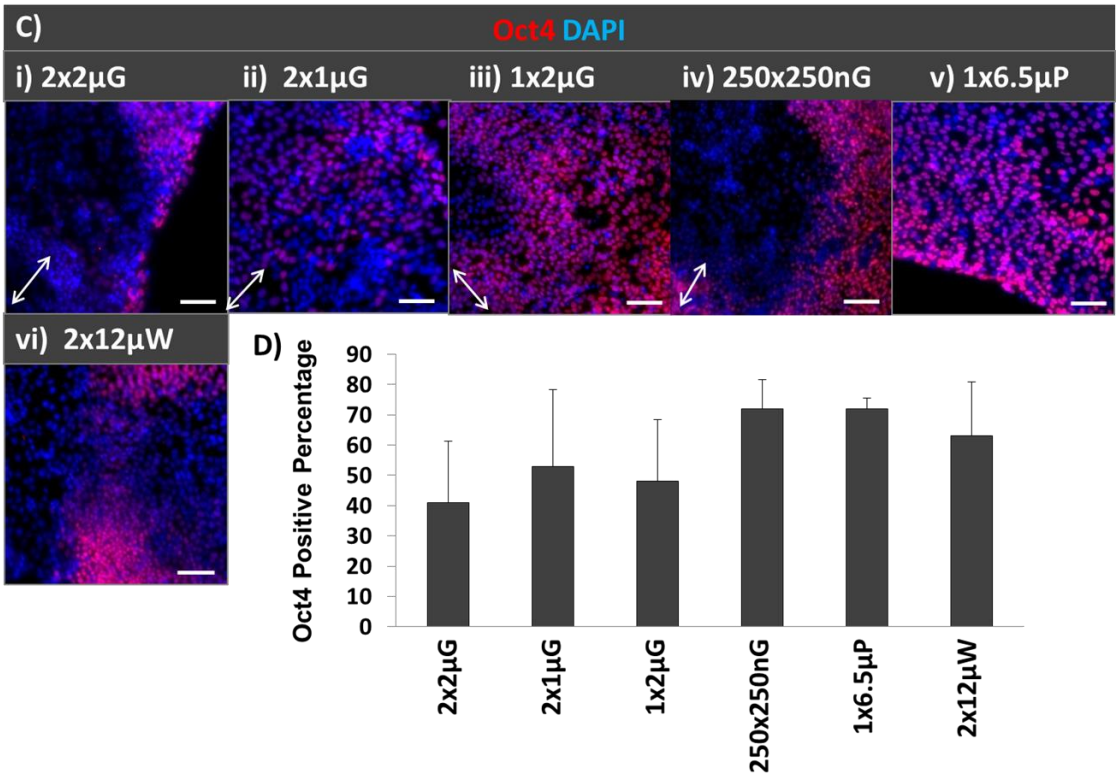

Figure 5.1 C) HES3 cells grown on the MARC chip in unconditioned media without growth factors were checked after ten days for a decrease in pluripotent marker Oct4, by immunostaining. The cells were stained for Oct4 (red) and DAPI (blue). The scale bars represent 100µm. i) Control (unpatterned PDMS). ii) 2µm grating with 2µm spacing and 2µm height (2x2µG). iii) 2µm grating with 1µm spacing and 120nm height (2x1µG). iv) 1µm grating with 2µm spacing and 80nm height (1x2µG). v) 250nm grating with 250nm spacing and 250nm height (250x250nG). vi) 1µm pillar with 6.5µm pitch and 1µm height (1x6.5µP). vii) 2µm wells with 12µm pitch and 2µm height (2x12µW). viii) Hierarchical structures with 2µm gratings perpendicular to 250nm gratings (2µG pr 250nG). **D)** The percentage of Oct4 positive cells present on different patterns after 10 days of culture in unconditioned media is shown. The white arrow marks show the direction of grating axis [193].

5.2.2 Neural marker expression of the hESCs on MARC

In the method termed 'direct differentiation', the hESCs were seeded directly onto PLO and laminin coated MARC; analysed after seven days of differentiation by immunofluorescence staining. The hESCs were stained (Figure 5.2 A) and quantified (Figure 5.2 B) for immature neuronal marker, β tubulin III (Tuj1), and astrocyte marker, Glial fibrillary acidic protein (GFAP). Human ESCs on the anisotropic micro- and nano-gratings showed a higher percentage of Tuj1-positive cells (2µm - 16% for H1 and 10% for H9; 250nm - 20% for H1 and H9) as compared to the GFAP-positive population

(2µm - 11% for H1 and 9% for H9, 250nm - 9% for H1 and 7% for H9). Contrastingly, a larger GFAP-positive population (31% in H1 and 23% in H9) was observed for cells grown on the isotropic pillar patterns as compared to the Tuj1-positive population (6% in H1 and 8% in H9). The ratio of Tuj1-positive to GFAP-positive cells, defined as N:A (neuron: astrocyte) ratio, was also higher for both H1 and H9 cells grown on nano-gratings (2.4 for H1 and H9) as compared to the hESC grown on 1µm pillars (0.19 for H1 and 0.02 for H9). The H9 grown on unpatterned control were observed to have a heterogeneous population comprising both Tuj1-positive (23% in H1 and 24% in H9) and GFAP-positive (44% in H1 and 27% in H9) populations at high levels comparable to those obtained with gratings or pillars respectively. The H1-derived cells were also stained for oligodendrocyte marker, O4, seven days after differentiation on the MARC. O4 expression was observed in the hESCs cultured on the 2µm wells and unpatterned PDMS (Figure 5.2 C).

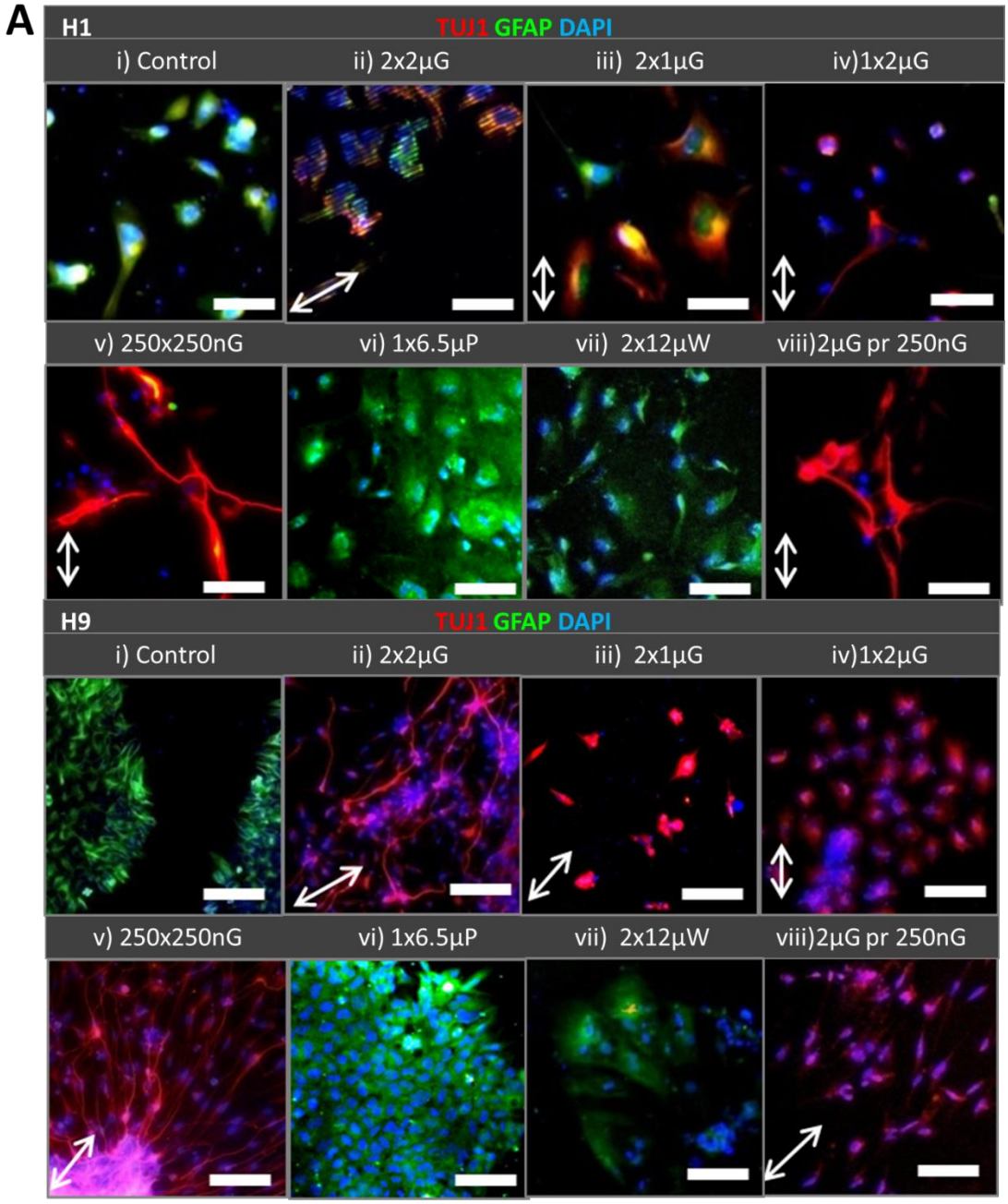

Figure 5.2 A) Cells were characterized as neuronal or glial by immunostaining after 7 days of direct neural differentiation on the MARC. Immunofluorescence images of H1- and H9-derived cells stained with immature neuronal marker, β tubulin III (Tuj1) in red; glial marker, glial fibrillary acidic protein (GFAP) in green, and nuclear marker, DAPI in blue. The white arrow indicates the direction of grating axis. i) Unpatterned PDMS control. ii) 2µm grating with 2µm spacing and 2µm height (2x2µG). iii) 2µm grating with 1µm spacing and 120nm height (2x1µG). iv) 1µm grating with 2µm spacing and 80nm height (1x2µG). v) 250nm grating with 250nm spacing and 250nm height (250x250nG). vi) 1µm pillar with 6.5µm pitch and 1µm height (1x6.5µP). vii) 2 m wells with 12µm pitch and 2µm height (2x12µW). viii) Hierarchical structures with 2µm gratings perpendicular to 250nm gratings (2µG pr 250nG). The white arrow marks show the direction of grating axis. The scale bars represent 100µm [193].

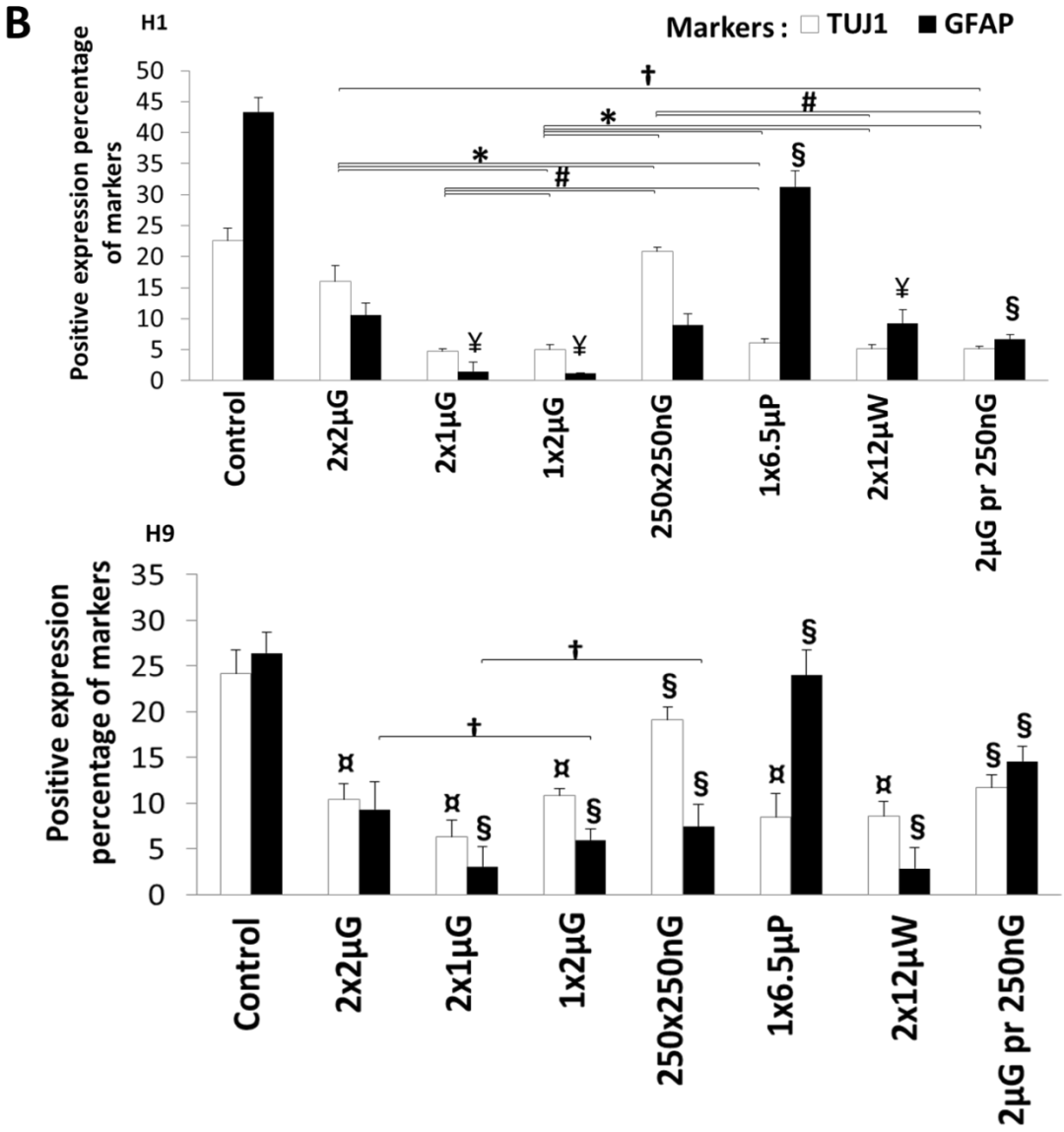

Figure 5.2 B) The percentages of Tuj1-positive and GFAP-positive cells on the various patterns after 7 days of direct differentiation on the MARC were quantified from the immunostaining images. The graph shows the percentage of H1 and H9-derived neuronal cells (Tuj1 positive) and glial cells (GFAP positive) on each pattern after 7 days of differentiation. Error bar shows standard error of the mean. † denotes values are significant with $p<0.05$, # denotes values are significant with $p<0.01$, * denotes values are significant with $p<0.001$, § denotes values that are significant in comparison with control, $p<0.05$, ¥ denotes values that are significant in comparison with control, $p<0.001$, ¤ denotes values are significant in comparison with control, $p<0.001$ [193].

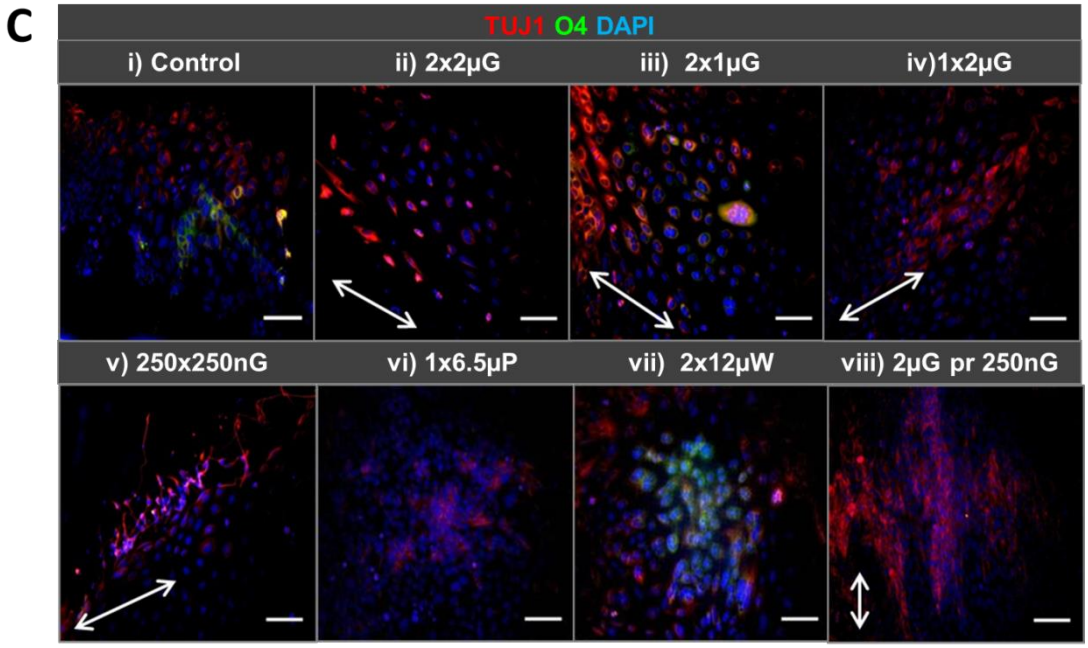

Figure 5.2 Human ESCs grown on wells by direct differentiation method express oligodendrocyte marker O4. **C)** Immunofluorescence images of H1 cells grown on Multi Architecture Chip (MARC) for seven days in N2B27 media are shown**.** Differentiated H1 cells were stained with neuronal and oligodendrocyte markers, Tuj1 (red) and O4 (green), respectively. The nucleus was counterstained with DAPI (blue). i) Control (unpatterned PDMS). ii) 2μm grating with 2μm spacing and 2μm height (2x2μG). iii) 2μm grating with 1μm spacing and 120nm height (2x1μG). iv) 1μm grating with 2μm spacing and 80nm height (1x2μG). v) 250nm grating with 250nm spacing and 250nm height (250x250nG). vi) 1μm pillar with 6.5μm pitch and 1μm height (1x6.5μP). vii) 2μm wells with 12μm pitch and 2μm height (2x12μW). viii) Hierarchical structures with 2μm gratings perpendicular to 250nm gratings (2μG pr 250nG). The white arrow marks show the direction of grating axis. The scale bars represent 100μm [193].

5.2.3 Mature Neuronal marker expression on anisotropic patterns

The immunostaining results also showed a significantly higher Microtubule-associated protein 2 (MAP2) positive population (12% for H1 and 8% for H9) for both H1 and H9 grown on the nano-gratings as compared to the micro-gratings, isotropic patterns (pillars and wells) and unpatterned control substrate (Figure 5.3 A, B, $p<0.05$). Although a variation between H1 and H9 in the percentage of positively-stained cells was observed, the trend was similar.

The efficiency of the direct differentiation method was compared against the conventional methods of neuronal differentiation via embryoid body (EB) formation using a well-established protocol [28]. The neural precursor cells derived by the conventional methods were grown on MARC for seven days and analyzed for Tuj1 and MAP2 positive populations (Chapter 4). Despite using the same or greater seeding density and longer culture duration, sufficient number of cells could not be generated for further statistical analysis by this method. The conventional differentiation method produced neurons with shorter neurite extensions (average 415µm for H1, n=20, standard error - 24.61µm), as compared to the direct differentiation (average 612µm for H1, n=35, standard error - 19.72µm). In addition, the conventional method only induced neuronal marker expression after multiple phases of differentiation and 20-30 days of differentiation, as compared to our one-step, seven day differentiation method.

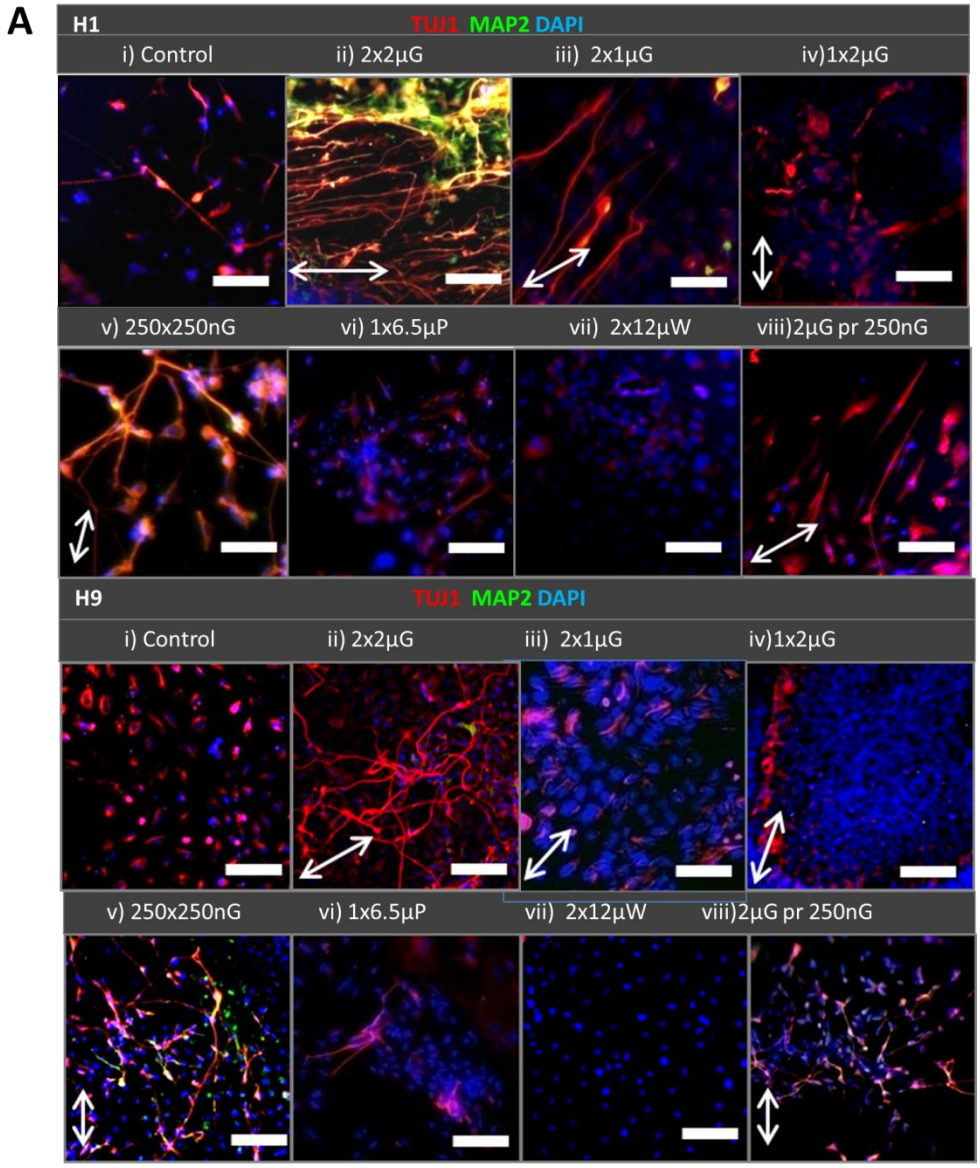

Figure 5.3 A) Gratings induce differentiated cells to express more of the mature neuronal marker, Microtubule associated protein 2 (MAP2). Immunofluorescence images of H1 and H9 cells grown on MARC for seven days and stained for immature neuronal marker, Tuj1 (red), mature neuronal marker, MAP2 (green), and nuclear marker, DAPI in blue. i) Unpatterned PDMS control. ii) 2µm grating with 2µm spacing and 2µm height (2x2µG). iii) 2µm grating with 1µm spacing and 120nm height (2x1µG). iv) 1µm grating with 2µm spacing and 80nm height (1x2µG). v) 250nm grating with 250nm spacing and 250nm height (250x250nG). vi) 1µm pillar with 6.5µm pitch and 1µm height (1x6.5µP). vii) 2µm wells with 12µm pitch and 2µm height (2x12µW). viii) Hierarchical structures with 2µm gratings perpendicular to 250nm gratings (2µG pr 250nG). The white arrow marks show the direction of grating axis. The scale bars represent 100µm [193].

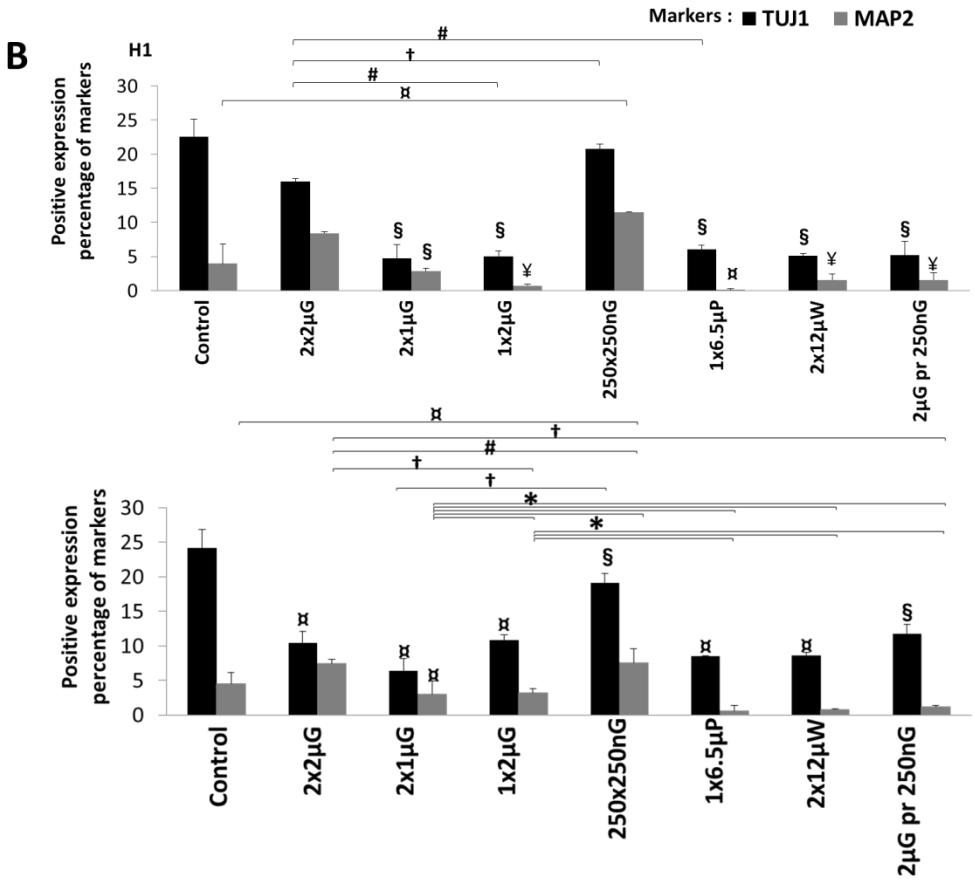

Figure 5.3 The percentages of Tuj1-positive and MAP2-positive cells on the various patterns after 7 days of direct differentiation on the MARC were quantified from the immunostaining images. **B)** The graph shows the percentage of H1and H9-derived neuronal cells (Tuj1 positive) and mature neuronal cells (MAP2 positive) on each pattern after 7 days of differentiation. Error bar shows standard error of the mean. † denotes values are significant with $p<0.05$, # denotes values are significant with $p<0.01$, * denotes values are significant with $p<0.001$, § denotes values that are significant in comparison with control, $p<0.05$, ¥ denotes values that are significant in comparison with control, $p<0.001$, ¤ denotes values are significant in comparison with control, $p<0.001$ [193].

5.2.4 Elongation and alignment of hESC-derived neurons

The alignment of neurites along the grating axis (Figure 5.4 A) was observed to be significantly higher on the 250nm gratings (64%) as compared to the 2µm gratings (60%) for H1-derived Tuj1-positive cells. No significant difference was observed between the 250nm gratings (50%) or 2µm gratings (50%) for the alignment of H9-derived Tuj1-positive cells.

The Tuj1-positive neurons derived from hESCs either by the conventional or direct differentiation method was compared for neuronal cell length ratio. The cell length ratio is measured as the ratio of length of long axis to length of short axis, along the 2µm and 250nm gratings (Figure 5.4 B and C for H1 and H9 derived cells, respectively). The Tuj1-positive cells obtained by direct differentiation of hESCs on nano-gratings were significantly more elongated. (Cell length ratio equal to 51 and 45 for H1 and H9 derived cells, respectively) as compared to the neurons derived from unpatterned control substrate (Cell length ratio equal to 25 and 21 for H1 and H9 derived cells, respectively). The neurons derived by conventional differentiation had shorter neurites, observed from their shorter cell length ratio (cell length ratio = 28 for H1 and cell length ratio = 32 for H9), as compared to the neurons derived by direct differentiation method on the nano-gratings.

Our system has also shown that mature neurons expressing MAP2 with longer neurite lengths, and higher degrees of elongation and alignment could be derived by the direct differentiation method. Alignment and elongation of the neurites are important design factors to be considered when designing scaffolds for neuronal regeneration, enabling the axons to send guided signals over a longer distance.

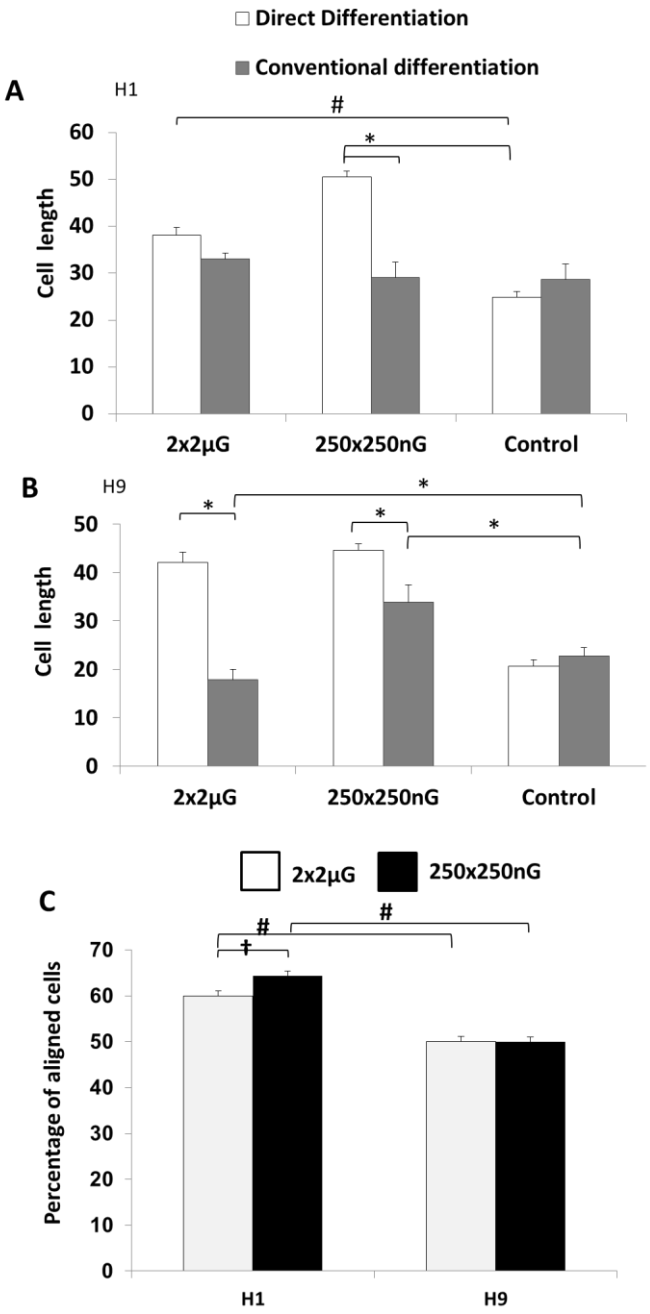

Figure 5.4 Neurons derived from hESCs were elongated and aligned along the grating axis. Graphs show the cell length (ratio of long axis : short axis) of neurons derived from **A)** H1 and **B)** H9 cell line by direct differentiation or conventional methods, along the 2µm (2µm spacing) and 250nm (250nm height) gratings with unpatterned PDMS as control. **C)** The graph shows the percentage of neurites aligned along the grating axis of 2 µm (2µm spacing) and 250nm (250nm height) gratings. The error bar is represented as the standard error of the mean. * denotes values are significant with $p<0.001$. # denotes values are significant with $p<0.01$. † denotes values are significant with $p<0.05$, § denotes values that are significant in comparison with control, $p<0.05$, ¥ denotes values that are significant in comparison with control, $p<0.001$, ¤ denotes values are significant in comparison with control, $p<0.001$[193].

5.2.5 Gene expression analysis of hESC-derived cells grown on the patterned substrates

RT–PCR and RT-qPCR were conducted to compare the gene expression of hESCs grown on the different patterns for seven days. RT-qPCR (Figure 5.5 Ai, Aii; Figure 5.6 Aii, Aiii, Bi, Bii) and RT-PCR was performed for pluripotent genes, early neural stem cell (NSC) markers and immature neurons, mature neuronal markers, subtype specific neuronal genes, synapse marker, and glial markers (Figures 5.5 – 5.9). Quantitative RT-qPCR analysis showed that the expression of pluripotent stem cell genes, Oct4 and nanog (Figure 5.5 Ai, Aii), were high in the undifferentiated cells at Day 0 and decreased for H1 grown on all the patterns by Day 7. The H9 cells grown on different patterns showed greater nanog expression and lower Oct4 expression as compared to the undifferentiated Day 0 population.

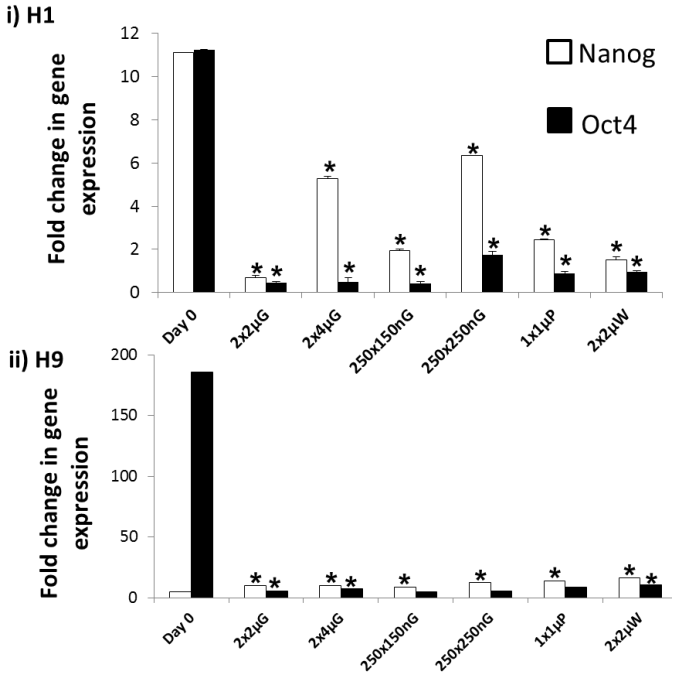

Figure 5.5 A) The graph shows the quantitative expression of pluripotent genes for i) H1 and ii) H9 cell lines seeded on individual topographies for seven days in the presence of neuronal differentiation media. * denotes values are significant with $p<0.001$ in comparison with control. Abbreviation: Day 0 (undifferentiated hESC control) [193].

The neural stem cell marker, Pax6 (Figure 5.5 Bi), was found to be elevated in H9 cells grown on the 2µm gratings and 250nm gratings. Only 30-50% of the total population of hESCs growing on the patterned substrate was neural cells. The significantly high expression of Nestin (observed from the RT-qPCR data, Figure 5.5 Bii, Biii) indicates that a fraction of the hESCs growing on the patterned substrates was in the neural stem cell stage. H1 and H9 grown on patterned substrates showed a different trend in expression levels of transcription factors, Sox1 and Sox2 (Figure 5.5 Bii, Biii), which are involved in neural determination and differentiation. H1 cells cultured on all anisotropic patterns expressed higher Sox1/2, while higher expression was observed for H9 cells cultured on pillars and wells.

Early neuronal genes, such as neural cell adhesion molecule (NCAM) and Tuj1 (Figure 5.6 Ai), were expressed uniformly for H1 and H9 across all the gratings. Correspondingly, NCAM expression was observed to be lower for H9 grown on wells and pillars. Nestin and MAP2 expression (Figure 5.6 Aii, Aiii and Figure 5.6 Bi, Bii respectively) were significantly higher in the hESCs grown on the gratings as compared to the control. H1 cells grown on patterned substrates showed a decrease in Musahi1 (Msi1, Figure 5.6 Aii, Aiii) and Neurofilament (NEFL, Figure 5.6 Bi, Bii), at Day 7 as compared to the undifferentiated cells (Day 0 control). However, significantly higher Msi1 expression was observed for H9 cells grown on the 2µm gratings and 2µm wells as compared to the Day 0 control.

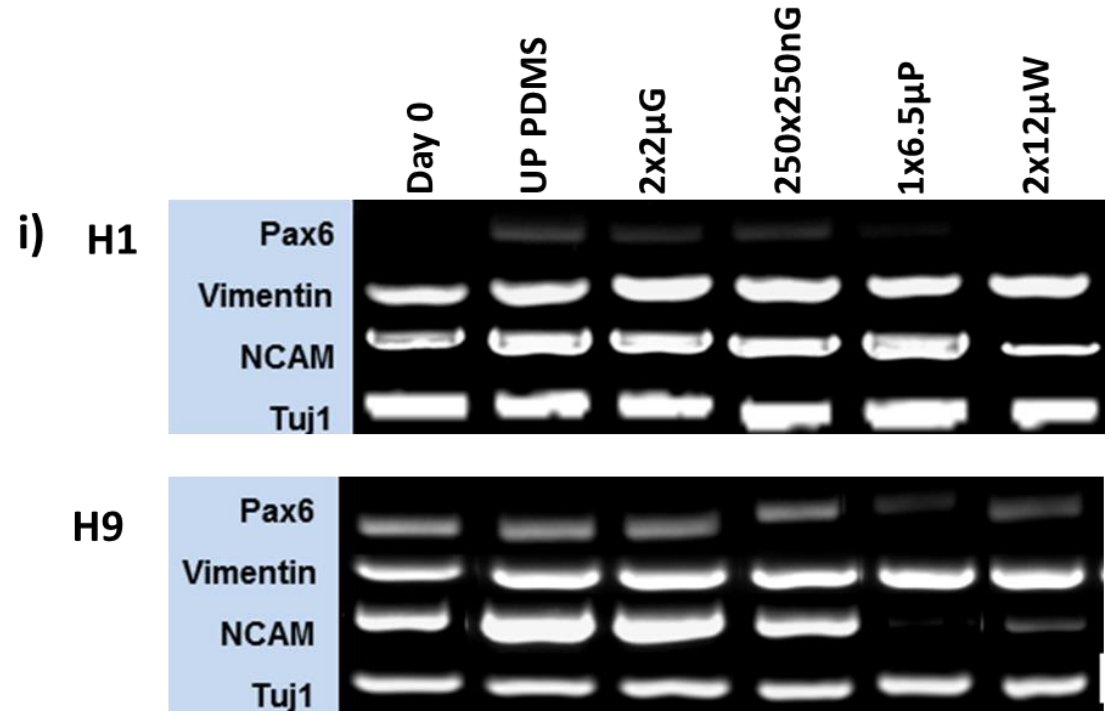

Figure 5.6 Ai) The image shows the early and immature neuronal gene expression pattern for H1 and H9 cell lines seeded on individual topographies for seven days in the presence of neuronal differentiation media. Abbreviations: Day 0 (undifferentiated hESC control), Unpatterned (UP) PDMS (control) [193]..

Varying expression level of mid-brain dopaminergic neuronal genes, Pax2, Ptx3 and lmx1b (Figure 5.7 i), were observed in hESCs grown on all patterns. H1-derived cells grown on 2µm wells showed lower expression levels of mid-brain markers as compared to the cells grown on other patterns. The dopamine transporter gene, DAT (Figure 5.7 ii), was up regulated in H1 grown on the 2µm gratings and H9 grown on 250nm gratings. The expression of dopaminergic neuronal genes in hESCs grown on the gratings was higher as compared to the wells; this confirms the effect of geometry on hESC fate during neural differentiation. The HI grown on the gratings expressed low levels of cholinergic acetyl transferase gene (ChAT gene codes for the ChAT enzyme important for the synthesis of acetylcholine, a neurotransmitter, Figure 5.7 iii). It is therefore possible to derive subtype specific neurons by varying the geometry and size of the topographies.

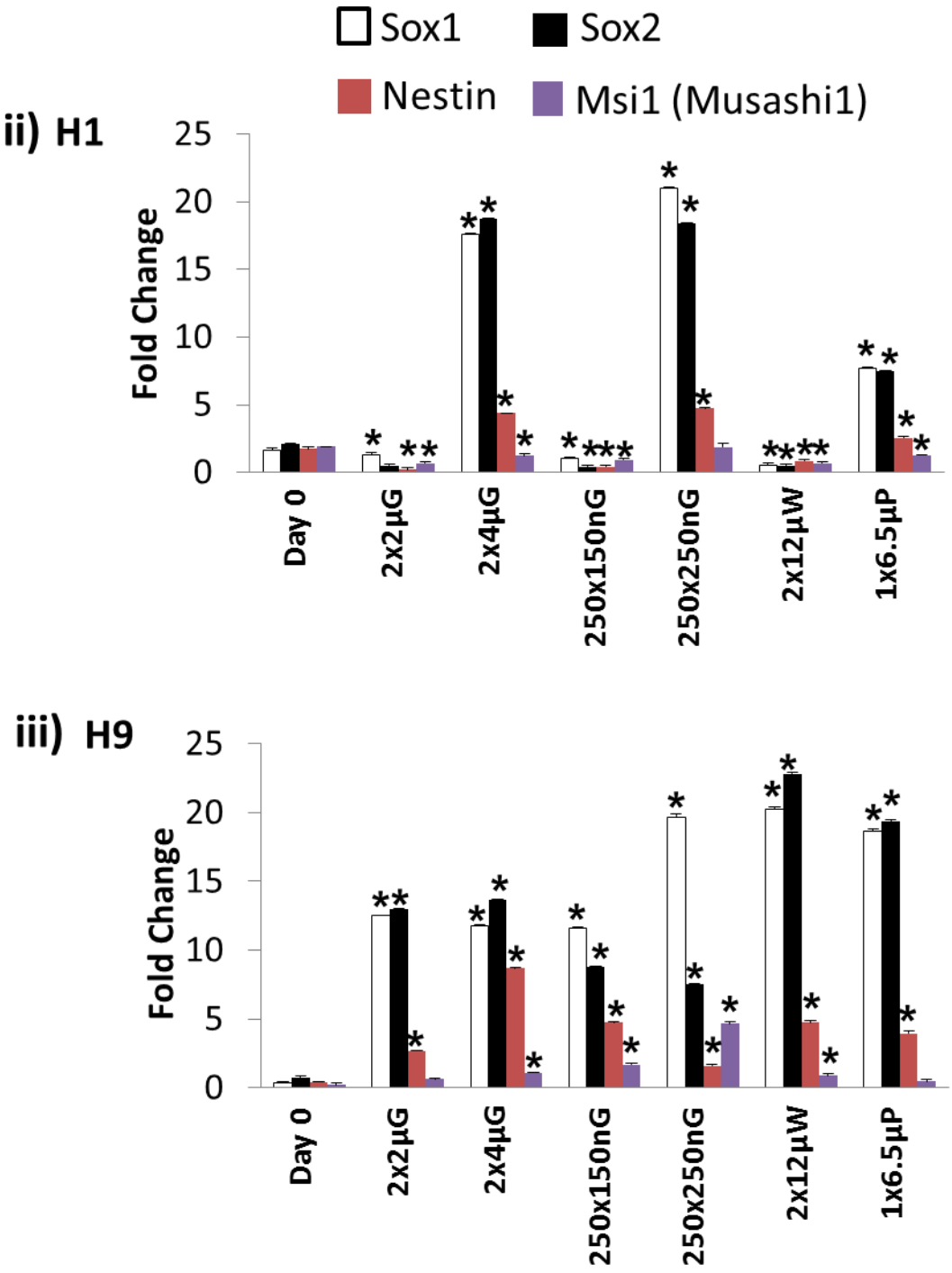

Figure 5.6 A) The graph shows the quantitative expression of pluripotent genes for **ii)** H1 and **iii)** H9 cell lines seeded on individual topographies for seven days in the presence of neuronal differentiation media. * denotes values are significant with $p<0.001$ in comparison with control. Abbreviation: Day 0 (undifferentiated hESC control) [193].

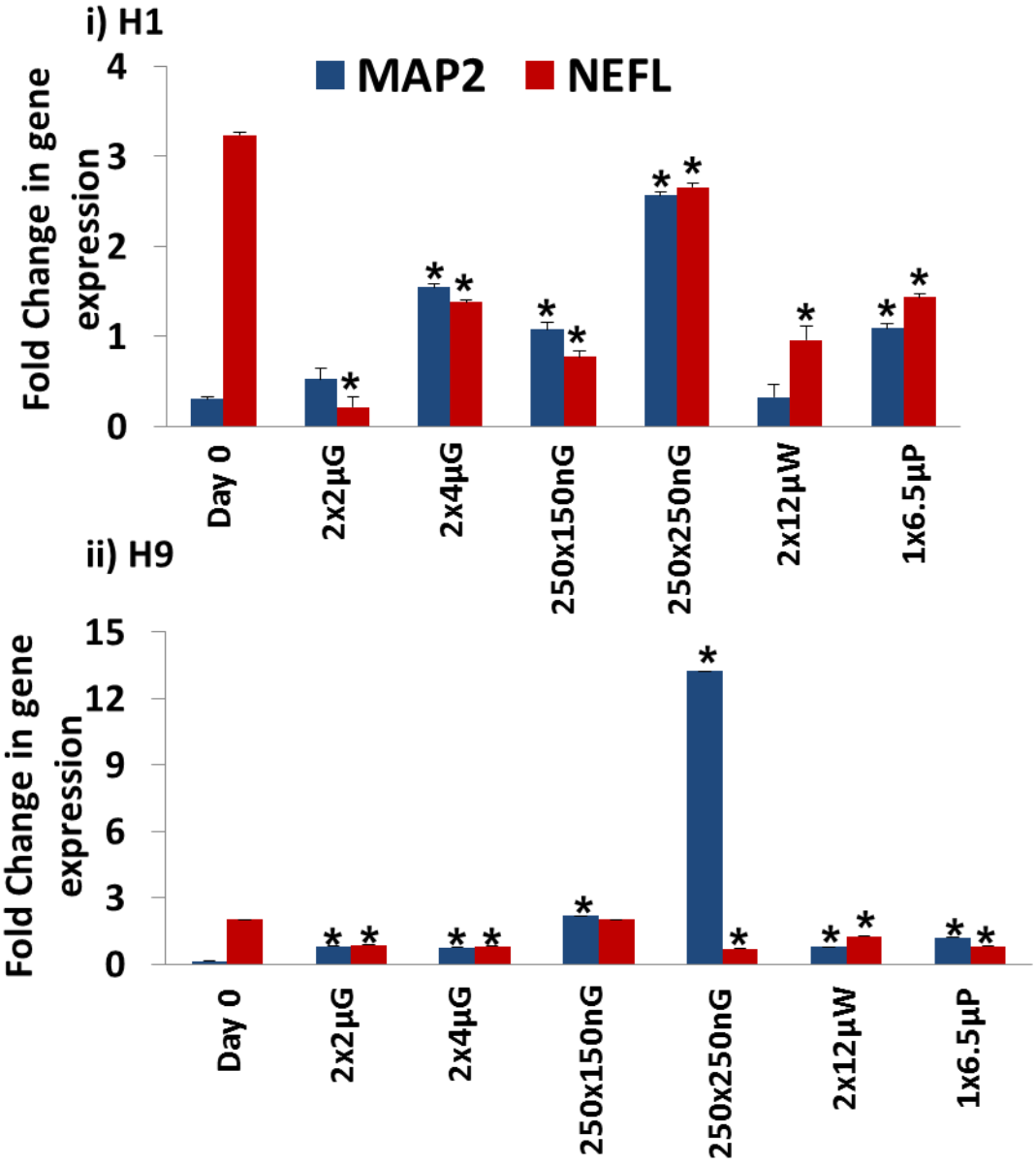

Figure 5.6 B) The graph shows the fold change of mature neuronal genes expression (RT-qPCR) for **i)** H1 and **ii)** H9 cell lines seeded on individual topographies for seven days in the presence of neuronal differentiation media. * denotes values are significant with $p<0.001$ in comparison with control. Abbreviation: Day 0 (undifferentiated hESC control) [193].

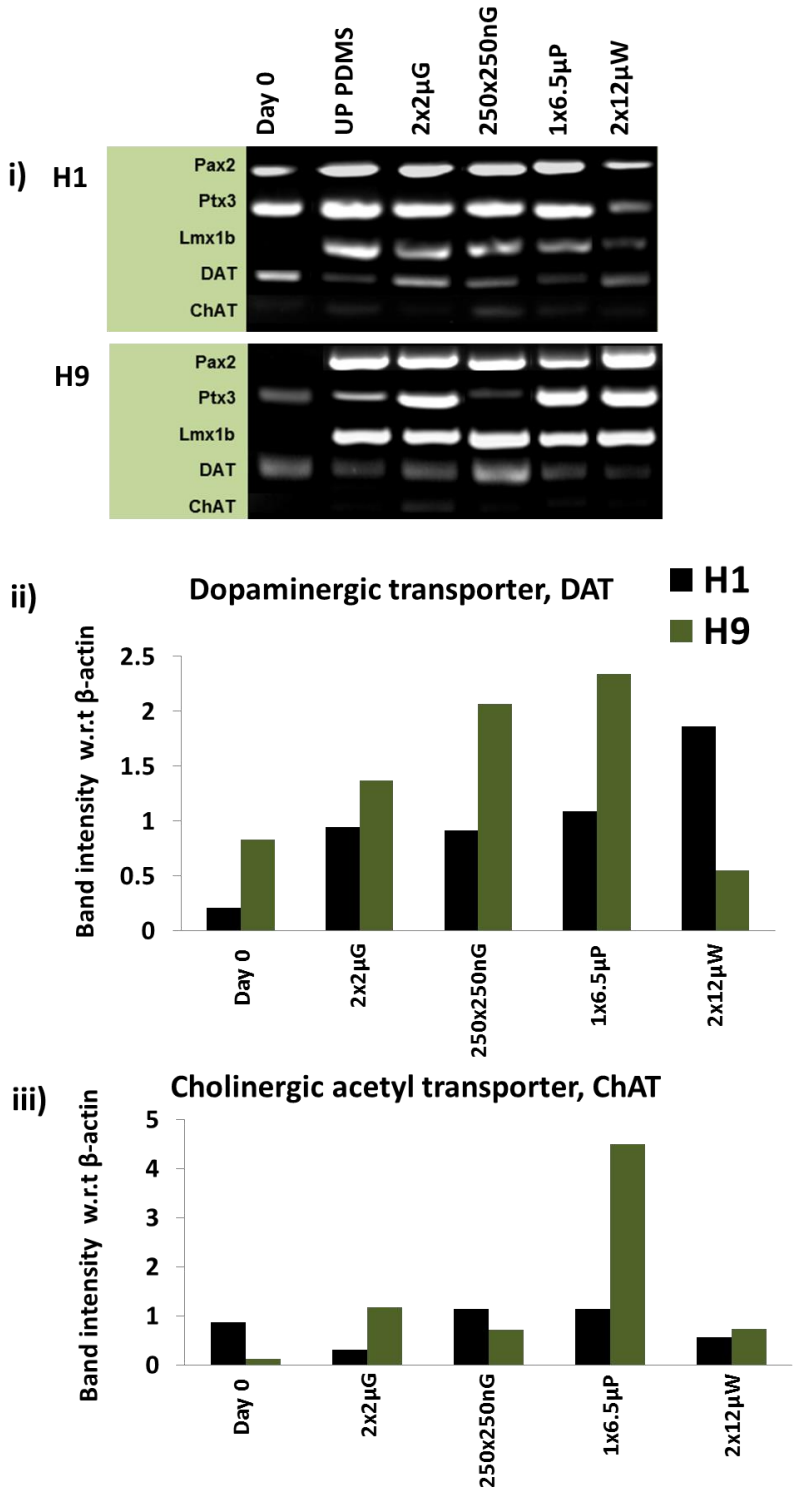

Figure 5.7 i) The image shows the region specific neuronal marker gene expression pattern for H1 and H9 cell lines seeded on individual topographies for seven days in the presence of neuronal differentiation media. The graph shows the densitometry analysis in arbitrary units (A.U) with respect to β-actin for **ii)** DAT and **iii)** ChAT bands obtained by reverse transcription PCR for H1 and H9 cell lines. Abbreviations: Day 0 (undifferentiated hESC), Unpatterned (UP) PDMS (control) [193].

Post synaptic density gene, PSD95, and the synaptogenesis gene, synapsin, were also expressed in hESCs on all the patterns (Figure 5.8). The gene expression of synaptophysin and PSD95 in cells grown on patterned substrates suggests that the synapse marker protein expression might be observed if the cells were maintained for longer duration on the topographies. In general, the patterned substrates had higher synaptophysin as compared to unpatterned control.

The oligodendrocyte marker, Olig1 (Figure 5.9), was expressed at lower levels for hESCs grown on TCPS. Higher levels of Olig1 was expressed on 2µm wells as compared to 1µm pillars while the astrocytic gene, GFAP (Figure 5.9), was higher in the hESCs grown on the 2µm wells as compared to 1µm pillars. These results suggest that though isotropic patterns like pillars and wells promote glial differentiation, the oligodendrocyte and glial differentiation can be further manipulated by varying the geometry and size of the isotropic topography.

This RT-PCR and RT-qPCR results confirmed that the pluripotent gene expression decreased and the neuronal gene expression increased by Day 7 for hESCs grown on the patterned substrates. Further investigating the influence of height by RT-qPCR suggested that the hESCs were sensitive to both the spacing as well as the height. Both micro- and nano-gratings with a greater height: width (D: W) aspect ratio showed significantly higher expression of neuronal genes like Nestin, Sox1, Sox2 and MAP2 for H1; Nestin, Sox1 and Msi1 for H9 (data not shown). The quantitative RT- qPCR data showed that hESC differentiation on the nano-scale grating is significantly different from the micron scale. The nano-scaled grating showed a greater enhancement of neuronal differentiation compared to the other topographies in H1.

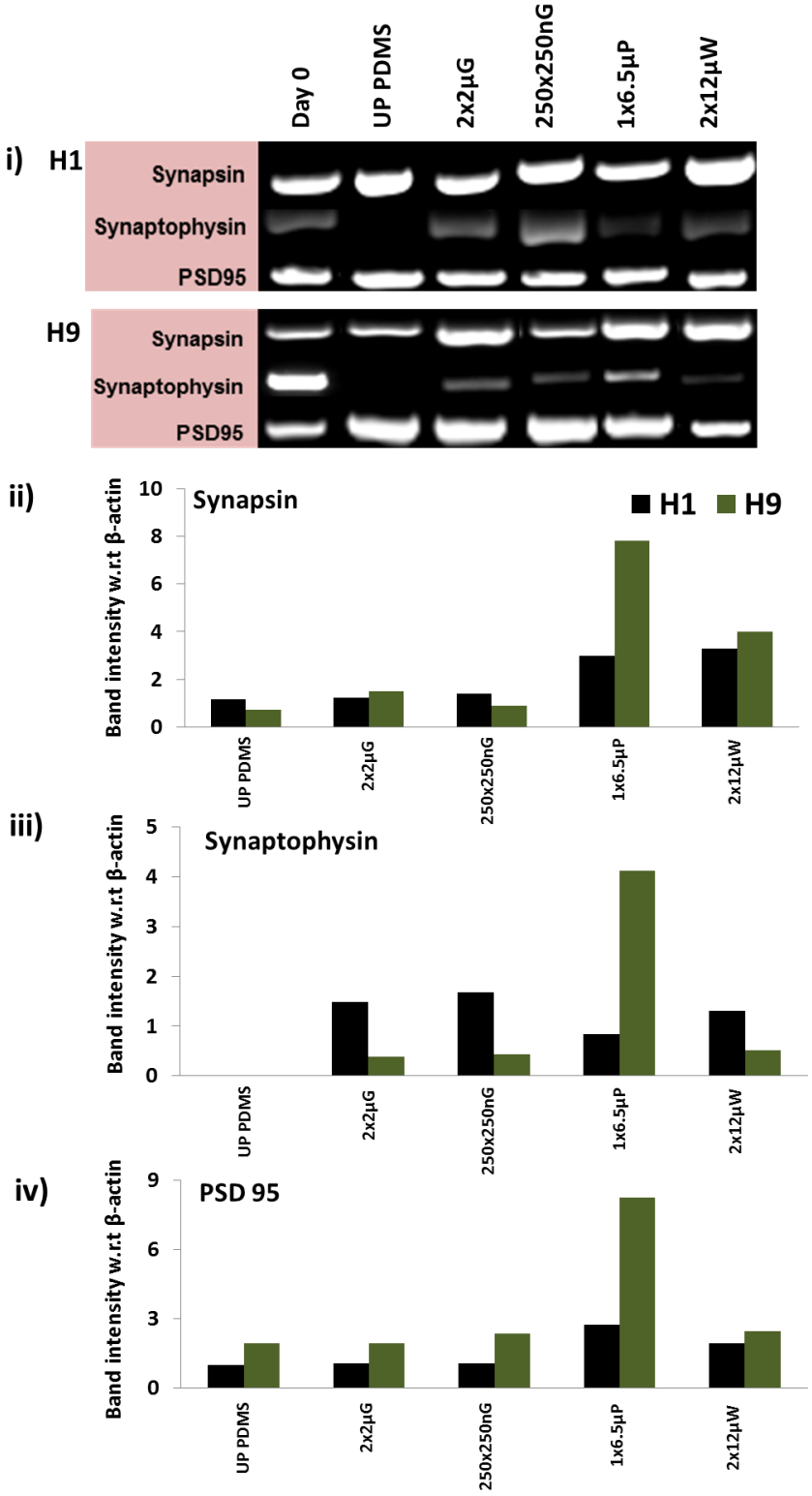

Figure 5.8 i) The image shows the synapse marker gene expression pattern for H1 and H9 cell lines seeded on individual topographies for seven days in the presence of neuronal differentiation media. The graph shows the densitometry analysis in arbitrary units (A.U) with respect to β-actin for **ii)** synapsin, **iii)** synaptophysin, **iv)** PSD 95 bands obtained by reverse transcription PCR for H1 and H9 cell lines. Abbreviations: Day 0 (undifferentiated hESC control), Unpatterned (UP) PDMS (control) [193].

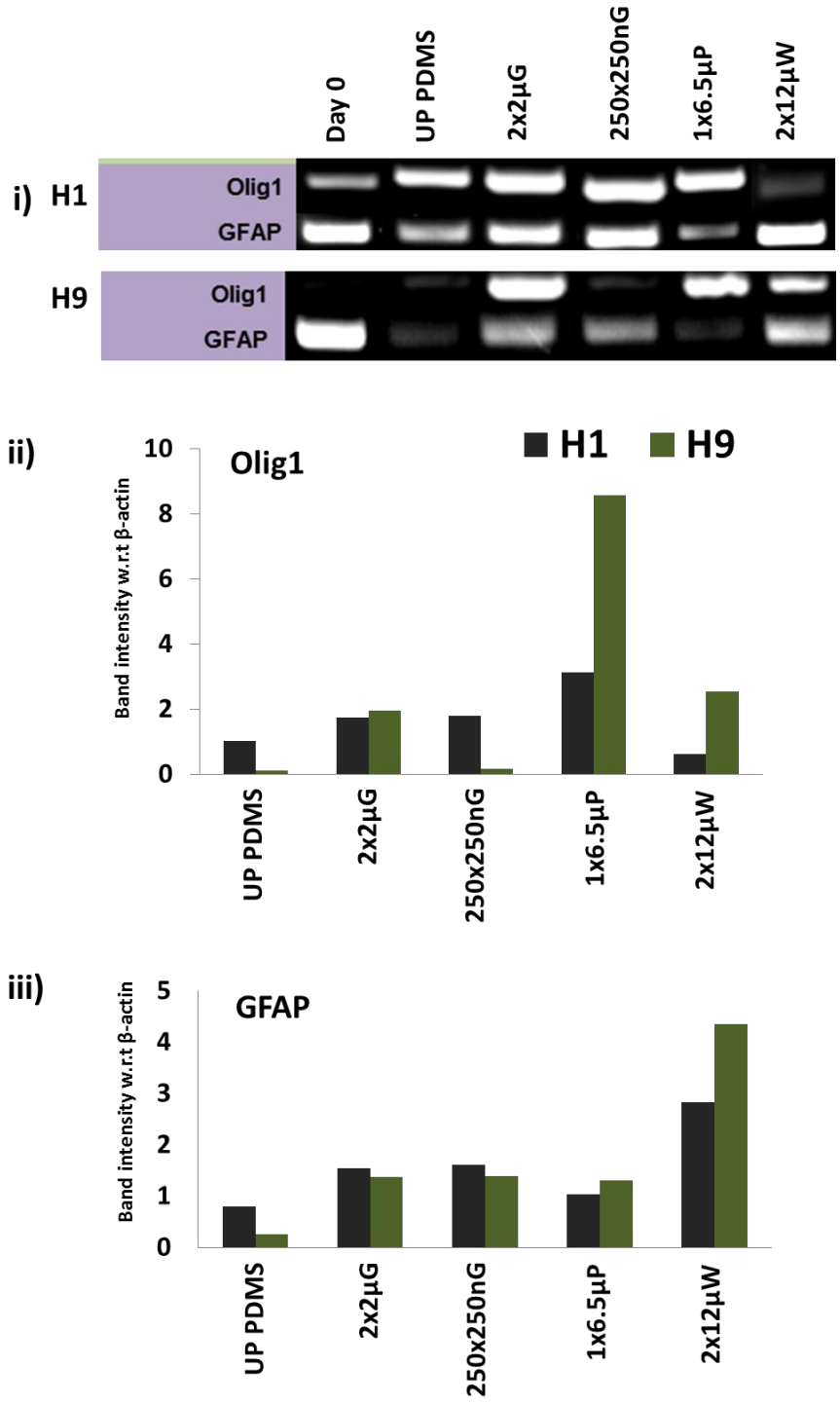

Figure 5.9 i) The image shows the synapse marker gene expression pattern for H1 and H9 cell lines seeded on individual topographies for seven days in the presence of neuronal differentiation media. The graph shows the densitometry analysis in arbitrary units (A.U) with respect to β-actin for **ii)** Olig1, **iii)** GFAP bands obtained by reverse transcription PCR for H1 and H9 cell lines. Abbreviations: D0 TCPS (undifferentiated hESC control), Unpatterned (UP) PDMS (control) [193].

5.3 Discussion

Pluripotent hESCs when subjected to direct differentiation on the anisotropic patterns exhibited elongated cell bodies and the neurites aligned along the grating axis. The cells spread and extended branches in all directions on the isotropic patterns, pillars and wells, promoting glial differentiation. This dependency on the substrate geometry for the differentiation of hESCs into glia or neurons was demonstrated at both protein and mRNA expression level by immunofluorescence staining and RT-PCR in this study. A schematic showing the neuronal differentiation of hESCs on MARC PDMS by either "conventional differentiation" or 'direct differentiation' method is shown in Figure 5.10.

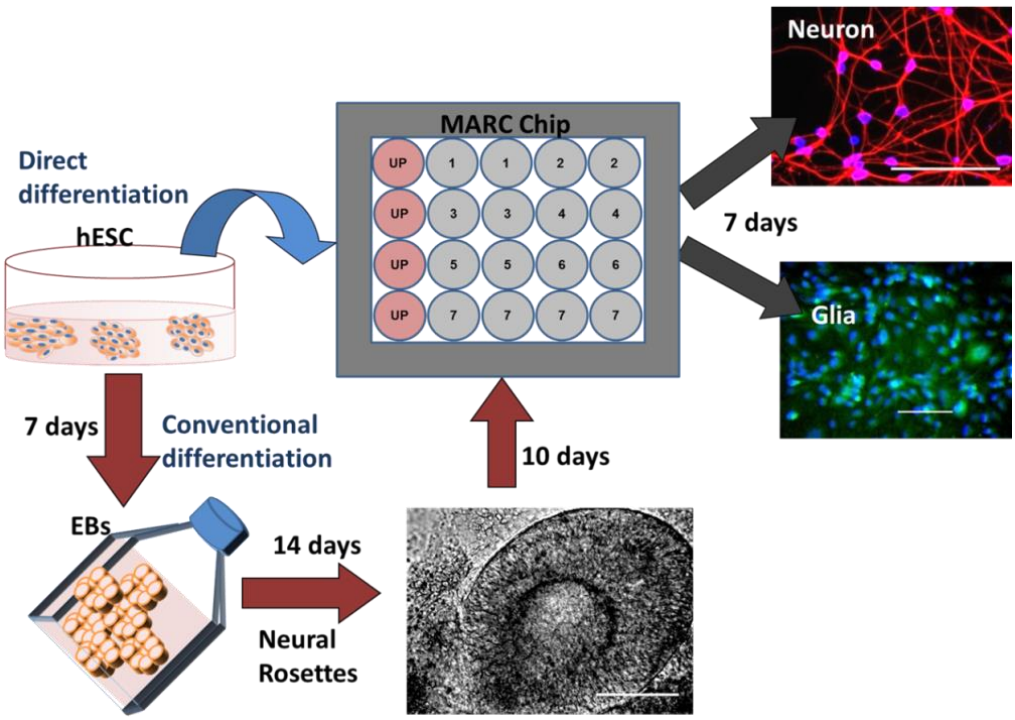

Figure 5.10 The **s**chematic of human embryonic stem cell (hESC) neural differentiation on the Multi Architecture Chip (MARC) by the direct or conventional method is shown. In "direct differentiation" (blue arrow), the hESCs were seeded directly on the MARC and analysed for neural markers after seven days. In "conventional methods" (red arrows) of differentiation, hESCs were grown as embryoid bodies and neurospheres before seeding onto the MARC. On the MARC, each pattern is represented by a circle and has a duplicate. The red circles represent the unpatterned control surface. The scale bar represents 100µm [193].

The media and the method of differentiation chosen were also essential factors to be optimised in order for the stem cells to respond to topographical cues. When mTESR1 media (expansion media containing strong chemokines for maintenance of pluripotency) was used, the hESCs on all topographies remained undifferentiated. The effect of topographies was superseded in the presence of strong chemical cues. This prompted the use of basal media (DMEM/F12 and knockout serum replacement without growth factors) but did not give satisfactory results hence a neuronal differentiation media containing minimal neuronal supplements was designed for the study using MARC and hESCs.

The N2B27 medium and ECM induced both glial and neuronal differentiation equally as evidenced from the expression of Tuj1- and GFAP-positive population on the unpatterned control; however, a higher percentage of a biased population was observed when grown on the topographies. A higher proportion of glial positive cells were observed when hESCs were grown on the isotropic patterns such as pillars and well, and a higher proportion of neuronal cells were observed when hESCs were grown on the anisotropic micro- and nano-gratings. The topography may also preferentially support the survival of a specific cell type. Anderson *et al*. postulated about the selective and inductive mechanisms of growth factor influences on stem cell fate determination [208]. To date, studies for neural differentiation of hESCs primarily consisted of inducing neural fate with growth factors, but our study suggests that topographies can also determine the fate of hESC either by a selective or inductive mechanism.

One can also postulate that the plating cell density also plays a role in neural fate determination. In this study, care was taken to keep the cell density within a consistent range between 20 – 25 x 10^3 / cm^2 for all the experiments to avoid the effect of cell density on neural fate determination. Preliminary data from our group showed that the

use of ROCK inhibitor (Y27632) to obtain single cell suspension affected the actin cytoskeleton, which in turn affects the efficiency of hESC differentiation. Therefore, the hESCs were plated onto the topographies as small clusters, and ROCK inhibitor was not used in the experimental design.

The hESCs were cultured on topographies for seven days with the direct differentiation method, whereas with the conventional method, the EBs are grown on tissue culture polystyrene (TCPS) without any topography induction until the neural precursor stage (Day 21). We speculate that the biophysical induction of topography, used in the direct differentiation method could play a significant role in the neural differentiation of hESCs. Another possible contribution could be the stiffness of the substrate; PDMS MARC chip used in this study is softer (1.43 ± 0.26 MPa, [209]) in comparison to the traditionally used, tissue culture polystyrene, TCPS (2 GPa, [210]). In the conventional method, TCPS might be unable to provide the optimal mechanical cues for neural differentiation; hence, longer duration (> 20 days) was needed to derive MAP2-positive neurons. Succinctly, in the direct differentiation method, neural differentiation was accelerated due to the combination of topography, softer substrate, and neuronal supplements. We conceive that when hESCs are grown directly on topographies for an extended culture duration with biochemical cues such as dorso-ventral patterning factors [6], more mature and functional neurons could be derived by the direct differentiation method.

The RT-qPCR analysis of H1 gene expression showed atleast 10 folds decrease in pluripotent transcription factor, Oct 4 when grown on patterned substrates. Interestingly, nanog gene expression, decreased only by 2 folds for micron and nano-gratings whereas decreased by almost 5 folds for cells grown on pillars and wells. Other studies have shown that nanog could promote osteogenic differentiation by modulating

the BMP pathway [211, 212]. In this study it is speculated that nanog might play a role in neuronal differentiation but not astrocyte differentiation. It would be presumed that the cells grown on gratings would differentiate into specialised sub-type specific neurons but the RT-PCR results showed that the dopamine transporter gene and cholinergic acetyl transporter gene were upregulated for H1 and H9 grown on pillars and not on micron gratings. It could be speculated that since the isotropic patterns support astrocytes, the neurons growing on these pillars are in a co-culture system and hence co-erced to a more mature neuronal subtype [213-216]. Supporting this speculation and results from previous studies which have shown that astrocyte co-culture could aid synapse formation in neurons higher synapse gene expression was observed for hESCs grown on pillars.

Studies conducted on hESCs differentiation have shown that there is a variation in the differentiation potential of H1 and H9 [217] and another study on the neuronal differentiation potential of iPSCs has also shown that there are differences in the neuronal differentiation potential amongst the cell lines [218]. Similarly, in this study, we observed variations in the levels of gene expression for H1- and H9-derived cells. Biologically, the discrepancies between mRNA and protein expression could be caused by post-transcriptional regulation, as well as differences in mRNA and protein turnover rates [219-221]. However, the trend of neuronal genes being expressed in hESCs growing on the anisotropic patterns and glial genes being preferentially expressed in cells growing on the isotropic patterns remained the same.

The present study highlights that the MARC is a versatile system that can be used to screen for both micro- and nano-topographies simultaneously on the same platform, affecting the neural fate of hESCs. Pluripotent hESCs when subjected to direct differentiation on the anisotropic patterns exhibited elongated cell bodies and the

neurites aligned along the grating axis along with high N:A ratio and MAP2 positive population (Figure 5.2 B, 5.3 B); meanwhile, they were rounded, spread and extended branches in all directions on the isotropic patterns, like pillars and wells, promoting glial differentiation. This dependency on the substrate geometry and size for the fate determination of hESCs differentiation into glia or neurons was demonstrated at both protein and mRNA expression level by immunofluorescence staining and PCR in this study.

5.4 Conclusion

In this chapter, a suitable media and an efficient protocol namely the "direct differentiation" method was devised. The hypothesis was tested with PDMS MARC chip and it was understood from gene and protein expression studies that the isotropic patterns favoured glial differentiation while the anisotropic patterns favoured the neuronal differentiation. The percentage of aligned cells and elongation of Tuj1 positive cells derived by direct differentiation method were higher as compared to those derived by conventional methods of neuronal differentiation. Human ESCs respond differently to different topographies and undergo cytoskeletal reorganization as a result of the underlying substrate geometry. It is essential to understand how the physical forces from the substrate are transduced to the cells and result in lineage specification. The actin cytoskeleton transduces this stretching force to the nucleus that may result in chromatin modifications and lineage specific gene expression (neuronal genes in this case). The next two chapters will focus on the changes in acto-myosin contractility and nucleus shape when hESCs are subjected to nano-gratings (250nm gratings with 250nm depth); to unravel the molecular mechanism behind topography mediated neural fate determination.

Chapter 6

6. The role of acto-myosin components in mediating the neuronal differentiation of hESCs.

6.1 Introduction

The previous chapters have indicated that the hESCs could be tuned to differentiate into neuronal or glial lineage based on the arrangement, geometry and size of the topography used. It was also observed that with the use of nano-gratings, more number of mature neurons could be derived as compared to hESCs grown on unpatterned substrates. These observations along with the change in the morphology of the cells grown on nano-grating substrate where the cells and their nuclei were more elongated are of special interest in this study. Studies on adult stem cells have shown that the topographies can affect the differentiation fate by inducing a shape change through the cytoskeletal elements, actin and myosin [53, 68, 222-225]. Hence, here it is hypothesised that the acto-myosin contractility is necessary for faster maturation of neurons derived from hESCs.

This chapter aims to understand the role of acto-myosin contractility on hESCs grown on unpatterned PDMS substrate only with the minimal biochemical cues (N2B27 media without any growth factor supplements) and without any topographical cues. Temporal studies were conducted with H1 cell line using direct differentiation method. Inhibitors of myosin contractility (blebbistatin), myosin light chain kinase (ML-7) and ROCK activity (Y-27632) were used to understand the role of these components during neuronal differentiation of hESCs.

6.2 Results

6.2.1 Temporal expression of mature neuronal marker

The hESCs (H1 cell line) were subjected to neuronal differentiation in N2B27 media (Neurobasal media and DMEM/F12 at 1:1 ratio supplemented with 1x N2 and B27 supplements) on unpatterned PDMS substrate. They were fixed at Day 1, 4 and 7 and immunostained for mature neuronal marker, MAP2 (Figure 6.1). The intensity of MAP2 protein expression increased, and there was a 2.5 folds increase in cell size from Day 1 to Day 7.

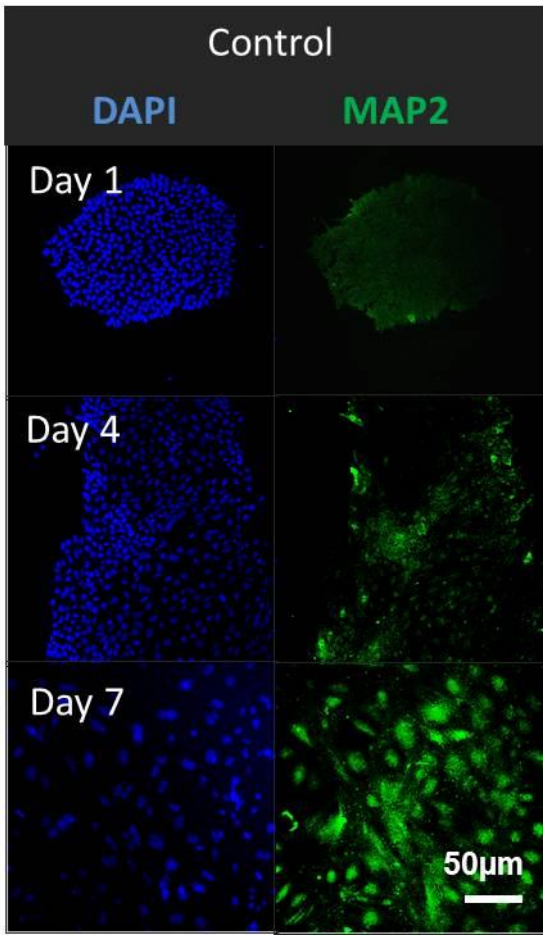

Figure 6.1 Temporal expression of mature neuronal marker, MAP2 (stained in green). The nuclei were counter stained with DAPI in blue. The cells on unpatterned PDMS were analysed at Day 1, 4 and 7. Highest intensity of MAP2 was observed on Day 7 of neuronal differentiation. The scale bar represents 50µm.

6.2.2 Temporal expression and analysis of acto-myosin components during neuronal differentiation of hESCs

The hESCs seeded on unpatterned substrates were immunostained for phosphorylated myosin light chain (pMLC) and counterstained for filamentous actin (F-actin) using fluorescently labelled phalloidin dye (Figure 6.2 A), to observe the extent of activated myosin (Figure 6.2 B), at Day 1, 4 and 7. In hESCs, F-actin and pMLC was seen primarily on the periphery of the cell (cortical actin) by Day 1. The F-actin formed ring like structures within the cortical actin while the activated myosin as seen from pMLC staining, was seen primarily at the nodes of cell-cell junction by Day 4. The intensity of F-actin and pMLC increased to the highest by Day 7 of differentiation. The intensity measurements showed that the increase in pMLC was significantly higher by Day 1 of differentiation. The intensity of each cell for F-actin and pMLC was quantified using ImageJ and represented as an average value in the graphs (Figures 6.2 C, D).

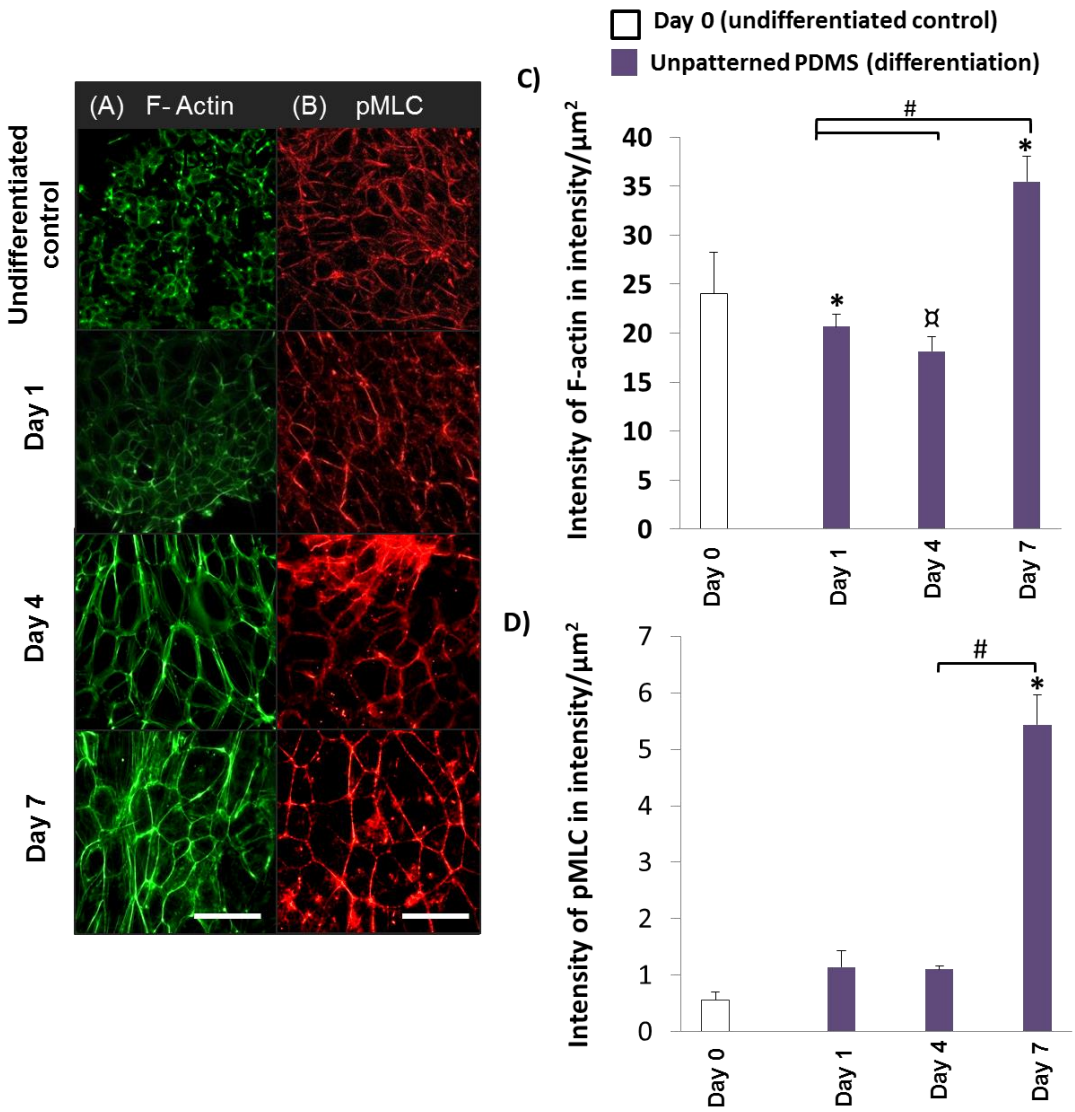

Figure 6.2 Temporal expression of F-actin **(A)** stained in green and pMLC **(B)** stained in red, of hESCs seeded on unpatterned PDMS substrates. F-actin and pMLC expression is seen even on undifferentiated cells but at much lower levels compared to differentiated cell population as seen from Day 7 staining. The scale bar represents 100µm. The plot shows the semi quantitative analysis of F-actin **(C)** and pMLC **(D)** protein expression intensity using Image J. The intensity is expressed in intensity/µm2. * represents significance at $p<0.001$ as compared to Day 0, undifferentiated control, ¤ represents significance at $p<0.01$ as compared to control, # represents significance at $p<0.05$.

6.2.3 Temporal expression of vinculin in hESCs undergoing neuronal differentiation

The hESCs were fixed and stained for vinculin after stabilisation with cytoskeleton buffer (refer to chapter 3, materials and methods). Figure 6.3 shows that vinculin expression was observed primarily at the nodes of cell-cell junction on the undifferentiated hESCs and were less in number compared to differentiated hESCs. The merged higher magnification images of vinculin and F-actin showed that vinculin co-localised with F-actin specifically at cell-cell junction during Day 1 and 4 of differentiation. Vinculin expressing focal adhesions were seen by Day 7 allowing the formation of stress fibers as seen from the high magnifcation merged image.

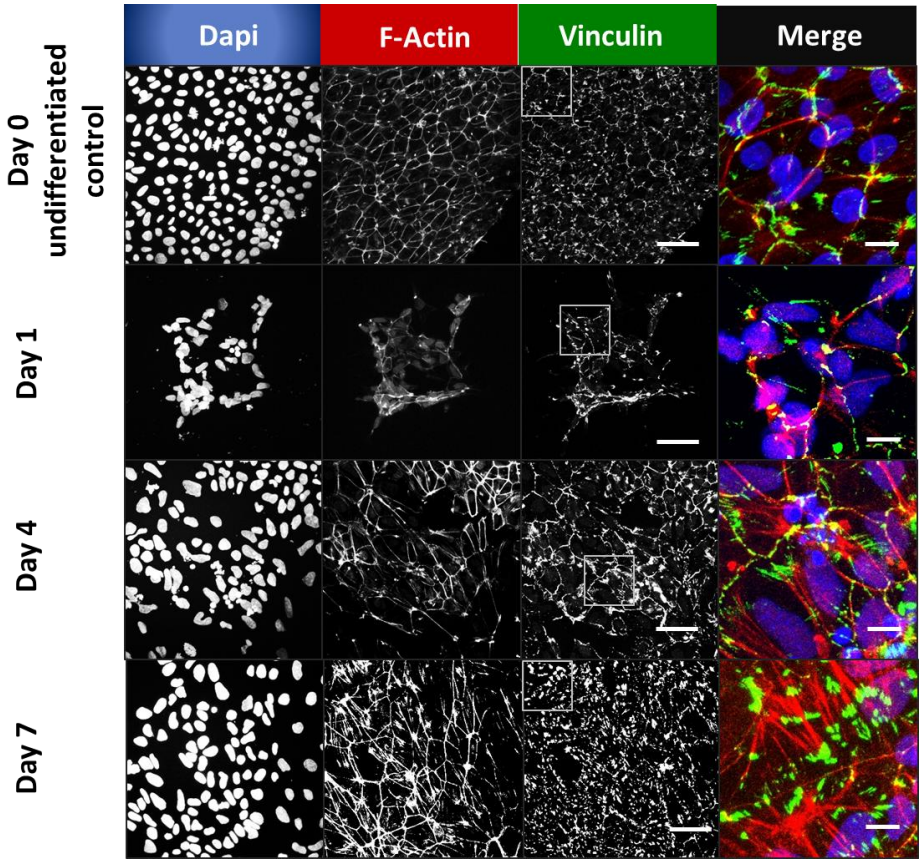

Figure 6.3 Temporal expression pattern of vinculin in hESCs during neuronal differentiation. The nucleus were stained with DAPI (blue) and F-actin was stained red with Alexa Fluor phalloidin 546 while vinculin was stained green, as seen from the merge panel. The scale bar for Dapi, F-actin and vinculin represents 50µm while the scale for images in merged panel represents 10µm.

6.2.4 Optimal inhibitor concentration determination during neuronal differentiation of hESCs

Inhibitors of non-muscle myosin II (blebbistatin), myosin light chain kinase (MLCK, inhibited by ML-7), Rho associated protein kinase activity (ROCK inhibited by Y-27632) and polymerisation of F-actin (cytochalasin D) were used in this study to determine the role of acto-myosin components during the neuronal differentiation of hESCs. Optimization was necessary to determine a suitable concentration for each inhibitor that would not be cytotoxic to the cells while being able to inhibit the specific cytoskeletal components. The samples were fixed and stained for neuronal marker Tuj1and F-actin at Day 4.

Three different concentrations per inhibitor were chosen based on the literature for other stem cells [153, 158, 226]. A concentration of 10µM would be the optimal with expected inhibition of the targeted cytoskeletal component and reduced cytotoxicity for blebbistatin (Figure 6.4 A), ML-7 (Figure 6.4 B) and Y-27632 (Figure 6.4 C). The inhibitor of actin polymerisation, Cytochalasin D was very cytotoxic to cells even at low concentrations of 0.1µM (Figure 6.4 D). Hence cytochalasin D was not used for further experiments.

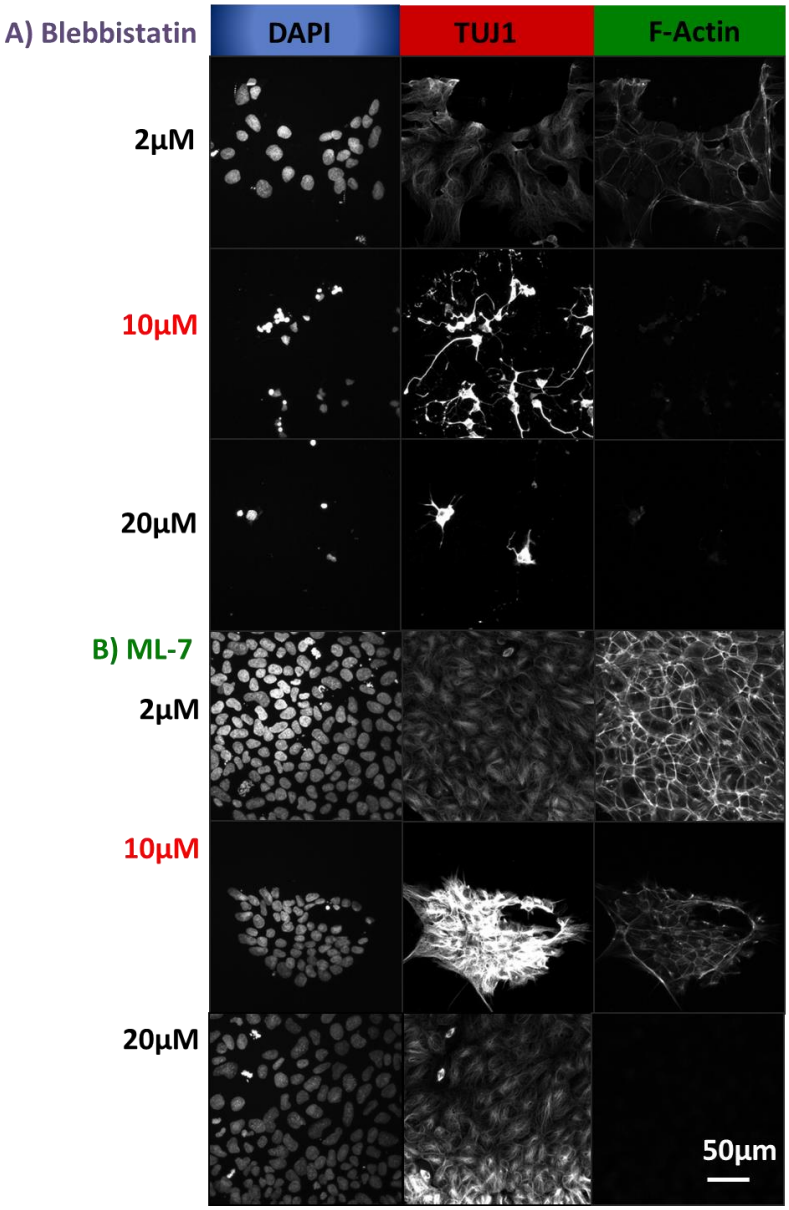

Figure 6.4 Determination of the optimal inhibitor concentration to inhibit acto-myosin contractility during neuronal differentiation of hESCs. **A)** Blebbistatin, to inhibit non-muscle myosin II. **B)** ML-7, to inhibit the phosphorylation of myosin light chain kinase (PMLCK). The cells were stained for nucleus with DAPI, neuronal marker, Tuj1 and filamentous actin with fluorescently labelled phalloidin. The scale bar represents 50µm.

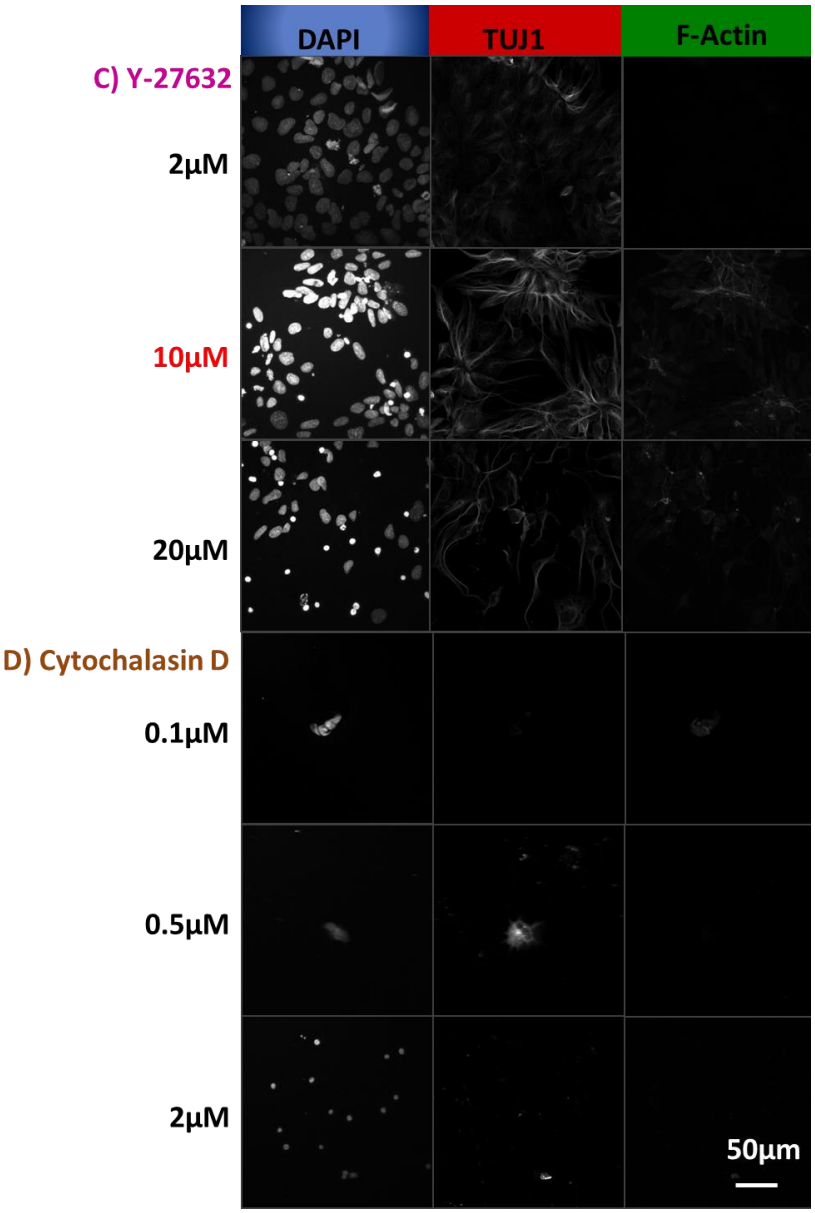

Figure 6.4 Determination of optimal inhibitor concentration to inhibit acto-myosin during neuronal differentiation of hESCs. **C)** Y-27632, to inhibit Rho-associated kinase (ROCK) activity and **D)** Cytochalasin D to inhibit actin polymerisation. The cells were stained for nucleus with DAPI, neuronal marker, Tuj1 and filamentous actin with fluorescently labelled phalloidin.The scale bar represents 50µm.

6.2.5 Effect of myosin and ROCK inhibitors on vinculin and early focal adhesion formation

The hESCs were plated and allowed to attach and stabilize for 24 hours before the addition of 2µM and 10µM concentrations of blebbistatin, 10µM concentration of ML-7 and Y-27632 for 2 days (Day 2 and Day 3) to understand the role played by myosin, phosphorylated myosin and ROCK respectively. The samples were fixed at Day 4 and immuno-stained for vinculin and MLC. The Day 4 samples without inhibitor treatment showed vinculin expression mostly at cell-cell junctions. When the myosin contractility and ROCK activity were inhibited by blebbistatin and Y-27632 respectively, the vinculin expression at cell-cell junction was decreased, but when the myosin contractility was inhibited by ML7, the vinculin expression at cell-cell junction increased (Figure 6.5 A). Early focal adhesions like phosphorylated focal adhesion kinase (pFAK) and paxillin were not prominent on hESCs undergoing differentiation with or without inhibitors (Figure 6.5 B).

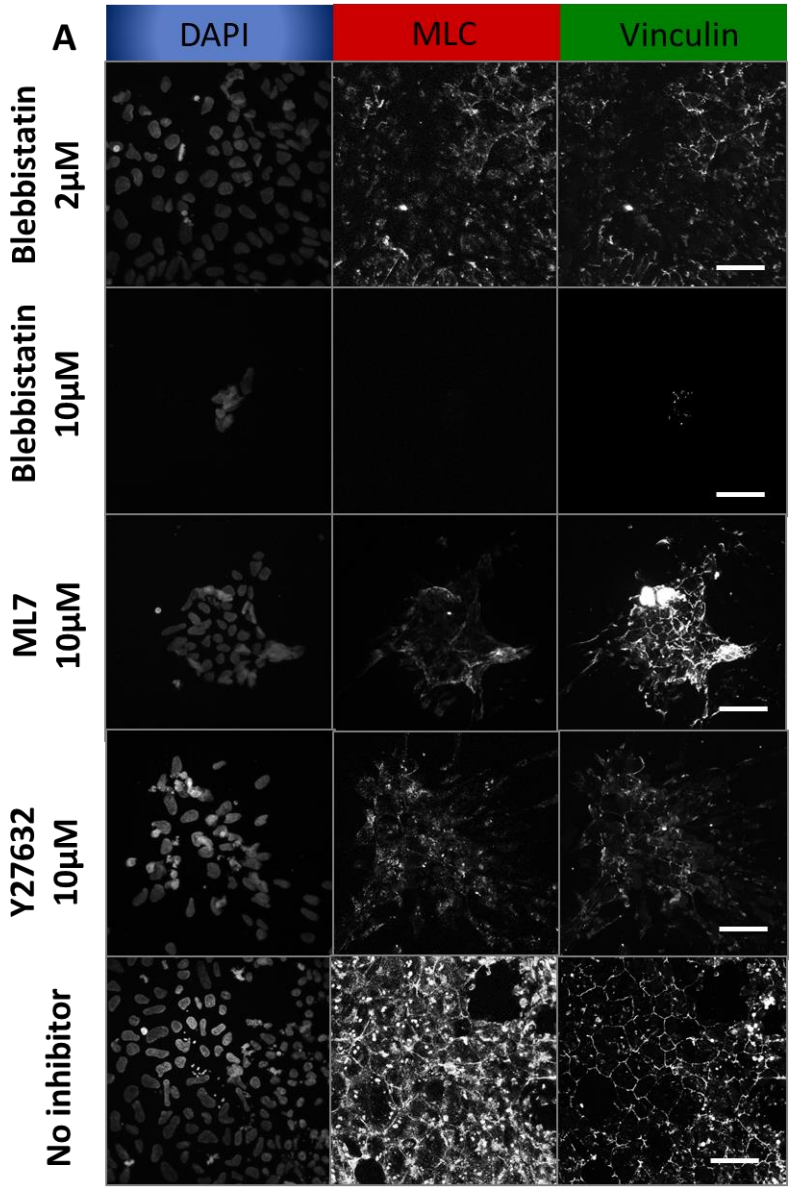

Figure 6.5 Effect of myosin and ROCK inhibitors on vinculin expressing focal adhesion **A)**. The cells grown on unpatterned substrates were immunostained for myosin light chain, vinculin and counterstained with DAPI for nucleus. The scale bar represents 50µm.

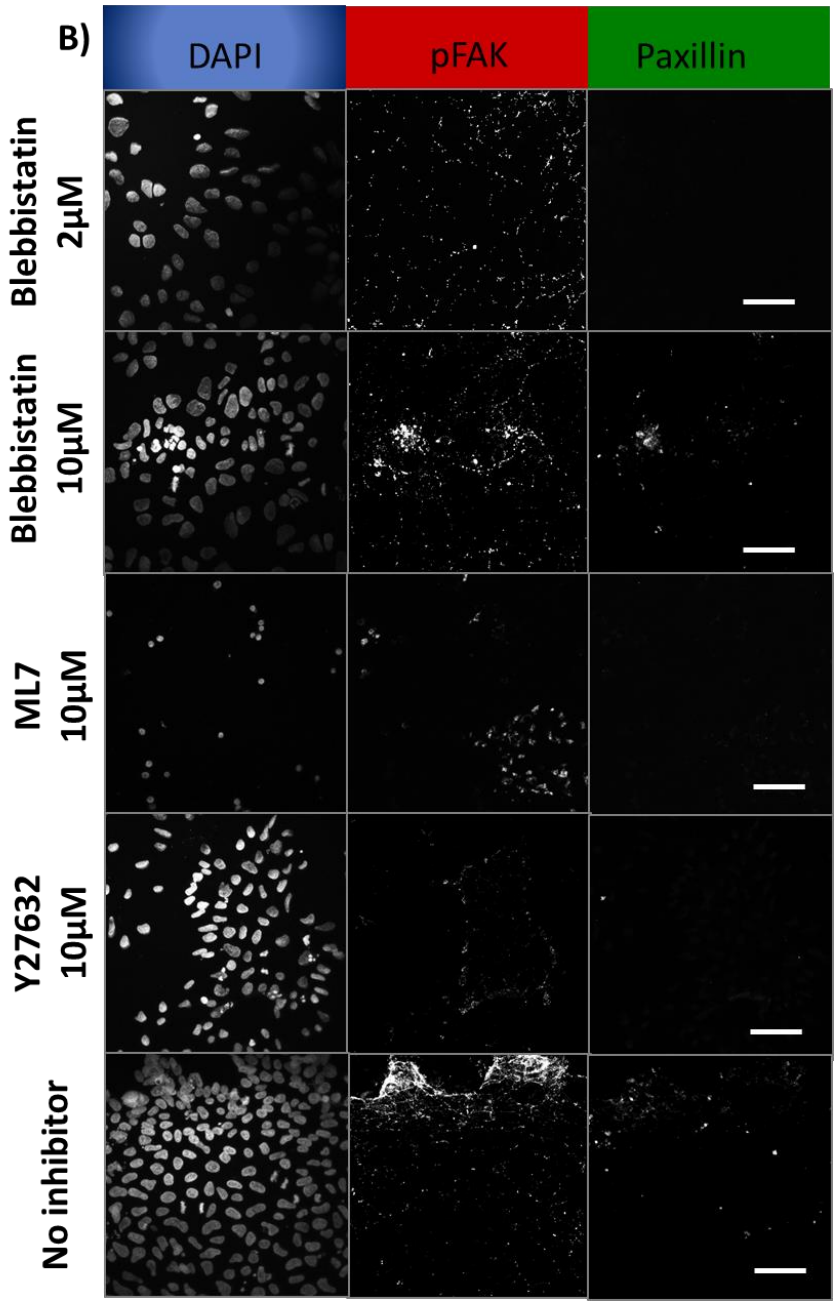

Figure 6.5 B) Effect of myosin and ROCK inhibitors on early formation of early focal adhesions like paxillin and phosphorylated focal adhesion kinase (pFAK). The cells were stained for nucleus with DAPI. The scale bar represents 50µm.

6.2.6 Inhibition of ROCK pathway aids neuritogenesis

When subjected to myosin and ROCK inhibitors for 2 days (fixed on Day 4, Figure 6.6 A), early inhibition of myosin contractility by blebbistatin did not affect the expression of immature neuronal marker, Tuj1, in the hESCs; however, inhibition of ROCK activity increased the neurite formation in Tuj1 positive cells. In order to verify if the Tuj1 expression was sensitive to the duration and concentration of myosin-contractility inhibition, the hESCs were treated with 5, 10 and 20μM blebbistatin for 5 days (fixed at Day 7). The prolonged exposure to different concentrations still did not affect the Tuj1 expression (Figure 6.6 B).

6.2.7 Maturation of neurons is a myosin dependent process

Mature neuronal marker, MAP2, expression was very weak when acto-myosin contractility was inhibited. The MAP2 expression when treated with blebbistatin and ML7 were comparable to that of samples which were not treated with any inhibitor, while the samples treated with ROCK inhibitor had higher MAP2 expression (Figure 6.7 A). It was also observed that Y-27632 did not inhibit the phosphorylated myosin as seen from the pMLC staining. The Figure 6.7 B shows the expression of MAP2, pMLC and EdU for cells treated with blebbistatin for 5 days and fixed at Day 7. Higher concentrations of 20μM blebbistatin inhibited MAP2 to a greater extent. EdU indicated the proliferating population, indicated by EdU, decreased when hESCs were treated with blebbistatin at 10μM concentration.

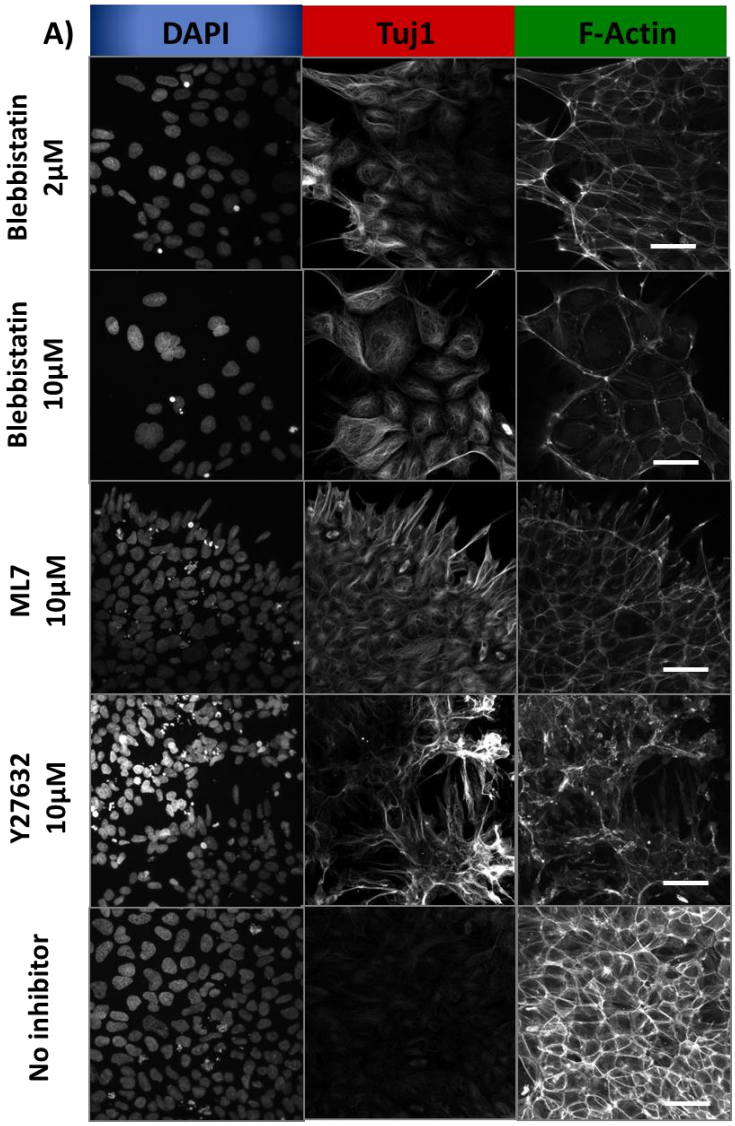

Figure 6.6 Inhibition of myosin or phosphorylated myosin did not affect the immature neuronal marker, Tuj1 expression. In parallel, ROCK activity inhibition by Y-27632 affects neurite formation in Tuj1 positive cells. **A)** The cells were stained for Tuj1, filamentous actin using fluorescently labelled phalloidin and counterstained for nuclei with DAPI. The scale bar represents 50μm.

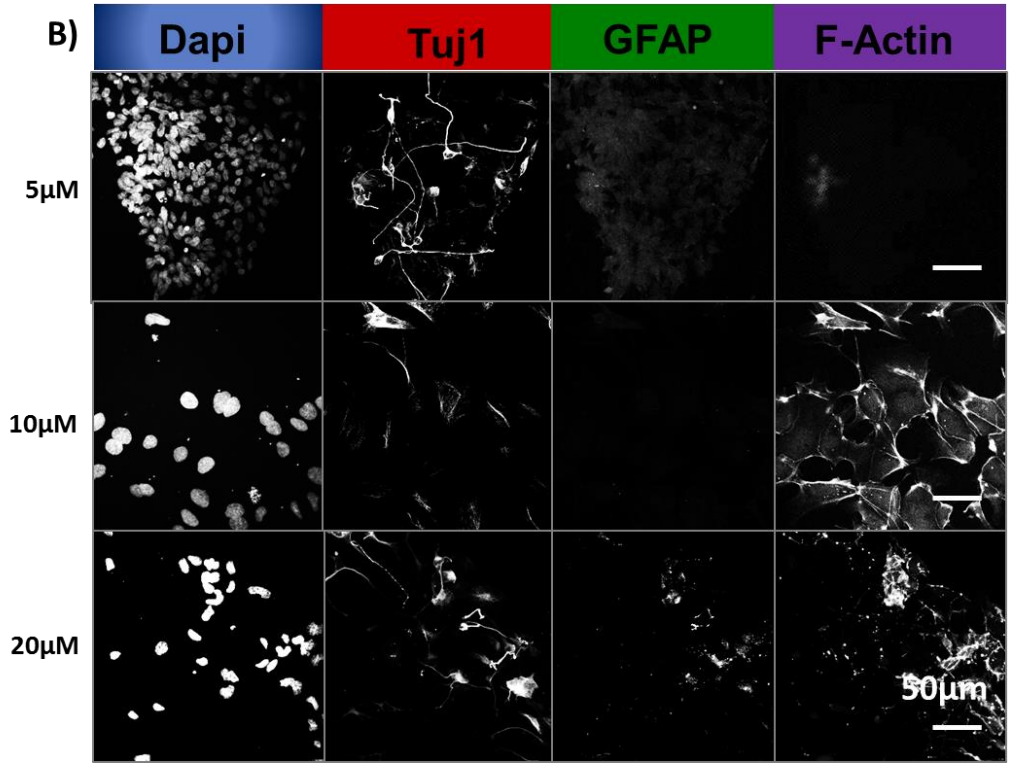

Figure 6.6 The hESCs were exposed to myosin inhibitor, blebbistatin for 5 days at three different concentrations. The neuronal marker, Tuj1 and glial marker, GFAP expression was not inhibited by exposure to myosin inhibitors at higher concentrations or for longer duration. **B)** The cells were stained for neuronal marker, Tuj1; Glial marker, GFAP, filamentous actin using fluorescently labelled phalloidin and counterstained for nuclei with DAPI. The scale bar represents 50µm.

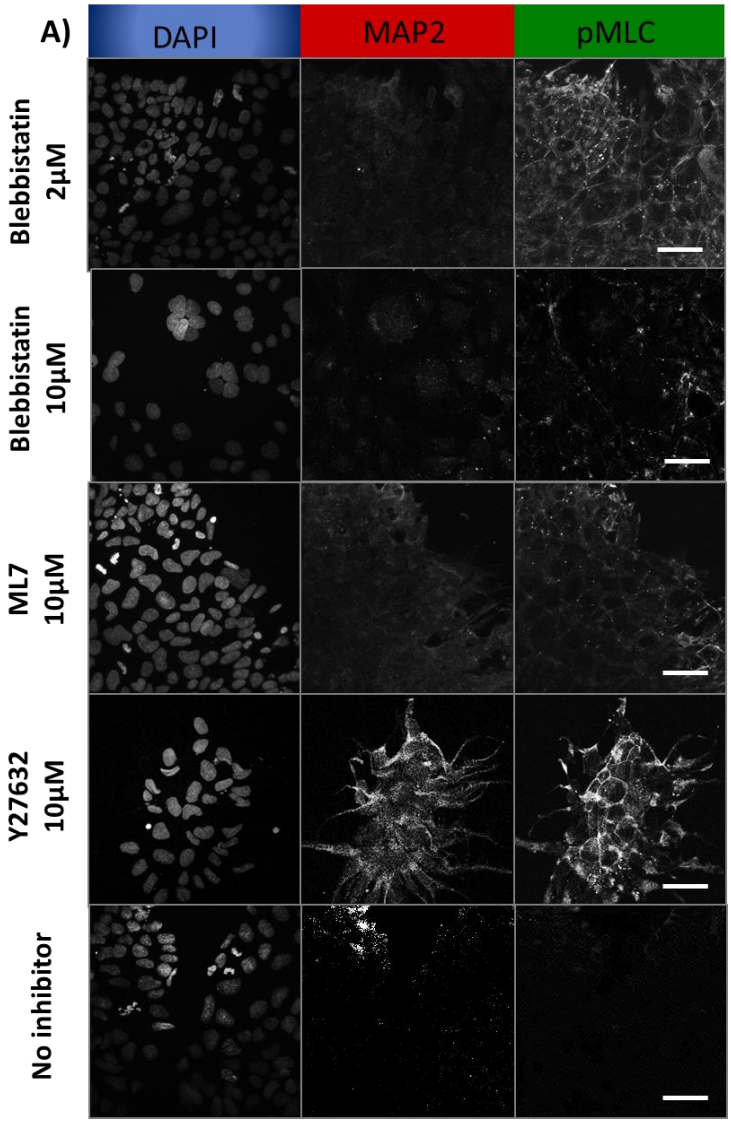

Figure 6.7 Inhibition of myosin contractility affected the expression of mature neuronal marker MAP2. **A)** The hESCs were subjected to blebbistatin, ML7 and Y-27632 inhibitors for 2 days and analysed for the expression of mature neuronal marker, MAP2 and pMLC. The scale bar represents 50µm.

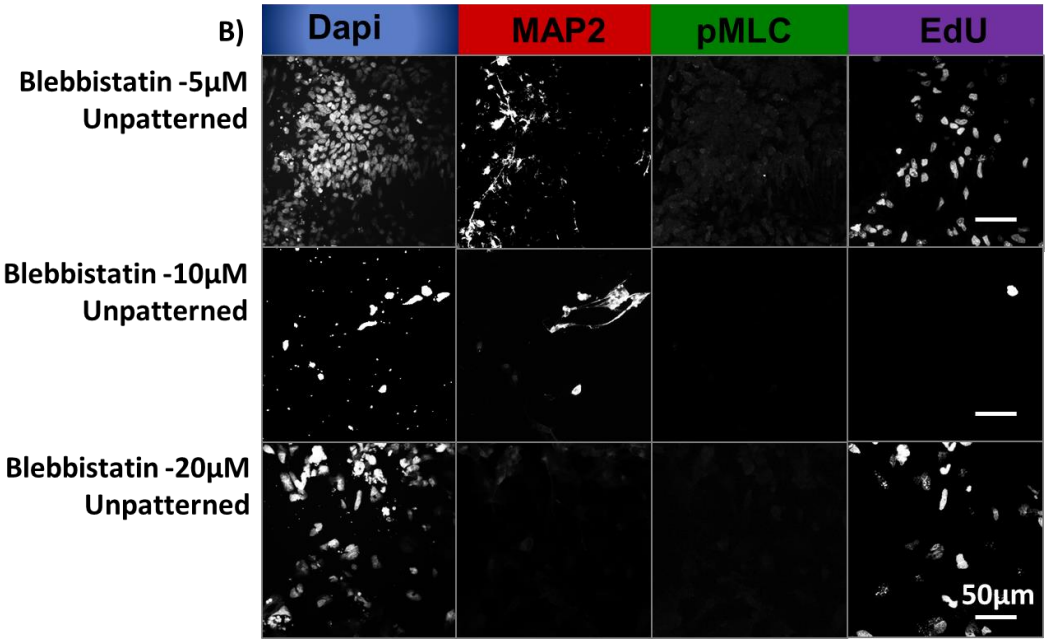

Figure 6.7 Inhibition of myosin contractility affected the expression of mature neuronal marker, MAP2. It was verified with long term exposure (5 days) and at higher dose of blebbistatin that maturation of neurons was myosin dependent. **B**) The samples were also stained for phosphorylated myosin light chain, EdU to observe the proliferating population and DAPI for visualising the nucleus. The scale bar represents 50µm.

6.3 Discussion

The hESCs undergo neuronal differentiation when provided with optimal topographical and biochemical cues. Chapter 5 demonstrated that the geometry and size of the topography could determine the neural fate of hESCs. The time taken for differentiation was reduced to 7 days by the "direct differentiation method" as compared to > 21 days by "conventional method" of differentiation. The aim of the study in chapter 6 was to elucidate the role of acto-myosin contractility during neuronal differentiation of hESCs without the presence of topography. It is hypothesised that the acto-myosin contractility was necessary for faster maturation of neurons derived from hESCs.

A temporal study of mature neuronal marker MAP2 protein expression showed that the intensity of MAP2 increased with time. In corollary, cells grown on unpatterned PDMS substrates showed significantly high intensity expression of F-actin and pMLC on Day 7 though its intensity was maintained at basal levels (comparable to undifferentiated cells) at Day 1 and Day 4.

The optimal concentrations of inhibitors chosen were based on the efficiency of inhibition and minimal cytotoxicity. The effect of ML-7 and Y-27632 was prominent at 10µM (Figure 6.4 B and C). Cytochalasin D was cytotoxic to cells even at very low concentrations of 0.1µM indicating that F-actin was indeed essential for the survival of hESCs (Figure 6.4 D) and hence not used in the studies discussed in the later part of this chapter. Blebbistatin had shown an interesting result when the cells were treated at 10µM concentration; the Tuj1 positive cells had branched neurite morphology but this was not observed with treatments at lower (2µM) or higher (20µM) concentrations. Hence, it was decided to use both 2µM and 10µM concentrations of blebbistatin in the rest of the experiments carried out in this thesis to provide a better comparison.

Earlier studies have shown that ROCK activity through its downstream elements could affect myosin contractility and also the stabilisation of F-actin [227]. In our studies, we observed that inhibiting myosin with blebbistatin at 2µM did not affect the F-actin expression but reduced the MLC protein expression. The samples treated with 10µM blebbistatin showed a greater inhibition of the MLC expression and F-actin expression was also reduced but not completely inhibited thereby decreasing the acto-myosin contractility (Figure 6.4 A and 6.5 A).

Once the cells adhere to the substrate, the integrins recruit paxillin by a mechanism which is still not clearly understood [228-230]. The early or immature focal adhesions (FAs), which were identified by the expression of paxillin or pFAK, were not prominent on hESCs and their expression was not affected by treatment with myosin contractility and ROCK inhibitors. It is speculated that cytoskeletal contractility is not one of the essential factors for the expression of early FA formation in hESCs.

The recruitment of vinculin observed at the cell-cell junction (Day 1 and 4 of differentiation) to cell - matrix focal adhesions by Day 7 also correspond to the increase in contractility at the 7 day time point. This prompted the investigation of the importance of acto-myosin contractility in vinculin expressing focal adhesion. Unexpectedly, decrease in acto-myosin contractility with ML-7 treatment increased the vinculin expression at cell-cell junction but when acto-myosin contractility was decreased with blebbistatin, vinculin expression was decreased both at cell-cell junction and at cell-matrix focal adhesions (cell-substrate interaction) [231]. The samples treated with 10µM blebbistatin exhibited decreased or no expression of vinculin containing focal adhesion, but they showed a higher number of immature focal adhesions, as compared to samples treated with ML-7 or Y-27632 (Figure 6.5). The results agreed with previous studies on mouse embryonic fibroblasts where the researchers showed that paxillin formation is independent of myosin II contractility and was not affected even by prolonged exposure to blebbistatin [230]. It is speculated that the feedback mechanism from acto-myosin contractility to vinculin allows the recruitment of vinculin to cell-matrix focal adhesions by Day 7 of neuronal differentiation.

Researchers have shown that 10µM concentration of ROCK inhibitor could be used to culture hESCs as single cells while maintaining its pluripotent state [232]. In this study, interestingly, the inhibition of the ROCK activity helped in neuritogenesis of Tuj1 positive cells (Figure 6.6 A). Previous study with mouse neuroblastoma cell line has shown that ROCK could also be involved in neurite retraction [233]. The work done by Da Silva *et al*. in 2003 with rat embryonic hippocampal neurons showed that inhibiting ROCK leads to neurite extensions through a profilin mediated pathway [234]. The study done by Scaife *et al*. established that when the ROCK activity was inhibited in 3T3 fibroblasts, microtubule rich extensions were formed and the formation of these extensions were not affected even by depolymerisation of F-actin [235]. Thus the results in this study on neuronal differentiation of hESCs where ROCK inhibition increased neurite extensions (Figure 6.6) correlates with previous studies.

Another interesting observation was that the maturation of neurons seems to be dependent on acto-myosin contractility although the expression of immature neuronal markers was independent of acto- myosin contractility, as seen from Figure 6.7A, B in which the cells were treated with blebbistatin. It is speculated that acto-myosin contractility plays a role in organization of tubulin into microtubules but not the expression of tubulin itself and hence affects neuronal maturation (expression of microtubules in mature neurons). It is also observed that the proliferating cell population EdU was independent of myosin activity as seen from Figure 6.7B. It has to be noted that, in general, MAP2 expression would be much lower on unpatterned PDMS substrates as compared to anisotropic patterned substrates (Chapter 5). This low level of MAP2 expression is speculated to be due to the lower acto-myosin contractility in hESCs on unpatterned surfaces.

6.4 Conclusion

This chapter has elaborated the role of cytoskeletal components especially non-muscle myosin II during the neuronal differentiation of hESCs without any topographical cues. The maturation of focal adhesions and the expression of mature neuronal markers like MAP2 were dependent on myosin activity while ROCK inhibition promoted neurite extension. A schematic of the proposed pathway is shown in Figure 6.8. The ROCK and myosin light chain kinase (MLCK) individually modulate the phosphorylation of myosin and hence the acto-myosin contractility. The use of blebbistatin and ML-7 to inhibit acto-myosin contractility has different effects on vinculin and Tuj1 expression. This leads to the speculation that the blebbistatin and MLCK might be following different pathways to cause acto-myosin contractility. It is well known that the stress fibers are stabilized by vinculin expressing focal adhesions. It is thought that vinculin might activate the wnt pathway of neuronal differentiation through β-catenin. In this chapter we understood the role of acto-myosin contractility in expression of MAP2 and neuritogenesis while the next chapter will discuss the contribution of topography in promoting higher number of MAP2 positive cells and longer neurite extensions.

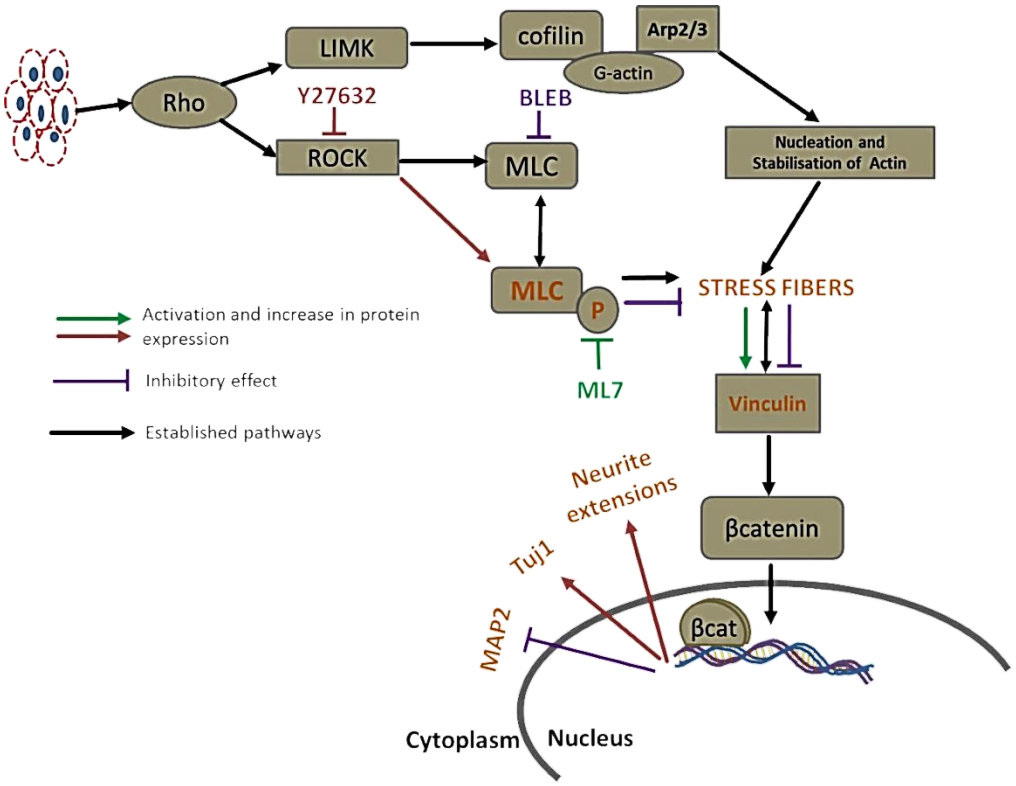

Figure 6.8 Proposed pathway for the role of acto-myosin contractility on neuronal differentiation of hESCs. The bold lines indicate the function that has been well studied while the dashed lines indicate the proposed pathway which is not studied yet. The action of blebbistatin is shown in violet, action of Y-27632 in maroon and action of ML-7 in green.

Chapter 7

7. Understanding the role of acto-myosin contractility during topography mediated neuronal differentiation

7.1 **Introduction**

The cell-matrix contacts are dynamic and cells seem to evaluate the forces from the extracellular environment as the cytoskeletal filaments assemble, break down and reassemble [236]. Recent studies have shown that cells can sense the nano- and micro-scaled topographies and change in spacing by the changes in integrin clustering [147, 237, 238]. The cytoskeletal elements can transduce stresses over long range distance through various focal adhesion proteins and SUN domains linking the actin to the nucleus lamin [239, 240].

The role of acto-myosin components during neuronal differentiation of hESCs was studied in the previous chapter. It was understood from the temporal inhibitor study that neuronal maturation is indeed dependent on acto-myosin contractility. This chapter will further investigate the hypothesis that hESCs grown on nano-gratings have higher contractility than the unpatterned substrates, resulting in elongation and alignment along the grating axis and the neural fate regulation.

The role of acto-myosin contractility in the presence of topographical cues in modulating the neural fate of H1 will be studied temporally using myosin contractility and ROCK activity inhibitors on the 250 nm nano-grating patterned PDMS substrate by "direct differentiation" method. The study will also elaborate the morphological and epigenetic changes observed in the nucleus temporally as neuronal differentiation proceeds on the nano-grating PDMS substrate.

7.2 Results

7.2.1 Early formation of stress fibers in hESCs cultured on nano-gratings

The hESCs were cultured on 250 nano-grating patterned (nano-patterned) and unpatterned PDMS substrates in N2B27 media. The samples were fixed and analysed for F-actin at Day 1, 4 and 7. Figure 7.1 A shows a series of confocal stack images of F-actin in hESCs grown on unpatterned substrate while Figure 7.1 B shows the confocal stack images of F-actin in hESCs grown on 250 nano-grating patterned substrate at Day 1. The cells grown on nano-patterned substrates even had stress fibre formation (indicated by the white arrows) while the cells on unpatterned substrates only had cortical actin around the periphery of the cells at Day 1 of differentiation. The maximum intensity projection images of F-actin in hESCs grown on unpatterned and patterned substrates and fixed at different time points (Day 1, 4 and 7) are shown in Figure 7.1 C. F-actin was localised to the periphery of hESCs on unpatterned substrates at Day 1 and Day 4, while stress fibers started appearing only by Day 7. The hESCs grown on patterned substrates showed stress fibers that were aligned to the grating axis even as early as Day 1. Figure 7.1 D shows the intensity of F-actin in hESCs measured using ImageJ. The hESCs on patterned and unpatterned substrates showed highest intensity only at Day 7. In the hESCs grown on 2μm gratings, the F-actin intensity decreased over time and the intensity at Day 7 was significantly lower than in the cells grown on nano-grating or unpatterned substrates (data shown in Appendix B, Figure B.1).

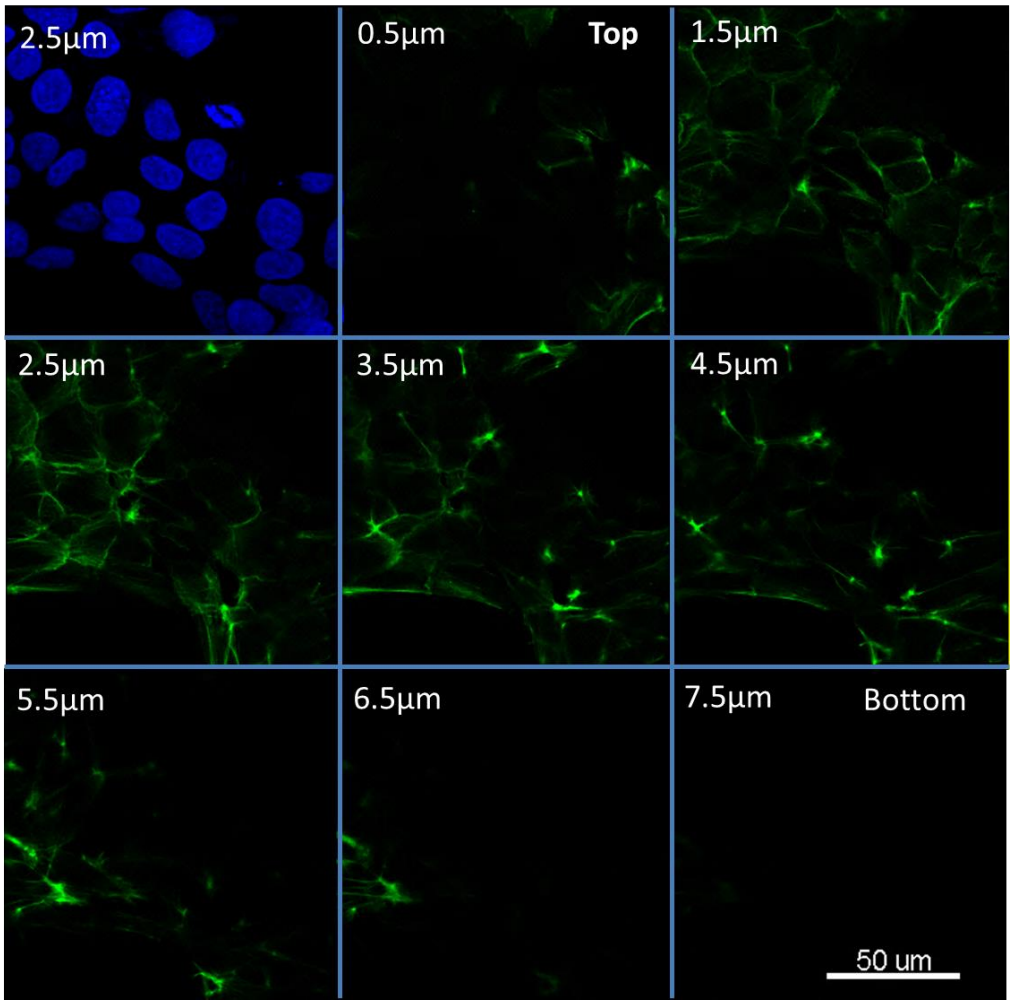

Figure 7.1 Gallery view of cortical actin from the apical surface of the cell to the basal part attached to the ECM at Day 1 of differentiation. **A)** Confocal stack of F-actin in hESCs grown on unpatterned PDMS substrates. The nucleus counterstained with DAPI in blue is shown for Z = 2.5µm. The slice is set at 1µm thickness and the Z-depth is shown on the image. The scale bar represents 50µm

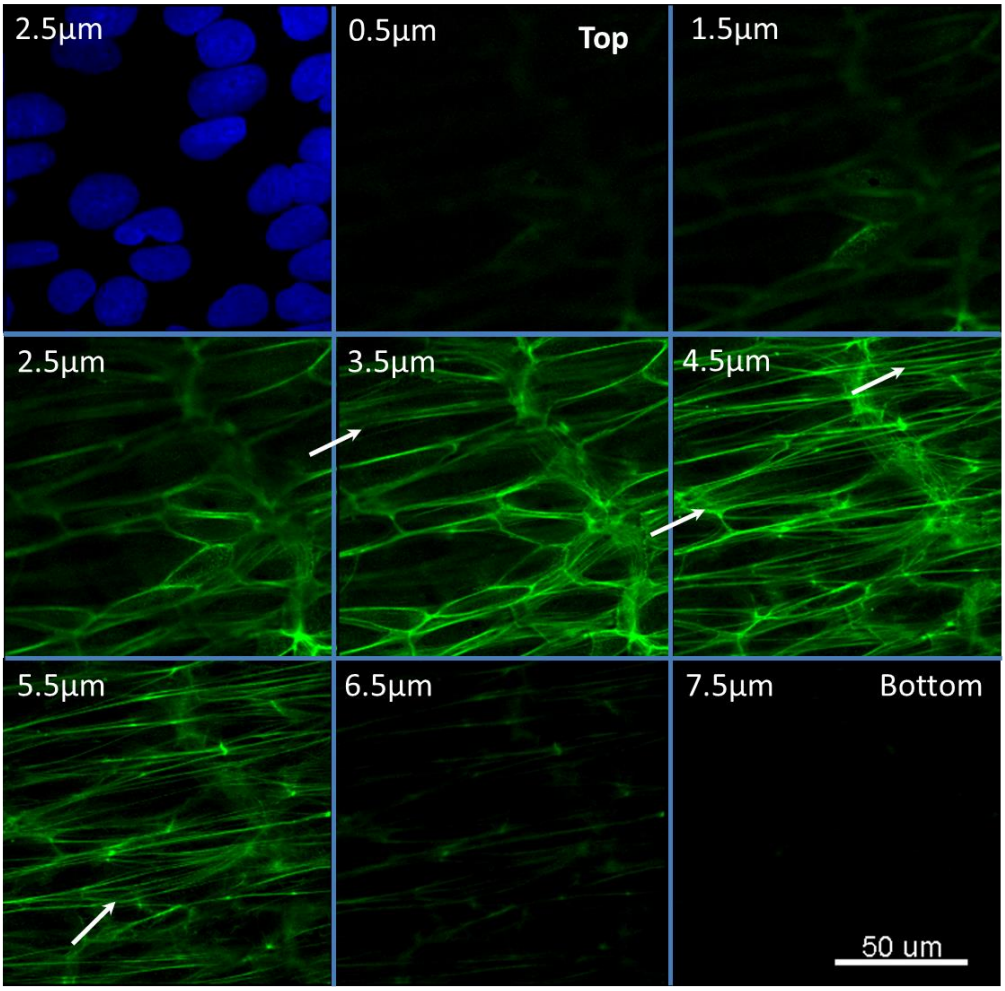

Figure 7.1 Gallery view of filamentous actin forming stress fibers on Day 1 of differentiation. **B)** Confocal stack of F-actin in hESCs grown on 250 nano-grating patterned PDMS substrates. The nucleus counterstained with DAPI in blue is shown for Z = 2.5µm.The slice is set at 1µm thickness and the Z-depth is shown on the image. The scale bar represents 50µm.

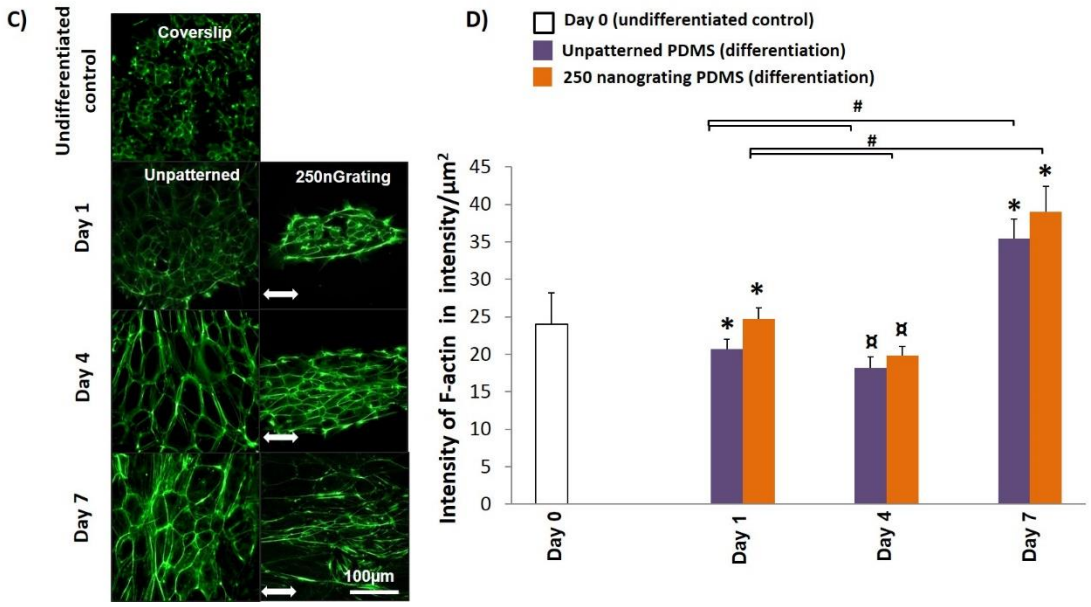

Figure 7.1 C) The hESCs grown on unpatterned and patterned substrates were fixed at Day 1, 4 and 7 and stained for F-actin with fluorescently labelled phalloidin, shown in green. The undifferentiated control shows hESCs grown on coverslips with matrigel and mTESR1 (expansion media). The scale bar represents 100µm. The bidirectional arrow represents the direction of grating axis. **D)** Intensity measurements of F-actin represented as intensity/µm^2, calculated using image J is plotted here. The F-actin intensity in hESCs grown on unpatterned and nano-patterned substrates was compared. * represents significance at $p<0.001$ as compared to Day 0, undifferentiated control, ¤ represents significance at $p<0.01$ as compared to control, # represents significance at $p<0.05$.

7.2.2 Increase in phosphorylated myosin light chain (pMLC) by Day 1 for cells grown on nano-patterned substrates

The hESCs grown on nano-patterned and unpatterned substrates were fixed at Day 1, 4 and 7 and immunostained for pMLC. The pMLC was mainly found around the periphery of the cells at all-time points whereas for hESCs grown on nano-patterned substrates, pMLC was observed on the periphery until Day 4 of differentiation and formed stress fibers by Day 7 (Figure 7.2 A). The semi-quantitative image analysis of fluorescence intensity of pMLC using ImageJ (Figure 7.2 B) showed that pMLC expression significantly increased from Day 4 to the highest intensity on Day 7 for cells grown on unpatterned substrates but for hESCs on nano-patterned substrates, the highest intensity of pMLC was observed on Day 4.

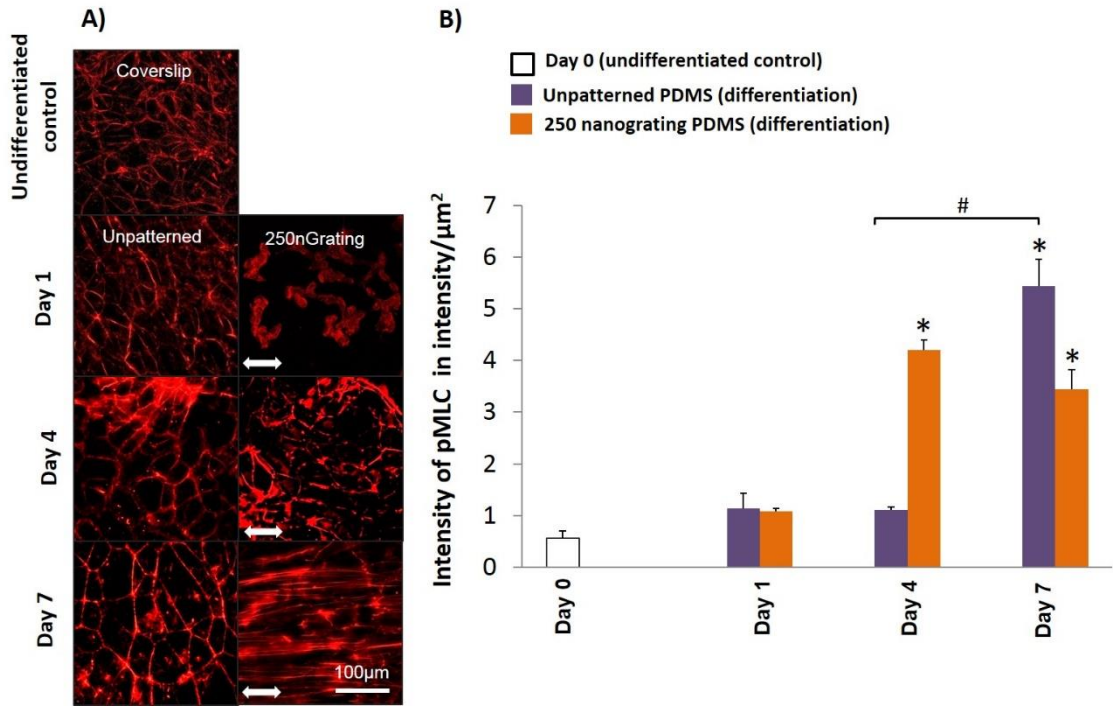

Figure 7.2 A) Human ESCs grown on unpatterned and 250 nano-grating patterned substrates were immunostained for phosphorylated myosin light chain (pMLC) at Day 1, 4 and 7. The scale bar represents 100µm. The bidirectional arrow represents the direction of grating axis. **B)** Intensity of hESCs expressing pMLC was quantified using ImageJ. * represents significance at $p<0.001$ as compared to the Day 0, undifferentiated control, # represents significance at $p<0.05$.

7.2.3 Vinculin expressing focal adhesions align to the nano-grating.

Vinculin was present at the cell-cell junction in undifferentiated cells while it was present along the periphery of the cell-cell junction at Day 1 and 4 in cells grown on nano-patterned and unpatterned substrates (Figure 7.3). On Day 7, more number of vinculin expressing focal adhesions were observed rather than vinculin at the cell- cell junctions. It was also observed that the vinculin-expressing cell-matrix focal adhesions were aligned along the grating axis whereas a random localisation was observed on unpatterned surfaces at Day 7 of differentiation.

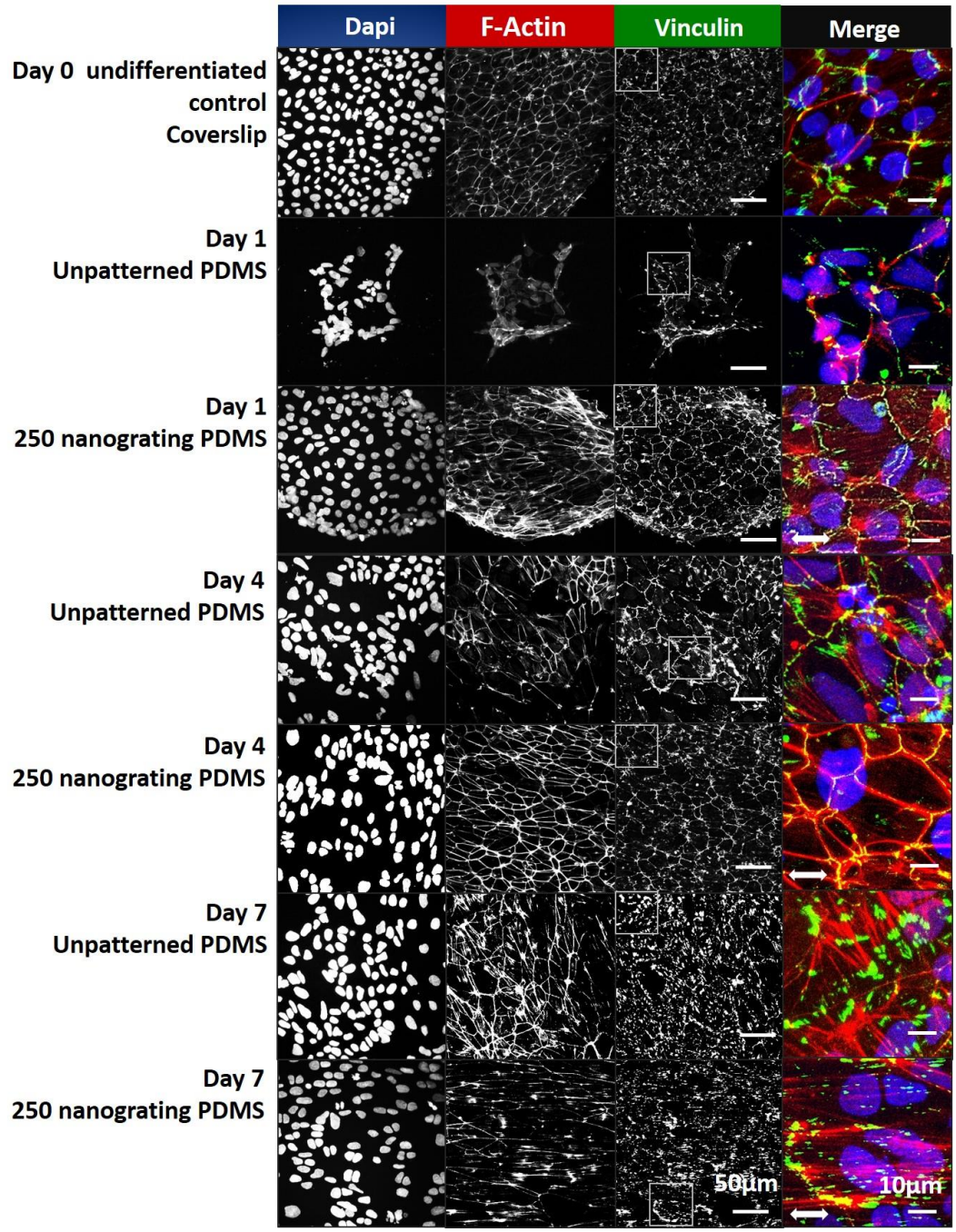

Figure 7.3 Human embryonic stem cells grown on patterned and unpatterned substrates were fixed at Day 1, 4 and 7; fluorescently labelled for F-actin is shown in red, immunostained vinculin are shown in green. The cells are counterstained with DAPI for nucleus shown in blue. The zoomed insert is shown in colour and merge of all the three channels. The scale bar represents 10µm for the zoomed images while it represents 50µm for other images. The bidirectional arrow represents the direction of grating axis.

7.2.4 Expression of immature focal adhesions is independent of acto-myosin contractility

The hESCs were treated with blebbistatin, ML-7 or Y-27632 and fixed at Day 4. Figure 7.4 A shows that the cells grown on unpatterned substrate had low vinculin expression when treated with blebbistatin, but the intensity of vinculin expressing focal adhesions was higher when treated with ML7. The hESCs on gratings were able to overcome the effect of blebbistatin and maintained the normal expression of vinculin, similar to cells not treated with inhibitors. The cells grown on gratings did not show a higher expression of vinculin expressing focal adhesion when treated with ML-7. The expression of early focal adhesions like pFAK and paxillin were not affected by treatment with inhibitors (Figure 7.4 B). It is to be noted that in general, there was higher expression of pFAK in cells grown on nano-patterned substrates as compared to cells grown on unpatterned substrates.

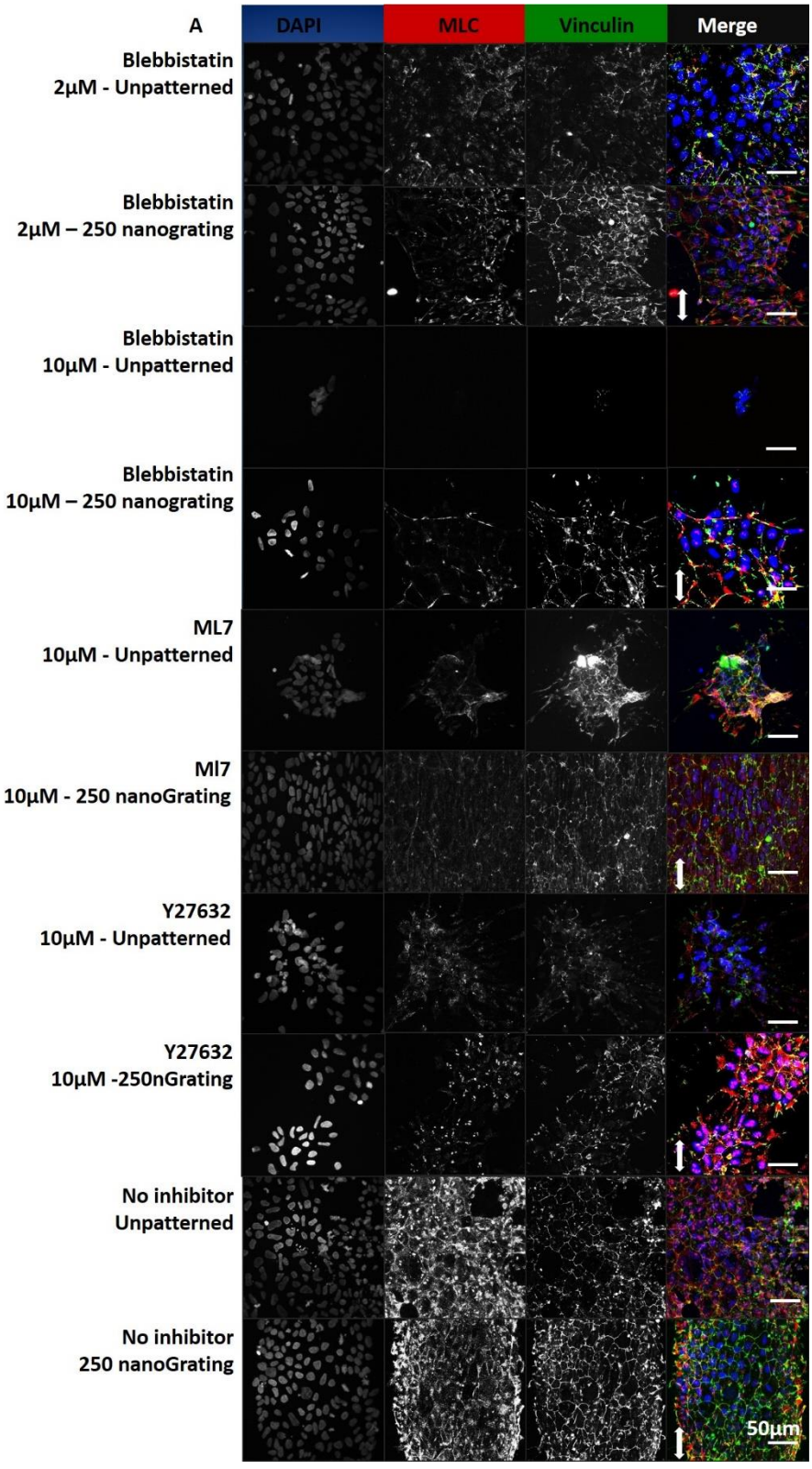

Figure 7.4 Panel of immunofluorescently stained images showing the expression of vinculin. **A)** Human ESCs immunostained for vinculin in green, pMLC in red and the nucleus counterstained with DAPI in blue. The scale bar represents 50µm. The bidirectional arrow represents the direction of grating axis.

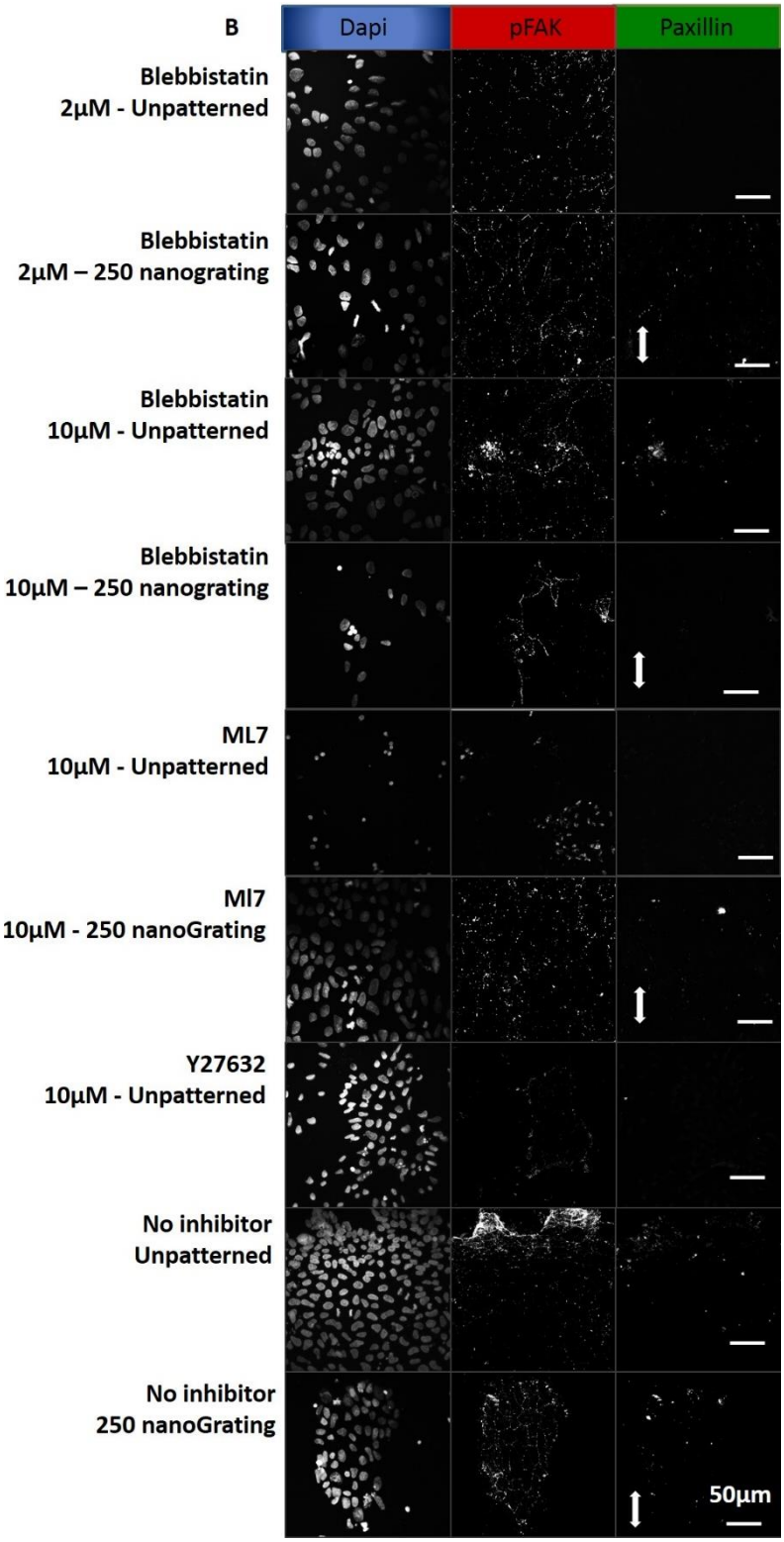

Figure 7.4 Panel of immunofluorescently stained images showing the expression of immature focal adhesions like pFAK and paxillin. **B)** Human ESCs stained with early focal adhesions like phosphorylated focal adhesion kinase (pFAK) and paxillin. The scale bar represents 50µm. The bidirectional arrow represents the direction of grating axis.

7.2.5 Grating topography aids the extension of neurites when treated with ROCK inhibitor or Blebbistatin

In the previous chapter, it was observed that the inhibition of the ROCK activity aided neuritogenesis. However, from Figure 7.5 A, the inhibition of acto-myosin contractility with blebbistatin in cells grown on gratings could also enhance expression of immature neuronal marker Tuj1 and were observed to have longer neurite extensions. The hESCs were still aligned to the grating axis when treated with ML-7 and Y-27632 but they lost alignment when treated with blebbistatin. When the hESCs were treated for longer duration (5 days) with different concentrations of blebbistatin (5, 10 and 20µM), Tuj1 expression was higher in cells grown on gratings as compared to cells grown on unpatterned substrates at a concentration of 10µM but not with the concentrations of 5 and 20µM (Figure 7.5 B).

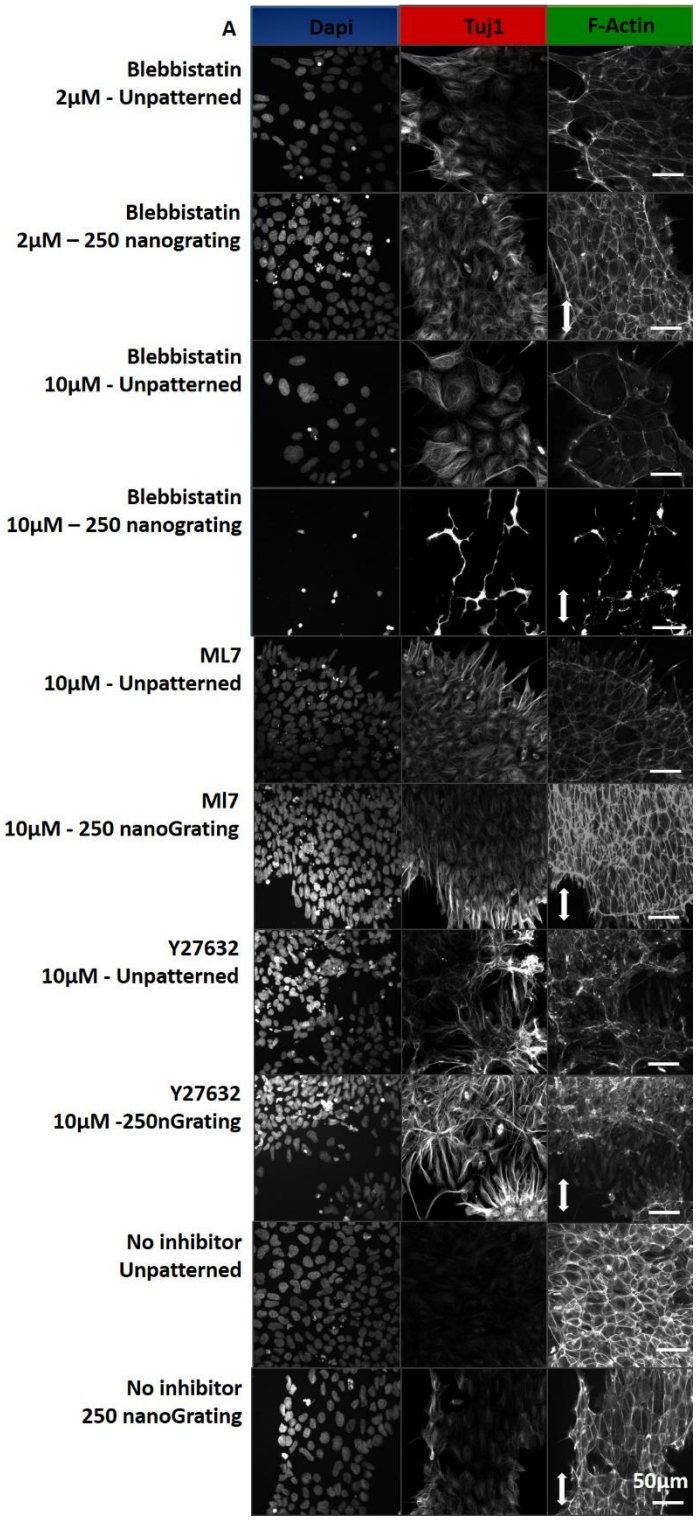

Figure 7.5 H1 grown on unpatterned and nano-patterned substrates were treated with blebbistatin, ML-7 and Y-27632 for 2 days and fixed at Day 4. **A)** The cells were immunostained for immature neuronal marker, Tuj1 and F-actin. The samples were counterstained with DAPI for visualisation of nucleus. The scale bar represents 50µm. The bidirectional arrow represents the direction of grating axis.

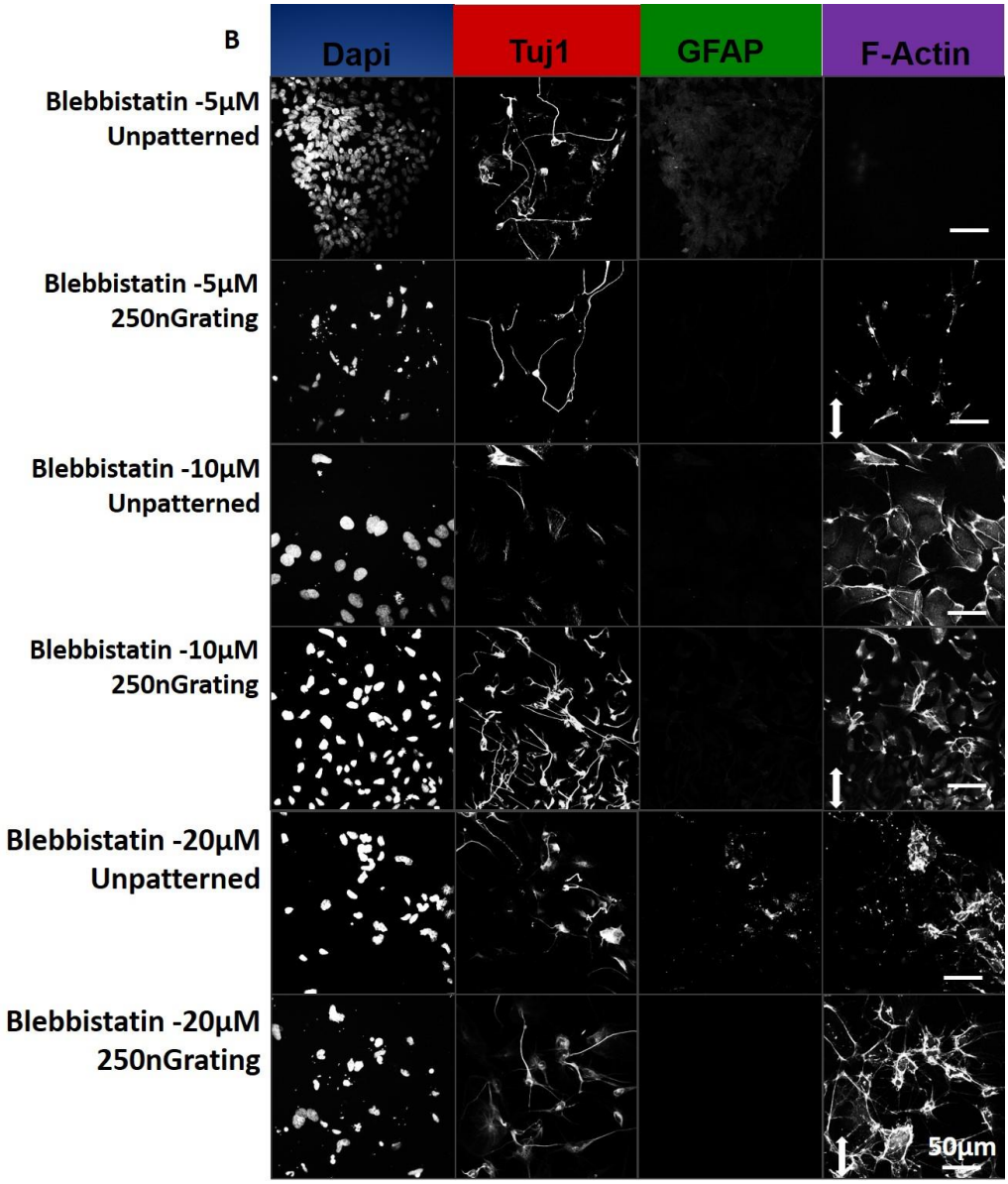

Figure 7.5 The hESCs grown on unpatterned and nano-patterned substrates were treated with 2, 10 and 20µM concentrations of blebbistatin for 5 days and fixed on Day 7 **B)** The cells were immunostained for early neuronal marker, Tuj1; glial marker, GFAP and F-actin. The samples were counterstained with DAPI for visualising the nucleus. The scale bar represents 50µm. The bidirectional arrow represents the direction of grating axis.

7.2.6 Maturation of neurons is myosin dependent and is enhanced when hESCs are grown on nano-gratings.

The human ESCs grown on nano-grating substrate showed lower expression of MAP2 when exposed to myosin II and pMLCK inhibitors. However, the MAP2 expression in cells grown on unpatterned and nano-patterned substrate was maintained or enhanced when exposed to ROCK inhibitor (Figure 7.6 A). By Day 4, the expression of MAP2 was low even on samples without inhibitor treatment irrespective of being grown on patterned and unpatterned substrates. When the exposure to blebbistatin was increased to 5 days (Figure 7.6 B), the cells grown on gratings were able to overcome the effect of even high concentrations of the drug (20µM) more effectively and express the mature neuronal marker MAP2. The EdU staining showed that the proliferating population were present when grown on either the patterned or unpatterned substrates.

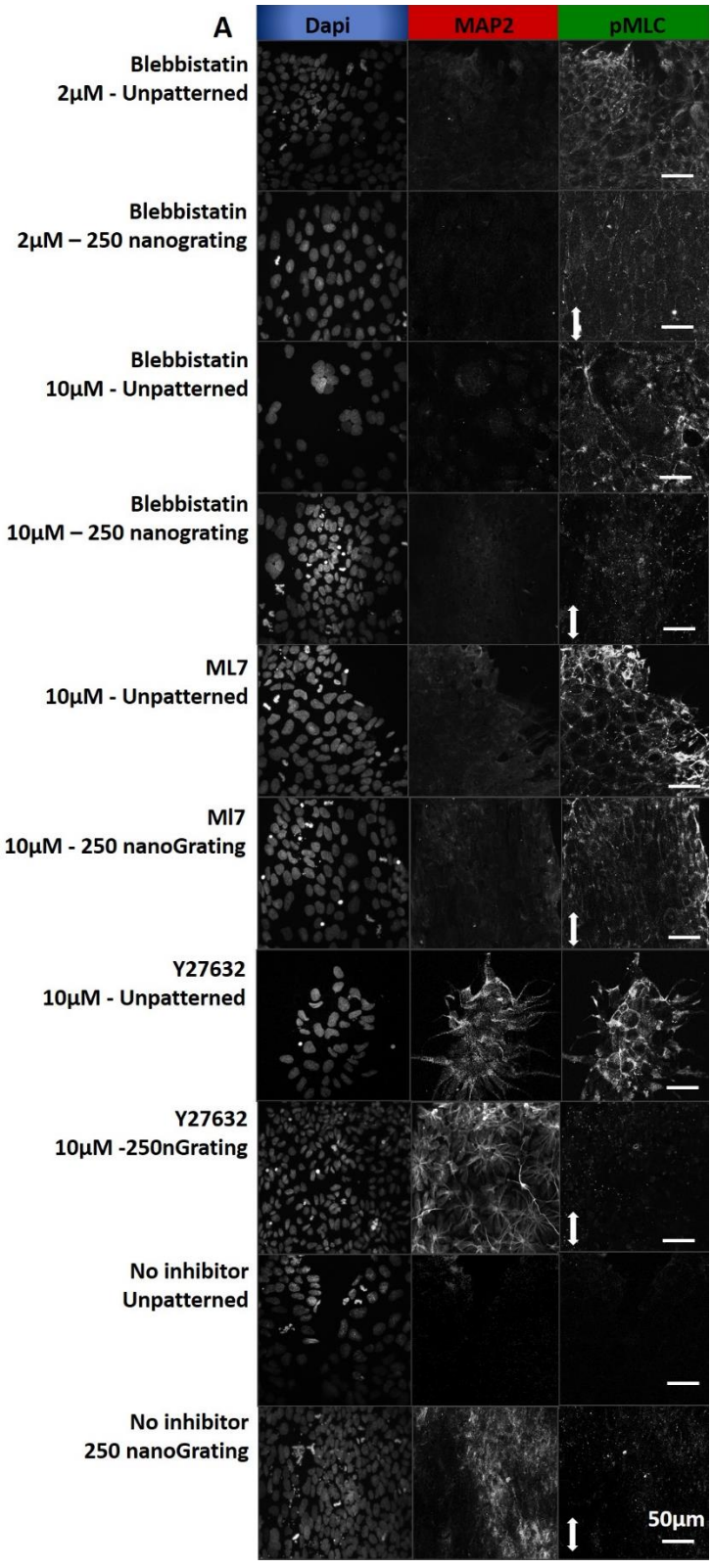

Figure 7.6 A) The hESCs were treated with inhibitors for 2 days and fixed on Day 4. The samples were immunostained for mature neuronal marker, MAP2 and phosphorylated myosin light chain, pMLC. The samples were counterstained with DAPI for nucleus. The scale bar represents 50µm. The bidirectional arrow represents the direction of grating axis.

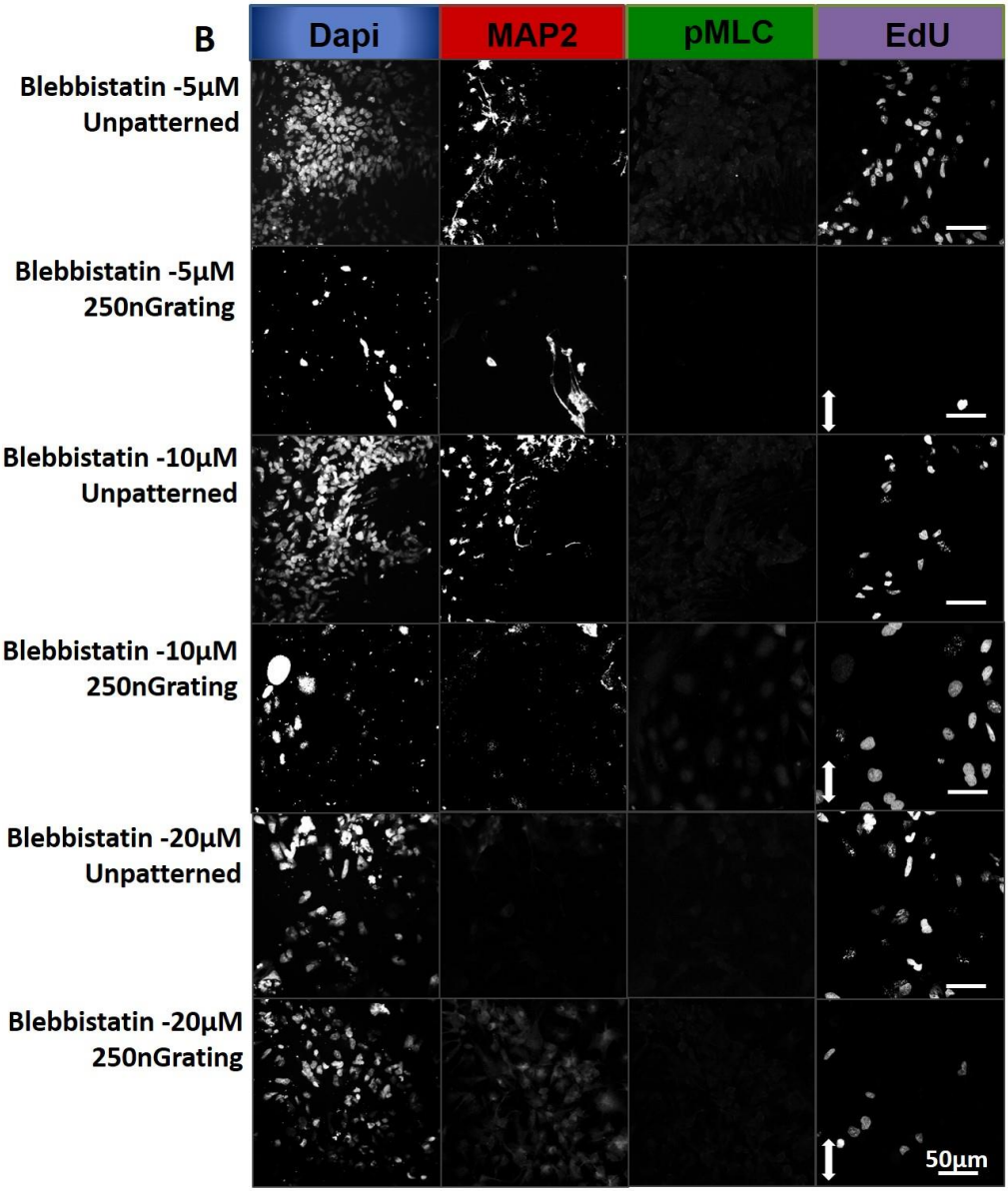

Figure 7.6 B) The hESCs were treated with different concentrations of blebbistatin for 5 days and fixed on Day 7. The samples were immunostained for MAP2, pMLC and EdU. The samples were counterstained with DAPI for nucleus. The scale bar represents 50µm. The bidirectional arrow represents the direction of grating axis.

7.2.7 Temporal gene and protein expression of mature neuronal marker, MAP2, and pluripotent transcription factor, nanog.

The MAP2 protein expression and alignment of the hESCs grown on nano-patterned substrates were the highest at Day 4 (Figure 7.7 A). The quantitative real time RT-qPCR gene expression results are shown in Figure 7.7 B as fold increase (relative gene expression normalised to the gene expression on unpatterned PDMS and GAPDH (endogenous control). , For cells grown on 250 nano-grating substrates, the MAP2 gene expression increased at Day 4 and again decreased by Day 7 whereas the nanog gene expression decreased over time (Figure 7.7 B). A similar trend of MAP2 gene expression was also seen when hESCs were grown on the 2µm gratings (Appendix B, Figure B.2).

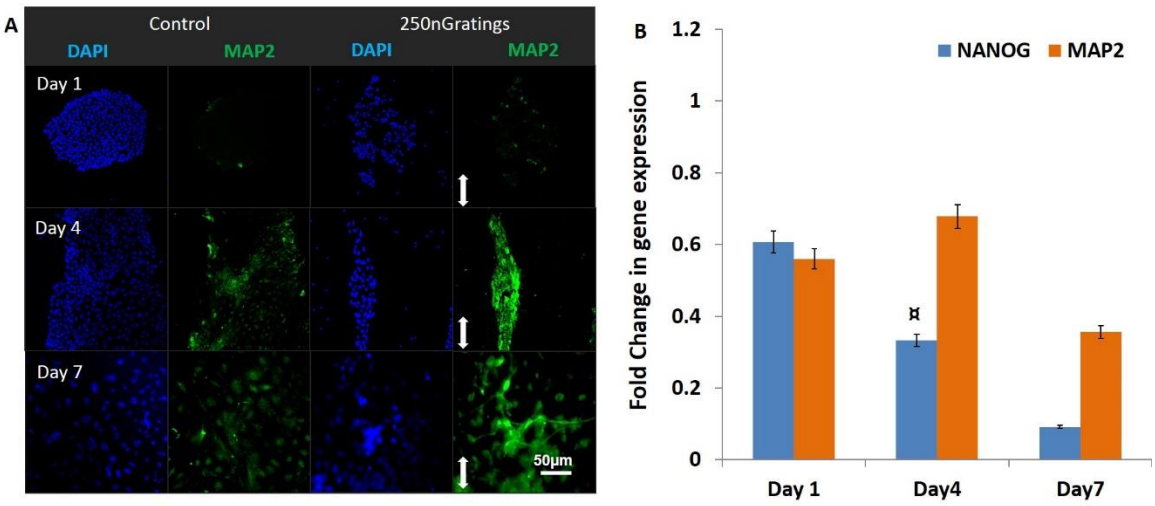

Figure 7.7 A) The temporal changes in protein expression of MAP2 on unpatterned and nano-patterned substrates during neuronal differentiation of hESCs. The samples are immunostained in green for MAP2 and the nucleus is counterstained with DAPI in blue. The scale bar represents 50µm. The bidirectional arrow represents the direction of grating axis. **B)** The plot shows the gene expression fold change for hESCs grown on nano-patterned substrates, obtained from real time RT-QPCR. The blue bar shows the pluripotent transcription factor, nanog gene expression while the orange bar shows the neuronal marker, MAP2 gene expression. ¤ represents significance at $p<0.01$ as compared to gene expression at Day 1 of neuronal differentiation.

Nanog (pluripotent marker and transcription factor located in the nuclei) protein expression was interestingly observed in the cytoplasm as well as nucleus (Figures 7.7 C, D, E and F). The cytoplasmic fraction of nanog protein increased as differentiation proceeded. The hESCs grown on unpatterned substrates have a more spread morphology by Day 4, while cells grown on patterned substrates are still confined to a compact, aligned colony. The intensity of nuclear and cytoplasmic nanog was plotted in Figure 7.7 D and E. The cytoplasmic and nuclear nanog followed a decreasing trend for cells grown on the nano-gratings. The cells grown on the unpatterned substrates showed an increase in cytoplasmic and nuclear nanog intensity at Day 4 followed by a decrease on Day 7. The ratio of nuclear: cytoplasmic nanog intensity, from Figure 7.7 F showed that the rate of decrease in nanog is faster for cells grown on unpatterned substrates than for cells grown on patterned substrates.

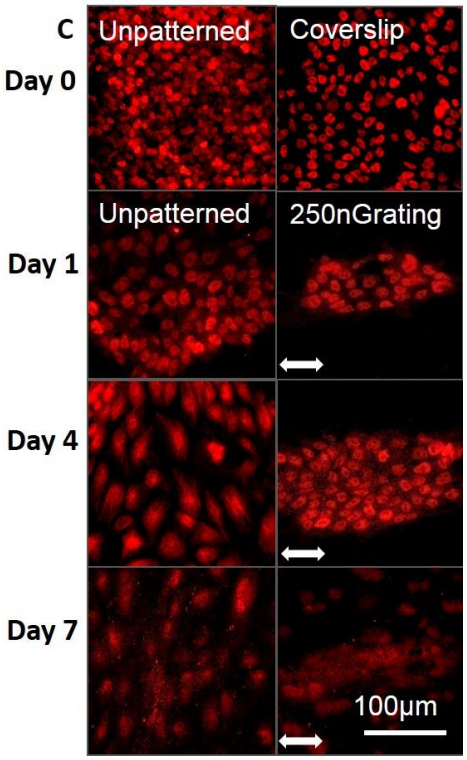

Figure 7.7 The temporal protein expression of the pluripotent transcription factor, nanog, in hESCs grown on unpatterned and nano-patterned substrates. **C)** The samples are immunostained for nanog in red and the white arrows indicate the direction of grating axis. The scale bar represents 100µm. The bidirectional arrow represents the direction of grating axis.

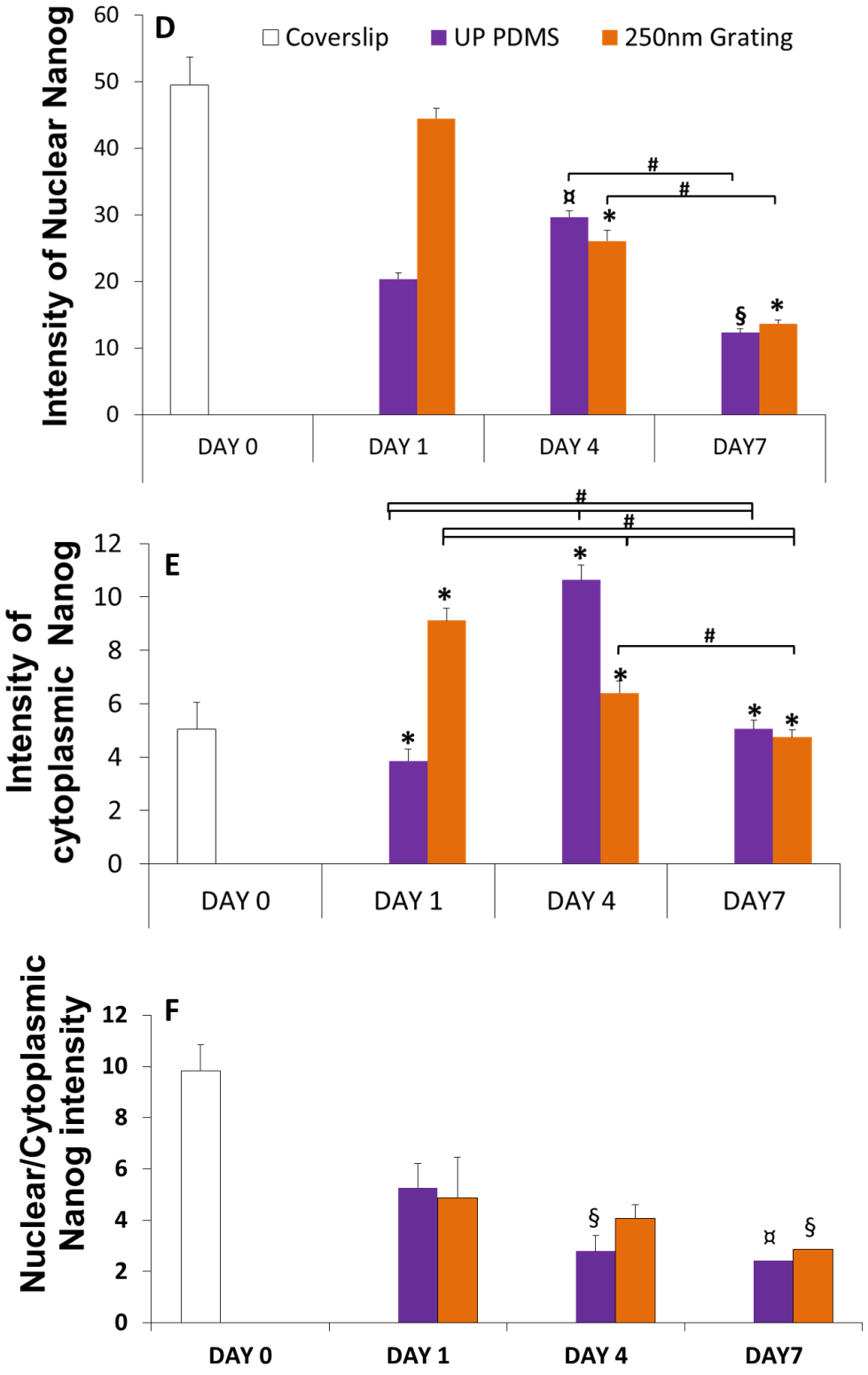

Figure 7.7 Intensity analysis plots for nanog expression in the cytoplasm and nucleus when grown on unpatterned or patterned substrates at Day 1, 4 and 7. **D)** The intensity plot of nanog protein in the nucleus. E) The intensity plot of nanog protein in the cytoplasm. F) The ratio of intensity of nanog protein in nucleus to the intensity of nanog in the cytoplasm. * represents significance at $p<0.001$ as compared to Day 0, undifferentiated control, ¤ represents significance at $p<0.01$ as compared to control, § represents significance at $p<0.05$ as compared to control, # represents significance at $p<0.05$.

7.2.8 Temporal changes in the nucleus morphology and size during neuronal differentiation of hESCs

The changes in the cytoskeleton could be correlated with the changes in the nucleus. The circularity index (values closer to 1 indicate more circularity) showed that the undifferentiated cells were more circular (0.8) as compared to the cells differentiated on nano-gratings on Day 4 and 7 (0.70 and 0.73 respectively, Figure 7.8 A). The hESCs were more circular on unpatterned substrates by Day 4 (0.76) but reached similar values of circularity (0.72 for cells on unpatterned substrates) as compared to cells grown on gratings by Day 7. The elongation index (higher values represent higher elongation) correlates with the circularity values in trend but the elongation of hESC nuclei on nano-patterned or unpatterned substrates reached a high value of elongation index 0.73 for cells on gratings and 0.54 for cells on unpatterned substrates by Day 1 of differentiation but no significant change was observed after that time point (Figure 7.8 B). However, the elongation of hESC nucleus on nano-patterned substrates was much higher (0.73) than for the nucleus of cells grown on unpatterned substrates (0.54).

The nuclei were more aligned (40%) by Day 7 of neuronal differentiation when grown on nano-patterned substrates (Figure 7.8 C). The cells grown on unpatterned substrates showed an increase in nucleus and cell area at Day 4 (258.4μm^2 for nucleus area and 1050.4μm^2 for cell area) but showed a slight decrease at Day 7 (211.1μm^2 for nucleus area and 864.1μm^2 for cell area, Figures 7.8 D and E). The cells grown on nano-patterned substrates showed an increase in nucleus and cell area between Day 1 (175μm^2 for nucleus and 493.1μm^2 for cell area) of differentiation to Day 4 (225.4μm^2 for nucleus and 918.7μm^2 for cell area). The nucleus and cell area showed fewer changes at Day 7 (237.1μm^2 for nucleus area and 948.9μm^2 for cell area) for cells grown on nano-patterned substrates. It however has to be noted that the areas of nucleus and cell were

lesser (211.1μm^2 for nucleus area and 864.1μm^2 for cell area) for hESC grown on unpatterned substrates than for hESC grown on patterned substrates (237.1μm^2 for nucleus area and 948.9μm^2 for cell area) at Day 7. The ratio of nuclear : cytoplasmic area (Figure 7.8 F) decreased from Day 1 (0.49 for cells on unpatterned substrates, 0.42 for cells on nano-gratings) to Day 4 (0.28 for cells on unpatterned substrates, 0.30 for cells on nano-gratings).

The nucleus volume was significantly higher for cells grown on unpatterned substrates as compared to cells grown on the nano-patterned substrates. The nucleus volume (Figure 7.8 G) increased significantly from Day 1 ($73x10^3\mu m^3$) to Day 4 ($10x10^3\mu m^3$) and then decreased to smaller volumes (as compared to undifferentiated cells whose nucleus volume measured $44x10^3\mu m^3$) by Day 7 ($35x10^3\mu m^3$) for cells grown on unpatterned substrates. The nucleus volume of hESCs grown on nano-patterned substrates showed a significant decrease in volume on Day 1 ($19x10^3\mu m^3$) of differentiation as compared to undifferentiated cells ($44x10^3\mu m^3$). The nucleus volume reached the highest value of $71x10^3\mu m^3$ by Day 4 of differentiation and then decreased 1.5 folds ($47x10^3\mu m^3$) by Day 7 of neuronal differentiation when cells were grown on nano-patterned substrates.

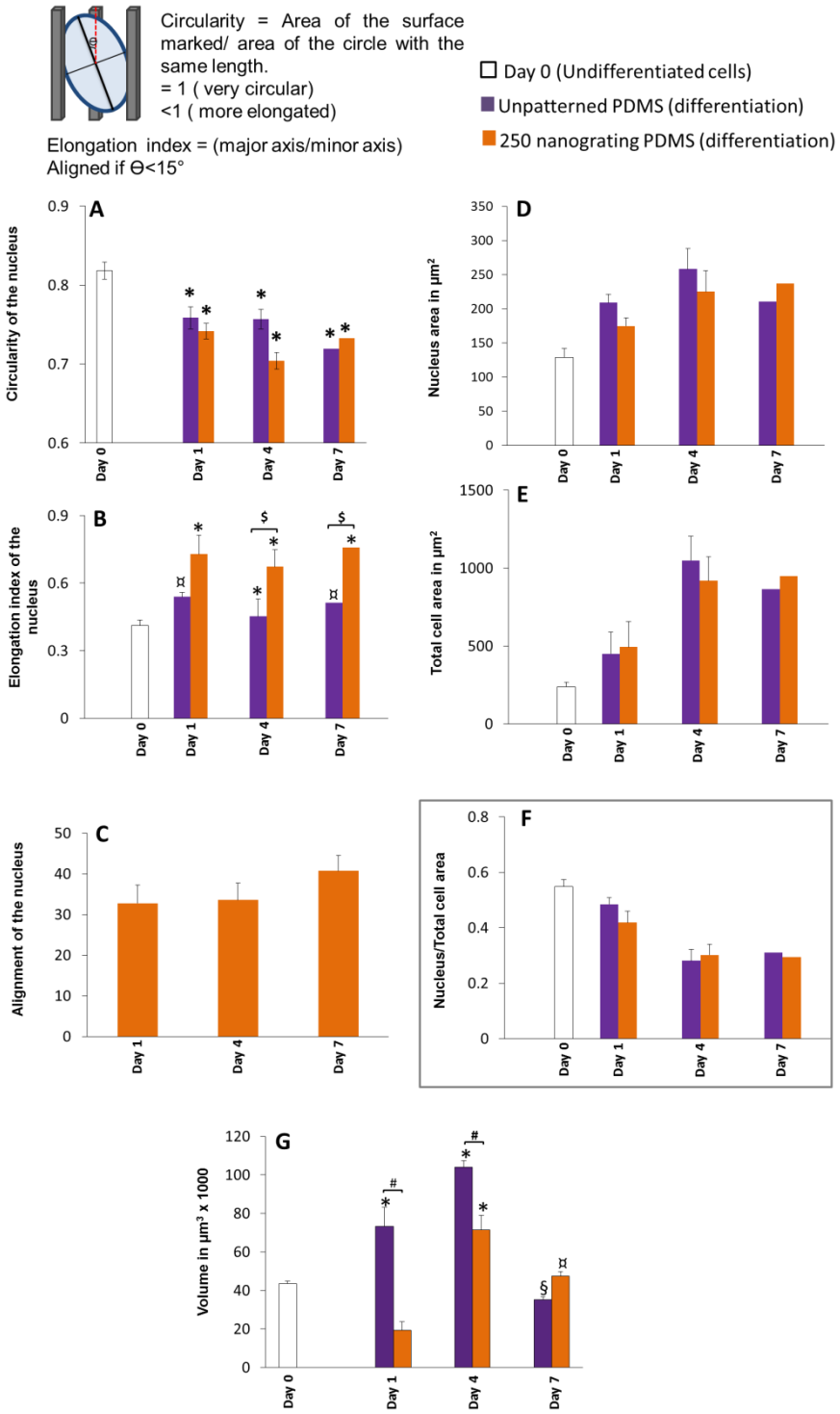

Figure 7.8 Temporal changes in nucleus morphology of hESCs grown on unpatterned and nano-patterned substrates during differentiation. **A)** The Figure shows the plot of nucleus circularity. **B)** The Figure shows nucleus elongation of hESCs. **C)** The Figure shows the **D)** The Figure shows the changes in the area of nucleus. **E)** The Figure shows the temporal changes in the total area of the cell. **F)** The Figure shows the ratio of nucleus area to total cell area. **G)** The Figure shows the temporal changes in the nucleus volume. * represents significance at $p<0.001$ as compared to Day 0, undifferentiated control, ¤ represents significance at $p<0.01$ as compared to control, § represents significance at $p<0.05$ as compared to control, # represents significance at $p<0.05$. $ represents significance at $p<0.01$.

7.2.9 Temporal changes in the histone markers during neuronal differentiation of hESCs

The hESCs grown on unpatterned and nano-patterned substrates were fixed at Day 1, 4 and 7; immunostained for two histone markers, histone 3 trimethylation on Lysine 9 (H3K9me3) and histone 3 acetylation on Lysine 9 (H3K9ac). Figure 7.9 shows that both the histone markers were strongly visible in the undifferentiated state while they were much weaker in the hESCs grown on unpatterned as well as patterned substrate in the presence of differentiation media, N2B27.

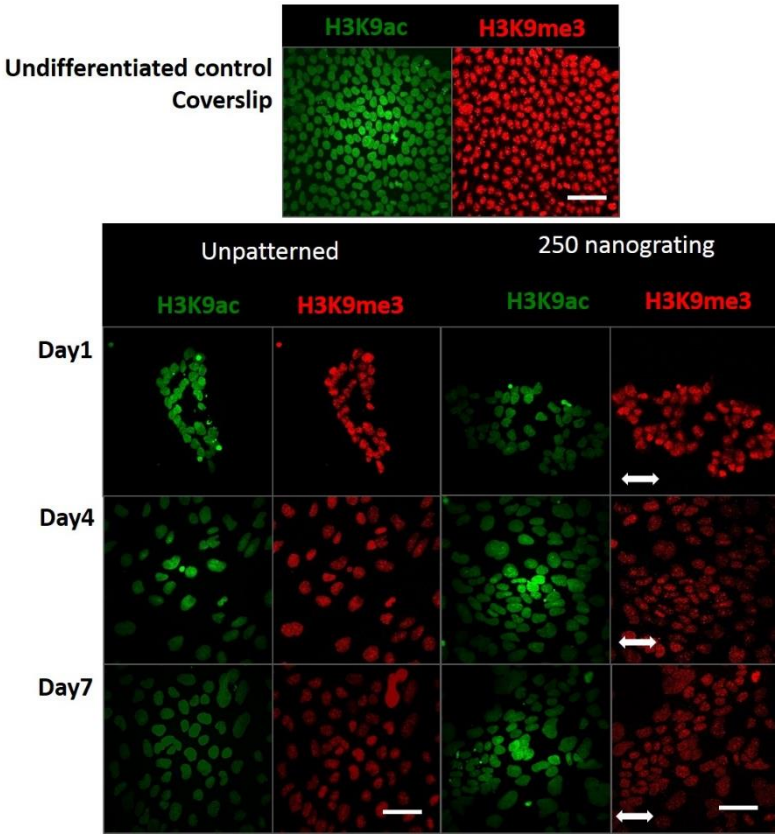

Figure 7.9 The hESCs were immunostained for histone methylation (H3K9me3) in red and acetylation marks (H3K9ac) in green. The scale bar represents 50µm. The bidirectional arrow represents the direction of grating axis.

7.3 **Discussion**

The hESCs when grown on nano-patterned substrates in the presence of N2 and B27 supplements preferentially differentiate into neurons than astrocytes. The neuronal maturation was also higher when hESC were grown on substrates with nano-sized gratings. From Chapter 6, it is understood that the acto-myosin contractility plays an important role in neuronal maturation while the ROCK plays a role in the neurite extension. This chapter focuses on the role of nano-grating topography in improving the efficiency of differentiation, by increasing the neuron: astrocyte ratio and the MAP2 positive population in a short time of 7 days. It is hypothesised that the hESCs seeded on nano-gratings have a higher contractility, resulting in elongation and alignment of cytoskeletal components and the nuclei along the grating during neuronal differentiation. It is speculated that the cytoskeletal contractility causes changes in the nucleus morphology and histone modifications thereby promoting neuronal differentiation.

The confocal stack images (Figure 7.1 A and B) clearly show the formation of cortical actin around the periphery of the human ES cells on the unpatterned substrate, while stress fibers were evident in hESCs grown on the nano-patterned substrate at the early stage of neuronal differentiation (Day 1). The intensity of F-actin in the hESCs grown on either unpatterned or nano-patterned substrates showed a significant increase from Day 4 to Day 7. The intensity of F-actin reached the highest value only by Day 7, and the stress fibers were evident only after 4 days of differentiation on unpatterned substrates. On the contrary, the stress fibers were formed as early as Day 1 in cells grown on nano-patterned substrates. The interesting observation is that the phosphorylated myosin light chain, which binds to F-actin to increase the acto-myosin contractility [241, 242], reached the maximum intensity by Day 4 when hESCs were grown on nano-patterned substrates. The pMLC expression reached maximum intensity

(Figure 7.2 B) only on Day 7 for hESCs grown on unpatterned substrates. There was early onset of acto-myosin contractility in cells grown on nano-patterned substrates as compared to unpatterned substrates. The results from Chapter 6 show that acto-myosin contractility plays a role in the expression of MAP2 and vinculin expressing focal adhesions. The increase in the number of mature neuronal population when grown on nano-gratings could be speculated to be due to the early onset of acto-myosin contractility.

The nano-grating topography increased the cytoskeletal contractility of hESCs and hence is speculated that the vinculin from cell-cell junction will be recruited to the mature focal adhesions. The vinculin expressing focal adhesions were also aligned to the grating axis by Day 7 of neuronal differentiation (Figure 7.4 A). Interestingly, the hESCs grown on nanopatterned substrates showed less reduction in the myosin contractility as compared to cells grown on unpatterned substrates (Figure 7.4 A). The nano-grating topography might help to partially recover the loss of contractility force, in spite of treatment with strong and specific inhibitors like blebbistatin. On the other hand, the cells grown on unpatterned substrates had a significant decrease in myosin contractility when treated with blebbistatin. The hESCs treated with blebbistatin showed lack of polarisation but not when treated with ML-7 or Y-27632.

Studies done by Ferrari *et al*. on PC12 neurite polarisation have shown that focal adhesions respond to the contractility forces by sensing and confirming the cell morphology to the underlying substrate [243]. In this study where a nano-grating substrate was used, the vinculin expressing focal adhesions could sense the direction of force and hence align the stress fibers along the grating axis through a feedback mechanism with the acto-myosin components. The expression of focal contacts and the

organisation of stress fibres in response to substrate geometry and topography has long-term effects on stem cell differentiation [237].

The changes in the cytoskeletal contractility were followed by changes in the nucleus shape, size and expression of histone markers. The undifferentiated hESCs are characterised by a very high nuclear to cytoplasmic ratio (0.5) [244]. The intermediate filaments and filamentous actin are coupled to the nucleus, transduce the mechanical signals from the substrate to the nucleus [245]. The increase in contractility on Day 4 correlates to a decrease in the ratio of nucleus area: cytoplasm area of the cells grown on patterned and unpatterned substrates, suggesting that the cells are increasing in size to become more differentiated. The review by M.J. Dalby on the mechanotransduction of topographical cues to a cell suggests that the increase in genome response correlates to the extent of deformation of the cell by the topography [237].

The decrease in cell area on unpatterned substrates by Day 7 correlates with the increase in acto-myosin contractility for hESCs on unpatterned substrates. The hESCs grown on patterned substrates showed a decrease in cell area as early as Day 1, which suggests that the cells were subjected to high contractility forces in an earlier stage of differentiation when grown on nano-grating substrates.

Interestingly, the volume of the nucleus reached the highest value by Day 4 of differentiation when grown on both unpatterned and nano-patterned substrates. The nucleus volume decreased by 2.24 folds at Day 1 of differentiation on nano-patterned substrates while it increased by 1.7 folds for cells grown on unpatterned substrates. Studies done by Trindade *et al*. have shown that during embryonic stem cell differentiation global rates of transcription would change by varying the nucleus volume while the transcription site density remains the same [246]. The same group also showed

that the ESCs exhibited either higher or lower nucleus volume depending on the differentiation pathway that the cell was subjected. In this study we observe that the dynamics of change in nucleus volume is different for hESCs grown on unpatterned versus patterned substrates. It could be speculated that the hESCs differentiate into neurons through different pathways when grown on unpatterned substrates as compared to patterned substrates.

Apart from morphological changes, the histone markers also showed temporal changes in their expression during neuronal differentiation of hESCs. The histone markers H3K9me3 and H3K9ac were expressed as punctae in the nuclei (Figure 7.9), which decreased as hESCs underwent differentiation. Studies conducted by Lagarkova *et al*. and Yeo *et al*. show that undifferentiated ES cells have active DNA methylation, while the demethylation may regulate the transcription of key developmental genes [247, 248]. A comprehensive review by Peterson *et al*. suggested that the site specific combination of histone modifications correlates with specific biological functions. The trimethylation of Lysine 9 on Histone 3 is associated with transcriptional repression, while the acetylation at Lysine 9 of histone 3 correlates to increase in histone deposition. In this study, the undifferentiated hESCs showed a higher expression of methylation markers, which might correlate with the transcriptionally repressive state of differentiation genes. These markers were decreased during neuronal differentiation of hESCs.

It is well known that the substrate topography acts at an early time-point on the cytoskeletal components followed by changes in the nucleus, thereby directing the stem cell behaviour and function. The chromatins are mechanically linked to the cytoskeleton through the lamin network and are responsive to forces transduced from the surrounding cell environment [249]. However, the expression of lamin A/C during neuronal

differentiation of hESCs occurred only during later stage of differentiation (14 days, shown in Appendix B, Figure 3) but not at Day 7. It is speculated that the cytoskeleton interacts with the nuclear membrane through different components in ESCs as compared to lamin A/C in adult stem cells. This might suggest that when the cells were presented with topography along with biochemical cues like N2 and B27 supplements, they undergo a different neuronal differentiation pathway as compared to cells grown on unpatterned substrates with just biochemical cues. The results from Chapter 5 clearly indicated that during neuronal differentiation of hESCs on unpatterned substrates, a mixture of neuronal and glial population was derived, whereas when cells were grown on nano-gratings, the hESCs were preferentially differentiated into neurons.

7.4 **Conclusion**

The acto-myosin contractility was observed to be higher in hESCs grown on nano-grating substrates as compared to those grown on unpatterned substrates. From the previous chapter, it was understood that MAP2 expression was dependent on the acto-myosin contractility. In this chapter it was elucidated that the higher number of MAP2 positive cells on nano-gratings correlated with the early onset of acto-myosin contractility. The inhibitor study also indicated that the alignment and elongation of neurites were affected with changes in contractility. This study went a step further to understand how the mechanical forces from the substrate were transduced to the nucleus. The hESCs grown on nano-gratings had an increase in volume of the nucleus on Day 4 that also corresponded with the highest expression of activated myosin light chain. It was also observed that the pluripotent epigenetic marks were decreased faster for cells grown on nano-gratings. This study has contributed significantly to the understanding of mechanotransduction of forces from the underlying topographical substrate to hESCs during neuronal differentiation.

Chapter 8

8. Conclusion and Future Work

8.1. Conclusion

The extracellular environment of the stem cell niche *in vivo* regulates the stem cell behaviours like adhesion, migration, proliferation and differentiation. A bioengineer's approach to selectively differentiate the stem cells to a particular lineage would involve an assortment of scaffolds, stem cells and growth factors. In the first part of the study, which aimed in deriving neurons from hESCs more efficiently, focuses is laid on the characterisation of hESCs and optimise the neuronal differentiation on the multi architectural (MARC) chip containing fields of topographies made of various geometries, spacing and dimensions. The topographies chosen were based on the literature for both maintenance and differentiation of stem cells, including anisotropic patterns like the gratings and isotropic patterns like the pillars and wells. The MARC chip can be used for high throughput screening of desired stem cell behaviour at low cost and completely customisable design of the chip that can easily fits into a 6 well multiwell plate. From this study it was understood that for neuronal differentiation of ESCs, neuronal supplements were necessary to complement the topographical cues. The results from "conventional method" of differentiation also indicated that when hESC derived neural progenitor cells were subjected to topographical cues, most of them differentiated into neurons irrespective of the topographical cue. This might suggest that the stage at which topographical cues are presented is important. The aim of the second part of the study was to determine the optimal geometry and size of topographical cues for neuronal or glial differentiation of hESCs using the PDMS MARC chip. The gene and protein expression from the results of RT-qPCR and immunostaining, respectively,

indicated that the anisotropic patterns favoured higher neuronal differentiation as seen from the higher neuron: astrocyte ratio (N:A, the ratio of Tuj1 positive cells : GFAP positive cells). The isotropic patterns favoured more glial differentiation as seen from the lower N: A ratio. These results were verified in two different cell lines, H1 and H9. The "direct differentiation" method allowed the derivation of neurons or glial cells in from hESCs more specifically (neurons: astrocyte population) depending on the topography used in a relatively short time (7 days) as compared to the "conventional method".

The third part of the study presented in this thesis aims to understand the role of acto-myosin contractility in neuronal differentiation of hESCs without topographical cues. From the literature, it is understood that the cells sense their ECM through integrins and focal adhesions. The mechanical cues from the underlying substrate is transduced to the cells dynamically in a short time ranging from seconds to minutes with the help of focal adhesion complexes and cytoskeletal elements, actin and myosin. This is one of the first studies to my knowledge presenting a temporal analysis of cytoskeletal components like actin and non-muscle myosin II in hESCs during neuronal differentiation. The filamentous actin remains as cortical actin during the first half of differentiation while it starts forming stress fibers between Day 4 to Day 7 of differentiation. The F-actin expression corresponds with the expression of activated non-muscle myosin II, as seen from the immunostaining of pMLC (phosphorylated myosin light chain) in hESCs. The inhibitor study with blebbistatin further confirms that MAP2, a mature neuronal marker expression is dependent on the acto-myosin contractility, in accord with the hypothesis. It is speculated that the acto-myosin contractility enforced by the ROCK activity, causes changes in the nucleus resulting in changes in gene expression. The MAP2 expression was dependent on the acto-myosin contractility and

hence could be speculated that the contractile force is necessary for organisation of tubulin into microtubules (seen in mature neurons). Having understood the general role of cytoskeletal components in sensing the underlying substrate, we extended the study to determine the role of nano-gratings in increasing the mechanical cues to achieve a rapid neuronal differentiation. The hESCs grown on nano-grating PDMS substrates were compared with previously established results on unpatterned PDMS substrates. The differences were distinct and significant especially in the expression of stress fibers (on Day 1) and expression of pMLC (peak at Day 4). The vinculin-expressing focal adhesions were also arranged anisotropically along the grating axis, which was disrupted with the use of inhibitors like blebbistatin, ML-7 and Y-27632. The continuous exposure of hESCs to topography allowed the cells to overcome the effect of blebbistatin and expressed higher level of actin and vinculin (at the levels comparable to cells not treated with any inhibitors).It is speculated that the maturation of neurons occurred faster for hESCs grown on nano-grating substrates because of the increase in acto-myosin contractility contributed by the topography at an early stage. The hESCs were able to elongate and align along the grating axis because of the increased acto-myosin contractility observed in hESCs grown on nano-grating substrates. The expressions of histone marker, H3K9me3, associated with pluripotency factors were also decreased and the volume of the nucleus showed a dynamic response in correlation with the expression of pMLC for hESCs grown on nano-gratings.

In conclusion, this study has contributed significantly in designing a simple high-throughput method for screening topographies. The MARC chip could be used to compare the effect of various topographies more accurately by subjecting all of them to the same experimental conditions. Fast, cheap and easy design allows the screening to be done more efficiently. This chip has been applied for the study of neural

differentiation in hESCs and it was clearly observed that anisotropic patterns supported the neuronal differentiation while the isotropic patterns supported the glial population. The mechanistic insights during neuronal differentiation of hESCs indicate the importance of providing topographical cues that can substantially increase the acto-myosin contractility in order to increase the mature neuronal population. The nano-grating not only increases the acto-myosin contractility but also provides a directional guidance for the stem cells allowing them to align and elongate along the grating axis during neuronal differentiation. A schematic summarising the results is shown in Figure 8.1 A, B and Figure 5.6. This study can be extended for longer time points with additional growth factors to study the derivation of region specific neurons that could be used for *in vitro* drug testing, understanding the molecular mechanisms of differentiation and the stem cell niche.

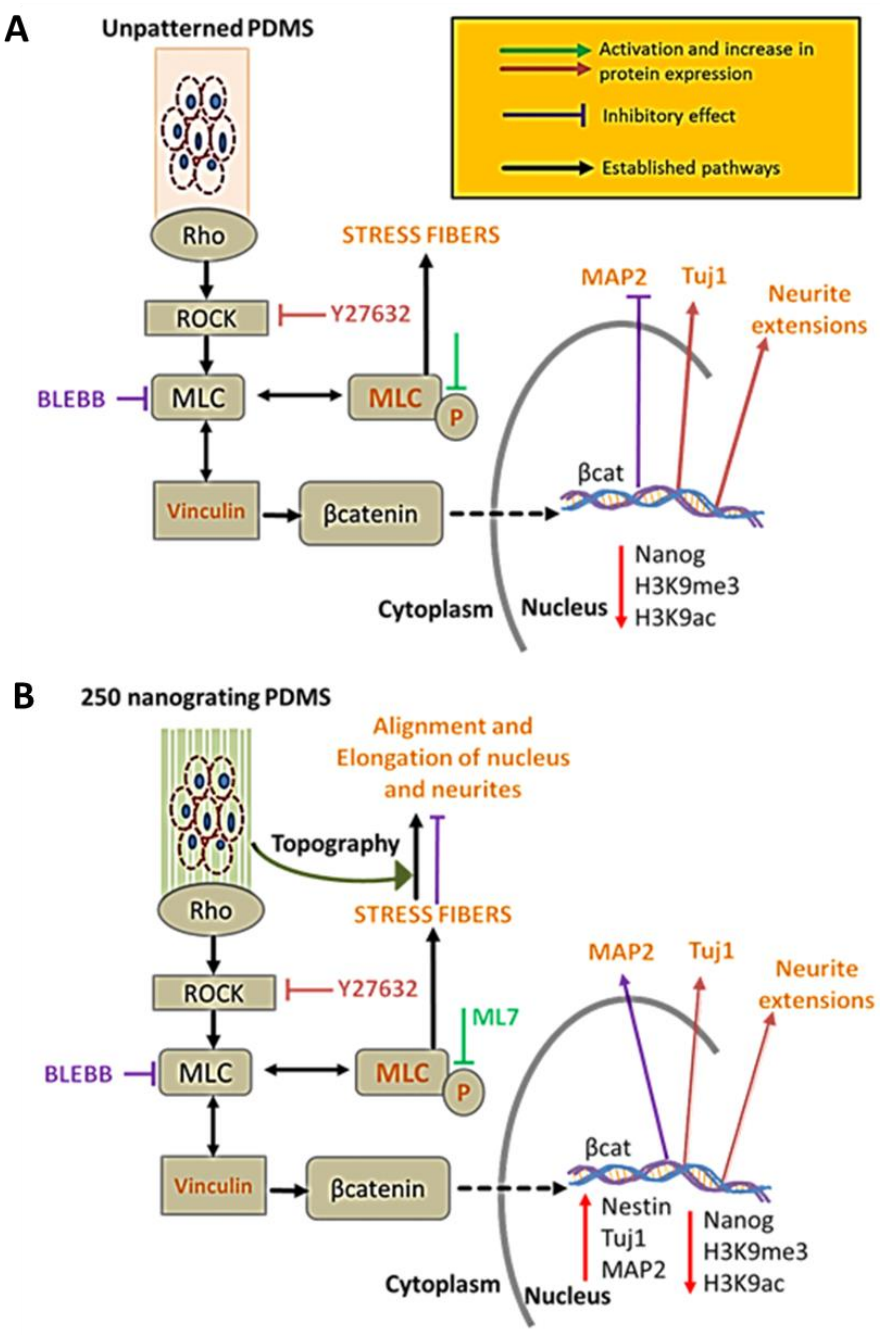

Figure 8.1 The proposed role of acto-myosin contractility in the neuronal differentiation of hESCS both in the absence **(A)** and presence **(B)** of topography is shown. Myosin contractility is essential for expression of mature neuronal markers, MAP2 as well as alignment and elongation of neurites along the grating axis. The effect of myosin contractility inhibitor, blebbistatin is shown in purple lines, the effect of ML7 (inhibitor of myosin light chain phosphorylation) is shown in green and the effect of ROCK inhibitor (Y-27632) is shown in maroon.

8.2. Future Work

The following future work is suggested in order to improve the current understanding of topography driven neuronal differentiation of human embryonic stem cells.

8.2.1. To derive region specific neuronal cells

The current work showed that certain topographies have an affinity towards a particular lineage when subjected to differentiation conditions. Banking on this property, it would be interesting to study the topographies that would aid in differentiating the hESCs to a region specific neuronal subtype for example using SHH, FGF8 along with suitable topographical cues to drive them to a dopaminergic lineage which would open more possibilities for cell therapy to treat degenerative disorders.

8.2.2. To understand the mechanism of topography directed neuronal differentiation of hESCs.

The work presented in this thesis showed that the acto-myosin contractility played an important role in neuronal maturation, and the alignment and elongation of neuronal precursor cells. However, a washout experiment (for example, 1 day washout experiment would involve addition of blebbistatin at Day 1 followed by culture in N2B27 media without inhibitor for 6 days and the samples will be fixed at Day 7; for 3 days washout experiment, the samples would be treated with blebbistatin for 3 days followed by culture in N2B27 media without inhibitors for 3 days and fixed on Day 7) of blebbistatin would allow us to determine the crucial time point for acto-myosin contractility, in order to mature the cells faster on nano-grating substrates. This experiment could be supplemented with western blotting of cytoskeletal proteins to see quantitative changes in actin, tubulin, non-muscle myosin II, and phosphorylated myosin

light chain. Studies have shown that globular actin (G-actin) could act as a transcription factor [250] hence assaying the ratio of G-actin : F-actin at different time points during neuronal differentiation could help us understand the role of cytoskeleton in transducing the force to the nucleus. The epigenetic marks could be studied in detail by using nuclear fraction of the protein and by performing co-immunoprecipitation to check if H3K9me3 is associated with nanog.

8.2.3. To study if glial cells have lower acto-myosin contractility

The PDMS MARC chip results were interesting especially the observation that the arrangement of the topography in isotropic or anisotropic manner could lead to fate specification of hESCs. It has been observed that there is increased acto-myosin contractility for the cells grown on nano-gratings. These observations lead to the speculation that the hESCs grown on isotropic patterns may be subjected to lower contractility forces and hence coerced into a glial lineage. Similar kind of inhibitor studies can be conducted for cells grown on pillars or wells to verify this speculation.

References

[1] Schmidt CE, Leach JB. Neural tissue engineering: strategies for repair and regeneration. Annual review of biomedical engineering 2003;5:293-347.

[2] An Y, Tsang KK, Zhang H. Potential of stem cell based therapy and tissue engineering in the regeneration of the central nervous system. Biomed Mater 2006;1:R38-44.

[3] Subramanian A, Krishnan U, Sethuraman S. Development of biomaterial scaffold for nerve tissue engineering: Biomaterial mediated neural regeneration. Journal of Biomedical Science 2009;16:108.

[4] Mackinnon SE. New directions in peripheral nerve surgery. Annals of plastic surgery 1989;22:257-273.

[5] Lundborg G. Richard P. Bunge memorial lecture. Nerve injury and repair--a challenge to the plastic brain. Journal of the peripheral nervous system : JPNS 2003;8:209-226.

[6] Erceg S, Ronaghi M, Stojkovic M. Human embryonic stem cell differentiation toward regional specific neural precursors. Stem Cells 2009;27:78-87.

[7] Carpenter MK, Inokuma MS, Denham J, Mujtaba T, Chiu CP, Rao MS. Enrichment of neurons and neural precursors from human embryonic stem cells. Exp Neurol 2001;172:383-397.

[8] Hu BY, Weick JP, Yu J, Ma LX, Zhang XQ, Thomson JA, Zhang SC. Neural differentiation of human induced pluripotent stem cells follows developmental principles but with variable potency. Proceedings of the National Academy of Sciences of the United States of America 2010;107:4335-4340.

[9] Serra M, Brito C, Costa E, Sousa M, Alves P. Integrating human stem cell expansion and neuronal differentiation in bioreactors. BMC Biotechnology 2009;9:82.

[10] Yim EKF, Pang SW, Leong KW. Synthetic nanostructures inducing differentiation of human mesenchymal stem cells into neuronal lineage. Exp Cell Res 2007;313:1820-1829.

[11] Teo BK, Ankam S, Yim EF. Stem Cell Interaction with Topography. In: Roy K, editor. Biomaterials as Stem Cell Niche: Springer Berlin Heidelberg; 2010. p. 61-87.

[12] Kumar M, Bagchi B, Gupta SK, Meena AS, Gressens P, Mani S. Neurospheres derived from human embryoid bodies treated with retinoic Acid show an increase in nestin and ngn2 expression that correlates with the proportion of tyrosine hydroxylase-positive cells. Stem cells and development 2007;16:667-681.

[13] Bakeine GJ, Ban J, Grenci G, Pozzato A, Zilio SD, Prasciolu M, Businaro L, et al. Design, fabrication and evaluation of nanoscale surface topography as a tool in directing differentiation and organisation of embryonic stem-cell-derived neural precursors. Microelectron Eng 2009;86:1435-1438.

[14] Recknor JB, Sakaguchi DS, Mallapragada SK. Directed growth and selective differentiation of neural progenitor cells on micropatterned polymer substrates. Biomaterials 2006;27:4098-4108.

[15] Christopherson GT, Song H, Mao HQ. The influence of fiber diameter of electrospun substrates on neural stem cell differentiation and proliferation. Biomaterials 2009;30:556-564.

[16] Ding S, Schultz PG. A role for chemistry in stem cell biology. Nature biotechnology 2004;22:833-840.

[17] Stojkovic M, Lako M, Strachan T, Murdoch A. Derivation, growth and applications of human embryonic stem cells. Reproduction 2004;128:259-267.

[18] Takahashi K, Yamanaka S. Induction of pluripotent stem cells from mouse embryonic and adult fibroblast cultures by defined factors. Cell 2006;126:663-676.

[19] Dang SM, Kyba M, Perlingeiro R, Daley GQ, Zandstra PW. Efficiency of embryoid body formation and hematopoietic development from

embryonic stem cells in different culture systems. Biotechnol Bioeng 2002;78:442-453.

[20] Cameron C, Hu W, Kaufman D. Improved development of human embryonic stem cell-derived embryoid bodies by stirred vessel cultivation. Biotechnol Bioeng 2006;94:938 - 948.

[21] Kurosawa H. Methods for inducing embryoid body formation: in vitro differentiation system of embryonic stem cells. J Biosci Bioeng 2007;103:389-398.

[22] Ungrin MD, Joshi C, Nica A, Bauwens C, Zandstra PW. Reproducible, ultra high-throughput formation of multicellular organization from single cell suspension-derived human embryonic stem cell aggregates. Plos One 2008;3:e1565.

[23] Gerecht S, Burdick JA, Ferreira LS, Townsend SA, Langer R, Vunjak-Novakovic G. Hyaluronic acid hydrogel for controlled self-renewal and differentiation of human embryonic stem cells. Proceedings of the National Academy of Sciences 2007;104:11298-11303.

[24] Steven D. Sheridan VS, Raj R. Rao. Analysis of Embryoid Bodies Derived from Human Induced Pluripotent Stem Cells as a Means to Assess Pluripotency. Stem Cells International 2012;2012.

[25] LaVaute TM, Yoo YD, Pankratz MT, Weick JP, Gerstner JR, Zhang SC. Regulation of neural specification from human embryonic stem cells by BMP and FGF. Stem Cells 2009;27:1741-1749.

[26] Chambers SM, Fasano CA, Papapetrou EP, Tomishima M, Sadelain M, Studer L. Highly efficient neural conversion of human ES and iPS cells by dual inhibition of SMAD signaling. Nature biotechnology 2009;27:275-280.

[27] Choi YY, Chung BG, Lee DH, Khademhosseini A, Kim JH, Lee SH. Controlled-size embryoid body formation in concave microwell arrays. Biomaterials 2010;31:4296-4303.

[28] Zhang XQ, Zhang SC. Differentiation of neural precursors and dopaminergic neurons from human embryonic stem cells. Methods Mol Biol 2010;584:355-366.

[29] Maden M. Retinoic acid in the development, regeneration and maintenance of the nervous system. Nature reviews Neuroscience 2007;8:755-765.

[30] Gerrard L, Rodgers L, Cui W. Differentiation of human embryonic stem cells to neural lineages in adherent culture by blocking bone morphogenetic protein signaling. Stem Cells 2005;23:1234-1241.

[31] Perrier AL, Tabar V, Barberi T, Rubio ME, Bruses J, Topf N, Harrison NL, et al. Derivation of midbrain dopamine neurons from human embryonic stem cells. Proceedings of the National Academy of Sciences of the United States of America 2004;101:12543-12548.

[32] Salehi H, Karbalaie K, Razavi S, Tanhaee S, Nematollahi M, Sagha M, Nasr-Esfahani MH, et al. Neuronal induction and regional identity by co-culture of adherent human embryonic stem cells with chicken notochords and somites. The International journal of developmental biology 2011;55:321-326.

[33] Zhou J, Su P, Li D, Tsang S, Duan E, Wang F. High-Efficiency Induction of Neural Conversion in Human ESCs and Human Induced Pluripotent Stem Cells with a Single Chemical Inhibitor of Transforming Growth Factor Beta Superfamily Receptors. Stem Cells 2010;28:1741-1750.

[34] Baharvand H, Mehrjardi NZ, Hatami M, Kiani S, Rao M, Haghighi MM. Neural differentiation from human embryonic stem cells in a defined adherent culture condition. The International journal of developmental biology 2007;51:371-378.

[35] Fuchs E, Tumbar T, Guasch G. Socializing with the neighbors: stem cells and their niche. Cell 2004;116:769-778.

[36] Moore KA, Lemischka IR. Stem cells and their niches. Science 2006;311:1880-1885.

[37] Rao BM, Zandstra PW. Culture development for human embryonic stem cell propagation: molecular aspects and challenges. Curr Opin Biotechnol 2005;16:568-576.

[38] Takahashi K, Tanabe K, Ohnuki M, Narita M, Ichisaka T, Tomoda K, Yamanaka S. Induction of pluripotent stem cells from adult human fibroblasts by defined factors. Cell 2007;131:861-872.

[39] Yamanaka S. Induced pluripotent stem cells: past, present, and future. Cell stem cell 2012;10:678-684.

[40] Hoffman LM, Carpenter MK. Characterization and culture of human embryonic stem cells. Nature biotechnology 2005;23:699-708.

[41] Ullmann U, In't Veld P, Gilles C, Sermon K, De Rycke M, Van de Velde H, Van Steirteghem A, et al. Epithelial-mesenchymal transition process in human embryonic stem cells cultured in feeder-free conditions. Mol Hum Reprod 2007;13:21-32.

[42] Amit M, Carpenter MK, Inokuma MS, Chiu CP, Harris CP, Waknitz MA, Itskovitz-Eldor J, et al. Clonally derived human embryonic stem cell lines maintain pluripotency and proliferative potential for prolonged periods of culture. Developmental biology 2000;227:271-278.

[43] Peerani R, Onishi K, Mahdavi A, Kumacheva E, Zandstra PW. Manipulation of Signaling Thresholds in â€œEngineered Stem Cell Nichesâ€• Identifies Design Criteria for Pluripotent Stem Cell Screens. Plos One 2009;4:e6438.

[44] Wang G, Zhang H, Zhao Y, Li J, Cai J, Wang P, Meng S, et al. Noggin and bFGF cooperate to maintain the pluripotency of human embryonic stem cells in the absence of feeder layers. Biochem Biophys Res Commun 2005;330:934-942.

[45] Skottman H, Hovatta O. Culture conditions for human embryonic stem cells. Reproduction 2006;132:691-698.

[46] Chin AC, Padmanabhan J, Oh SK, Choo AB. Defined and serum-free media support undifferentiated human embryonic stem cell growth. Stem cells and development 2009.

[47] Wang X, Yang P. In vitro differentiation of mouse embryonic stem (mES) cells using the hanging drop method. Journal of visualized experiments : JoVE 2008.

[48] Dang SM, Zandstra PW. Scalable production of embryonic stem cell-derived cells. Methods Mol Biol 2005;290:353-364.

[49] Smith LA, Liu X, Hu J, Wang P, Ma PX. Enhancing Osteogenic Differentiation of Mouse Embryonic Stem Cells by Nanofibers. Tissue Engineering Part A 2009;15:1855-1864.

[50] Chan LY, Birch WR, Yim EK, Choo AB. Temporal application of topography to increase the rate of neural differentiation from human pluripotent stem cells. Biomaterials 2013;34:382-392.

[51] Lovmand J, Justesen J, Foss M, Lauridsen RH, Lovmand M, Modin C, Besenbacher F, et al. The use of combinatorial topographical libraries for the screening of enhanced osteogenic expression and mineralization. Biomaterials 2009;30:2015-2022.

[52] Markert LD, Lovmand J, Foss M, Lauridsen RH, Lovmand M, Fuchtbauer EM, Fuchtbauer A, et al. Identification of distinct topographical surface microstructures favoring either undifferentiated expansion or differentiation of murine embryonic stem cells. Stem cells and development 2009;18:1331-1342.

[53] Peerani R, Rao BM, Bauwens C, Yin T, Wood GA, Nagy A, Kumacheva E, et al. Niche-mediated control of human embryonic stem cell self-renewal and differentiation. EMBO J 2007;26:4744-4755.

[54] Sasaki D, Shimizu T, Masuda S, Kobayashi J, Itoga K, Tsuda Y, Yamashita JK, et al. Mass preparation of size-controlled mouse embryonic stem cell aggregates and induction of cardiac differentiation by cell patterning method. Biomaterials 2009;30:4384-4389.

[55] Mohr JC, de Pablo JJ, Palecek SP. 3-D microwell culture of human embryonic stem cells. Biomaterials 2006;27:6032-6042.

[56] Khademhosseini A, Ferreira L, Blumling J, 3rd, Yeh J, Karp JM, Fukuda J, Langer R. Co-culture of human embryonic stem cells with murine embryonic fibroblasts on microwell-patterned substrates. Biomaterials 2006;27:5968-5977.

[57] Even-Ram S, Artym V, Yamada KM. Matrix Control of Stem Cell Fate. Cell 2006;126:645-647.

[58] Ciapetti G, Ambrosio L, Marletta G, Baldini N, Giunti A. Human bone marrow stromal cells: In vitro expansion and differentiation for bone engineering. Biomaterials 2006;27:6150-6160.

[59] Sanchez-Ramos J, Song S, Cardozo-Pelaez F, Hazzi C, Stedeford T, Willing A, Freeman TB, et al. Adult Bone Marrow Stromal Cells Differentiate into Neural Cells in Vitro. Experimental neurology 2000;164:247-256.

[60] Caplan AI. Mesenchymal stem cells. J Orthop Res 1991;9:641-650.

[61] Caplan AI, Dennis JE. Mesenchymal stem cells as trophic mediators. J Cell Biochem 2006;98:1076-1084.

[62] Farrell E, O'Brien FJ, Doyle P, Fischer J, Yannas I, Harley BA, O'Connell B, et al. A Collagen-glycosaminoglycan Scaffold Supports Adult Rat Mesenchymal Stem Cell Differentiation Along Osteogenic and Chondrogenic Routes. Tissue Engineering 2006;12:459-468.

[63] Drost AC, Weng S, Feil G, Sch, fer J, Baumann S, Kanz L, et al. In vitro Myogenic Differentiation of Human Bone MarrowDerived Mesenchymal Stem Cells as a Potential Treatment for Urethral Sphincter Muscle Repair. Annals of the New York Academy of Sciences 2009;1176:135-143.

[64] Yim EK, Pang SW, Leong KW. Synthetic nanostructures inducing differentiation of human mesenchymal stem cells into neuronal lineage. Exp Cell Res 2007;313:1820-1829.

[65] Sekiya I, Larson BL, Vuoristo JT, Cui J-G, Prockop DJ. Adipogenic Differentiation of Human Adult Stem Cells From Bone Marrow Stroma (MSCs). Journal of Bone and Mineral Research 2004;19:256-264.

[66] Dalby MJ, Gadegaard N, Tare R, Andar A, Riehle MO, Herzyk P, Wilkinson CDW, et al. The control of human mesenchymal cell differentiation using nanoscale symmetry and disorder. Nat Mater 2007;6:997-1003.

[67] Huang NF, Li S. Mesenchymal stem cells for vascular regeneration. Regenerative Medicine 2008;3:877-892.

[68] McBeath R, Pirone DM, Nelson CM, Bhadriraju K, Chen CS. Cell Shape, Cytoskeletal Tension, and RhoA Regulate Stem Cell Lineage Commitment. Developmental cell 2004;6:483-495.

[69] Martino S, D'Angelo F, Armentano I, Tiribuzi R, Pennacchi M, Dottori M, Mattioli S, et al. Hydrogenated Amorphous Carbon Nanopatterned Film Designs Drive Human Bone Marrow Mesenchymal Stem Cell Cytoskeleton Architecture. Tissue Engineering Part A 2009.

[70] Khor HL, Kuan Y, Kukula H, Tamada K, Knoll W, Moeller M, Hutmacher DW. Response of cells on surface-induced nanopatterns: fibroblasts and mesenchymal progenitor cells. Biomacromolecules 2007;8:1530-1540.

[71] Dulgar-Tulloch AJ, Bizios R, Siegel RW. Human mesenchymal stem cell adhesion and proliferation in response to ceramic chemistry and nanoscale topography. J Biomed Mater Res A 2009;90:586-594.

[72] Park J, Bauer S, von der Mark K, Schmuki P. Nanosize and Vitality: TiO2 Nanotube Diameter Directs Cell Fate. Nano Lett 2007;7:1686-1691.

[73] Engel E, Martínez E, Mills CA, Funes M, Planell JA, Samitier J. Mesenchymal stem cell differentiation on microstructured poly (methyl methacrylate) substrates. Annals of Anatomy - Anatomischer Anzeiger 2009;191:136-144.

[74] Martínez E, Engel E, Planell JA, Samitier J. Effects of artificial micro- and nano-structured surfaces on cell behaviour. Annals of Anatomy - Anatomischer Anzeiger 2009;191:126-135.

[75] Terje Ssm, Matthew JD, Andrew H, Rahul T, Richard OCO, Bo S. Fabrication of pillar-like titania nanostructures on titanium and their interactions with human skeletal stem cells. Acta Biomaterialia 2009;5:1433-1441.

[76] Hosseinkhani H, Hosseinkhani M, Tian F, Kobayashi H, Tabata Y. Osteogenic differentiation of mesenchymal stem cells in self-assembled peptide-amphiphile nanofibers. Biomaterials 2006;27:4079-4086.

[77] Dang JM, Leong KW. Myogenic Induction of Aligned Mesenchymal Stem Cell Sheets by Culture on Thermally Responsive Electrospun Nanofibers. Adv Mater 2007;19:2775-2779.

[78] Guvendiren M, Burdick JA. The control of stem cell morphology and differentiation by hydrogel surface wrinkles. Biomaterials 2010;31:6511-6518.

[79] Prabhakaran MP, Venugopal JR, Ramakrishna S. Mesenchymal stem cell differentiation to neuronal cells on electrospun nanofibrous substrates for nerve tissue engineering. Biomaterials 2009;30:4996-5003.

[80] Kantawong F, Burgess KEV, Jayawardena K, Hart A, Burchmore RJ, Gadegaard N, Oreffo ROC, et al. Whole proteome analysis of osteoprogenitor differentiation induced by disordered nanotopography and mediated by ERK signalling. Biomaterials 2009;30:4723-4731.

[81] Le DM, Kulangara K, Adler AF, Leong KW, Ashby VS. Dynamic Topographical Control of Mesenchymal Stem Cells by Culture on Responsive Poly(ϵ-caprolactone) Surfaces. Adv Mater 2011;23:3278-3283.

[82] Morshead CM, Reynolds BA, Craig CG, McBurney MW, Staines WA, Morassutti D, Weiss S, et al. Neural stem cells in the adult mammalian forebrain: A relatively quiescent subpopulation of subependymal cells. Neuron 1994;13:1071-1082.

[83] Johansson CB, Momma S, Clarke DL, Risling M, Lendahl U, Frisén J. Identification of a Neural Stem Cell in the Adult Mammalian Central Nervous System. Cell 1999;96:25-34.

[84] Goldman SA. Neural Progenitor Cells of the Adult Human Brain. Neural Development and Stem Cells2006. p. 267-297.

[85] Steven AG, Abdellatif B, Eva C, Keyoung HM, Marta N, Neeta SR, Amer S, et al. Isolation and induction of adult neural progenitor cells. 2002;2:70-79.

[86] Johansson CB, Svensson M, Wallstedt L, Janson AM, Frisén J. Neural Stem Cells in the Adult Human Brain. Exp Cell Res 1999;253:733-736.

[87] Svendsen CN, Caldwell MA, Ostenfeld T. Human Neural Stem Cells: Isolation, Expansion and Transplantation. Brain Pathology 1999;9:499-513.

[88] Scolding N, Franklin R, Stevens S, Heldin CH, Compston A, Newcombe J. Oligodendrocyte progenitors are present in the normal adult

human CNS and in the lesions of multiple sclerosis. Brain 1998;121:2221-2228.

[89] Roy NS, Wang S, Harrison-Restelli C, Benraiss A, Fraser RAR, Gravel M, Braun PE, et al. Identification, Isolation, and Promoter-Defined Separation of Mitotic Oligodendrocyte Progenitor Cells from the Adult Human Subcortical White Matter. Journal of Neuroscience 1999;19:9986-9995.

[90] Boote Jones EN, Mallapragada SK. Directed growth and differentiation of stem cells towards neural cell fates using soluble and surface-mediated cues. J Biomater Sci Polym Ed 2007;18:999-1015.

[91] Obayashi S, Tabunoki H, Kim SU, Satoh J. Gene expression profiling of human neural progenitor cells following the serum-induced astrocyte differentiation. Cell Mol Neurobiol 2009;29:423-438.

[92] Park JY, Kim SK, Woo DH, Lee EJ, Kim JH, Lee SH. Differentiation of neural progenitor cells in a microfluidic chip-generated cytokine gradient. Stem Cells 2009;27:2646-2654.

[93] Leipzig ND, Shoichet MS. The effect of substrate stiffness on adult neural stem cell behavior. Biomaterials 2009;30:6867-6878.

[94] Christopherson GT, Song H, Mao H-Q. The influence of fiber diameter of electrospun substrates on neural stem cell differentiation and proliferation. Biomaterials 2009;30:556-564.

[95] Park S, Lee KS, Lee YJ, Shin HA, Cho HY, Wang KC, Kim YS, et al. Generation of dopaminergic neurons in vitro from human embryonic stem cells treated with neurotrophic factors. Neuroscience letters 2004;359:99-103.

[96] Yue F, Cui L, Johkura K, Ogiwara N, Sasaki K. Induction of midbrain dopaminergic neurons from primate embryonic stem cells by coculture with sertoli cells. Stem Cells 2006;24:1695-1706.

[97] Silva GA, Czeisler C, Niece KL, Beniash E, Harrington DA, Kessler JA, Stupp SI. Selective Differentiation of Neural Progenitor Cells by High-Epitope Density Nanofibers. Science 2004;303:1352-1355.

[98] Peerani R, Zandstra PW. Enabling stem cell therapies through synthetic stem cell-niche engineering. The Journal of clinical investigation;120:60-70.

[99] Kirouac DC, Madlambayan GJ, Yu M, Sykes EA, Ito C, Zandstra PW. Cell-cell interaction networks regulate blood stem and progenitor cell fate. Mol Syst Biol 2009;5:293.

[100] Chua KN, Chai C, Lee PC, Tang YN, Ramakrishna S, Leong KW, Mao HQ. Surface-aminated electrospun nanofibers enhance adhesion and expansion of human umbilical cord blood hematopoietic stem/progenitor cells. Biomaterials 2006;27:6043-6051.

[101] Chua KN, Chai C, Lee PC, Ramakrishna S, Leong KW, Mao HQ. Functional nanofiber scaffolds with different spacers modulate adhesion and expansion of cryopreserved umbilical cord blood hematopoietic stem/progenitor cells. Exp Hematol 2007;35:771-781.

[102] Anderson DG, Levenberg S, Langer R. Nanoliter-scale synthesis of arrayed biomaterials and application to human embryonic stem cells. Nature biotechnology 2004;22:863-866.

[103] Anderson DG, Putnam D, Lavik EB, Mahmood TA, Langer R. Biomaterial microarrays: rapid, microscale screening of polymer–cell interaction. Biomaterials 2005;26:4892-4897.

[104] Mei Y, Saha K, Bogatyrev SR, Yang J, Hook AL, Kalcioglu ZI, Cho SW, et al. Combinatorial development of biomaterials for clonal growth of human pluripotent stem cells. Nature materials 2010;9:768-778.

[105] Flaim CJ, Chien S, Bhatia SN. An extracellular matrix microarray for probing cellular differentiation. Nature methods 2005;2:119-125.

[106] Soen Y, Mori A, Palmer TD, Brown PO. Exploring the regulation of human neural precursor cell differentiation using arrays of signaling microenvironments. Mol Syst Biol 2006;2.

[107] Flaim CJ, Teng D, Chien S, Bhatia SN. Combinatorial signaling microenvironments for studying stem cell fate. Stem Cells Dev 2008;17:29-39.

[108] Brafman DA, Shah KD, Fellner T, Chien S, Willert K. Defining long-term maintenance conditions of human embryonic stem cells with arrayed cellular microenvironment technology. Stem Cells Dev 2009;18:1141-1154.

[109] Unadkat HV, Hulsman M, Cornelissen K, Papenburg BJ, Truckenmuller RK, Carpenter AE, Wessling M, et al. An algorithm-based topographical biomaterials library to instruct cell fate. Proceedings of the National Academy of Sciences of the United States of America 2011;108:16565-16570.

[110] Timpl R, Rohde H, Robey PG, Rennard SI, Foidart JM, Martin GR. Laminin--a glycoprotein from basement membranes. The Journal of biological chemistry 1979;254:9933-9937.

[111] Engel J, Odermatt E, Engel A, Madri JA, Furthmayr H, Rohde H, Timpl R. Shapes, domain organizations and flexibility of laminin and fibronectin, two multifunctional proteins of the extracellular matrix. Journal of molecular biology 1981;150:97-120.

[112] Sanes JR. Extracellular-Matrix Molecules That Influence Neural Development. Annu Rev Neurosci 1989;12:491-516.

[113] Liesi P. Extracellular matrix and neuronal movement. Experientia 1990;46:900-907.

[114] Luckenbill-Edds L, Kaiser CA, Rodgers TR, Powell DD. Localization of the 110 kDa receptor for laminin in brains of embryonic and postnatal mice. Cell and tissue research 1995;279:371-377.

[115] Leivo I, Vaheri A, Timpl R, Wartiovaara J. Appearance and distribution of collagens and laminin in the early mouse embryo. Developmental biology 1980;76:100-114.

[116] Cooper AR, MacQueen HA. Subunits of laminin are differentially synthesized in mouse eggs and early embryos. Developmental biology 1983;96:467-471.

[117] Dziadek M, Timpl R. Expression of nidogen and laminin in basement membranes during mouse embryogenesis and in teratocarcinoma cells. Developmental biology 1985;111:372-382.

[118] Aumailley M, Krieg T. Laminins: a family of diverse multifunctional molecules of basement membranes. The Journal of investigative dermatology 1996;106:209-214.

[119] Edgar D. The expression and distribution of laminin in the developing nervous system. Journal of cell science Supplement 1991;15:9-12.

[120] Liesi P. Laminin-Immunoreactive Glia Distinguish Regenerative Adult Cns Systems from Non-Regenerative Ones. Embo Journal 1985;4:2505-2511.

[121] Cornbrooks CJ, Carey DJ, McDonald JA, Timpl R, Bunge RP. In vivo and in vitro observations on laminin production by Schwann cells. Proceedings of the National Academy of Sciences of the United States of America 1983;80:3850-3854.

[122] Madison R, Dasilva CF, Dikkes P, Chiu TH, Sidman RL. Increased Rate of Peripheral-Nerve Regeneration Using Bioresorbable Nerve Guides and a Laminin-Containing Gel. Experimental neurology 1985;88:767-772.

[123] Madison RD, Dasilva C, Dikkes P, Sidman RL, Chiu TH. Peripheral-Nerve Regeneration with Entubulation Repair - Comparison of Biodegradeable Nerve Guides Versus Polyethylene Tubes and the Effects of a Laminin-Containing Gel. Experimental neurology 1987;95:378-390.

[124] Bailey SB, Eichler ME, Villadiego A, Rich KM. The influence of fibronectin and laminin during Schwann cell migration and peripheral nerve regeneration through silicon chambers. Journal of neurocytology 1993;22:176-184.

[125] Labrador RO, Buti M, Navarro X. Influence of collagen and laminin gels concentration on nerve regeneration after resection and tube repair. Experimental neurology 1998;149:243-252.

[126] Tong XJ, Hirai K, Shimada H, Mizutani Y, Izumi T, Toda N, Yu P. Sciatic nerve regeneration navigated by laminin-fibronectin double coated biodegradable collagen grafts in rats. Brain research 1994;663:155-162.

[127] David S, Braun PE, Jackson DL, Kottis V, McKerracher L. Laminin overrides the inhibitory effects of peripheral nervous system and central nervous system myelin-derived inhibitors of neurite growth. Journal of neuroscience research 1995;42:594-602.

[128] Timpl R, Brown JC. The laminins. Matrix biology : journal of the International Society for Matrix Biology 1994;14:275-281.

[129] Forsberg E, Ek B, Engstrom A, Johansson S. Purification and Characterization of Integrin Alpha-9-Beta-1. Experimental cell research 1994;213:183-190.

[130] Mckerracher L, David S, Jackson DL, Kottis V, Dunn RJ, Braun PE. Identification of Myelin-Associated Glycoprotein as a Major Myelin-Derived Inhibitor of Neurite Growth. Neuron 1994;13:805-811.

[131] Edgar D, Timpl R, Thoenen H. The Heparin-Binding Domain of Laminin Is Responsible for Its Effects on Neurite Outgrowth and Neuronal Survival. Embo Journal 1984;3:1463-1468.

[132] Aumailley M, Nurcombe V, Edgar D, Paulsson M, Timpl R. The Cellular Interactions of Laminin Fragments - Cell-Adhesion Correlates with 2 Fragment-Specific High-Affinity Binding-Sites. Journal of Biological Chemistry 1987;262:11532-11538.

[133] Skubitz APN, Letourneau PC, Wayner E, Furcht LT. Synthetic Peptides from the Carboxy-Terminal Globular Domain of the a Chain of Laminin - Their Ability to Promote Cell-Adhesion and Neurite Outgrowth, and Interact with Heparin and the Beta-1 Integrin Subunit. Journal of Cell Biology 1991;115:1137-1148.

[134] Folkman J, Moscona A. Role of cell shape in growth control. Nature 1978;273:345-349.

[135] Manasek FJ, Burnside MB, Waterman RE. Myocardial cell shape change as a mechanism of embryonic heart looping. Developmental biology 1972;29:349-371.

[136] Ingber DE. Control of capillary growth and differentiation by extracellular matrix. Use of a tensegrity (tensional integrity) mechanism for signal processing. Chest 1991;99:34S-40S.

[137] Meyers J, Craig J, Odde DJ. Potential for control of signaling pathways via cell size and shape. Curr Biol 2006;16:1685-1693.

[138] Brunette DM, Chehroudi B. The effects of the surface topography of micromachined titanium substrata on cell behavior in vitro and in vivo. J Biomech Eng 1999;121:49-57.

[139] Dunn GA, Brown AF. Alignment of fibroblasts on grooved surfaces described by a simple geometric transformation. J Cell Sci 1986;83:313-340.

[140] Bissell MJ, Weaver VM, Lelievre SA, Wang F, Petersen OW, Schmeichel KL. Tissue structure, nuclear organization, and gene expression in normal and malignant breast. Cancer Res 1999;59:1757-1763s; discussion 1763s-1764s.

[141] Lutolf MP, Hubbell JA. Synthetic biomaterials as instructive extracellular microenvironments for morphogenesis in tissue engineering. Nature biotechnology 2005;23:47-55.

[142] Ingber DE. Tensegrity II. How structural networks influence cellular information processing networks. J Cell Sci 2003;116:1397-1408.

[143] Ingber DE. Tensegrity I. Cell structure and hierarchical systems biology. J Cell Sci 2003;116:1157-1173.

[144] Ingber DE. Tensegrity-based mechanosensing from macro to micro. Prog Biophys Mol Biol 2008;97:163-179.

[145] Bissell MJ, Hall HG, Parry G. How does the extracellular matrix direct gene expression? J Theor Biol 1982;99:31-68.

[146] Nelson CM, Bissell MJ. Of extracellular matrix, scaffolds, and signaling: tissue architecture regulates development, homeostasis, and cancer. Annual review of cell and developmental biology 2006;22:287-309.

[147] Geiger B, Spatz JP, Bershadsky AD. Environmental sensing through focal adhesions. Nature reviews Molecular cell biology 2009;10:21-33.

[148] Dalby MJ, Childs S, Riehle MO, Johnstone HJ, Affrossman S, Curtis AS. Fibroblast reaction to island topography: changes in cytoskeleton and morphology with time. Biomaterials 2003;24:927-935.

[149] Riveline D, Zamir E, Balaban NQ, Schwarz US, Ishizaki T, Narumiya S, Kam Z, et al. Focal contacts as mechanosensors: externally applied local

mechanical force induces growth of focal contacts by an mDia1-dependent and ROCK-independent mechanism. The Journal of cell biology 2001;153:1175-1186.

[150] Yim EK, Sheetz MP. Force-dependent cell signaling in stem cell differentiation. Stem cell research & therapy 2012;3:41.

[151] Berrier AL, Yamada KM. Cell-matrix adhesion. Journal of cellular physiology 2007;213:565-573.

[152] Delon I, Brown NH. Integrins and the actin cytoskeleton. Curr Opin Cell Biol 2007;19:43-50.

[153] Engler AJ, Sen S, Sweeney HL, Discher DE. Matrix elasticity directs stem cell lineage specification. Cell 2006;126:677-689.

[154] Harris AK, Wild P, Stopak D. Silicone rubber substrata: a new wrinkle in the study of cell locomotion. Science 1980;208:177-179.

[155] Tan JL, Tien J, Pirone DM, Gray DS, Bhadriraju K, Chen CS. Cells lying on a bed of microneedles: an approach to isolate mechanical force. Proceedings of the National Academy of Sciences of the United States of America 2003;100:1484-1489.

[156] Fujita S, Ohshima M, Iwata H. Time-lapse observation of cell alignment on nanogrooved patterns. J R Soc Interface 2009;6 Suppl 3:S269-277.

[157] Gerecht S, Bettinger CJ, Zhang Z, Borenstein JT, Vunjak-Novakovic G, Langer R. The effect of actin disrupting agents on contact guidance of human embryonic stem cells. Biomaterials 2007;28:4068-4077.

[158] Chowdhury F, Na S, Li D, Poh YC, Tanaka TS, Wang F, Wang N. Material properties of the cell dictate stress-induced spreading and differentiation in embryonic stem cells. Nat Mater;9:82-88.

[159] Engler AJ, Carag-Krieger C, Johnson CP, Raab M, Tang HY, Speicher DW, Sanger JW, et al. Embryonic cardiomyocytes beat best on a matrix with heart-like elasticity: scar-like rigidity inhibits beating. J Cell Sci 2008;121:3794-3802.

[160] Reilly GC, Engler AJ. Intrinsic extracellular matrix properties regulate stem cell differentiation. Journal of biomechanics;43:55-62.

[161] Galbraith CG, Yamada KM, Sheetz MP. The relationship between force and focal complex development. The Journal of cell biology 2002;159:695-705.

[162] Vicente-Manzanares M, Ma X, Adelstein RS, Horwitz AR. Non-muscle myosin II takes centre stage in cell adhesion and migration. Nature reviews Molecular cell biology 2009;10:778-790.

[163] Paszek MJ, Zahir N, Johnson KR, Lakins JN, Rozenberg GI, Gefen A, Reinhart-King CA, et al. Tensional homeostasis and the malignant phenotype. Cancer Cell 2005;8:241-254.

[164] Chrzanowska-Wodnicka M, Burridge K. Rho-stimulated contractility drives the formation of stress fibers and focal adhesions. The Journal of cell biology 1996;133:1403-1415.

[165] Hall A. Rho GTPases and the actin cytoskeleton. Science 1998;279:509-514.

[166] Zhang Q, Skepper JN, Yang F, Davies JD, Hegyi L, Roberts RG, Weissberg PL, et al. Nesprins: a novel family of spectrin-repeat-containing proteins that localize to the nuclear membrane in multiple tissues. J Cell Sci 2001;114:4485-4498.

[167] Crisp M, Liu Q, Roux K, Rattner JB, Shanahan C, Burke B, Stahl PD, et al. Coupling of the nucleus and cytoplasm: role of the LINC complex. The Journal of cell biology 2006;172:41-53.

[168] Alberts B BD, Lewis J, Raff M, Watson J. Molecular biology of the cell. Garland Publishing Inc.; New York: 1994.

[169] Dechat T, Pfleghaar K, Sengupta K, Shimi T, Shumaker DK, Solimando L, Goldman RD. Nuclear lamins: major factors in the structural organization and function of the nucleus and chromatin. Genes Dev 2008;22:832-853.

[170] Gieni RS, Hendzel MJ. Mechanotransduction from the ECM to the genome: are the pieces now in place? J Cell Biochem 2008;104:1964-1987.

[171] Wang N, Tytell JD, Ingber DE. Mechanotransduction at a distance: mechanically coupling the extracellular matrix with the nucleus. Nature reviews Molecular cell biology 2009;10:75-82.

[172] Fey EG, Wan KM, Penman S. Epithelial cytoskeletal framework and nuclear matrix-intermediate filament scaffold: three-dimensional organization and protein composition. The Journal of cell biology 1984;98:1973-1984.

[173] Maniotis AJ, Chen CS, Ingber DE. Demonstration of mechanical connections between integrins, cytoskeletal filaments, and nucleoplasm that stabilize nuclear structure. Proc Natl Acad Sci U S A 1997;94:849-854.

[174] Hu S, Chen J, Butler JP, Wang N. Prestress mediates force propagation into the nucleus. Biochem Biophys Res Commun 2005;329:423-428.

[175] Hu S, Chen J, Fabry B, Numaguchi Y, Gouldstone A, Ingber DE, Fredberg JJ, et al. Intracellular stress tomography reveals stress focusing and structural anisotropy in cytoskeleton of living cells. Am J Physiol Cell Physiol 2003;285:C1082-1090.

[176] Dalby MJ, Gadegaard N, Herzyk P, Sutherland D, Agheli H, Wilkinson CD, Curtis AS. Nanomechanotransduction and interphase nuclear organization influence on genomic control. J Cell Biochem 2007;102:1234-1244.

[177] Dalby MJ, Yarwood SJ, Riehle MO, Johnstone HJ, Affrossman S, Curtis AS. Increasing fibroblast response to materials using nanotopography: morphological and genetic measurements of cell response to 13-nm-high polymer demixed islands. Exp Cell Res 2002;276:1-9.

[178] Hughes CS, Postovit LM, Lajoie GA. Matrigel: a complex protein mixture required for optimal growth of cell culture. Proteomics;10:1886-1890.

[179] Moe AAK, Suryana M, Marcy G, Lim SK, Ankam S, Goh JZW, Jin J, et al. Microarray with Micro- and Nano-topographies Enables Identification of the Optimal Topography for Directing the Differentiation of Primary Murine Neural Progenitor Cells. Small 2012;8:3050-3061.

[180] Zhang F, Low HY. Anisotropic wettability on imprinted hierarchical structures. Langmuir : the ACS journal of surfaces and colloids 2007;23:7793-7798.

[181] Andersson AS, Backhed F, von Euler A, Richter-Dahlfors A, Sutherland D, Kasemo B. Nanoscale features influence epithelial cell morphology and cytokine production. Biomaterials 2003;24:3427-3436.

[182] Drago J, Nurcombe V, Bartlett PF. Laminin through Its Long Arm E8 Fragment Promotes the Proliferation and Differentiation of Murine Neuroepithelial Cells-Invitro. Exp Cell Res 1991;192:256-265.

[183] Choo A, Padmanabhan J, Chin A, Fong WJ, Oh SKW. Immortalized feeders for the scale-up of human embryonic stem cells in feeder and feeder-free conditions. Journal of Biotechnology 2006;122:130-141.

[184] Sun Y, Villa-Diaz LG, Lam RH, Chen W, Krebsbach PH, Fu J. Mechanics regulates fate decisions of human embryonic stem cells. Plos One 2012;7:e37178.

[185] Jordan PM, Ojeda LD, Thonhoff JR, Gao J, Boehning D, Yu Y, Wu P. Generation of spinal motor neurons from human fetal brain-derived neural stem cells: role of basic fibroblast growth factor. J Neurosci Res 2009;87:318-332.

[186] Horcas I, Fernandez R, Gomez-Rodriguez JM, Colchero J, Gomez-Herrero J, Baro AM. WSXM: a software for scanning probe microscopy and a tool for nanotechnology. Rev Sci Instrum 2007;78:013705.

[187] Lee MR, Kwon KW, Jung H, Kim HN, Suh KY, Kim K, Kim KS. Direct differentiation of human embryonic stem cells into selective neurons on nanoscale ridge/groove pattern arrays. Biomaterials 2010;31:4360-4366.

[188] Soen Y, Mori A, Palmer TD, Brown PO. Exploring the regulation of human neural precursor cell differentiation using arrays of signaling microenvironments. Molecular systems biology 2006;2:37.

[189] Unadkat HV, Hulsman M, Cornelissen K, Papenburg BJ, Truckenmuller RK, Post GF, Uetz M, et al. An algorithm-based topographical biomaterials library to instruct cell fate. Proceedings of the National Academy of Sciences of the United States of America 2011;108:16565-16570.

[190] Migliorini E, Grenci G, Ban J, Pozzato A, Tormen M, Lazzarino M, Torre V, et al. Acceleration of neuronal precursors differentiation induced by substrate nanotopography. Biotechnol Bioeng;108:2736-2746.

[191] Stevens RMD, Frederick NA, Smith BL, Morse DE, Stucky GD, Hansma PK. Carbon nanotubes as probes for atomic force microscopy. Nanotechnology 2000;11:1-5.

[192] Wang L, Sun B, Ziemer KS, Barabino GA, Carrier RL. Chemical and physical modifications to poly(dimethylsiloxane) surfaces affect adhesion of Caco-2 cells. J Biomed Mater Res A;93:1260-1271.

[193] Ankam S, Suryana M, Chan LY, Moe AAK, Teo BKK, Law JBK, Sheetz MP, et al. Substrate topography and size determine the fate of human embryonic stem cells to neuronal or glial lineage. Acta Biomaterialia 2013;9:4535-4545.

[194] Moe AA, Suryana M, Marcy G, Lim SK, Ankam S, Goh JZ, Jin J, et al. Microarray with Micro- and Nano-topographies Enables Identification of the Optimal Topography for Directing the Differentiation of Primary Murine Neural Progenitor Cells. Small 2012.

[195] Amit M, Carpenter MK, Inokuma MS, Chiu C-P, Harris CP, Waknitz MA, Itskovitz-Eldor J, et al. Clonally Derived Human Embryonic Stem Cell Lines Maintain Pluripotency and Proliferative Potential for Prolonged Periods of Culture. Developmental Biology 2000;227:271-278.

[196] Odorico JS, Kaufman DS, Thomson JA. Multilineage differentiation from human embryonic stem cell lines. Stem Cells 2001;19:193-204.

[197] Lindvall O, Kokaia Z. Stem cells in human neurodegenerative disorders--time for clinical translation? The Journal of clinical investigation 2010;120:29-40.

[198] Dottori M, Pebay A, Pera MF. Neural Differentiation of Human Embryonic Stem Cells. Protcols for Neural Cell Culture, Fourth Edition 2010:75-86.

[199] Chambers SM, Fasano CA, Papapetrou EP, Tomishima M, Sadelain M, Studer L. Highly efficient neural conversion of human ES and iPS cells by dual inhibition of SMAD signaling. Nat Biotech 2009;27:275-280.

[200] Roy NS, Cleren C, Singh SK, Yang L, Beal MF, Goldman SA. Functional engraftment of human ES cell-derived dopaminergic neurons enriched by coculture with telomerase-immortalized midbrain astrocytes. Nat Med 2006;12:1259-1268.

[201] Discher DE, Mooney DJ, Zandstra PW. Growth factors, matrices, and forces combine and control stem cells. Science 2009;324:1673-1677.

[202] Hoffman-Kim D, Mitchel JA, Bellamkonda RV. Topography, cell response, and nerve regeneration. Annual review of biomedical engineering 2010;12:203-231.

[203] Oh S, Brammer KS, Li YSJ, Teng D, Engler AJ, Chien S, Jin S. Stem cell fate dictated solely by altered nanotube dimension. Proceedings of the National Academy of Sciences 2009;106:2130-2135.

[204] Kilian KA, Bugarija B, Lahn BT, Mrksich M. Geometric cues for directing the differentiation of mesenchymal stem cells. Proceedings of the National Academy of Sciences of the United States of America 2010;107:4872-4877.

[205] Wan LQ, Kang SM, Eng G, Grayson WL, Lu XL, Huo B, Gimble J, et al. Geometric control of human stem cell morphology and differentiation. Integrative biology : quantitative biosciences from nano to macro 2010;2:346-353.

[206] Ludwig T, Thomson JA. Defined, feeder-independent medium for human embryonic stem cell culture. In: Patient R, Schlaeger T, Snyder E, Yamashita Y, editors. Current protocols in stem cell biology: John Wiley and Sons, inc; 2007. p. 1-16.

[207] Ankam S, Suryana M, Chan LY, Moe AA, Teo BK, Law JB, Sheetz MP, et al. Substrate topography and size determine the fate of human embryonic stem cells to neuronal or glial lineage. Acta biomaterialia 2013;9:4535-4545.

[208] Morrison SJ, Shah NM, Anderson DJ. Regulatory mechanisms in stem cell biology. Cell 1997;88:287-298.

[209] Brown XQ, Ookawa K, Wong JY. Evaluation of polydimethylsiloxane scaffolds with physiologically-relevant elastic

moduli: interplay of substrate mechanics and surface chemistry effects on vascular smooth muscle cell response. Biomaterials 2005;26:3123-3129.

[210] Callister WD. Fundamentals of Materials Science and Engineering: An Interactive E-Text. 5th ed. John Wiley and Sons, inc; Somerset, NJ: 2000. Ch7, p54 -55.

[211] Ogasawara T, Ohba S, Yano F, Kawaguchi H, Chung UI, Saito T, Yonehara Y, et al. Nanog promotes osteogenic differentiation of the mouse mesenchymal cell line C3H10T1/2 by modulating bone morphogenetic protein (BMP) signaling. Journal of cellular physiology 2013;228:163-171.

[212] Suzuki A, Raya A, Kawakami Y, Morita M, Matsui T, Nakashima K, Gage FH, et al. Nanog binds to Smad1 and blocks bone morphogenetic protein-induced differentiation of embryonic stem cells. Proceedings of the National Academy of Sciences of the United States of America 2006;103:10294-10299.

[213] Jones EV, Cook D, Murai KK. A neuron-astrocyte co-culture system to investigate astrocyte-secreted factors in mouse neuronal development. Methods Mol Biol 2012;814:341-352.

[214] Swanson RA, Liu J, Miller JW, Rothstein JD, Farrell K, Stein BA, Longuemare MC. Neuronal regulation of glutamate transporter subtype expression in astrocytes. J Neurosci 1997;17:932-940.

[215] Guizzetti M, Moore NH, Giordano G, Costa LG. Modulation of neuritogenesis by astrocyte muscarinic receptors. The Journal of biological chemistry 2008;283:31884-31897.

[216] Ullian EM, Harris BT, Wu A, Chan JR, Barres BA. Schwann cells and astrocytes induce synapse formation by spinal motor neurons in culture. Molecular and cellular neurosciences 2004;25:241-251.

[217] Melichar H, Li O, Ross J, Haber H, Cado D, Nolla H, Robey EA, et al. Comparative study of hematopoietic differentiation between human embryonic stem cell lines. Plos One;6:e19854.

[218] Hu BY, Weick JP, Yu J, Ma LX, Zhang XQ, Thomson JA, Zhang SC. Neural differentiation of human induced pluripotent stem cells follows developmental principles but with variable potency. Proceedings of the

National Academy of Sciences of the United States of America;107:4335-4340.

[219] Fu N, Drinnenberg I, Kelso J, Wu JR, Paabo S, Zeng R, Khaitovich P. Comparison of protein and mRNA expression evolution in humans and chimpanzees. Plos One 2007;2:e216.

[220] Preuss TM, Caceres M, Oldham MC, Geschwind DH. Human brain evolution: Insights from microarrays. Nature Reviews Genetics 2004;5:850-860.

[221] Cox B, Kislinger T, Emili A. Integrating gene and protein expression data: pattern analysis and profile mining. Methods 2005;35:303-314.

[222] McNamara LE, McMurray RJ, Biggs MJ, Kantawong F, Oreffo RO, Dalby MJ. Nanotopographical control of stem cell differentiation. Journal of tissue engineering 2010;2010:120623.

[223] Kilian KA, Bugarija B, Lahn BT, Mrksich M. Geometric cues for directing the differentiation of mesenchymal stem cells. P Natl Acad Sci USA 2010;107:4872-4877.

[224] Chen W, Villa-Diaz LG, Sun Y, Weng S, Kim JK, Lam RH, Han L, et al. Nanotopography influences adhesion, spreading, and self-renewal of human embryonic stem cells. Acs Nano 2012;6:4094-4103.

[225] Ruiz SA, Chen CS. Emergence of patterned stem cell differentiation within multicellular structures. Stem Cells 2008;26:2921-2927.

[226] Ohgushi M, Matsumura M, Eiraku M, Murakami K, Aramaki T, Nishiyama A, Muguruma K, et al. Molecular pathway and cell state responsible for dissociation-induced apoptosis in human pluripotent stem cells. Cell stem cell 2010;7:225-239.

[227] Riento K, Ridley AJ. Rocks: multifunctional kinases in cell behaviour. Nature reviews Molecular cell biology 2003;4:446-456.

[228] Laukaitis CM, Webb DJ, Donais K, Horwitz AF. Differential dynamics of alpha 5 integrin, paxillin, and alpha-actinin during formation and disassembly of adhesions in migrating cells. Journal of Cell Biology 2001;153:1427-1440.

[229] Webb DJ, Donais K, Whitmore LA, Thomas SM, Turner CE, Parsons JT, Horwitz AF. FAK-Src signalling through paxillin, ERK and MLCK regulates adhesion disassembly. Nat Cell Biol 2004;6:154-+.

[230] Sumida GM, Tomita TM, Shih WT, Yamada S. Myosin II activity dependent and independent vinculin recruitment to the sites of E-cadherin-mediated cell-cell adhesion. Bmc Cell Biol 2011;12.

[231] Dumbauld DW, Shin H, Gallant ND, Michael KE, Radhakrishna H, Garcia AJ. Contractility Modulates Cell Adhesion Strengthening Through Focal Adhesion Kinase and Assembly of Vinculin-Containing Focal Adhesions. Journal of cellular physiology 2010;223:746-756.

[232] Watanabe K, Ueno M, Kamiya D, Nishiyama A, Matsumura M, Wataya T, Takahashi JB, et al. A ROCK inhibitor permits survival of dissociated human embryonic stem cells. Nature biotechnology 2007;25:681-686.

[233] Amano M, Chihara K, Nakamura N, Fukata Y, Yano T, Shibata M, Ikebe M, et al. Myosin II activation promotes neurite retraction during the action of Rho and Rho-kinase. Genes to cells : devoted to molecular & cellular mechanisms 1998;3:177-188.

[234] Da Silva JS, Medina M, Zuliani C, Di Nardo A, Witke W, Dotti CG. RhoA/ROCK regulation of neuritogenesis via profilin IIa-mediated control of actin stability. The Journal of cell biology 2003;162:1267-1279.

[235] Scaife RM, Job D, Langdon WY. Rapid microtubule-dependent induction of neurite-like extensions in NIH 3T3 fibroblasts by inhibition of ROCK and Cbl. Molecular biology of the cell 2003;14:4605-4617.

[236] Vogel V, Sheetz M. Local force and geometry sensing regulate cell functions. Nature reviews Molecular cell biology 2006;7:265-275.

[237] Dalby MJ. Topographically induced direct cell mechanotransduction. Medical engineering & physics 2005;27:730-742.

[238] Arnold M, Cavalcanti-Adam EA, Glass R, Blummel J, Eck W, Kantlehner M, Kessler H, et al. Activation of integrin function by nanopatterned adhesive interfaces. Chemphyschem : a European journal of chemical physics and physical chemistry 2004;5:383-388.

[239] Shumaker DK, Kuczmarski ER, Goldman RD. The nucleoskeleton: lamins and actin are major players in essential nuclear functions. Curr Opin Cell Biol 2003;15:358-366.

[240] Razafsky D, Hodzic D. Bringing KASH under the SUN: the many faces of nucleo-cytoskeletal connections. The Journal of cell biology 2009;186:461-472.

[241] Somlyo AP, Somlyo AV. Signal transduction and regulation in smooth muscle. Nature 1994;372:231-236.

[242] AI I. Actin motors that drive formation and disassembly of epithelial apical junctions. Frontiers in Bioscience 2008;13:6662–6681.

[243] Ferrari A, Cecchini M, Serresi M, Faraci P, Pisignano D, Beltram F. Neuronal polarity selection by topography-induced focal adhesion control. Biomaterials 2010;31:4682-4694.

[244] Thomson JA, Itskovitz-Eldor J, Shapiro SS, Waknitz MA, Swiergiel JJ, Marshall VS, Jones JM. Embryonic stem cell lines derived from human blastocysts. Science 1998;282:1145-1147.

[245] Maniotis AJ, Chen CS, Ingber DE. Demonstration of mechanical connections between integrins cytoskeletal filaments, and nucleoplasm that stabilize nuclear structure. P Natl Acad Sci USA 1997;94:849-854.

[246] Faro-Trindade I, Cook PR. A Conserved Organization of Transcription during Embryonic Stem Cell Differentiation and in Cells with High C Value. Molecular biology of the cell 2006;17:2910-2920.

[247] Yeo S, Jeong S, Kim J, Han JS, Han YM, Kang YK. Characterization of DNA methylation change in stem cell marker genes during differentiation of human embryonic stem cells. Biochem Biophys Res Commun 2007;359:536-542.

[248] Lagarkova MA, Volchkov PY, Lyakisheva AV, Philonenko ES, Kiselev SL. Diverse epigenetic profile of novel human embryonic stem cell lines. Cell Cycle 2006;5:416-420.

[249] Dalby MJ, Biggs MJP, Gadegaard N, Kalna G, Wilkinson CDW, Curtis ASG. Nanotopographical stimulation of mechanotransduction and

changes in interphase centromere positioning. J Cell Biochem 2007;100:326-338.

[250] Miyamoto K, Pasque V, Jullien J, Gurdon JB. Nuclear actin polymerization is required for transcriptional reprogramming of Oct4 by oocytes. Genes & Development 2011;25:946-958.

Appendix A

Optimisation of the 250 nano-grating PDMS fabrication using soft-lithography.

Sylgard 184 has been used to make PDMS replicas of nanofeatures according to the manufacturer's protocol where 10 parts of the base is mixed to 1 part of the curing agent, mixed well and poured onto a master mold, degassed for 30 minutes and cured at 70˚ for minimum 2 hours. The aspect ratio (width: height) of the nano-grating chosen in this study is 1 (250nm width: 250nm height). During the course of the experiments, certain flaws were observed in the replicas made by the soft lithography method. This lead us to investigate a series of factors that might have affected the lithography process namely, the curing temperature (50˚ and 70˚), curing time (4 hours and overnight), material of the master mold (polycarbonate (PC) and polymethylmethacrylate (PMMA)), base: curing agent ratio (10:1, 10:1.3 and 5:1), surface treatment with surfactant (0.05% triton X) and silane, different batches of Sylgard 184 (named X and Y).

The results (Figures A.1 – A.5) were not so surprising but confirmed that the change in batch of Sylgard 184 along with fresh silanization of the master molds helped in successful replication of the nano-grating features. A master mold that had been used for more than 50 PDMS replicas was used with Batch Y PDMS and the lines were still merged (figure A.2). But from Figure A.5, it can be observed that both surface treatment and the batch of PDMS together impact on the replication fidelity. The silanized master molds were usable upto 50 replicas after which the surface treatment starts to wear off (X-ray photoelectron spectroscopy data not presented here) resulting in poor fabrication of nanofeatures having aspect ratios of ≥ 1. The results were also confirmed with tensile

testing for different batch of PDMS and water contact angle testing to check for the hydrophobicity of the material mold (data not shown here). Care is taken to make sure the master molds are silanised every 50 replications and every batch of PDMS is tested for nanofeature replication.

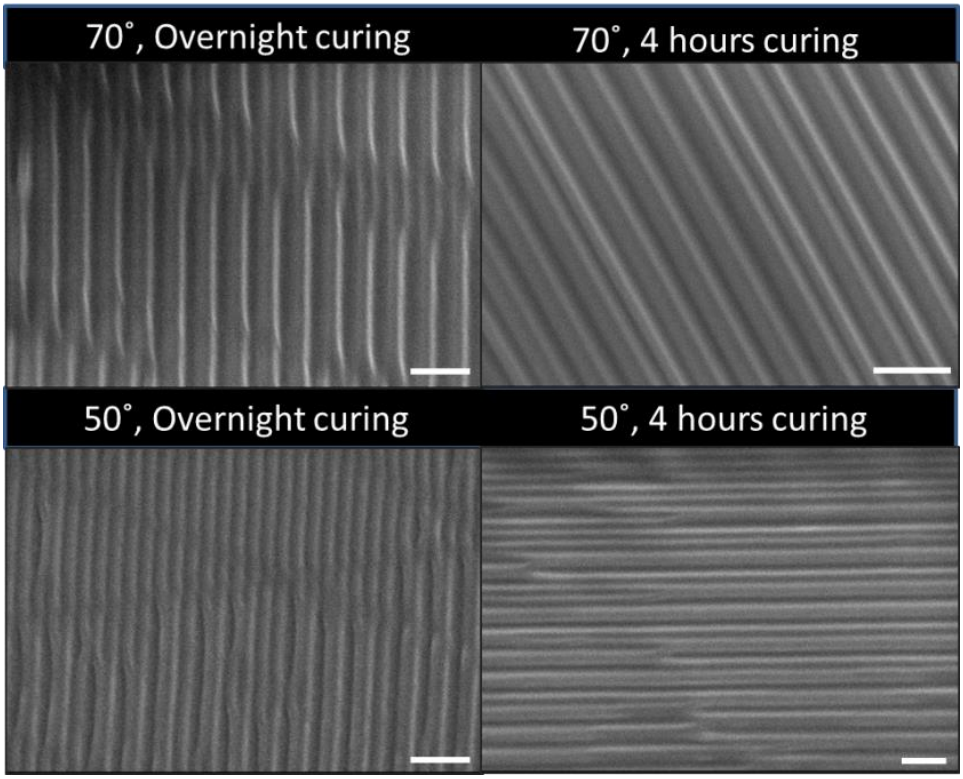

Figure A.1 The curing temperature and time makes lesser impact on replication fidelity. The Figure shows the scanning electron microscopy images of nano-grating PDMS replicated by soft lithography at different curing temperatures (50˚, 70˚) and at two different curing durations (overnight and 4 hours). It can be observed that the lines are merged in all the conditions. The scale bar represents 2µm.

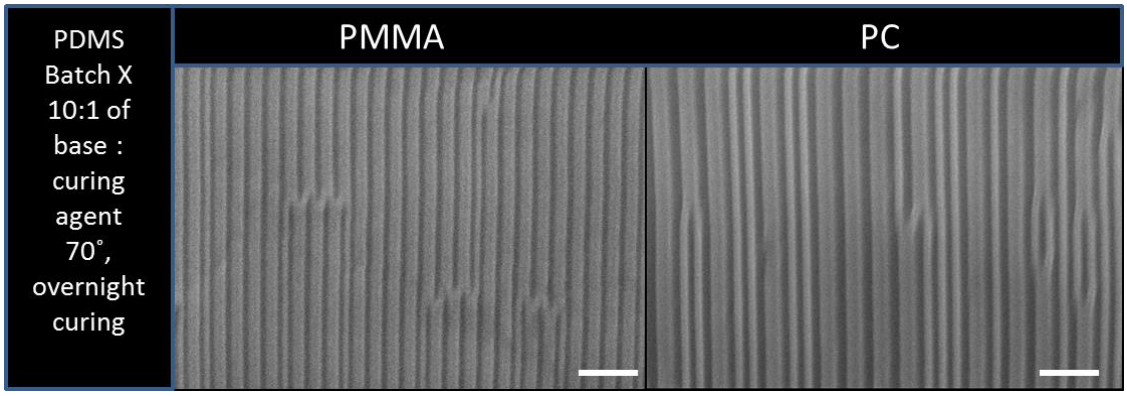

Figure A.2 Soft lithography can be done using a master mold made of either polycarbonate (PC) or polymethylmethacrylate (PMMA). Batch X PDMS which was routinely used for fabricating microstructures was used to fabricate nano-grating PDMS according to the manufacturer's protocol. The lines were merged using either PC or PMMA. The scale bar represents 2µm.

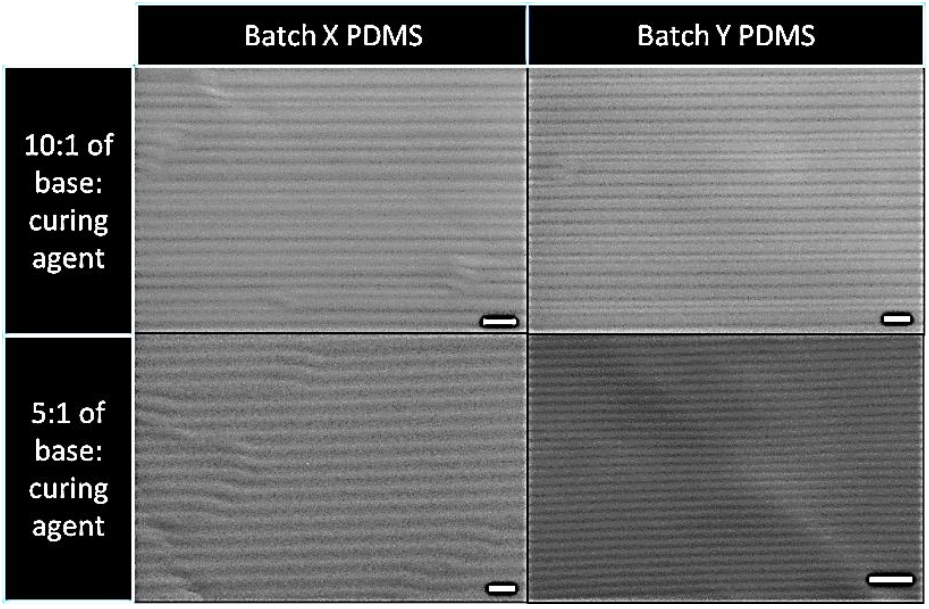

Figure A.3 The batch of Sylgard 184 used and the stiffness of the PDMS can affect the replication fidelity for nano features with aspect ratios ≥ 1. When Batch Y Sylgard 184 kit was used at either 10:1 or 5:1 base: curing agent ratios, the replication was more consistent as compared to the Batch X Sylgard 184 kit. The scale bars represent 2µm.

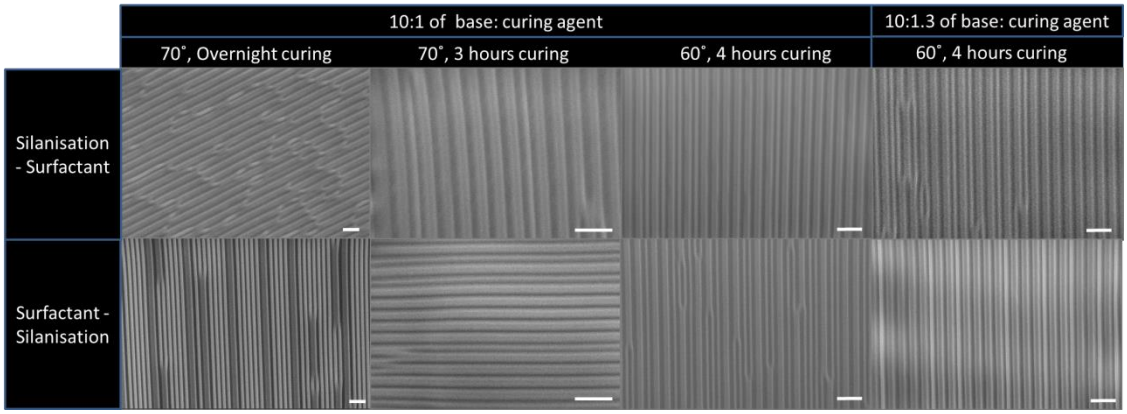

Figure A.4 The surface treatment of the master molds (polycarbonate) with either silane or just the surfactant was not sufficient to replicate nano-sized features. The figure shows PDMS replicas done using master molds treated with either silane (silanization-surfactant) or just surfactant (surfactant-silanization) at different curing temperatures, duration and base: curing agent ratios. The 250nano-gratings were merged under all conditions. The scale bars represent 2µm.

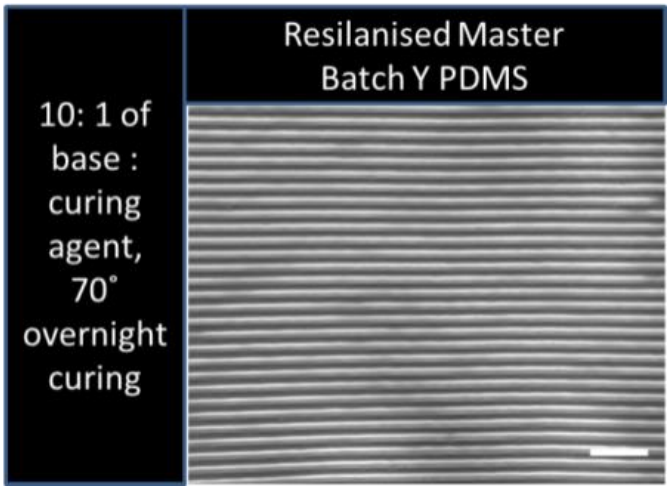

Figure A.5 The batch of Sylgard 184 kit and the surface treatment is important for replication fidelity of nano-gratings with aspect ratio, 1. The above image shows the PDMS replica from a freshly resilanised PMMA master mold and Batch Y Sylgard 184 kit. It can be observed that the 250nm lines were replicated without any merging with equal spacing. The scale bar represents 2µm.

Appendix B

Analysis of F-actin, Nanog and MAP2 expression on micron gratings

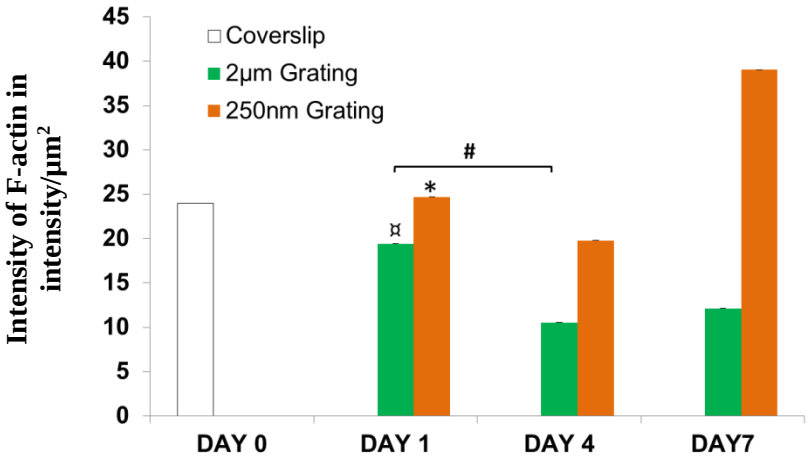

Figure B.1 Intensity measurements of F-actin in hESCs grown on micropatterned substrates (2µm gratings with 2µm spacing and height). The results are shown in intensity/µm^2. * represents significance at $p<0.001$ as compared to Day 0, undifferentiated control, ¤ represents significance at $p<0.01$ as compared to control, # represents significance at $p<0.05$.

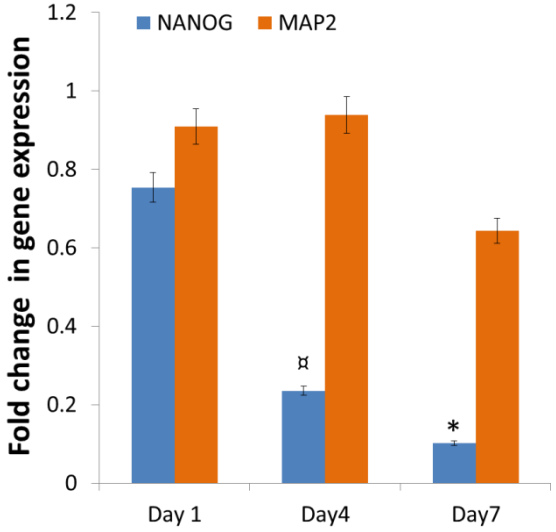

Figure B.2 The plot shows the gene expression fold change for hESCs grown on micro-patterned substrates (2µm grating with 2µm width and 2µm depth), obtained from real time RT-qPCR. The blue bar shows the pluripotent transcription factor, nanog gene expression while the orange bar shows the neuronal marker, MAP2 gene expression. ¤ represents significance at $p<0.01$ as compared to gene expression during Day 1 of neuronal differentiation

Expression of Lamin A/C on nano-patterned and unpatterned substrates

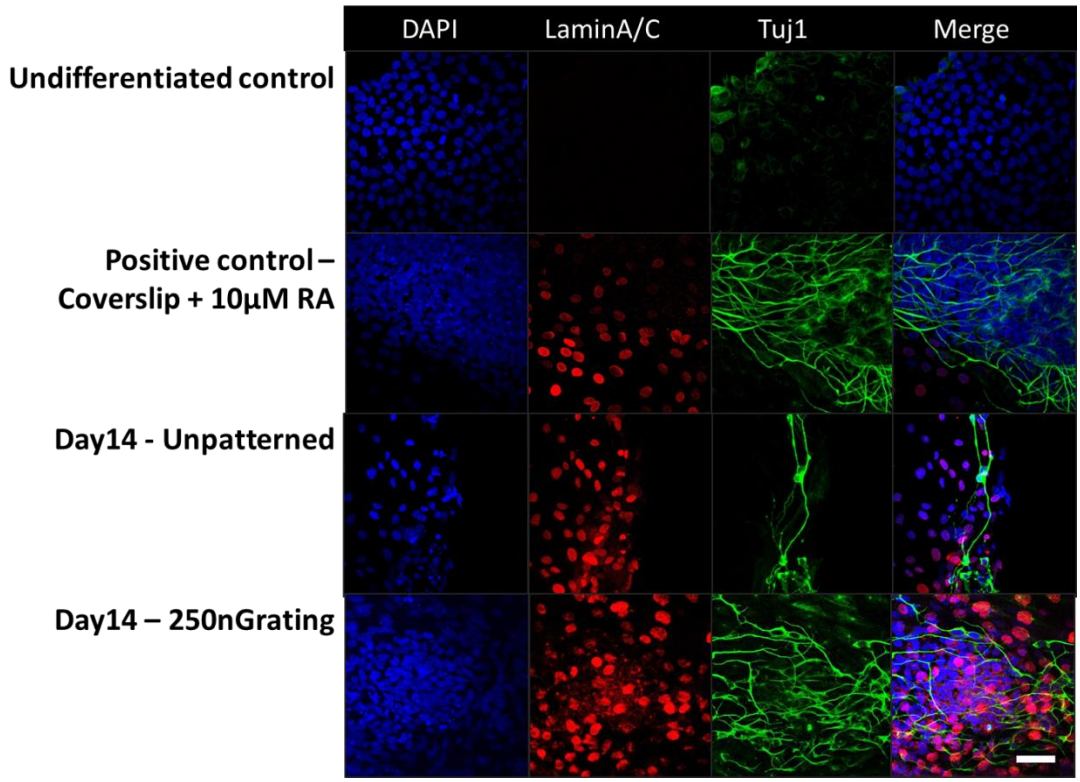

Figure B.3. The image shows the expression of lamin A/C in hESCs differentiated in neuronal differentiation media for longer durations (14 days) on unpatterned and nano-grating PDMS. Human ESCs grown on coverslips with retinoic acid is shown as the positive control while undifferentiated hESCs are shown as the negative control. The hESCs are immunostained for lamin A/C in red, Tuj1 in green and nucleus is counterstained with DAPI in blue. The scale bar represents 50µm.

Appendix C

1. Elongation, alignment, circularity and intensity measurement using Image J.

A. Open the image file of interest in Image J.

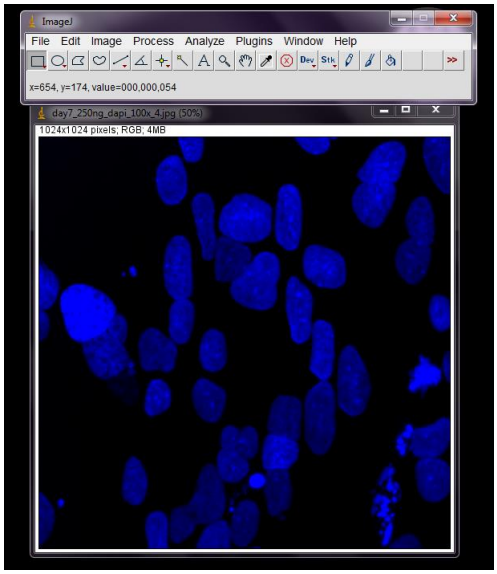

B. Calibrate the scale with known pixel values and choose measurements needed for analysis.

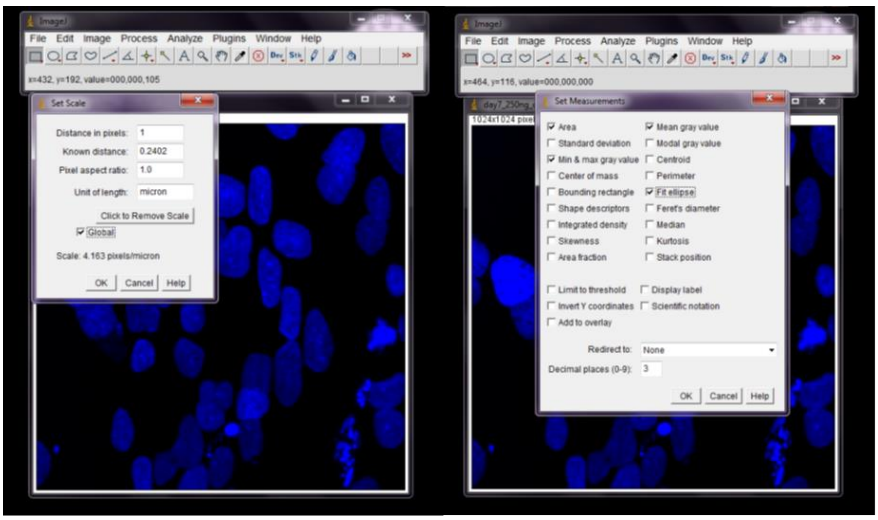

C. Mark the region of interest (ROI) using circle/ellipse/freehand tool.

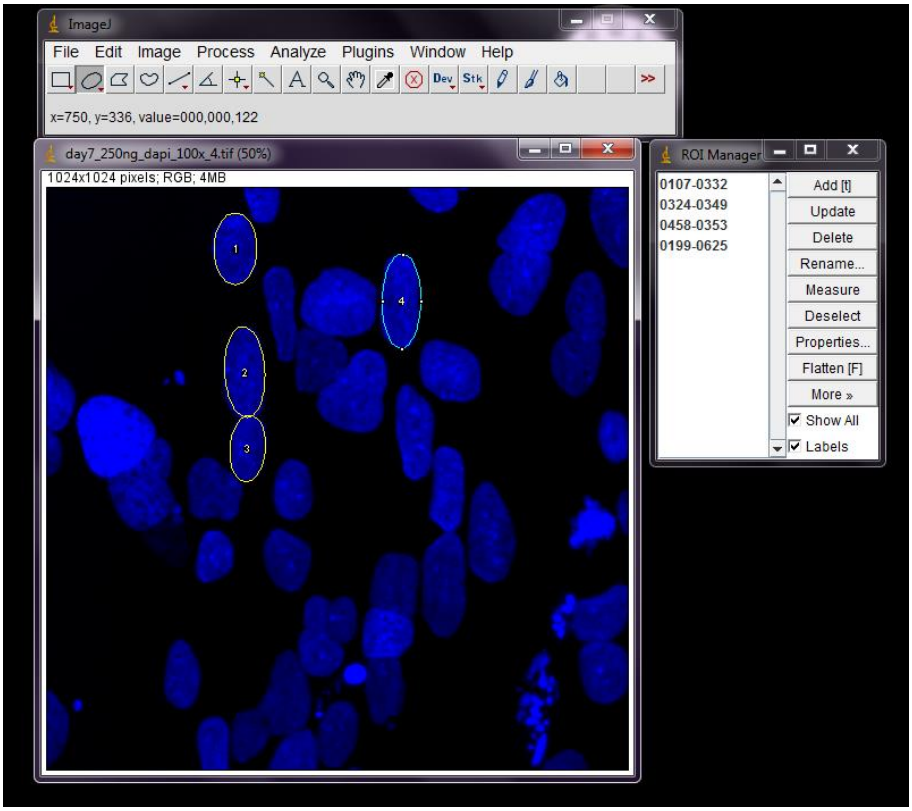

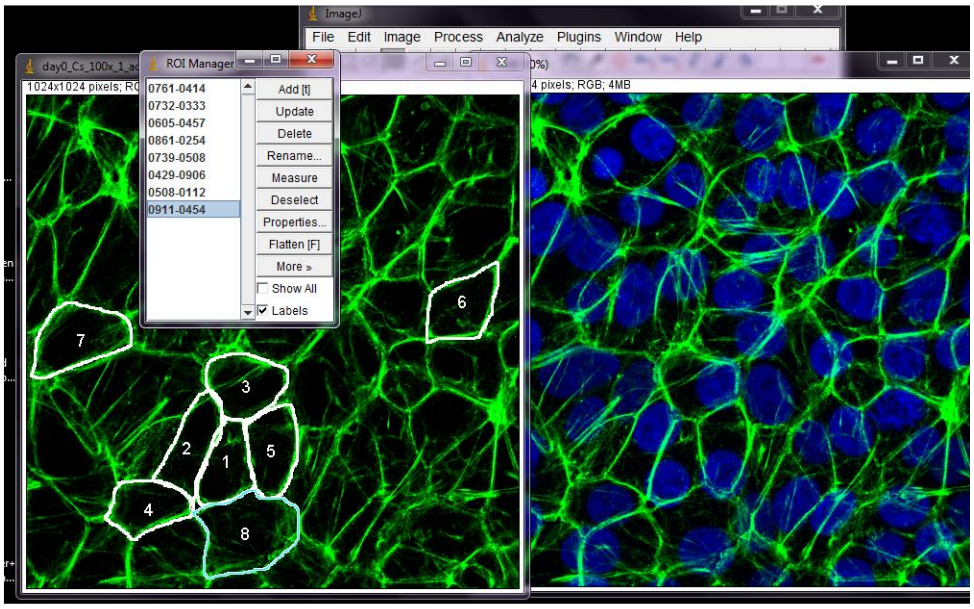

D. Export the measurements to excel file for statistical analysis.

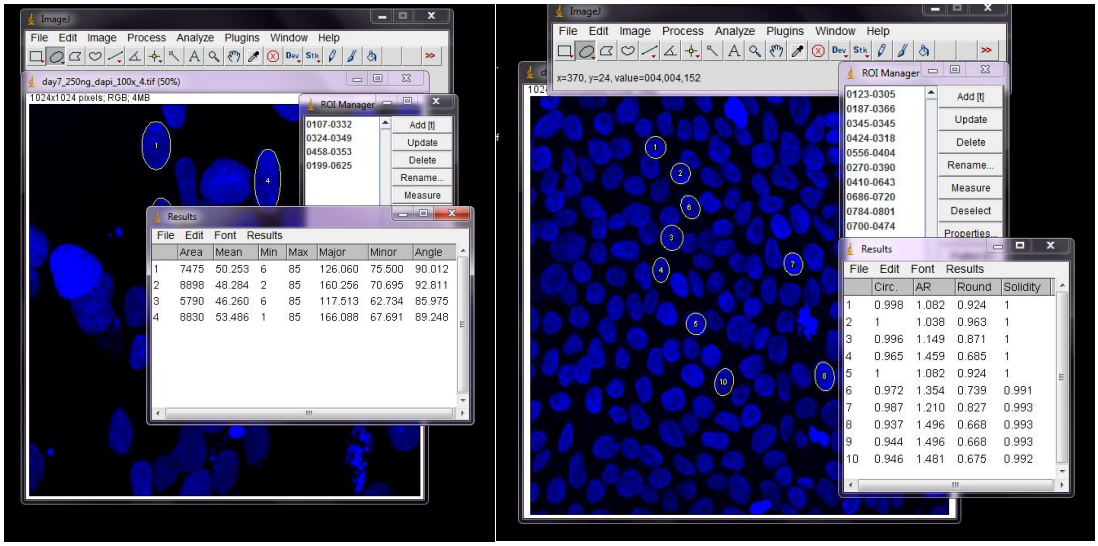

When an ellipse is used to fit the nucleus, it is possible to determine the length of major axis and minor axis, from which elongation of nucleus could be calculated.

Elongation index: Major axis/Minor axis. More elongated nucleus or cells have higher elongation index.

The Image J measurements for circularity are made based on the following formula:

Circularity: 4π X area/ (perimeter)^2. Values close to 1 indicate a perfect circle, while values close to 0 indicate elongated shape.

2. Measuring Volume of nucleus using Imaris.

A. Open image file in Imaris.

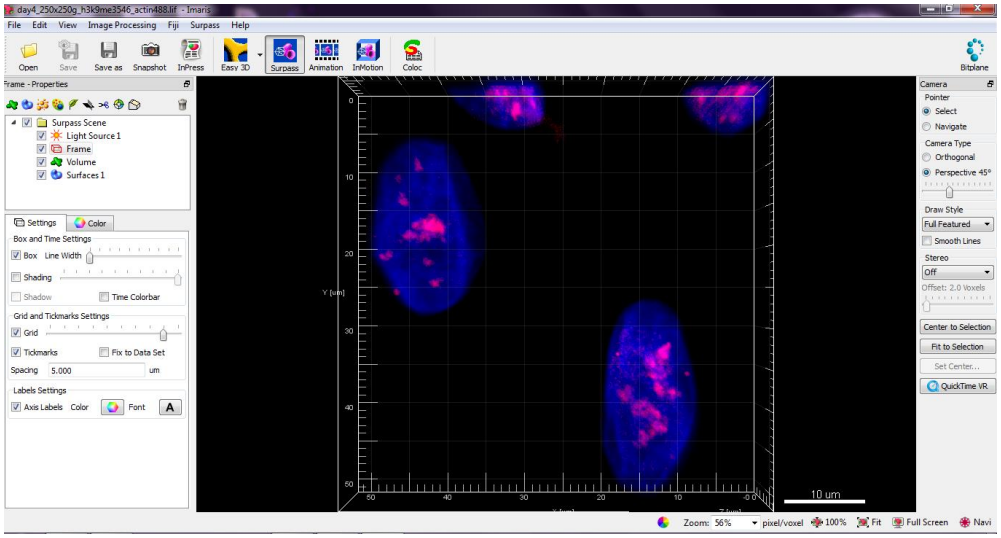

B. Create a surface mask for all the nucleus based on intensity.

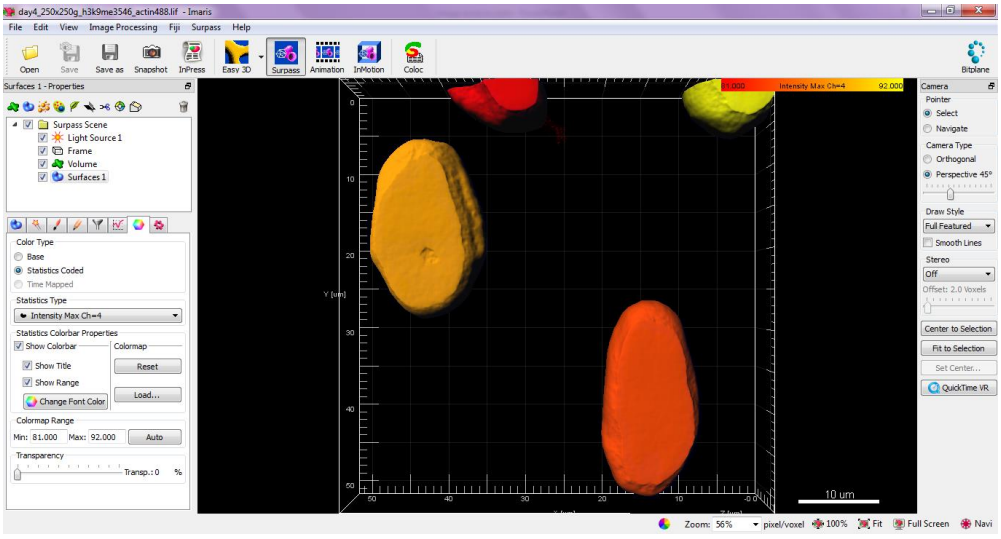

C. Measurements can be imported to excel for further statistical analysis.

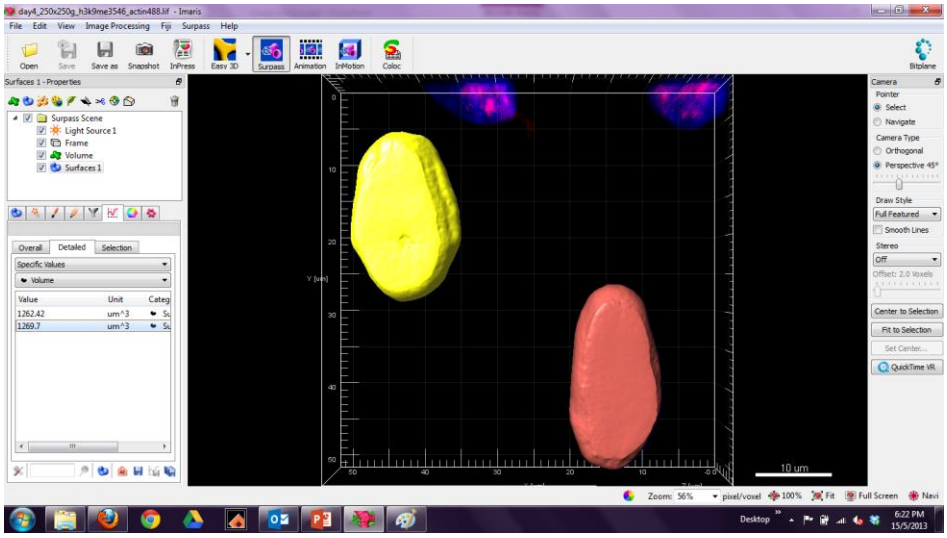

In general, volume of a 3D object can be calculated by the sum of areas for a particular ROI for the entire Z height (area of ROI at Z=0 + area of ROI at Z=1 + ……area of ROI at Z=n) or by using the formula (area of the ROI x height of the object).

Appendix D

List of publications, book chapters and conferences

PUBLICATIONS

1. Moe AAK, Suryana M, Marcy G, Lim SK, Ankam S, Goh JZW, Jin J, *et al*. Microarray with Micro- and Nano-topographies Enables Identification of the Optimal Topography for Directing the Differentiation of Primary Murine Neural Progenitor Cells. Small 2012; 8:3050-3061.

2. Ankam S, Suryana M, Chan LY, Moe AAK, Teo BKK, Law JBK, Sheetz MP, *et al*. Substrate topography and size determine the fate of human embryonic stem cells to neuronal or glial lineage. Acta Biomaterialia 2013; 9:4535-4545.

3. Ankam S, Teo BKK, Kukumberg M and Yim EKF. High throughput screening to investigate the interaction of stem cells with their extracellular microenvironment. Organogenesis July 2013.

BOOK CHAPTERS

1. Teo BKK, Ankam S, Chan LY, Yim EKF. Nanotopography/Mechanical Induction of Stem-Cell Differentiation. In: Shivashankar GV, editor. Methods in cell biology: Academic Press; 2010. p. 241-94.

2. Teo BK, Ankam S, Yim EF. Stem Cell Interaction with Topography. In: Roy K, editor. Biomaterials as Stem Cell Niche: Springer Berlin Heidelberg; 2010. p. 61-87.

CONFERENCES

1. **Ankam** Soneela, Lim Keat Sandy, Aung Aung Kywe Moe, Jerome Goh, Yim Evelyn. Nanotopographical cues enhance the neuronal differentiation of human embryonic stem cell. Society for Neuroscience conference held at San Diego, United States of America, November 2010.

2. **Ankam** Soneela, Yim Evelyn. Induction of stem cell differentiation using topographical cues. 5th East Asia Pacific student's workshop held at National University of Singapore, Singapore, December 2010.
3. Lim Keat Sandy, Aung Aung Kywe Moe, **Ankam** Soneela, Tann Jason, Thiery Marcy Guillaume, Goh L. K Eyleen, Yim Evelyn. Screening for cell culture substrate topography that enhance differentiation of neural progenitor cells into mature neurons. International Society for Stem cell Research, 9th Annual meeting held at Toronto, Canada, July 2011.
4. **Soneela Ankam**, Lim Keat Sandy, Aung Aung Kywe Moe, Yim Evelyn. Neural differentiation of human embryonic stem cells can be modulated by topography.

Tissue Engineering and Regenerative Medicine International Society (TERMIS-AP) held at Waterfront Conference Center, Singapore, August 2011.

5. Aung Aung Kywe Moe, Goh Jerome, Lim Keat Sandy, **Ankam** Soneela**,** Yim Evelyn. Neural differentiation of murine neural progenitor cells on nano-patterned polydimethylsiloxane substrates in different media compositions and different durations. Tissue Engineering and Regenerative Medicine International Society (TERMIS-AP) held at Waterfront Conference Center, Singapore, August 2011.

6. Aung Aung Kywe Moe, **Ankam** Soneela**,** Lim Keat Sandy, Mancuso J. James, Thiery Marcy Guillaume, Goh Jerome, Benjamin Teo Kim Kiat, Goh L. K. Eyleen, Augustine J. George, Yim Evelyn. Nano- and micro-gratings and micro-pillars promote neuronal differentiation of murine neural progenitor cells. Society for Neuroscience Conference held at Washington, D.C., United States of America, November 2011.

7. **Ankam** Soneela, G.V. Shivashankar, Yim Evelyn. Substrate nanotopography cause changes in nucleus shape and size during neuronal differentiation of human embryonic stem cells. Gordon Research seminar and Conference (GRS and GRC) on Signal Transduction by Engineered Extracellular Matrices held at University of New England, Maine, United States of America, July 2012.